

الجمهورية الجزائرية الديمقراطية الشعبية

République Algérienne Démocratique et Populaire
**Ministère de l'Enseignement Supérieur et de la Recherche
Scientifique**

Université Ferhat ABBAS Sétif-1

THESE

Présentée devant

**LE DEPARTEMENT DE GENIE DES PROCEDES
FACULTE DE TECHNOLOGIE**

En vue de l'obtention du diplôme de

Doctorat 3^{ème} cycle

Option : Matériaux Polymères

Par

M^{me} : KERAKRA SAMIA

**Préparation, fabrication et caractérisation des
armatures renforcées polymères/argile nanocomposites**

Soutenue le 27/06 /2018 devant le Jury :

Président :	Djafer BENACHOUR	Prof.	Université Ferhat ABBAS, Sétif-1
Examineur 1:	Hocine DJIDJELLI	Prof.	Université Abderrahmane MIRA, Bejaïa
Examineur 2 :	Rachida DOUFNOUNE	Prof.	Université Ferhat ABBAS, Sétif-1
Directeur de thèse :	Said BOUHELAL	Prof.	Université Ferhat ABBAS, Sétif-1
Co-Directeur de thèse:	Marc PONCOT	MC.	IJL École des mines, Nancy

Democratic and Popular Republic of Algeria
Ministry of Higher Education and Scientific Research

University of Ferhat ABBAS- Setif-1

DOCTORAL DISSERTATION

Presented in front of

**DEPARTMENT OF PROCESS ENGINEERING
FACULTY OF TECHNOLOGY**

In fulfillment of requirements for the degree of

3rd Cycle PhD

Option: Polymeric materials

By

M^{me} : KERAKRA SAMIA

**Preparation, fabrication and characterization of reinforced
frame polymer/clay nanocomposites**

Defended on 27/06 /2018 Front of the Jury

President :	Djafer BENACHOUR	Prof.	University Ferhat ABBAS, Sétif-1
Examiner 1:	Hocine DJIDJELLI	Prof.	University Abderrahmane MIRA, Bejaïa
Examiner 2 :	Rachida DOUFNOUNE	Prof.	University Ferhat ABBAS, Sétif-1
Advisor:	Said BOUHELAL	Prof.	University Ferhat ABBAS, Sétif-1
Co-advisor :	Marc PONÇOT	MC.	IJL École des mines, Nancy

Acknowledgements

I would like to thank my supervisor, Pr. Said Bouhelal, for providing me advices, mentoring, encouragement and research support through my PhD study. I have learned and grown tremendously under his guidance.

I would like to express my deepest gratitude to Dr. Marc Ponçot for his supervision and his support. Really, I am so thankful to him for providing me an unique opportunity to characterize my samples under his tutelage, as well as his timely advice and encouragement during the year that I spent in his laboratory at Jean Lamour Institute (IJL) in Nancy.

I am also indebted to Pr. Abdesselam Dahoun for his warm welcoming and his timely assistance and encouragement when I was at Jean Lamour Institute in Nancy.

Many many thanks to Mr. Olivier Godard for his assistance, long hours, infinite patience, humor, really, no words are enough to convey all my acknowledgements to him for helping me with equipments training.

A special thanks to Pr. Djafer Benachour, for his very careful review of my thesis and his insightful comments and correction that ensued.

I am thankful to my committee members, foremost the president of the committee members Pr.Benachour, and Pr. Rachida Doufnoune , Pr. Hocine Djidjelli for their valuable time, constructive criticisms and suggestions. Thank you for the opportunity to revise my thesis, I really appreciate your careful review.

I would like to thank Mr.Khitass Moncef and Miss. Ibtissem for their help as well. Many thanks also go to (IJL, LMPMP laboratory and Unit of Emergent Research Materials) groups members with whom I sheared the best moments of my life.

Finally, I would like to thank all my friends an all my family members for their encouragements and support, especially my best friend and sister “Taous”.

A special thanks to my husband “Samir” for his long time support, understanding, love, encouragement, and for bringing me a lot of happiness in my life.

I would like to thank my parents for their unconditional love and support. I would never be here without them.

List of Figures

Figure I.1. Young's modulus of Alfa fibers/clay/ polypropylene hybrid composites	5
Figure I.2. Dynamic mechanical analysis results of Alfa fibers/clay/ polypropylene hybrid composites as a function of temperature.....	6
Figure I.3. SEM micrographs of impact fractured surfaces of: (c) (PP: G15)/NC6; and (d) (PP: G15)/NC9. SEM: scanning electron microscopy; PP: polypropylene; NC: nanoclay G: glass fibers	7
Figure I.4. Variation of tensile strength and tensile modulus for PP/glass fiber composites and PP/glass fiber/nanosilica hybrid composites.....	8
Unmodified: short glass fiber/PP composite.....	8
Modified: hybrid composite modified by nanosilica	8
Figure I.5. Variation of storage modulus for PP/glass fiber composites and PP/glass fiber/nanosilica hybrid composite as a function of temperature	9
Figure II.2. Schematic picture of an ion-exchange reaction	18
Figure II.3. Illustration of different states of dispersion of organoclays in polymers with corresponding WAXS patterns and TEM results	19
Figure II.4. Schematic image of a polymer-clay nanocomposite material with completely exfoliated (molecular dispersed) clay sheets within the polymer matrix material	20
II.1.3. Reversibly crosslinked isotactic polypropylene/clay Nanocomposites.....	21
Figure II.5. Illustration of the hybrid structure of totally exfoliated iPP/clay nanocomposite material	22
Figure II.6. WAXS patterns of a- neat PB-1 and b- PB-1/clay nanocomposite at different aging times.....	23
Figure II.7. Spherulitic morphology of a- neat PB-1 and b- PB-1/ clay nanocomposite	24
Figure II.8. X-ray diffraction patterns for phase transformation in a- pure PB-1 and b- PB-1/clay nanocomposite	24
Figure II.9. Schematic illustration of network structure: a) for a polymer with tetrafunctional C-C bonds (arrows indicate crosslinks).....	28
Figure II.11. Nano-particle reinforcement of the matrix in a fibre composite	31
Figure II.12. Simulation of uniform distribution of short fibers in nanocomposite matrix	31
Figure III.1. Molecular structure of Polypropylene	39
Figure III.2. Molecular structure of polybutene-1	41

Figure III.3. Helical conformations of (a) Form-I, 3/1 helix.....	42
(b) Form-II, 11/3 helix	42
Figure III.4. Crystal-crystal transformations of PB-1	43
Figure III.5. SEM micrograph of the used hollow recycled PET fiber	45
Figure III.6. Three phase model of fiber structure	46
Figure III.7. Structure of Layered Silicates	47
Figure III.8. Experimental device of X-ray diffraction test	58
Figure III.9. a-Tensile micromachine b-Sample dimensions.....	62
Figure III.11. Determination of the true axial strain in the representative volume element (RVE)	63
Figure III.12. General diagram of the VidéoTraction TM system	64
Figure IV.1. Torque-time evolution of the different crosslinked PP.....	68
Figure IV.2. Variation of MFI for the crosslinked samples.....	68
Figure IV.3. Variation of the gel content of the crosslinked samples.....	69
Figure IV.4. DSC thermograms of first heating (a) and cooling (b) runs of PP (pellet and granule)	70
Figure IV.5. First (a) and second (b) heating runs of crosslinked PP samples.....	71
Figure IV.6. Cooling run of crosslinked PP samples.....	72
Figure IV.7. WAXS patterns of the different crosslinked PP samples.....	73
Figure IV.8. α and γ forms portion (%) as function of the crosslinking agent content.....	73
Figure IV.9. FTIR spectra of crosslinked PP samples in the region [1800-1700 cm^{-1}]	74
Figure IV.10. FTIR spectra of crosslinked PP samples. b. in the region [1500-800 cm^{-1}] c. in the region [800-400 cm^{-1}]	75
Figure IV.11. Mechanism of the reversible crosslinking reaction of polypropylene.....	76
Figure IV.12. 2D WAXS patterns of a) - 0.8 XPP b) - 3.2 XPP.....	77
Figure IV.13. Variation of the storage modulus (a) and storage modulus values (b) as a function of temperature for the neat PP and crosslinked PP.....	78
Figure IV.14. Variation of $\tan \delta$ as a function of temperature for the crosslinked PP materials..	79
Figure. IV.15. True tensile behavior of the crosslinked samples.....	80
Figure.IV.16. Impact strength of the PP crosslinked samples	81
Figure IV.17. Torque vs time data of neat PP and PP/h.r-PETfs composites.....	83
Figure IV.18. MFI of composites in function of different loading of r-PETfs.....	83

Figure IV.18. Variation of the Young's modulus and elongation at break for PP/ hollow r-PETfs (wt %) composites	85
Figure IV.20. Strain and stress at break of PP/ hollow r-PETfs (wt %) composites	85
Figure IV.21. Variation of the impact strength for PP/ hollow r-PETfs (wt %) composites	86
Figure IV.22. WAXS patterns of composites in different loading of r-PETfs.....	87
Figure IV.23. Thermograms of the second heating cycle of composites.....	87
Figure IV.24. Thermograms of the cooling cycle of composites	87
Figure IV.25. Optical microscopic images of polished plaques surface of 7wt% h.r-PETfs reinforced PP composite.....	88
Figure IV.26. Optical microscopic images of films surface of 7wt% h.r-PETfs reinforced PP composites.....	89
Figure IV.27. (a,b,c,d,e,f,g,h). SEM micrographs of the fractured surface of composite with 7wt%h.r-PETfs	90
Figure IV.28. In situ tensile Chromatography-slice images showing different kinds of damage	91
Figure IV.29. In situ tensile Chromatography -slice images of PP/ 7 wt% h.r-PETfs composite before loading (left) and after fracture (right)	92
Figure IV.30. Modulus (E') curves of composites PP/h. r-PETfs composites as a function of temperature	93
Figure IV.31. Tan delta curves of PP/h. r-PETfs composites as a function of temperature	94
Figure IV.32. Dynamic rheological analysis of crosslinked PP/h.r-PETfs (wt %) composites..	95
Figure IV.33. MFI measurement of crosslinked PP/h.r-PET fibers (wt %) composites.....	96
Figure IV.34. Young's Modulus of h.r-PET fibers (wt %) reinforcing (XPP/PP) matrices.....	97
Figure IV.35. Stress and strain at break of (unmodified/modified PP) /h.r-PET fibers (wt %) composites	98
Figure IV.36. Elongation at break of (unmodified/modified PP) /h.r-PET fibers (wt %) composites	98
Figure IV.37. Izod impact strength of crosslinked PP/PET fibers composites	99
Figure. IV.38. Variation of the storage modulus as a function of temperature for crosslinked PP/hollow PET fiber composites.....	100
Figure. IV.39. Variation of the tan delta as a function of temperature for crosslinked PP/ hollow PET fiber composites.....	101
Figure. IV.40. WAXS patterns of crosslinked PP/h.r-PET fibers composites.....	102
Figure. IV.41. Heating and cooling runs of unmodified and modified PP	103
Figure. IV.42. Heating and cooling runs of crosslinked PP/h.r-PETfs (wt%) composites.....	103

Figure. IV.43. a. SEM micrograph of 7wt% h.r-PET fiber/crosslinked PP composite b. optical image of 7wt% h.r-PET fiber/crosslinked PP composite.....	105
Figure. IV.44. FTIR spectra of 7wt % (treated/untreated) PET fiber/ (modified/unmodified) PP composites.....	106
Figure IV.45. Young's modulus of 7 wt% (treated/untreated) PET fiber/ (modified/unmodified) PP composites	107
Figure IV.46. Variation of elongation at break for 7 wt% (treated/untreated) PET fiber/ (modified/unmodified) PP composites.....	108
Figure IV.47. Variation of Izod impact strength for the treated PET fiber filled unmodified and modified PP matrices.....	109
Figure IV. 48. WAXS patterns of 7 wt% treated PET fiber / (unmodified and modified) PP composites	110
Figure IV.49. DSC thermograms of 7 wt% treated PET fiber / (unmodified and modified) PP composites.....	111
Figure IV.50. SEM micrographs of fractured surface of 7 wt% treated PET fiber /XPP composite	112
Figure IV.51.a. Torque vs time data of (3, 5 and 7 wt% PA fibers) /PP composites.....	113
Figure. IV.51. b. Torque evolution of (3, 5 and 7 wt% PA fibers)/ crosslinked PP composites.....	114
Figure IV.51.c. Torque stabilization values (Tc) of polyamide fibers/ (unmodified/crosslinked) PP composites.....	114
Figure IV.52. Variation of MFI values for (PP/XPP)/ wt% PAfs composites.....	115
Figure IV.53. Variation of Young's modulus for (PP/XPP)/ wt% PAfs composites as a function of PAfs loading	116
Figure IV.54. Variation of tensile strength for (PP/XPP)/ wt% PAfs composites as a function of PAfs loading	116
Figure IV.55. Variation of Izod impact strength for (PP/XPP)/ wt% PAfs composites.....	117
Figure IV.56. WAXS patterns of (PP/XPP)/ wt% PAfs composites.....	118
Figure IV.57. DSC thermograms of polyamide fiber/ (unmodified PP (a) and modified PP (b)) composites.....	119
Figure IV.58. Opticl microscopy image of PP/ 5 wt% polyamide fiber composite.....	120
Figure IV.59. SEM micrographs of fractured surface of crosslinked PP/ 5wt% polyamide fiber composite.....	120
FigureIV.60. FTIR spectra of a)-Unmodified Na-MMT; b, c, d)- PP ; PP/1wt% FA crosslinked PP ; 3,5and7wt%f-Na-MMT nanocomposites.....	122
Figure IV.61. FTIR spectra of PP, PP/5wt%PAfs, PP/5wt% t-PAfs composites.....	123

Figure IV.62. Fourier transform infrared spectroscopy (FTIR) spectra of a, b) - 5wt % t-PAfs/ 3, 5 and 7 wt% f-Na-MMT/PP hybrid composites.....	125
Figure IV.63. WAXS patterns of a)-5 wt% t-PAfs /PP composite b)- 1 wt% FA /PP crosslinked PP.....	126
Figure IV.64. WAXS patterns of 3, 5 and 7 wt%/PP nanocomposites.....	127
Figure IV.65. WAXS patterns of 5wt% t-PAfs/3, 5 and 7wt% f-Na-MMT/PP hybrid composites.....	128
Figure IV.66. DSC thermographs of second heating and cooling runs of 5wt%t-PAfs /PP composite.....	130
Figure IV.67. DSC thermographs of second heating and cooling runs of a)-f-Na-MMT/PP nanocomposite and b)-t-PAfs/f-Na-MMT/PP hybrid composites.....	131
Figure IV.68. Optical micrographs of a) 5wt% t-PAfs/PP composite b) 5wt% t-PAfs / 5wt% f-Na-MMT /PP hybrid composite.....	132
Figure IV.69. SEM micrographs of a) - Untreated PAfs b, c)-Treated PAfs.....	133
Figure IV.70. SEM micrographs of the tensile fractured surface of a) - 5wt% PAfs/PP composite	134
Figure IV.71. Variation of Young's modulus for the different composites.....	135
Figure IV.72. Variation of the tensile strength for the different composite	136
Figure IV.73. Variation of the Izod impact strength for the different composites.....	137
Figure IV.74. Evolution (Torque/time) for the different crosslinked PB-1 materials.....	138
Figure IV.75. Variation of T_C and T_B torque values for the cosslinked PB-1 materials.....	139
Figure IV.76. Variation of MFI values for the modified PB-1 samples.....	139
Figure IV.77. DSC thermograms of the neat PB-1 before and after one mixing cycle in the Brabender (pellet and mixed granule)	141
Figure IV.78. DSC thermograms of the first (a) and second (b) heating runs of the crosslinked PB materials.....	142
Figure IV.79. DSC Thermograms of the cooling run of the crosslinked samples.....	143
Figure IV.80. DSC thermograms of the first (a) and second (b) heating runs of the crosslinked samples (plates)	144
Figure IV.81. DSC Thermograms of the cooling run of the crosslinked samples (plates).....	145
Figure IV.82 . WAXS profiles of the crosslinked PB-1 samples.....	146
Figure IV.83. Variation of the crystallinity degree for form I and II of the crosslinked PB samples.....	147
Figure IV.84. FTIR spectra of the crosslinked PB-1 samples a- in the region [1200- 800 cm^{-1}] and b- in the region [750 - 400 cm^{-1}]	148
Figure IV.85. Mechanism of the crosslinking reaction of the polybutene-1	148

Figure IV.86. 2D WAXS patterns of the modified PB-1 samples.....	149
Figure IV.87. Variation of the storage modulus (a) and $\tan \delta$ (b) as a function of temperature for the crosslinked materials.....	150
Figure IV.88. True stress- true strain curves of the modified PB-1 materials.....	152
Figure IV.89. SEM micrographs of a- neat PB-1 and b- 0.8 XPB-1 samples.....	152
Figure IV.90. Torque evolution of the different composites.....	153
Figure IV.91. Variation of MFI for the different composites.....	154
Figure IV.92. First and second heating runs of the crosslinked PB-1, modified and unmodified PB-1 / treated PET fibers composites.....	156
Figure IV.93. First and second heating runs of PB-1/f-Na-MMT nanocomposite, PB-1 /7wt% hollow PET fibers composite and the hybrid composite	157
Figure IV.94. Cooling run of PB-1/f-Na-MMT nanocomposite, PB-1 /7wt% hollow PET fibers composite and the hybrid composite	157
Figure IV.95. WAXS patterns of the different composites	159
Figure IV.96. Variation of Young's modulus for the different composites.....	160
Figure IV.97. Variation of the stress (a) and strain (b) at break of the investigated composites.....	161
Figure IV.98.a. Storage modulus of the different composites as a function of temperature...	163
Figure IV.98. b. The damping factor ($\tan \delta$) of the composites as a function of temperature.	164
Figure 99. (a,b,c,d). SEM micrographs of the tensile fractured surface of the treated and untreated 7 wt% PET fiber /PP composite.....	165
Figure IV.100 (a,b,c,d). SEM micrographs of the tensile fractured surface of 7 wt% treated PET fiber/crosslinked PB-1 composite.....	166

List of tables

- Table I.1.** Reported works on fiber/nanofiller/polymer hybrid composites
- Table III.1.** Properties of the polypropylene (PP 510A) used
- Table III.2.** Some properties of the polypropylene (PP 510P) used
- Table III.3.** Isomorphous forms of polypropylene
- Table III.4.** Properties of the polybutene-1 used
- Table III.5.** Structural Characteristics for the Crystal Modifications of PB-1
- Table III.6.** Properties of the hollow recycled PET fibers
- Table III.7.** Polyamide fibers (PAfs) properties
- Table III.8.** Crosslinked PP samples designation and composition
- Table III.9.** Formulation of PP/short fibers composites
- Table III.10.** Formulation of crosslinked PP/short fibers composites
- Table III.11.** Sample designation and composition of hybrid composites.
- Table III.12.** Crosslinked PB-1 sample designation and composition
- Table III.13.** Formulation of PB-1/hollow PET fiber/Na-MMT hybrid composite
- Table III.14.** Remarkable values of $F_u \rightarrow / \rightarrow_x$ used for determining the material texture using Hermans' orientation factor.
- Table IV.1.** Gel content values of the different crosslinked PP
- Table IV.2.** DSC parameters of PP (pellet and granule)
- Table IV.3.** DSC parameters of the modified PP materials
- Table IV.4.** Crystallinity degrees of modified PP materials
- Table IV.5.** Mechanical parameter of the crosslinked PP samples
- Table IV.6.** Melting (T_m), crystallization temperatures (T_c) and enthalpies (ΔH_m , ΔH_c) for different samples and crystallinity degree (χ_c) obtained by DSC and WAXS.
- Table IV.7.** WAXS measurements: (χ_c^{WAXS}), X_β of β form and X_γ of the γ -form.
- Table IV.8.** Melting (T_m), crystallization temperatures (T_c) and enthalpies (ΔH_m , ΔH_c) for different samples and crystallinity degree (χ_c) obtained by DSC.
- Table IV.9.** WAXS measurements: (χ_c^{WAXS}), X_β of β form and X_γ of the γ -form
- Table IV.10.** DSC parameters of treated PET fiber/ modified and unmodified PP composites

Table IV.11. DSC parameters of polyamide fiber / (unmodified and modified) PP composites

Table IV.12. WAXS measurements: (χ_c^{WAXS}), X_β of β form and X_γ of the γ -form.

Table IV.13. Melting (T_m), crystallization temperatures (T_c) and enthalpies (ΔH_m , ΔH_c) for different samples and crystallinity degree (χ_c) obtained by DSC

Table IV.14. Variation of gel content for the crosslinked PB-1 samples

Table IV.15. DSC parameters of PB-1 pellet and granule (mixed)

Table IV.16. DSC results of the modified PB-1 samples

Table IV.17. DSC results of the modified PB-1 samples (plates)

Table IV.18. χ I , χ II and crystallinity degree of the modified PB-1 materials

Table IV.19. DMA parameters of the modified PB-1 samples

Table IV.20. DSC parameters of modified and unmodified PB-1/PET fiber composites

Table IV.21. DSC parameters of the composites investigated

Table IV. 221. Crystallinity degree of the different composites

Table IV.23. Impact strength of the different composites

Table IV.23. DMA parameters of the different composites

Table of contents

Introduction.....	1
Chapter I : Overview, objective and scope of the thesis	4
I.1 Overview	4
I.2 Properties and of the prepared materials	10
I.3 Limitations of the present research work	12
I.4 Objective	12
I.5 Scope.....	12
Chapter II : Fiber reinforced polymer nanocomposite.....	16
Introduction	16
II.1.Review on polymer–clay nanocomposite	17
II.1.1.Organic modification of clay	17
II.1.2.Nanocomposite formation	18
II.1.3. Reversibly crosslinked isotactic polypropylene/clay Nanocomposites.....	21
II.1.4. Polybutene-1/clay nanocomposites studies	22
II.2. Review on fiber-reinforced polymer composite.....	24
II.2.1. Methods for Adhesion Improvement.....	25
II.2.1.1.Review on chemical coupling agents	25
II.2.1.2. Matrix Modifications.....	26
II.2.1.3. Fiber Treatment and Matrix Modifications.....	27
II.2.1.4. Review on crosslinking reaction.....	27
II.3.Clay/fiber/polymer hybrid composite	29
II.3.1.The concept of a three phase composite.....	29
Chapter III : Materials and experimental techniques.....	38
III.1. General characteristics of the materials used	38
III.1.1. Polypropylene (PP).....	38
III.1.1.1.Microstructure of PP	39
III.1.2.Polybutene-1 (PB-1).....	40
III.1.3. Hollow recycled Poly (ethylene terephthalate) fibers	43
III.1.4. Polyamide fibers (PA 6).....	44
III.1.5.Stearic Acid.....	45
III.1.6. Montmorillonite (MMT).....	46
III.1.7.Crosslinking agent (Functionalizing agent)	47

III.2. Processing method	48
III.2.1. Crosslinked polypropylene	48
III.2.2. Composites preparation.....	48
a-Polypropylene (PP) matrix /short fibers composite.....	48
❖ Surface treatment of fibers.....	48
b-Crosslinked PP (XPP) matrix/short fibers composites	49
c-Hybrid composites preparation.....	50
c.1- Na-MMT/PP nanocomposites preparation	50
c.2- Crosslinked PP (PP/ 1wt% FA).....	50
c.3- PAfs/PP composites preparation	50
c.4- f-Na-MMT /PAfs /PP hybrid composites	51
III.2.2. Crosslinked Polybutene -1	51
III.2.1. Polybutene-1 /hollow PET fiber/ Na-MMT hybrid composites	55
III.3. Experimental techniques	56
III.3.1. Rheological characterizations	56
III.3.1.1. Dynamic rheological analysis	56
III.3.1.2. Melt flow index (MFI) measurements	56
III.3.2. Gel content	56
III.3.3. Microstructural characterization.....	56
III.3.3.1. FTIR measurements	56
III.3.3.2. Differential scanning calorimetry (DSC).....	56
III.3.3.3. Wide-angle X-ray scattering (WAXS).....	57
III.3.3.4. Macromolecular orientation (2D WAXS)	59
III.3.3.5. Dynamic Mechanical Analysis.....	60
III.3.3.6. Scanning electron microscope (SEM).....	60
III.3.3.7. Optical light polarized microscopy	60
III.3.3.8. Synchrotron X-ray tomography (SRXTM)	60
III.3.4.1. Tensile test.....	61
III.3.4.1.1. VidéoTraction™ system	61
III.3.4.1.2. Simple tensile test	64
III.3.4.2. IZOD impact strength tests.....	64
Chapter IV: Results and discussions.....	67
IV.1. Composite based on modified polypropylene matrix/fibers.....	67
IV.1.1. Crosslinking of polypropylene (PP).....	67

IV.1.1.1. Rheological results	67
1.1. Dynamic rheological analysis (DRA) results	68
1.2. Melt flow index (MFI) results	68
IV.1.1.2. Gel content test.....	69
IV.1.1.3. Structural study of the modified polypropylene samples	69
3.1. DSC measurements of crosslinked PP	69
3.2. X-ray diffraction results	72
3.3. Fourier transform infrared spectroscopy (FTIR)	74
IV.1.1.4. Mechanical study of the modified polypropylene.....	77
4.1. 2D-WAXS.....	77
4.2. DMA (Dynamic mechanical analysis)	77
4.3. True mechanical behavior.....	79
4.4. Impact strength	80
IV.1.1.5. General Conclusions	81
IV.1.2. Crosslinked PP matrix/short fiber composite	82
IV.1.2.1. Crosslinked PP/short hollow PET fiber composite.....	82
A. Influence of the Matrix modification.....	82
A.1. Study of unmodified PP/short hollow PET fibers composite.....	82
1.2. Rheological properties of composites.....	82
2.1. DRA results	82
2.2. MFI results	83
1.3. Mechanical Properties.....	84
1.4. Microstructural study of the composites.....	86
4.2. DSC Analysis	87
4.3. Optical microscopy observations.....	88
4.4. SEM Observation.....	89
4.5. Synchrotron X-ray tomography (SRXTM).....	91
4.6. Dynamic mechanical analysis (DMA).....	92
A.1.2. Conclusion	94
A.2. Study of crosslinked PP/ short hollow PET fibers composite	94
2.1. Rheological properties	94
1.1. DRA measurement.....	94
1.2. MFI Results	95
2.2. Mechanical properties.....	96
2.2.1. Tensile strength.....	96

2.2.2. Izod impact strength.....	99
2.2.3. Dynamic mechanical analysis (DMA)	99
2.3. Structural properties.....	101
2.3.1. X-ray diffraction Results	101
2.3.2. DSC results	103
2.3.3. Optical and scanning electron microscopy	104
A.2.2.Conclusion	105
B- Influence of the PET fiber treatment	105
1. Fourier transform infrared (FTIR).....	105
2. Mechanical properties	106
2.1. Tensile strength.....	106
2.2. IZOD Impact strength.....	108
3. X-ray diffraction results	109
4. DSC Results.....	110
5. SEM observation	111
B.2. Conclusion	112
IV.1.2.2. Crosslinked PP/short polyamide fiber composite	112
2.1. DRA results.....	112
2.2. MFI measurement.....	114
2.3. Mechanical properties	115
2.4. X-ray diffraction results	117
2.5. DSC measurement	118
2.6. Optical and scanning electronic microscopy	119
IV.1.2.2.2. Conclusion.....	121
IV.1.2.3. Na-Montmorillonite– short polyamide Fiber/polypropylene hybrid composite	121
3.1. Fourier transform infrared spectroscopy (FTIR)	121
3.2. Wide-angle X-ray scattering (WAXS).....	125
3.3. DSC Analysis.....	129
3.4. Optical and scanning electron microscopy	132
3.5. Mechanical properties (Tenseil strength).....	134
3.5.1. Izod impact strength.....	136
IV.2.3.2. Conclusion	137
IV.1.2.Crosslinking of polybutene-1 (PB-1)	137
IV.1.2.1.rheological results	137
2.1.1. DRA results.....	137

2.1.2. MFI measurements	139
IV.1.2.2. Gel content	140
IV.1.2.3. Structural study of the modified PB-1	140
2.3.1. DSC measurements	140
a/- DSC measurement of the granules	140
b/ DSC measurement of the plates	143
2.3.2. X-ray diffraction Results (Plates)	145
2.3.3. FTIR Results	147
2.3.4. 2D WAXS result	149
2.3.5. DMA results	150
2.3.6. True Stress-Strain behavior	151
2.3.7. SEM observation	152
IV.1.2.4. Conclusion	153
IV.2.2. Crosslinked PB-1/hollow PET fiber/clay Hybrid composites	153
2.1. DRA measurement	153
2.2. MFI measurement	154
2.3. DSC Measurements	154
2.4. X-ray diffraction X	158
2.5. Mechanical properties	159
2.6. Impact strength	161
2.7. DMA results	162
2.8. SEM observations	164
IV.2.3. Conclusion	167
General conclusions	170
Recommendations	172

Introduction

Introduction

Currently, polymer composite materials have replaced traditional ones in a variety of applications and they found in the most diverse engineering fields such as aerospace, automotive, sports goods, shipping industries, construction, etc. Thus, the optimization of their performance and characteristics is a challenge worldwide. Until today, scientific researchers are still looking for new lightweight, recyclable, low cost and performing composite materials based on polymer matrices.

Owing to the low cost, easy processing and superior mechanical properties of short fiber reinforced polymer composites, these materials are rapidly gaining market share in structural applications. On the other hand, another class of composite materials has attracted both academic and industrial attention because they exhibit great improvement in properties at very low filler contents, for which at least one dimension of the used filler (particles) is in the nanometer range. Subsequently, short fiber/ nanoparticle hybridization has been developed as a promising method to toughen composite polymer through synergistic effects of the properties of short fibers and nanoparticles.

In the last two decade, some studies have investigated the potential improvement in properties and performances of hybridization fillers reinforced polymer matrix materials [1-5]. The obtained hybrid composite material is a multi-phase system, for that it is necessary to ensure the adhesion between fillers and polymer matrix through control of the interfacial interactions. Most fillers (mainly polar) have compatibility problems with polymer matrices (mostly non-polar), leading to low compatibility and poor composite performances. To overcome this problem, several techniques were suggested to increase fillers–matrix interactions: surface grafting, compatibilizer/coupling agent addition, or chemical/physical/thermal surface treatments [6, 7].

The present work deals with the preparation and characterization of hybrid composites based on polypropylene and polybutene-1 (as matrices) and short synthetic fiber (PET and PA) / clay (as reinforcing fillers).

Direct melt-compounding of the polymer matrix with the fillers is the most widely used method for preparation of the polymer composites materials [8-13].

In this context, the different composites investigated in this present work were prepared by direct melt mixing and to overcome the compatibility problem between fibers and polymers matrices, a modification of the matrices structure (polypropylene and polybutene-1) was carried out using reversibly crosslinking reaction method [14] , also the fibers surfaces were treated using stearic

acid. Additionally, (hollow recycled PET and polyamide short fibers) /clay (sodium montmorillonite) / (polypropylene and polybutene -1) matrices hybrid composites were prepared using the developed route based on reversibly crosslinking reactive extrusion [15].

Polypropylene/Na- MMT and polybutene-1/Na-MMT nanocomposites were prepared, in which an organic peroxide/ sulfur mixture and tetramethyl thiuram disulfide as an activator for sulfur were used to functionalize Na-MMT then short treated fibers were added to the nanocomposites matrices leading to the hybrid composites.

The present thesis contains 4 chapters, the first one presents the overview, objective and scope of the research work, then a brief background and literature review on fiber reinforced polymer nanocomposite (polymer/clay nanocomposite, short fiber/polymer composite and hybrid composite) is detailed. Next, the materials utilized and experimental methods used for preparation of samples and evaluation are presented in chapter 3. Chapter 4 deals with the results obtained and their discussions. Finally, a general conclusion and some recommendations for future work are presented.

References

- [1] Lin L, Lee J, Hong C, Yoo G, Advani S.G. Preparation and characterization of layered silicate/glass fiber/epoxy hybrid nanocomposites via vacuum-assisted resin transfer molding (VARTM) , *Compo Sci and Technol*, 66, 2116-2125, 2006.
- [2] Haque A, Shamsuzzoha M, Hussain F, Dean D. S2-Glass/Epoxy Polymer nanocomposites: Manufacturing, Structures, Thermal and Mechanical Properties , *J Compo Mat*, 37(20), 1821-37, 2003.
- [3] Subramaniyan Ak, Sun CT. Interlaminar Fracture Behavior of Nanoclay Reinforced Glass Fiber Composites, *J Compo Mat*, 1-12, 2008.
- [4] Akkapeddi MK. Glass fiber Reinforced Polyamide-6 Nanocomposites , *Polym Compo*, 21(4), 576-585, 2000.
- [5] Vijay PV, Ganga Rao HVS, Krishnaswamy V. Manufacturing, Durability and Bond Behavior of FRP Bars with Nanoclay, *Special Publication*, 230, 77-98, 2005.
- [6] El Mechtali FZ, Essabir H, Nekhlaoui S, et al. Mechanical and thermal properties of polypropylene reinforced with almond shell particles: impact of chemical treatments, *J Bionic Eng*, 12, 483–494, 2015.
- [7] Essabir H, Bensalah MO, Rodrigue D, et al. Biocomposites based on Argan nut shell and a polymer matrix: effect of filler content and coupling agent, *Carb Polym*, 143, 70–83. 2016.
- [8] Jakopin, S. Compounding of additives. In *Proceedings of 37th Annual SPE Technical Conference (ANTEC 1979 Conference)*, Society of Plastics Engineers, Inc.: Brookfield, CT, USA, pp. 987–99, 1979.
- [9] Ess JW, Hornsby PR. Twin-screw extrusion compounding of mineral filled thermoplastics: Dispersive mixing effects, *Plast. Rubb, Process Appl*, 8, 147–156, 1987.
- [10] Mülhaupt R, Stricker F. PP compounds as engineering materials, *Kunststoffe*, 87, 482–486, 1997
- [11] Yang F, Nelson G.L. Polymer/silica nanocomposites prepared via extrusion. *Polym. Adv. Technol.*, 17, 320–326, 2006.
- [12] Kalaitzidou K, Fukushima H, Drzal L.T. A new compounding method for exfoliated graphitepolypropylene nanocomposites with enhanced flexural properties and lower percolation threshold, *Compos. Sci. Technol*, 67, 2045–2051, 2007.
- [13] Jankong S, Srikulkit K. Preparation of polypropylene/hydrophobic silica nanocomposites, *J.Met. Mater. Miner*, 18, 143–146, 2008.
- [14] Bouhelal S, US patent,;N° 7,517,942, April 17, 2009.
- [15] Bouhelal S, US patent,;N° 7,550,526, June 23, 2009.

Chapter I Overview
Objective and scope

Overview, objective and scope of the thesis

I.1 Overview

Among the different types of composites materials, short synthetic fibers/clay reinforced polymer composites are the most attractive materials for structural applications. Their high mechanical properties-to-weight ratio and affordable price make them the material of choice.

Polymers are traditionally reinforced with synthetic or natural inorganic fillers in order to improve their properties and reduce their costs [1]. Commonly used fillers are clay, talc, mica [2, 3] and fibrous like glass, carbon fibers, aramid and jute fibers [4, 5]. In order to improve or modify certain thermomechanical properties of polymers for specific applications, short fibers reinforced polymers find large applications in engineering and consumer products [6]. Increasing the adhesion between fiber and polymer matrix is one of the most effective ways to improve the reinforcement by fibers [7]. Numerous studies have been reported concerning the enhancement of the interfacial interaction between the polymer/fibers phases [5-10].

Polymer modification with polar molecules (such as maleic anhydride, bismaleimide, etc.) is one of the known ways to enhance the interfacial adhesion between fibers and polymer matrix, especially for polyolefin matrices [10]. Polymer modification appears as an effective method to provide good interfacial adhesion, in contrast to fiber modification, which mostly involves solvent based processes. For instance, maleated PP (PP-g-MAH) has been extensively used as compatibilizer in various polyolefin composites [10, 11].

Nowadays we are witnessing increasing use of nanocomposites that can enhance selected properties of related polymers [14]. Nanocomposites based on clay and layered silicates have been widely investigated [15]. Montmorillonite (MMT) is one of the most used layered silicates. It is a 2:1 aluminosilicate, which is formed by two silica tetrahedral layers shared an octahedral sheet of aluminium or magnesium hydroxide [16, 17].

Moreover, production of hybrid polymer composites systems based on fibers and nanoclay has shown recent achievements and activities [18-22].

F. Eslami *et al.* [18] studied the effect of nanoclay/basalt fiber on the mechanical properties of polypropylene. The authors proved that the presence of the layered structure in basalt fiber / propylene composite improved the interfacial adhesion of nanoclay and the fiber, leading to the improvement of the mechanical properties of composite.

Somaiah.M *et al.* [19] analyzed the mechanical and morphological properties of nanoclay/S-glass fiber/polyester hybrid composite. They studied the effect of nanoclay content on S-glass

fiber/polyester composite. The obtained results showed that the incorporation of nanoclay had a significant effect on the mechanical behavior of composites.

In the research work conducted by Radouane B. *et al.* [20], the hybrid composite based on Alfa fibers/clay / polypropylene was studied, the authors presented the mechanical, thermal, and structural properties of the hybrid composites prepared. The samples were compounded by twin-screw extrusion and injection molding, constant overall filler loading was used (30 wt %) to study the effect of the relative filler loading. To improve the adhesion with the matrix, Alfa fibers surface were treated using an alkali solution, while the clay was purified and grinded to reduce particle size. The authors concluded that natural fiber-reinforced polymers combined with natural particulate fillers have advantages in terms of mechanical properties improvement. Figure I.1 shows the obtained Young's modulus which indicates an important increase as function of fillers loading. It could be concluded from this study that the combination of two fillers led to a synergistic effect of their properties.

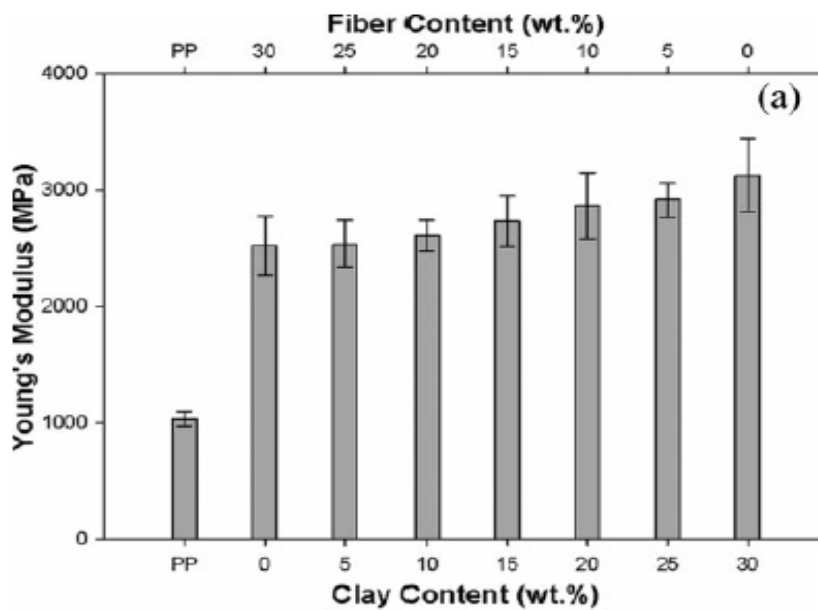


Figure I.1. Young's modulus of Alfa fibers/clay/ polypropylene hybrid composites [20].

Additionally, a research work realized by Normasmira. A *et al.* [21] studied the possibility of processing hybrid composites using nanoclay and glass fiber as reinforcement of polypropylene composite. The study entitled Polypropylene/glass fiber/nanoclay hybrid composites: morphological, thermal, dynamic mechanical and impact behaviors, in which PP/glass fiber (GF)

and PP/ nanoclay (NC) composites were prepared with different ratios of GF and clay powder. Compositions were physically premixed and then compounded using a twin-screw extruder. Dynamic mechanical analysis (see figure I.2) showed an increase in storage modulus indicating higher stiffness of the hybrid composites when compared to the glass fiber composites and the neat matrix. From the $\tan \delta$ curves, a strong influence of glass fiber and nanoclay content on the magnitude of $\tan \delta$ max value was observed.

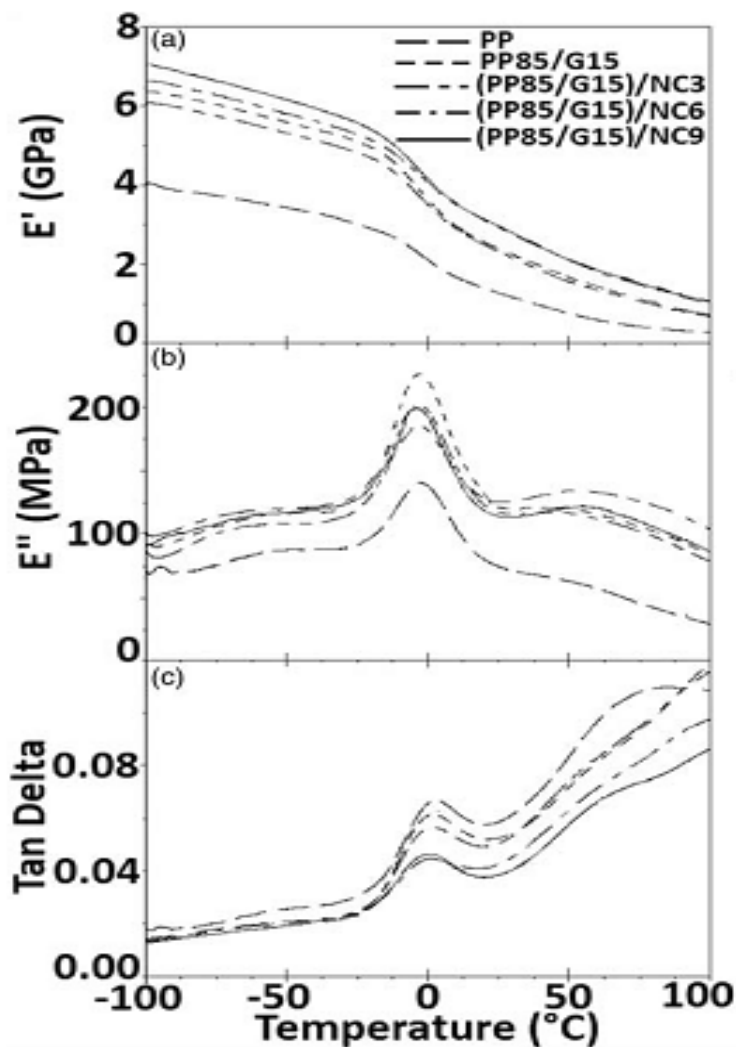


Figure I.2. Dynamic mechanical analysis results of Alfa fibers/clay/ polypropylene hybrid composites as a function of temperature [21]

Differential scanning calorimetric investigations showed that the incorporation of nanoclay into polypropylene/glass fiber composite shifted the melting temperature (T_m) to higher values. The degree of crystallinity (χ_c) was strongly influenced by the presence of the glass fiber and

nanoclay in the matrix. Impact test showed a reduction in the critical strain energy for hybrid composites with higher nanoclay loading.

Figure I.3. shows the SEM micrographs of the elaborated hybrid composite. The effect of the loading of clay on the adhesion of PP/glass fiber composites can be observed.

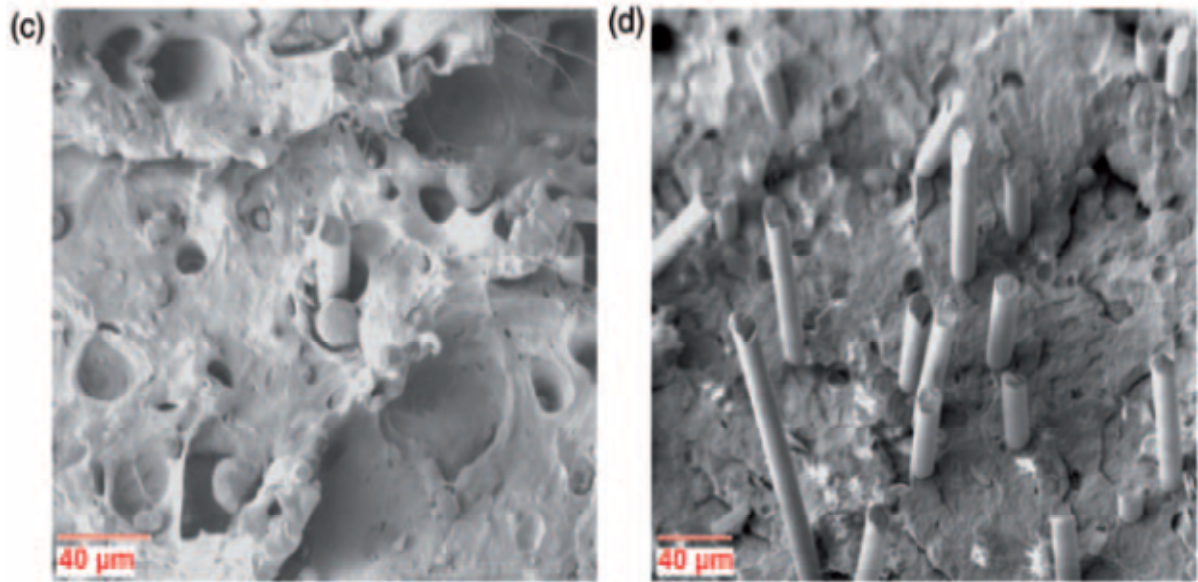


Figure I.3. SEM micrographs of impact fractured surfaces of: (c) (PP: G15)/NC6; and (d) (PP: G15)/NC9. SEM: scanning electron microscopy; PP: polypropylene; NC: nanoclay G: glass fibers [21].

Sinto. J *et al.* [22] conducted another study based on PP reinforced with short glass fibers /nanosilica and prepared by melt mixing. The weight of the glass fiber was varied while the nanosilica weight was at optimum level. Silica nanoparticles-glass fiber hybrid polypropylene composites were prepared by adding glass fiber into the nanosilica/polypropylene melt using melt mixing method in a Brabender.

The effect of glass fiber and glass fiber-nanosilica hybrid on mechanical properties of polypropylene is given in Figure I.4. From this figure it may be observed that the tensile strength of glass fiber/PP composite increase up to 40 wt. % fiber loading and then reaches a plateau height or slightly decrease. The glass fiber-nanosilica /PP hybrid composite shows superior property compared to glass fiber/PP reinforced composite. Tensile strength, tensile modulus, of glass fiber-nanosilica /PP hybrid composite are also found to increase up to 30 wt.% loading of glass fiber and then decrease. These results demonstrate that a small amount of nanosilica can

substantially enhance the mechanical strength of the PP composites and that glass fiber and nanosilica show synergistic reinforcement.

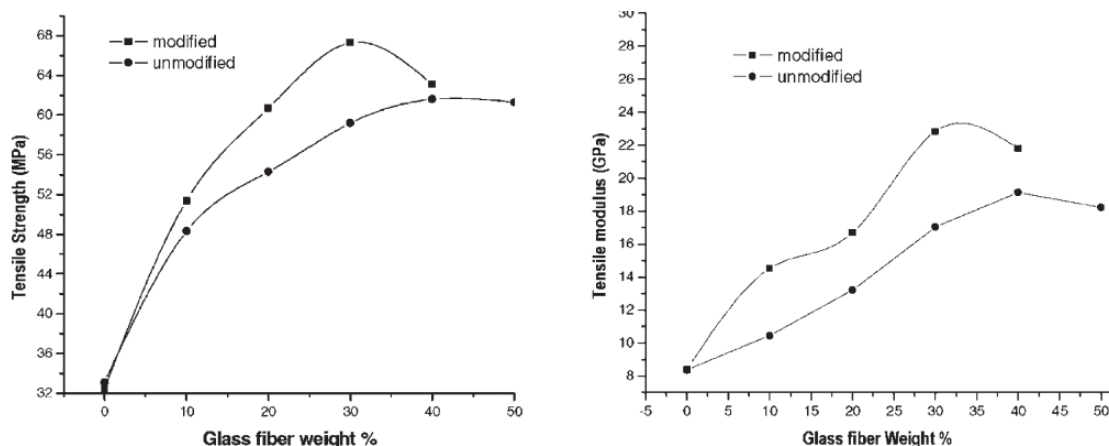


Figure I.4. Variation of tensile strength and tensile modulus for PP/glass fiber composites and PP/glass fiber/nanosilica hybrid composites
 Unmodified: short glass fiber/PP composite
 Modified: hybrid composite modified by nanosilica [22].

The results of dynamic mechanical analysis of the modified and unmodified PP/glass fiber composites and glass fiber/ nanosilica /PP hybrid composite are shown in Figure I.5. The storage modulus of PP is found to improve steadily with addition of short glass fiber. It was also found that the incorporation of glass fiber in the nanosilica/PP nanocomposite improved the storage modulus of PP. The presence of the two fillers in PP enhanced the stiffness of the PP matrix.

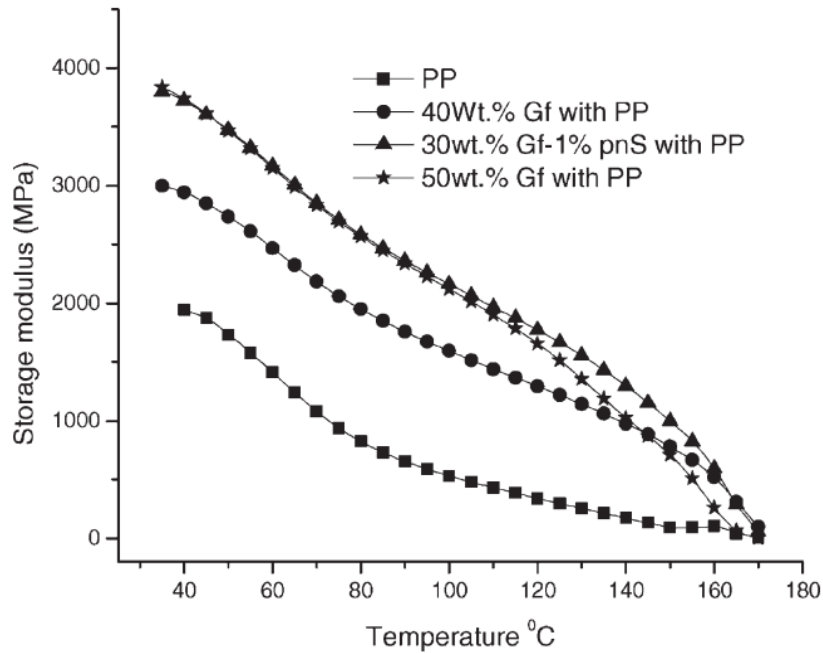


Figure I.5. Variation of storage modulus for PP/glass fiber composites and PP/glass fiber/nanosilica hybrid composite as a function of temperature [22].

Many research works related to polymer hybrid composites based on different classes of polymers were reported, For instance, a combination of short glass fibers and exfoliated layered silicate/polyamide 6 (PA6) was investigated, it was found that both fillers have a similar effect on the modulus. It was also shown that the combination of short glass fibers and 4 wt% layered silicate could add approximately 2 GPa to the tensile strength of the polyamide matrix, both in wet and dry conditions, independent of the fiber content [23].

Other studies focused on the preparation of carbon fiber / epoxy / montmorillonite hybrid composites [24, 25], several natural montmorillonite clays with different surfactants were used, mixed with and without the help of a solvent. The resulting nanocomposite matrices showed slightly increased storage modulus in the glassy state up to 20%, but the fracture toughness and the failure strain were somewhat reduced. The impregnation of the carbon fiber bundles with the nanocomposite resins was more difficult than with the unfilled epoxy resin, because of the much higher viscosity. No improvement in flexural strength of the fibre composites was found with nanofillers [26].

In addition, a research work at NASA [27] on nanocomposite matrix for fiber composites was done, in which firstly, layered silicate was exfoliated in a resin so-called PMR-15, which is a highly crosslinked at high-temperature resistant thermosetting polyimide with the addition of carbon fiber. It was shown that the exfoliated layered silicate reduced oxidation during ageing at high temperatures and reduced matrix cracking. The nanocomposite matrix was reported to increase the flexural strength, flexural modulus.

Table I.1, below summarizes the reported research works on fiber/nanofiller/polymer hybrid composites.

Table I.1. Reported works on fiber/nanofiller/polymer hybrid composites.

Matrix	Fillers	Ref
Polyamide (PA-6)	carbon fiber/glass fiber/nanoclay	[28]
Polyamide (PA-6)	chopped glass fibers/hectorite-type clays (nano size)	[29]
Polyamide (PA-6)	glass fiber/layered silicate	[30]
Polyamide 12 (PA-12)	Carbon nanotubes and nanofibers	[31]
Polyester	Nanoclay/glass fiber	[32]
Poly (vinyl ester)	Organoclay/glass fiber mats	[33]
High density polyethylene(HDPE)	nanoclay/rice husk	[34]
Ethylene-propylene copolymer	Nano clay/cellulose	[35]

I.2 Properties of the prepared materials

The prepared hybrid composites in this present thesis are characterized by different properties in terms of:

- **Recyclability**

The developed route based on reversibly crosslinking reactive extrusion, which is applied for both the crosslinking of polyolefins (PP, PB) and the development of polyolefins /clay nanocomposites [34, 35], is used in this research work. The reversible crosslinking of the used polyolefins allows the recyclability of their composites. We consider that our materials are recyclable because the preparation of recycled PP/f-Na-MMT nanocomposite has been successfully produced, in which the melt mixing cycle was repeated twice, so that after the PP/ f-Na-MMT nanocomposite is extruded the obtained blends were grinded, and re-fed in the

brabender chamber to reprocess the material with the addition of fibers. In addition, the different characterizations were carried out for the samples which could be molten again.

- **Light weighting**

The obtained materials are light in weight compared to the most composites regarding the low densities of the different materials used (hollow PET fiber, polyamide fiber, clay). In addition, the matrices used (Polypropylene and Polybutene -1) have the lowest densities among commodity plastics.

- **Practical and useful preparation method**

The different components were prepared by melt mixing, which is the simplest, most practical and economical method to be used in industry.

- **Simple treatment**

The functionalization of clay is a very useful and easy technique which is capable of exfoliating the raw clay without any restricted working conditions. On the other hand, the suggested treatment of the fiber surface is so simple, economical and efficient in the presence of the crosslinking agent as it has been found in this present work.

- **Synergistic properties of fillers effect**

Two different reinforcements in terms of size (nano, micro), morphology (fibers, layer), nature (inorganic, organic), and origin (synthetic or natural) were dispersed in the matrix with the aim of improving the properties of polyolefins/filler composites. The idea is to obtain a combination of properties of both fillers. For instance, the Young's modulus of the polymer (matrices) used increased when fibers were incorporated. Nevertheless, the resulting composites are less ductile with lower elongation at break. Meanwhile, the exfoliation of the clay in polypropylene matrix increased the elongation at break of composites.

- ❖ **Application**

Automotive components (bumpers, step assist) can be produced using composite and hybrid composites based on crosslinked polypropylene filled with PET fiber or polyamide fibers and clay.

Composite based on polybutene-1 matrix and reinforced with PET fiber and clay can be used to produce the subject pipes.

I.3 Limitations of the present research work

The major challenge in the developed clay/short fiber/polymer hybrid composite systems is the lack of even simple structure-property models. Progress in the engineering of hybrid composites has remained largely empirical. Thus, similarly, predicting the ultimate material limits or maximum performance for different classes of hybrid composites, is almost impossible.

As far as the hybrid class of fiber reinforced polymer-clay nanocomposites for structural applications is concerned, the research has not yet been done for mass utilization or field applications. Being a new class of materials, adequate data are not yet available to predict the long term performance of nanoclay composites, though durability is the corner stone of any design of infrastructure systems. This lack of experience gives rise to the need of further investigation on product durability issues.

Likewise, though the mechanical properties like stiffness and modulus are significantly enhanced, there are some properties like toughness and impact resistance which are slightly increased. Therefore, a careful consideration is required to determine the parameters causing this behavior.

In addition, it is still so difficult to control the couple interface/dispersion of two fillers in the same matrix and, regarding the functionalizing agent used (peroxide, sulfur and accelerator), it is still difficult to argue their type of reaction with polymer matrix and filler.

I.4 Objective

Development of hybrid composites based on polypropylene/clay/short synthetic fibers for the purpose of obtaining a lightweight, recyclable and performing material which achieves strong interfacial interactions between filler and matrix, fiber dispersion and clay layer exfoliation in matrices (polypropylene and polybutene-1) is the topic of this research work.

I.5 Scope

The scope of this research work includes:

- I. Modification of polymer (PP and PB) by chemical crosslinking.
- II. Chemical treatment of fibers and its effect on crosslinked (PP and PB)/short fibers (PET and polyamide fibers) composites.
- III. Recyclability of PP/clay noncomposite.

IV. Elaboration of recyclable nanocomposite/treated fibers hybrid composites.

V. Compatibility of two types of fibers (hollow PET and polyamide fibers) and PP/clay nanocomposites.

References

- [1] Pavlidou S, Papaspyrides CDA. Review on polymer-layered silicate nanocomposites, *Progr.Polym.Sci*, 33, 1119–1198, 2008.
- [2] Velasco JI, De Saja JA, Martinez AB. Crystallization behavior of polypropylene filled with surface-modified talc, *J. Appl. Polym. Sci*, 61,125-132, 1996.
- [3] Qiu W, Mai K, Zeng H. Effect of silane-grafted polypropylene on the mechanical properties and crystallization behavior of Talc/polypropylene composites, *J.Appl.Polym.Sci*, 77, 2974–2977,2000.
- [4] Moe MT, Kin L. Durability of bamboo-glass fiber reinforced polymer matrix hybrid composites, *Compos. Sci. Tech*, 63, 375–387, 2003.
- [5] Rana AK, Mandal A, Mitra BC, Jacobson R, Rowell R, Banerjee, AN. Short jute fiber-reinforced polypropylene composites: Effect of compatibilizer, *J.Appl. Polym. Sci*, 69,329–338, 1998.
- [6] Mallick P.K. *Fiber Reinforced Composites Materials. Manufacturing, and Design*, 3rd ed.; Publisher: Taylor & Francis group, Boca Raton, London, pp.5-26. 2007.
- [7] Jiang S, Li Q, Zhao Y, Wang J, Kang M. Effect of surface silanization of carbon fiber on mechanical properties of carbon fiber reinforced polyurethane composites, *Compos. Sci. Tech*, 110, 87–94, 2015.
- [8] John M, Bellman C, Anandjiwala R. Kenaf-polypropylene composites: Effect of amphiphilic coupling agent on surface properties of fibers and composites, *Carbohydr Polym*, 82, 549- 554, 2010.
- [9] Asumani O, Reid R, Paskaramoorthy R. Effect of alkali-silane treatment on the tensile and flexural properties of short fiber non-woven kenaf reinforced PP composites, *Compos Part A: Appl S*, 43, 1431-1440, 2012.
- [10] Chand N, Dwivedi U. Effect of coupling agent on abrasive wear behaviour of chopped jute fiber reinforced PP composites. *Wear*.vol .26, 1057-1063, 2006.
- [11] Prakash M, Pravin G. The Effect of Coupling Agent on the Properties of Short Non-Woven PET Microfiber Reinforced Polypropylene (PP) Composites, *IJCEBS*,vol. 2, 2320–4087, 2014.
- [12] Qiu W, Mai K, Zeng H. Effect of silane-grafted polypropylene on the mechanical properties and crystallization behavior of Talc/polypropylene composites, *J.Appl.Polym.Sci*,vol, 77, 2974–2977, 2000.
- [13] Moe MT, Kin L. Durability of bamboo-glass fiber reinforced polymer matrix hybrid composites. *Compos, Sci. Tech*, vol, 63, 375–387, 2003.
- [14] Chow WS, Mohd Ishak ZA. Mechanical, morphological and rheological properties of polyamide 6/organo-montmorillonite nanocomposites, *Express Polym Lett*, 1, 77-83, 2007.
- [15] Gorrasi G, Tortora M, Vittoria, V , Galli G, Chiellini E. Transport and mechanical properties of blends of poly(-caprolactone) and a modified montmorillonite–poly(-caprolactone) nanocomposite. *J Polym Sci Polym Phys*, 40, 11, 18–24, 2002.
- [16] Okada A, Usuki A. Twenty Years of Polymer-Clay Nanocomposites, *Macromol Mat Eng*, 291, 1449–1476. 2006.
- [17] Giannelis EP, *Polymer Layered Silicate Nanocomposites*, *Adv Mater*, 8, 29-35, 1996.
- [18] Eslami-Farsani R, Reza Khalili SM, Hedayatnasab Z, Soleimani N. Influence of thermal conditions on the tensile properties of basalt fiber reinforced polypropylene-clay nanocomposites. *Mater. Des*, 53, 540–549, 2014.
- [19] Somaiah C, Niranjana K MSR. Effect of Nanoclay on the Mechanical properties of Polyester and S-Glass Fiber (Al), *IJSAT*, 74, 35-42, 2015.
- [20] Radouane B, Charles A, Souad N, Hamid E, Mohammed OB, Denis R, Rachid B, Abou el kacem Q. Alfa fibers/clay hybrid composites based on polypropylene: Mechanical, thermal, and structural properties, *J Therm CompoMat*, 1–18, 2017.

- [21] Normasmira A, Rahman A, Yahya R, Lafia-Araga RA, Hornsby PR . Polypropylene/glass fiber/nanoclay hybrid composites: morphological, thermal, dynamic mechanical and impact behaviors, *J Reinforced Plastics and Composites*, 31(18) 1247–1257, 2012.
- [22] Sinto J, Suma K, Jude M, Abhilash G, George K. Modification of Polypropylene/Glass Fiber Composites with Nanosilica, *Macromol. Symp*, 277, 138–143, 2009.
- [23] Akkapeddi MK. Glass fiber reinforced polyamide-6 nanocomposites. *Polymer Composites*, 21, 576–585, 2000.
- [24] Chen CG, Curliss D. Resin matrix composites: Organoclay-aerospace epoxy nanocomposites, Part II. *Sampe Journal* , 37(5):11-18, 2001.
- [25] Rice BP, Chen CG, Cloos L, Curliss D. Carbon fiber composites: Organoclay aerospace epoxy nanocomposites, Part I. *Sampe Journal*;37(5):7-9, 2001.
- [26] Rice BP, Chen CG, Cloos L, Curliss D. Carbon fiber composites: Organoclay aerospace epoxy nanocomposites, Part I. *Sampe Journal*;37(5):7-9, 2001.
- [27] Campbell S, Scheiman D, Faile M, Papadopoulos D. PMR-15/ layered silicate nanocomposites for improved thermal stability and mechanical properties. 2002
- [28] Wu SH, Wang FY, Ma CCM, Chang WC. Mechanical, thermal and morphological properties of glass fiber and carbon fiber reinforced polyamide-6 and polyamide-6/clay nanocomposites, *Mater. Lett.*, 49, 327–333, 2001.
- [29] Akkapeddi MK. Glass fiber reinforced polyamide-6 nanocomposites. *Polym. Compos*, 21, 576–585, 2000.
- [30] Vlasveld DPN, Parlevliet PP, Bersee HEN, Picken SJ. Fibre-matrix adhesion in glass-fibre reinforced polyamide-6 silicate nanocomposites, *Compos. A Appl. Sci. Manuf.*, 36, 1–11, 2005.
- [31] Sandler JKW, Pegel S, Cadek M, Gojny F, Van ESM, Lohmar J, Blau W.J, Schulte K, Windle AH, Shaffer MSP, A comparative study of melt spun polyamide-12 fibres reinforced with carbon nanotubes and nanofibres, *Polymer*, 45, 2001–2015. 2004.
- [32] Jawahar P, Balasubramanian M. Influence of nanosize clay platelets on the mechanical properties of glass fiber reinforced polyester composites, *J. Nanosci. Nanotechnol.*, 6, 3973–3976, 2006.
- [33] Chandradass J, Kumar MR., Velmurugan R. Effect of nanoclay addition on vibration properties of glass fibre reinforced vinyl ester composites, *Mater. Lett.*, 61, 4385–4388, 2007.
- [34] Kord B. Nanofiller reinforcement effects on the thermal, dynamic mechanical, and morphological behavior of HDPE/rice husk flour composites, *BioResources*, 6, 1351–1358, 2011.
- [35] Singh AP, Pal KR. Novel hybrid of clay, cellulose, and thermoplastics. I. Preparation and characterization of composites of ethylene-propylene copolymer, *J. Appl. Polym. Sci.*, 104, 2672–2682, 2007.

Chapter II Fiber
reinforced polymer
nanocomposites

Fiber reinforced polymer nanocomposites

Introduction

Polymer nanocomposites are relatively a new class of composites, for which at least one dimensions of the dispersed particles, is in the nanometer range [1-4]. Short fiber reinforced thermoplastic polymer composites are another development within the field of composites [5].

In this work, the possibility of a combination of these two new types of composites is investigated. The concept of combining nanoclay and short fibers in the same matrix has been proposed. This combination consists of a three-phase composite, in which the main reinforcing phase are the short fibers and the matrix consists of a thermoplastic polymer nanocomposite.

To be able to understand the properties of this new type of composites, several aspects of the individual components need to be understood first. For this reason, the first chapter focuses on the polymer/clay nanocomposite material, followed by a review on fiber composites, and finally, a definition of the aspect of the three-phase composite will be presented.

Polymer thermoplastic nanocomposite matrices based on clay have been reviewed in this present research work, because the clay material is easily available and its intercalation chemistry has been studied for a long time [6].

The thermoplastic polymer matrices chosen in this present work are polypropylene (PP) and polybutene-1 (PB-1), because they are known from previous research that important nanocomposites can be produced with those polymers.

First, PP is a versatile polymer, which has attractive properties (recyclable, easy of processing, low cost...) that make it the polymer of choice for many applications. However, PP has some disadvantages such as low strength, high notch sensitivity and high flammability. For enhancing its mechanical properties (stiffness, strength and toughness...), fillers are usually added to PP, such as calcium carbonate, glass fiber [7], clay [8], PET fiber [9].

Secondly, Polybutene -1 (PB-1), is a polymer with excellent properties. It exhibits advantages over other polyolefins in toughness, flexibility, creep, stress cracking resistance, impact resistance, abrasion resistance and high-temperature resistance [10]. Polybutene-1 crystallizes in numerous polymorphs; however only tetragonal phase II and hexagonal phase I are of practical interest. Form II is kinetically favored when the polymer is crystallized from the melt. At room temperature, this form is metastable and it transforms to the hexagonal phase I.

The II-I transition brings about important structural changes, such as, density, crystallinity, hardness, rigidity, stiffness and tensile strength. The II-I phase transition requires several days to

be completed and this slow kinetics is the principal reason why the commercial development of polybutene-1 has been much delayed. A great deal of research has thus been oriented towards finding solutions to accelerate this transition [11-16].

II.1.Review on polymer–clay nanocomposites

Recent research work in the field of polymer/clay nanocomposites are reported in this review. Structure, properties, preparation methods are discussed in general.

II.1.1.Organic modification of clay

Clay is incompatible with most polymers due to its strong hydrophilic character. Thus, a direct melt mixing of both components is not realizable. To overcome this difficulty, as a first step, the surface of the clay has to be modified by using an organophilic agent, thus giving rise to the so-called organophilic clay or organoclay [17, 18].

Generally, this can be done by ion-exchange reactions with cationic surfactants, as shown in Figure II.1. Alkylammonium ions are mostly used, although other “onium” salts can be used, such as sulfonium and phosphonium. Alkylammonium or alkylphosphonium cations in the organosilicates lower the surface energy of the inorganic host and improve the wetting characteristics of the polymer matrix, and result in a larger interlayer spacing [1, 19-21]

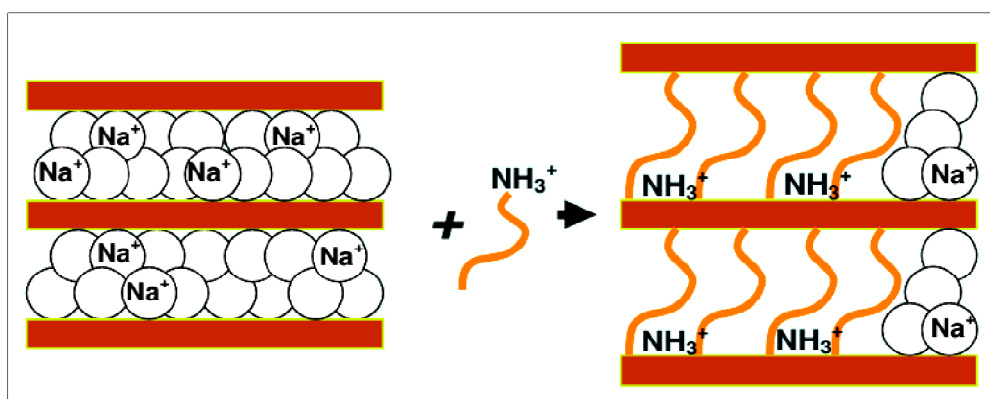


Figure II.1. Ion Exchange Reaction between Na-MMT and Alkyl Ammonium Molecules [19].

Figure II.2 depicts a schematic picture of an ion-exchange reaction. The inorganic, relatively small (sodium) ions are exchanged against more voluminous organic onium cations. This ion-exchange reaction has two consequences: the first one, the gap between the single sheets is

widened, enabling polymer chains to move in between them. The second one, the surface properties of each single sheet are changed from being hydrophilic to hydrophobic [2].

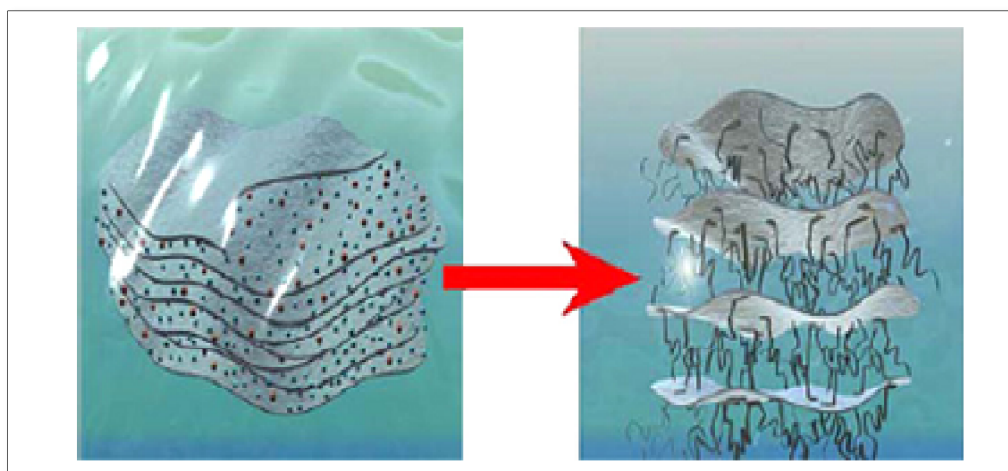


Figure II.2. Schematic picture of an ion-exchange reaction [2].

II.1.2. Nanocomposites formation

Numerous ways can be used to obtain exfoliated nanocomposite using clays and organoclays including in situ polymerization [4, 6, 22–28] and solution [29, 30] methods.

However, the greatest interest has involved melt processing [31– 32] because of several reasons: it is more economical, more flexible for formulation, easier and more practical method.

The main objective of the different preparation methods is to achieve a complete exfoliation of the clay platelets in the polymer matrix, i.e., separation of platelets from one another and dispersed individually in the polymer matrix. Nevertheless, this desired morphology is frequently not achieved and varying degrees of dispersion are more common.

The literature commonly refers to three types of morphology: immiscible (conventional or microcomposite), intercalated, and miscible or exfoliated. These are illustrated schematically in Figure II.3 along with example transmission electron microscopic (TEM) photographs and the expected wide angle X-ray patterns [29, 30, 33-37].

For the case called immiscible in figure II.3, the organoclay platelets exist in particles comprised of tactoids or aggregates of tactoids, i.e., no separation of platelets. Thus, the wide angle X-ray pattern of the polymer composite is expected to be the same as that obtained for the organoclay alone; there is no shifting of the X-ray d-spacing.

The second case is shown in figure II.3, it can be seen from the x-ray pattern that the peak of the organoclay shifts, indicating that the gallery has expanded, and it is usually assumed that polymer chains have entered or have been intercalated in the galleries.

For the last case (exfoliated organoclay), no wide angle X-ray peak is expected for the nanocomposite since there is no regular spacing of the platelets and the distances between platelets would be larger than what wide angle X-ray scattering can detect.

The early literature seemed to suggest that “intercalation” would be useful and perhaps a precursor to exfoliation. Subsequent research has suggested alternative ideas about how the exfoliation process may occur in melt processing and how the detail of the mixing equipment and conditions affects the state of dispersion achieved [38-41].

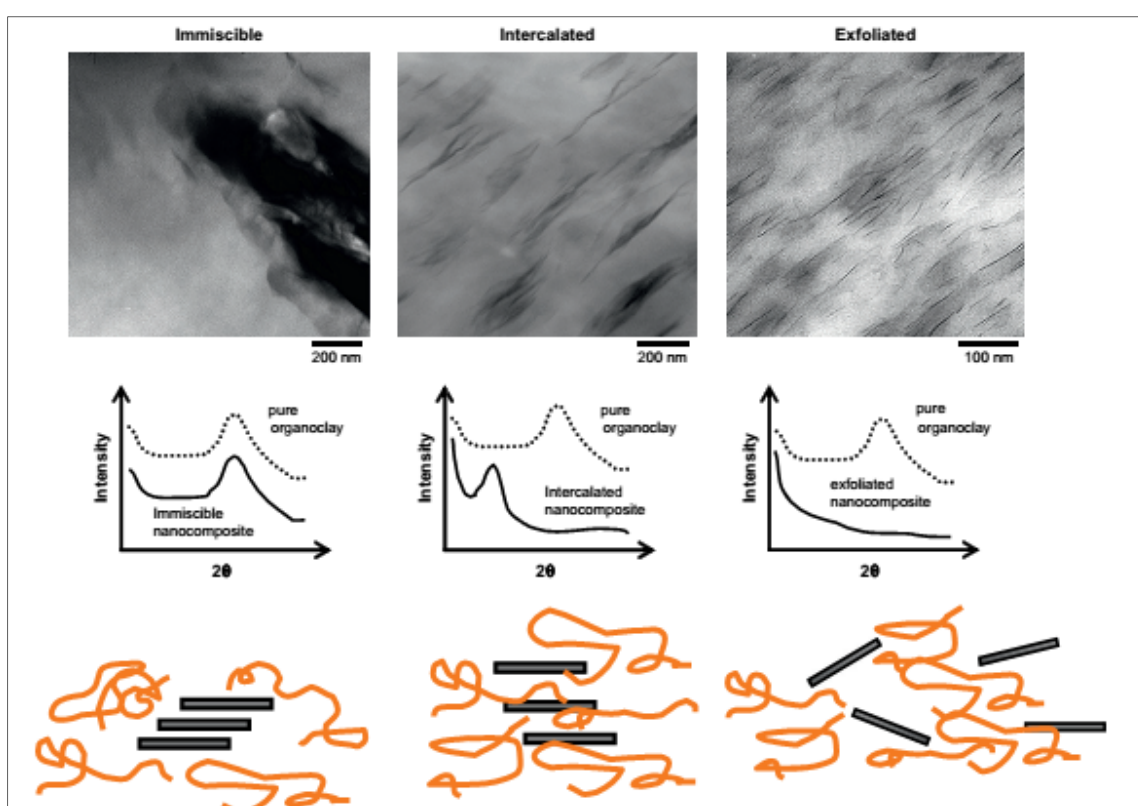


Figure II.3. Illustration of different states of dispersion of organoclays in polymers with corresponding WAXS patterns and TEM results [42].

There is a general agreement in the literature that exfoliated systems lead to better mechanical properties, particularly higher modulus, than intercalated nanocomposites [43]. Figure II.4 shows an ideal image how polymers surface active agents favor in a subsequent separation of the

platelets from each other forming finally the matrix material with homogeneously dispersed platelets.

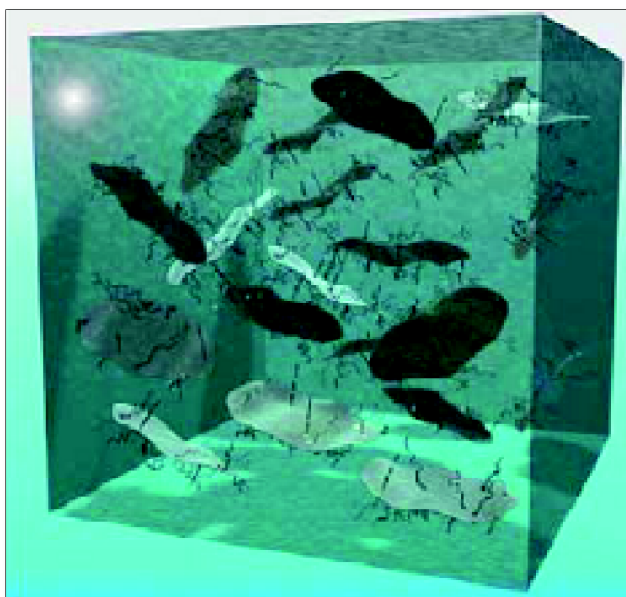


Figure II.4. Schematic image of a polymer-clay nanocomposite material with completely exfoliated (molecular dispersed) clay sheets within the polymer matrix material [2].

A key factor in the polymer–organoclay interactions is the affinity between the polymer matrix and the silicate surface [44 - 48]. For example, Nylon 6 appears to have good affinity for the silicate surface, perhaps by hydrogen bonding, and, as a result, very high levels of exfoliation can be achieved in this matrix provided the processing conditions and melt rheology are properly selected [49].

Even under the best of circumstances exfoliation of organoclays in neat polyolefins like PP, or PE, is not very good and far less than that observed in PA, PU, and some other polar polymers [50, 51]. It has been found that a small amount of a polyolefin that has been lightly grafted with maleic anhydride, w1% MA by weight is typical, can act as a very effective “compatibilizer” for dispersing the organoclay in the parent polyolefin [52, 53, 54, 55, 56–61].

This does not lead to the high level of exfoliation that can be achieved in polyamides, but this approach has allowed such nanocomposites to move forward in commercial applications, particularly in automotive parts [62].

II.1.3. Reversibly crosslinked isotactic polypropylene/clay Nanocomposites

In the present thesis, a new route based on reversibly crosslinking reactive extrusion is applied for the development of iPP/clay nanocomposites. Isotactic polypropylene (iPP)/clay nanocomposites, prepared by two different methods (i.e., conventional and in situ). In both methods, the clay only has to be separated from the rest of minerals or impurities by washing the raw material with distilled water followed by centrifugation. It is not necessary to perform any other chemical treatment or purification step.

In the so called conventional method, iPP, crosslinking agent (peroxide, sulfur and accelerator), potassium persulfate, and dried clay, were mixed in the solid state with appropriate weight % ratios, together with a few drops of a vegetable oil, which facilitates the powder dispersion within iPP granules. The resulting mixture was subsequently introduced into a single screw laboratory extruder.

In the in situ method, first acetone and then dried clay were added to the crosslinking agent. The acetone volume was, at least, equal to three times the volume of the solid phase (total solid $\frac{1}{4}$ crosslinking agent + clay). After a few minutes, two separate phases appeared. The solid phase contained the functionalized clay, while the liquid one contained acetone plus some impurities. After one day of mixing, the solid phase was ready to be blended with iPP in the desired amount. This way, the penetration and diffusion of the agents between the interlayer spaces of the clay was favored. It is to be noted that the main role played by the acetone at this step of the process is to protect the clay from the water absorption before the blending process takes place. The iPP and the functionalized clay have been processed in an extruder (a single screw laboratory extruder (Prolabo1989)).

From the results obtained of the both methods, it is found that the presence of clay significantly affected the value of long spacing in iPP, as well as the coherence length of lamellar stacks. FTIR and DMTA results proved the grafting of iPP chains onto the clay lamellae. Thus, in the FTIR study, two new sharp peaks appear at 923 and 769 cm^{-1} , that are associated to Si-O-C bonds created between the iPP chain and the tetrahedral structure of the inorganic Si-O-Si clay plane. The obtained DMTA results show the appearance of two Tg values in the composite with 4% of clay, clearly demonstrating that the clay is completely exfoliated. Similarly to the scheme represented in the article by D. Gournis and coworkers [63]. Figure II.5 shows the morphology of the hybrid structure in case of total exfoliation.

The most relevant point is that the reported technique of crosslinking by reactive extrusion gives rise to a partial or total exfoliation (4 wt % clay) with absence of intercalated structure.

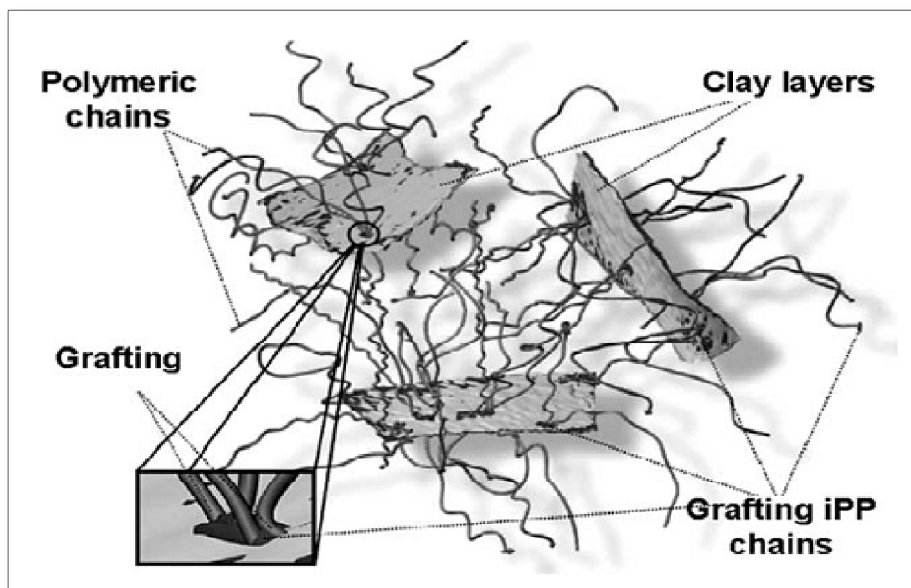


Figure II.5. Illustration of the hybrid structure of totally exfoliated iPP/clay nanocomposite material [63].

II.1.4. Polybutene-1/clay nanocomposites studies

Addition of layered silicate fillers, such as montmorillonite clay, to prepare nanocomposites is likely to improve the mechanical performance of polybutene-1 and to have a significant influence on the kinetics of the II/I transition [64–65]. Wanjale and Jog [64, 66] studied nanocomposites based on PB and organoclay prepared by melt-blending. They observed that formation of an intercalated clay network produced significant changes in the crystallization behavior and accelerated the II-I phase transition. Moreover, addition of clay nanofiller brought about a different response to stress during tensile straining [65].

The same approach was adopted in the research work conducted by Valerio Causin *et al.* [67], but the formulation was optimized with a maleated polypropylene-based compatibilizer that improved the polymer–clay interaction. It was found that the incorporation of the montmorillonite in the polybutene-1 showed a significant improvement of some physical and mechanical properties without exfoliation of the filler (see figure II.6), but only by a reduction in the size of the tactoids and by a slight intercalation. In addition, It may be noted that, as a consequence of the phase transition, with increasing time the intensity of the peaks typical of the hexagonal phase I (i.e. (110) at $9.98\ 2\theta$) increases, whereas the intensity of peaks related to the tetragonal phase II (i.e. (200) at $11.98\ 2\theta$) decreases. A quite striking difference in the polymorphism of the two samples (neat PB-1 and PB-1/clay nanocomposite) can be noted in the

diffractograms taken at the initial time. While in PB-1 almost 100% phase II is detected, in PB-1/clay a relevant amount of phase I co-exists with form II right after the cooling from the melt. Montmorillonite seems then to act as a nucleant for phase I. Noteworthy that, in the study of the crystallization of poly(1-butene) conducted by Kaszonyiova and co-workers [68] it was found that nucleating agents did not influence the polymorphism of polybutene-1.

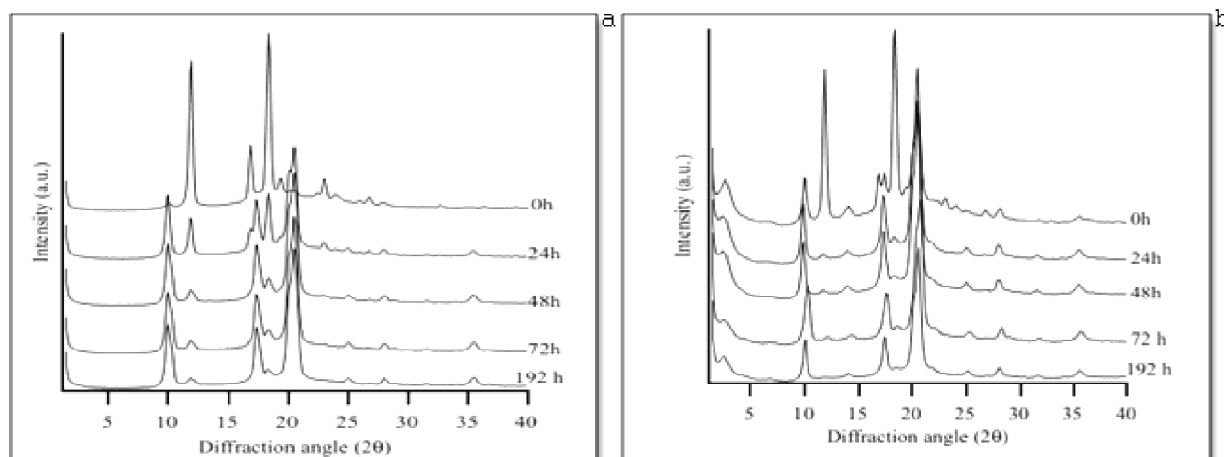


Figure II.6. WAXS patterns of **a-** neat PB-1 and **b-** PB-1/clay nanocomposite at different aging times[67]

Additionally, Santosh D *et al.* [69] studied the structure of PB-1/clay nanocomposite, the investigated composites were prepared by melt intercalation using an organically modified clay. Isothermal crystallization studies clearly indicated enhancement in crystallization rate by the clay. Also, the phase transformation studies revealed that the phase transformation from form II to form I at room temperature takes place faster in the case of PB-1 nanocomposites. It was found also that the PB-1 exhibited a well-defined spherulitic morphology compared to that of the PB-1/clay nanocomposite (see figure II.6), in which, the presence of clay layers seems to disturb the compactness of the spherulites.

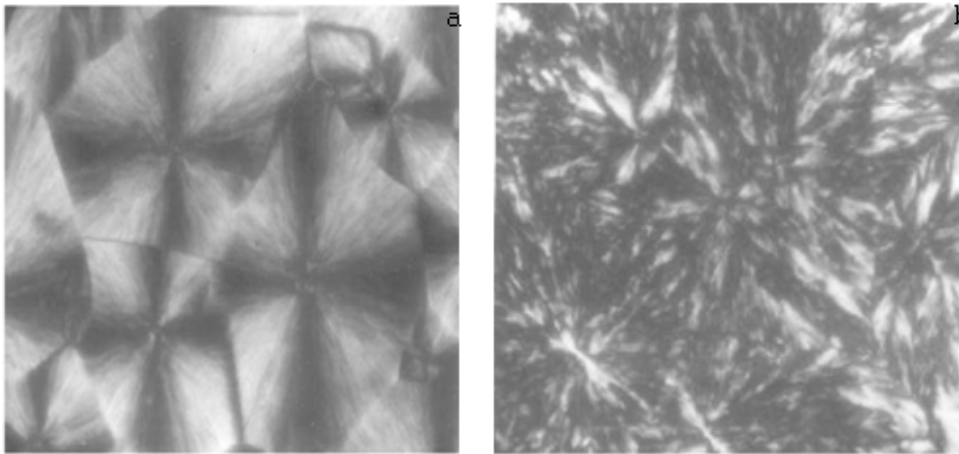


Figure II.7. Spherulitic morphology of **a-** neat PB-1 and **b-** PB-1/ clay nanocomposite [69].

According to their study also [69], the x-ray diffraction patterns revealed that there was no exfoliation without exfoliation of the clay layer in the PB-1 (see figure II.7). However, a slight intercalation of layer was shown.

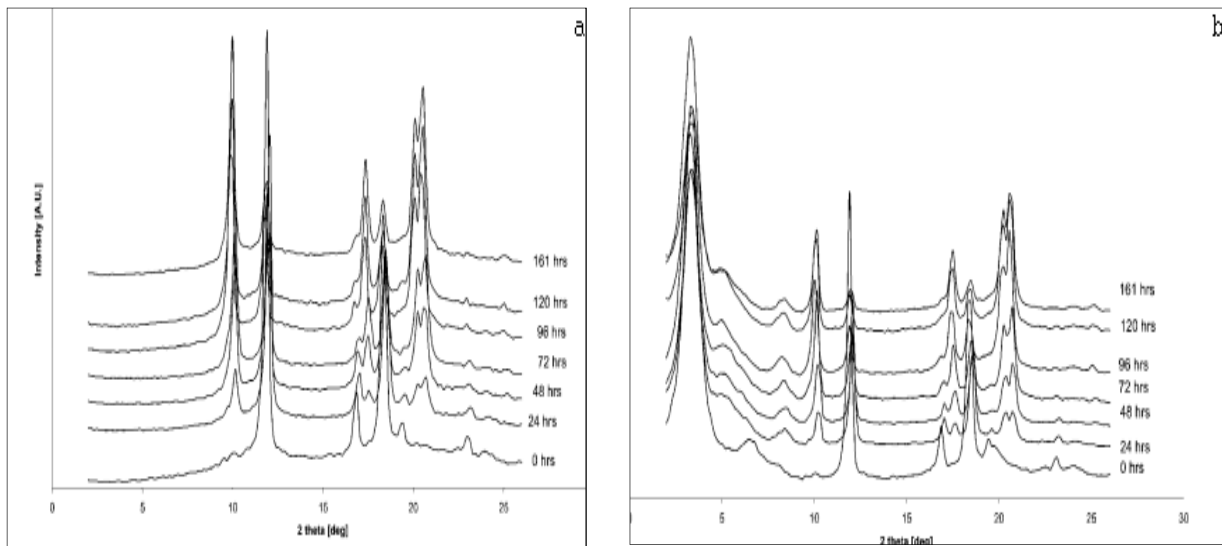


Figure II.8. X-ray diffraction patterns for phase transformation in **a-** pure PB-1 and **b-** PB-1/clay nanocomposite [69].

II.2. Review on fiber-reinforced polymer composite

Fiber-reinforced polymer composite materials consist of strength fibers embedded in a polymer matrix. The composite has a combination of properties of both fibers and matrix that cannot be achieved with either of the constituents alone. In general, fibers are the main load-carrying parts,

while the matrix function is to transfer stresses between the fibers, and to protecting the fiber surface from mechanical abrasion [70, 71].

Polymer composites have been used in several of industrial applications like construction, sporting goods, home appliances, furniture, etc. Over traditional materials, polymer composites present better mechanical properties, lighter weight, better dimensional stability, higher corrosion resistance, and flexibility [72]. However, a critical factor needed in determining the final properties of the composite material, particularly its mechanical properties [70, 73-75], which is the adhesion between fibers and matrix, especially in the case of nonpolar polyolefines matrices such as PE, PP...

The fiber-matrix adhesion is confined to the interphase between the two phases (fiber/matrix), where stress transfer occurs. It is located between the fiber and the matrix [76].

II.2.1. Methods for Adhesion Improvement

Matrix-reinforcement interphases have been the main objective of a lot of research work, particularly in thermoplastic composite polymers. Several methods of treatments are necessary to improve the interfacial adhesion [77].

Compatibility can be increased by either fiber surface treatment or modification of polymer matrix or both [70, 78].

II.2.1.1. Review on chemical coupling agents

There are many types of chemical coupling agents used in the elaboration of polypropylene composites. A coupling agent is defined as a substance that bonds the filler to the polymer matrix [70]. So, to achieve this property, the used coupling agent must have a unique structure that be able to interact with the filler, which is polar function in nature, at the same time it must be compatible with the nonpolar (case of polyolefines) or polar molecular chains of the polymer matrix.

Some of the oldest types of coupling agents used are organofunctional silanes. Silane coupling agents are molecules that have this unique structure. One end has a hydrolyzable group, which is an intermediate in the formation of silanol groups, for chemical bonding to the surface of the filler. On the other end, silanes have an organofunctional group that entangles with polymer molecular chains by physical-type interactions [79].

In general, the type of functional group needed depends on the chemical structure of the polymer matrix. Many types of organofunctional groups of silanes are available: epoxy, methacrylate, amine, mercapto, and vinyl.

Zulkifli investigated the effect of different types of silane and their concentrations in the interphase chemistry of the filler particle or fiber reinforcement in a polymer matrix and their influences on the fracture properties [80].

II.2.1.2. Matrix Modifications

One of the other known ways to enhance the adhesion between fiber and thermoplastic polymer is to modify the polymer by introducing polar functional groups to it. For instance, the introduction of polar functional groups to the polypropylene chains can improve compatibility with polar strengthening and achieve a homogenous dispersion of additives, fillers and reinforcements.

The polar groups are introduced by reactions with species that contain specific functional groups in their structures, such as ester, carboxylic acid or anhydride groups. This kind of strategy is used for PP/glass fiber composites in which a maleic anhydride grafted polypropylene (PP-g-MA) is added in order to react with the amine group of the silanized glass surface [81, 82].

A similar methodology was adopted by Di Benedetto *et al.* [83], who used oligomers of poly(sulfone) and poly(carbonate) to promote the fiber bonding with different matrices.

Lee *et al.* [89] evaluated the ability of hydroxylated polypropylene with aim of improving the adhesion between PP and glass laminates filler. They found evidence for chemical bonding between PP-OH and glass surfaces with a subsequent interfacial interaction.

Van den Overt *et al.* [84] investigated the influence of PP-g-MA on fatigue behavior in continuous glass-fiber-reinforced polypropylene composites. It was found that a slight improvement in fatigue strength was shown when the maleic anhydride (MA) was grafted to the PP (PP-g-MA).

Bogoeva-Gaceva *et al.* [85] also investigated the properties of a PP-g-MA as an adhesion promoter for glass fiber composites. They showed that the shear strength of single-fiber model composites with PP-g-MA-modified matrix was increased compared to that with neat PP. Noteworthy that melted PP is subject to a grafting reaction with maleic anhydride (MA) in the presence of peroxide initiators. The use of peroxide initiators together with the required processing conditions largely causes the degradation of PP; this fact makes PP-g-MA only attractive as an additive to blend with pure PP [86].

II.2.1.3. Fiber Treatment and Matrix Modifications

With view of obtaining a composite with a better adhesion and large interactions between fiber and matrix, several processing methods have been reported allowing both the treatment of fiber and modification of polymer matrix at the same time. Numerous studies have been performed in order to determine the effect of treatment of glass fiber and modification of polypropylene on the mechanical properties, by modifying the fibers with aminopropyl trieth oxysilane and grafted maleic anhydride to the PP. The obtained results showed that physical and chemical interactions established in the composite improved the interfacial strength and mechanical properties [87–94].

In the present work, the modification of the polyolefins used as matrices was carried out by reversibly crosslinking reaction. The reversibly crosslinking reaction allows the introduction of polar functional groups to the polyolefins polymers chains that can improve compatibility with fibers.

II.2.1.4. Review on crosslinking reaction

The modification of polyolefins is of great interest in recent years. Functional and engineered polyolefins are becoming more and more commercially important and expanding their applications because of their superior properties [95-100]. The most widely used modification method of polyolefins to be functionalized or engineered is the chemical modification. Indeed, the chemical modification of polymers is important because it leads to modify the bulk properties of polymers by grating, copolymerization or crosslinking. In addition, the surface chemistry and physics of polymers can be modified by several chemical surface modifying techniques like surface degradation, surface hydrolysis and catalytic-initiated graft copolymerization... [101].

Crosslinking is a widely method used for modification of polymer properties. The crosslinking process consists in a formation of a tri-dimensional network structure. Vulcanized rubbers and thermosetting resins can be cited as the common examples of crosslinked systems. Meanwhile, crosslinked polyolefins are of significant interest as well. Figure II.9, shows a schematic illustration of the possible network structure [102].

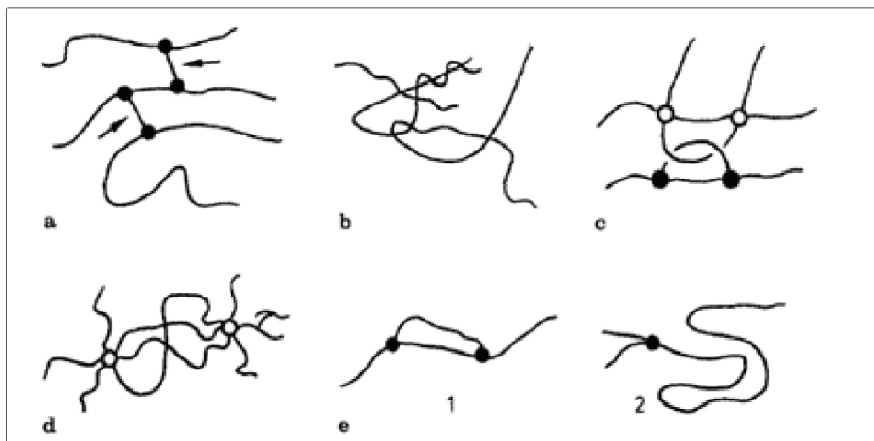


Figure II.9. Schematic illustration of network structure: a) for a polymer with tetrafunctional C-C bonds (arrows indicate crosslinks).

b) Physical entanglements of macromolecular chains

c) Three-functional branching points, *open circles* tetrafunctional branching points.

d) Crosslinked structure with polyfunctional branching points

e) Noneffective three functional branching points

1 -- of intramolecular cycles

2 -- at the chain ends

Various methods are used for initiation of polyolefin crosslinking. All processes used are based on a formation of polyalkene macroradicals in certain stage of the process. Common ways of crosslinking initiation consist in macroradicals formation via thermal decomposition of organic peroxides, high energy irradiation (gamma or electron beam), ultraviolet radiation in the presence of ultraviolet sensitizer, and grafting of silane groups onto the polyolefin backbone with subsequent crosslink formation via hydrolysis of the silanole moieties. Other procedures of initiating polyolefin crosslinking are rarely used or are only investigated in the laboratory [102,103].

Polyethylene could be crosslinked easily, in contrast, polypropylene and polybutene-1 have been considered until very recently as noncrosslinkable polymers. This is due to the fact that, if they are either irradiated, or subjected to the action of peroxide, the degradation process predominates

over the crosslinking mechanism particularly at the tertiary carbons of PP and PB-1. Nevertheless, new methods to achieve the crosslinking of the PP have been developed [104-106]. The crosslinking method used in the present work deals with a patented method that allows the preparation of reversibly crosslinked iPP. It is utilized for the preparation of both crosslinking PP and PB-1 materials.

This method, with slight variations, can be used to obtain crosslinked blends of PP and low or high density PE, copolymers of iPP or their blends with elastomers. In addition, the polymers to be crosslinked can be freshly prepared, recycled, restored, etc. The reversible crosslinking reaction is the newest method developed to obtain modified polyolefins.

The principle of the crosslinking mechanism is to create macroradicals and cause them to act immediately on sulfur before the reaction of termination occurs.

The crosslinking process takes place by a homolytic chemical reaction. The initiation reaction is originated by the peroxide decomposition, which gives rise to the formation of macroradicals with a very short lifetime. The sulfur atoms link the chains (coupling reaction) through the formation of a tridimensional, heat-resistant, network. The interchain bridges can be a sulfur atom, a polysulfide (S)_x, or a cyclic S-compound. Accelerators increase the sulfur activation rate. In this way, the macroradicals' formation and their coupling reaction with the sulfur takes place simultaneously, thus obtaining an optimum crosslinking degree for each formulation. The potassium persulfate increases the macroradicals' lifetime.

In crosslinked PP [107], the change in the molecular weight has a direct effect on the behavior of the material. The composition of the initiating system, especially the presence or absence of the coagent, is important in respect to the degradation-crosslinking ratio.

Generally, crosslinking leads to an increase in viscosity of polymer melt; however, with small initiator amount, when degradation and branching are dominant, a decrease in PP viscosity is common. Crosslinking was also investigated as an alternative for compatibilization in blends containing PP [108].

II.3. Clay/fiber/polymer hybrid composites

II.3.1. The concept of a three phase composite

The scales of microcomposites, such as fiber/polymer composite, and nanofiller/polymer nanocomposite are so different that the two can be combined. On the scale of the fibers the

nanofiller particles are still very small, for example, the thickness of an exfoliated silicate sheet is 10000 times smaller than the diameter of an average glass fiber (see figure II.10) [109].

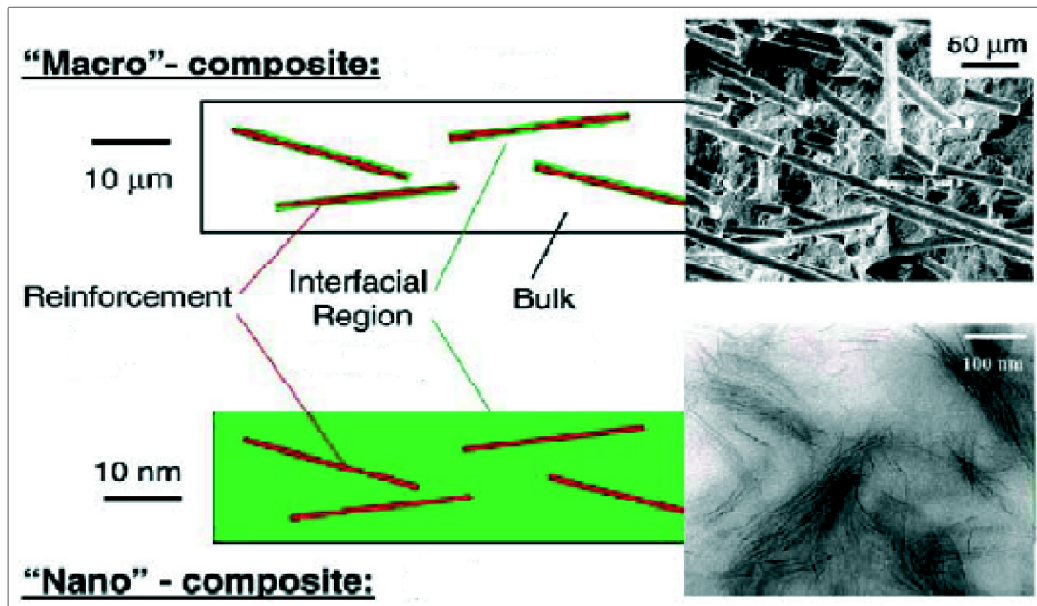


Figure II.10. Schematic comparison of macro-composite containing fibers to that of a nano-composite at the same volume fraction of filler [109].

Figure II.11 depicts the concept of a three phase composite model, the presented fibers are long, and the nanoparticles fit between them without reducing the fiber volume fraction. In this three phase composite it is not the goal to replace any of the fibers with nanofillers, the goal is still to use a high volume fraction of fibers as the main reinforcement [110].

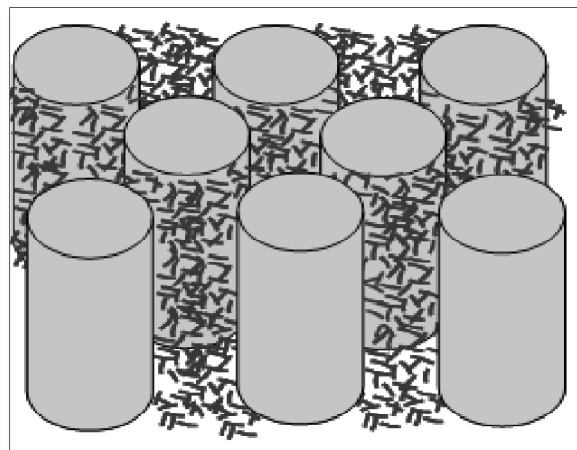


Figure II.11. Nano-particle reinforcement of the matrix in a fibre composite [110].

Figure II.12. Simulated progress of a nanoparticle/short fiber/polymer hybrid composite in which nanoparticles and short fibers are evenly distributed in the pure polymer matrix [111].

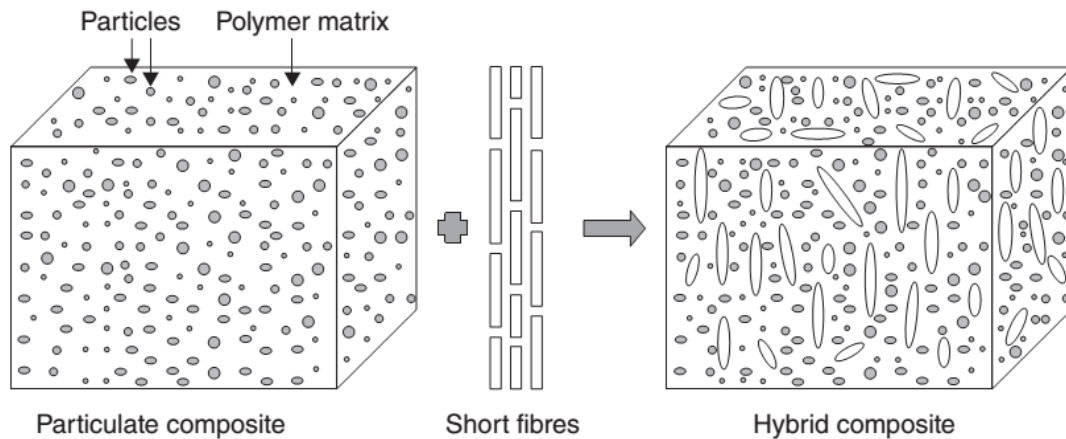


Figure II.12. Simulation of uniform distribution of short fibers in nanocomposite matrix [111].

The short fibers that are present in the matrix polymer are only intended to improve the matrix-dominated properties of the nanoparticle composite. The most important improvement that the nanocomposite matrix could provide is an increase in the compressive and flexural strength, modulus and the tensile strength of the fiber composite. The compressive strength, and therefore also the flexural strength of a short fiber composite, depends on the modulus of the matrix [110]. Because the modulus of the composite matrix increases with the addition of nanofillers, the compressive and flexural strength of the composite are expected to increase in such a three-phase composite.

References

- [1] Alexandre M, Dubois P. Polymer-layered silicate nanocomposites: preparation, properties and uses of a new class of materials. *MaterSciEng R*; 28:1–63, 2000.
- [2] Fischer H. Polymer nanocomposites: from fundamental research to specific applications. *Mater SciEng C*; 23:763–72, 2003.
- [3] Lagaly G. Introduction: from clay mineral-polymer interactions to clay mineral-polymer nanocomposites. *Appl Clay Sci*; 15:1–9, 1999.
- [4] Giannelis EP. Polymer layered silicate nanocomposites. *Adv Mater*; 8:29–35, 1996.
- [5] Fu SY, Mai YW. Science and engineering of short fibre reinforced polymer composites. Woodhead Publishing Limited and CRC Press LLC.: Boca Raton, 2009.
- [6] Gorrasi G, Tortora M, Vittoria V, Galli G, Chiellini E. Transport and mechanical properties of blends of poly(ϵ -caprolactone) and a modified montmorillonite-poly(ϵ -caprolactone) nanocomposite. *J Polym Sci Polym Phys*, 40:1118–24, 2002.
- [7] Karian Harutun G. Handbook of polypropylene and polypropylene composites, Marcei Dekker, Inc, Newyork p. 736.2003.
- [8] Pavlidou S, Papaspyrides CD. A review on polymer-layered silicate nanocomposites, *Progress in Polymer Science*, 33, 1119–1198, 2008.
- [9] Palova S, Sérgio H. Mechanical properties of polypropylene reinforced with recycled-pet fibres, *J.Mater.Process.Technol*, 520 143–144, 2003.
- [10] Jeremy PS. The processing, structure and properties of poly(1-butene) monofilaments, Phd Thesis, Loughborough University Institutional Repository, UK, 1987.
- [11] Azzurri F, Flores A, Alfonso GC, Balta Calleja FJ. Polymorphism of isotactic poly(1-butene) as revealed by microindentation hardness. Kinetics of the transformation. *Macromolecules*, 35: 9069–9073, 2002.
- [12] Azzurri F, Flores A, Alfonso GC, Sics I, Hsiao BS, Balta ´ Calleja FJ. *Polymer*, 44:1641.2003.
- [13] Nakafuku C, Miyaki T. Effect of pressure on the melting and crystallization behaviour of isotactic polybutene-1, *Polymer*, 24, 141–148, 1983.
- [14] Boor J.J, Mitchell J.C. Kinetics of crystallization and a crystal-crystal transition in poly-1-butene. *J. Polym. Sci.,A1*, 59–66, 1963.
- [15] Alfonso G, Azzurri F, Castellano M. Analysis of calorimetric curves detected during the polymorphic transformation of isotactic-p-1, *J Therm Anal Calorim*, 66, 197-207, 2001.
- [16] Kaszonyiova M, Rybnikar F, Geil PH. Crystallization and transformation of polybutene-1, *J. Macromol. Sci. Phys.*, B43: 1095, 2004.
- [17] Kawasumi M, Hasegawa N, Kato M, Usuki A, Okada A. Preparation and mechanical properties of polypropylene-clay hybrids, *Macromolecules*, 30, 6333–6338, 1997.
- [18] Kato M, Usuki A, Okada A. Synthesis of polypropylene oligomer-clay intercalation compounds, *J App Polym Sc*, 66, 1781–1785, 1997.
- [19] Manias E, Touny A, Wu L, Strawhecker K, Lu B, Chung TC. Polypropylene/montmorillonite nanocomposites. Review of the synthetic routes and materials properties. *Chem Mater*, 13:3516–23, 2001.

- [20] Zanetti M, Lomakin S, Camino G. Polymer layered silicate nanocomposites. *Macromol Mater Eng*, 279:1–9, 2000.
- [21] Kornmann X, Lindberg H, Berglund LA. Synthesis of epoxy–clay nanocomposites: influence of the nature of the clay on structure. *Polymer*, 42:1303–10, 2001.
- [22] Loo LS, Gleason KK. Fourier transforms infrared investigation of the deformation behavior of montmorillonite in nylon 6/nanoclay nanocomposite. *Macromolecules*, 36:2587–90, 2003.
- [23] Wu HD, Tseng CR, Chang FC. Chain conformation and crystallization behavior of the syndiotactic polystyrene nanocomposites studied using Fourier transform infrared analysis. *Macromolecules*, 34:2992–9, 2001.
- [24] Fomes TD, Paul DR. Modelling properties of nylon 6/clay nanocomposites using composite theories, *Polymer*; 44:4993– 5013, 2003.
- [25] Kim SW, Jo WH, Lee MS, Ko MB, Jho JY. Preparation of clay– dispersed poly(styrene co-acrylonitrile) nanocomposites using poly(ϵ -caprolactone) as a compatibilizer. *Polymer*, 42: 9837–42, 2001.
- [26] Vaia RA, Giannelis EP. Lattice of polymer melt intercalation in organically modified layered silicates. *Macromolecules*, 30:7990–9, 1997.
- [27] Arada P, Ruiz-Hitzky E. Polymer–salt intercalation complexes in layer silicates. *Adv Mater*, 2:545–7, 1990.
- [28] Arada P, Ruiz-Hitzky E. Poly (ethylene oxide)–silicate intercalation materials. *Chem Mater*; 4:1395–403, 1992.
- [29] Fomes TD, Yoon PJ, Hunter DL, Keskkula H, Paul DR. Effect of organoclay structure on nylon 6 nanocomposite morphology and properties. *Polymer*; 43:5915–33, 2002.
- [30] Wu S-H, Wang F-Y, Ma C-CM, Chang W-C, Kuo C-T, Kuan H-C, et al. Mechanical, thermal and morphological properties of glass fiber and carbon fiber reinforced polyamide 6 and polyamide 6/clay nanocomposites. *Mater Lett*, 49:327–33, 2001.
- [31] Theng BKG. *Formation and properties of clay–polymer complexes*. Amsterdam: Elsevier; 1979.
- [32] Suh D, Lim Y, Park O. The property and formation mechanism of unsaturated polyester–layered silicate nanocomposite depending on the fabrication methods. *Polymer*, 41, 8557–8563, 2000.
- [33] Yu ZZ, Yang M, Zhang Q, Zhao C, Mai YW. Dispersion and distribution of organically modified montmorillonite in nylon-66 matrix. *J Polym Sci Polym Phys*, 41:1234–43, 2003.
- [34] Wang KH, Choi MH, Koo CM, Choi CM, Chung IJ. Synthesis and characterization of maleated polyethylene/clay nanocomposites. *Polymer*, 42:9819–26, 2001.
- [35] Ray SS, Bousima M. Biodegradable polymers and their layered silicate nanocomposites: in greening the 21st century materials world. *Prog Mater Sci*, 50:962–1079, 2005.
- [36] Dennis HR, Hunter DL, Chang D, Kim S, White JL, Cho JW, et al. Effect of melt processing conditions on the extent of exfoliation in organoclay-based nanocomposites. *Polymer*, 42:9513– 22, 2001.
- [37] Krikorian V, Pochan D. Poly(l-lactide acid)/layered silicate nanocomposite: fabrication,

- characterization, and properties. *Chem Mater*, 15:4317–24, 2003.
- [38] Krishnamoorti R, Giannelis EP. Rheology of end-tethered polymer layered silicate nanocomposites. *Macromolecules*, 30:4097–102, 1997.
- [39] Tseng C-R, Wu J-Y, Lee H-Y, Chang F-C. Preparation and crystallization behavior of syndiotactic polystyrene–clay nanocomposites. *Polymer*, 42:10063–70, 2001.
- [40] Chang J-H, Uk-An Y, Sur GS. Poly(lactic acid) nanocomposites with various organoclays. I. thermomechanical properties, morphology, and gas permeability. *J Polym Sci Polym Phys*, 41:94–103, 2003.
- [42] Paul DR, Robeson LM, *Polymer nanotechnology: Nanocomposites*. *Polymer* 49 3187–3204, 2008.
- [43] Jordan J, Jacobb K, Tannenbaumc R, Sharafb M, Jasiukd I. Experimental trends in polymer nanocomposites. *Materials Science and Engineering A* 393:1–11, 2005.
- [44] Yano K, Usuki A, Okada A, Kurauchi T, Kamigaito O. Synthesis and properties of polyimide/clay hybrid. *J Polym Sci Polym Chem*, 31:2493–8, 1993.
- [45] Kojima Y, Usuki A, Kawasumi M, Okada A, Kurauchi T, Kamigaito O. Synthesis of nylon-6 hybrid by montmorillonite intercalated with ϵ -caprolactam. *J Polym Sci Polym Chem*; 31:983–6, 1993.
- [46] Doh JG, Cho I. Synthesis and properties of polystyrene– organoammonium montmorillonite hybrid. *Polym Bull*; 41:511–8, 1998.
- [47] Wang Z, Pinnavaia TJ. Nanolayer reinforcement of elastomeric polyurethane. *Chem Mater*, 10:3769–71, 1998.
- [48] Yao KJ, Song M, Hourston DJ, Luo DZ. Polymer/layered clay nanocomposites: 2 polyurethane nanocomposites. *Polymer*, 43:1017–20, 2002.
- [49] Pantoustier N, Lepoittevin B, Alexandre M, Kubies D, Calberg C, Jerome R. Biodegradable polyester layered silicate nanocomposites based on poly(ϵ -caprolactone). *Polym Eng Sci*, 42:1928–37, 2002.
- [50] Reichert P, Kressler J, Thomann R, Mulhaupt R, Stoppelmann G. Nanocomposites based on a synthetic layer silicate and polyamide- 12. *Acta Polym*, 49:116–23, 1998.
- [51] Hsu SLC, Chang KC. Synthesis and properties of polybenzoxazole–clay nanocomposites. *Polymer*, 43:4097–101, 2002.
- [52] Bergman JS, Chen H, Giannelis EP, Thomas MG, Coates GW. Synthesis and characterization of polyolefin–silicate nanocomposites: a catalyst intercalation and in situ polymerization approach. *J Chem Soc Chem Commun*, 21:2179–80, 1999.
- [53] Ke YC, Long CF, Qi ZN. Crystallization, properties, and crystal and nanoscale morphology of PET–clay nanocomposites. *J Appl Polym Sci*, 71:1139–46, 1999.
- [54] Messersmith PB, Giannelis EP. Polymer–layered silicate nanocomposites: in-situ intercalative polymerization of ϵ -caprolactone in layered silicates. *Chem Mater*, 5:1064–6, 1993.
- [55] Messersmith PB, Giannelis EP. Synthesis and barrier properties of poly(ϵ -caprolactone)–layered silicate nanocomposites. *J Polym Sci Polym Chem*, 33:1047–57, 1995.
- [56] Zilg C, Thomann R, Mulhaupt R, Finter J. Polyurethane nanocomposites containing laminated anisotropic nanoparticles derived from organophilic layered silicates. *Adv*

- Mater, 11, 49–52, 1999.
- [57] Berta M, Lindsay C, Pans G, Camino G. Effect of chemical structure on combustion and thermal behaviour of polyurethane elastomer layered silicate nanocomposites. *Polym Degrad Stabil*, 91, 1179–1191, 2006.
- [58] Gao X, Lee J, Widya T, Macosko C. Polyurethane/clay nanocomposites foams: processing, structure and properties. *Polymer*, 46:775–83, 2005.
- [59] Liu X, Wu Q. Polyamide 66/clay nanocomposites via melt intercalation. *Macromol Mater Eng*, 287:180–6, 2002.
- [60] Phang IY, Liu T, Mohamed A, Pramoda KP, Chen L, Shen L. Morphology, thermal and mechanical properties of nylon 12/organoclay nanocomposites prepared by melt compounding. *Polym Int*, 54:456–64, 2005.
- [61] Davis CH, Mathias LJ, Gilman JW, Schiraldi DA, Shields JR, Trulove P. Effects of melt-processing conditions on the quality of poly(ethylene terephthalate) montmorillonite clay nanocomposites. *J Polym Sci Polym Phys*, 40:2661–6, 2002.
- [62] Okamoto M, Morita S, Kotaka T. Dispersed structure and ionic conductivity of smectic clay/polymer nanocomposites. *Polymer*, 42:2685–8, 2001.
- [63] Gournis D, Karakassides MA, Baka T, Boukos N. Catalytic synthesis of carbon nanotubes on clay minerals, *Carbon* 40, 2641–2646, 2002.
- [64] Wanjale SD, Jog JP. Effect of modified layered silicates and compatibilizer on properties of PMP/clay nanocomposites. *J Appl Polym Sci*, 90(12), 3233, 2003.
- [65] Nathani, H, Dasari, A, Misra, RDK. On the reduced susceptibility to stress whitening behavior of melt intercalated polybutene-clay nanocomposites during tensile straining. *Acta Mater*, 52: 3217–3227, 2004.
- [66] Wanjale SD, Jog JP. Poly (1-butene)/Clay Nanocomposites: Preparation and Properties. *Journal of Polymer Science: Part B: Polymer Physics*, 41, 1014–1021, 2003.
- [67] Valerio C , Carla M , Antonio M , Giuseppe F , Gulnaz I , Fabiana F. Morphology, structure and properties of a poly(1 butene)/montmorillonite nanocomposite. *Polymer* 47 4773–4780, 2006.
- [68] Kaszonyiova M, Rybnikar F, Geil PH. *J Macromol Sci Phys* 2004; B43,1095.
- [69] Wanjale SD , Jog JP. Poly (1-Butene)/ Clay Nanocomposites: A crystallization study. *Journal of macromolecular science Part B- Physics* .Vol. B42, No. 6, pp. 1141–1152, 2003.
- [70] Mallick, P.K. *Fiber Reinforced Composites. Materials, Manufacturing and Design*; Marcel Dekker Inc.: New York, NY, USA, 1997.
- [71] Hull, D.; Clyne, T.W. *An Introduction to Composite Materials*, 2nd ed.; Cambridge University Press: Cambridge, UK, 1996.
- [72] Folkes MJ. *Multicomponent Polymer Systems*; Miles, I.S., Rostami, S., Eds.; Longman Scientific and Technical: Essex, UK, Chapter 8, 1992.
- [73] Yosoyima R, Morimoto K, Susuki T, Nakajima A. *Adhesion and Bonding in Composites*; Marcel Dekker Inc.: New York, NY, USA, 1990.
- [74] Yosoyima R, Morimoto K, Suzuki T. The reaction of glass fiber with diisocyanate and its application. *J. Appl. Polym. Sci.*, 29, 671–679, 1984.
- [75] Pukánszky B, Maurer-Frans HJ, Boode JW. Impact testing of polypropylene blends and

- composites. *Polym. Eng. Sci.*, 35, 1962–1971, 1995.
- [76] Utracki, L. *Polymer Blends Handbook*; Kluwer Academic Publishers: Dordrecht, The Netherlands, 2002.
- [77] Gatenholm P, Felix J. Methods for improvement of properties of cellulose-polymer composites. In *Wood Fiber/Polymer Composites: Fundamental Concepts, Process, and Material Options*; Forest Product Society: Madison, WI, USA, 3, pp. 57–62. 1993.
- [78] Monte SJ. *Functional Fillers for Plastics*; Xantos, M., Ed.; Wiley-VCH: Hoboken, NJ, USA, pp. 85–102, 2005.
- [79] Plueddemann EP. *Silane Coupling Agents*; Plenum: New York, NY, USA, 1982.
- [80] Zulkifli R. Surface fracture analysis of glass fibre reinforced epoxy composites treated with different type of coupling agent. *Eur. J. Sci. Res.*, 29, 55–65, 2009.
- [81] Rijdsdijk HA, Contant M, Peijs J.M. Continuous-glass-fibre-reinforced polypropylene composites I. Influence of maleic-anhydride modified polypropylene on mechanical properties. *Compos. Sci. Technol.*, 48, 161–172, 1993.
- [82] Mäder E, Jacobasch HJ, Grundke K, Gietzelt T. Influence of an optimized interphase on the properties of polypropylene/glass fibre composites. *Compos. Part A Appl. Sci. Manuf*, 27, 907–912, 1996.
- [83] DigBenedetto AT. Measurement of the thermomechanical stability of interphases by the embedded single fiber test. *Compos. Sci. Technol.*, 42, 103–123, 1991.
- [84] Lee SH, Li CL, Chung T. Evaluation of poly(propylene-co-hexen-6-ol) as an interfacial agent in pp/glass laminates. *Polymer*, 35, 2979–2988, 1994.
- [85] Bogoeva-Gaceva G, Grozdanov A. Crystallization of isotactic polypropylene: The effect of fiber surface. *J. Serb. Chem. Soc.*, 71, 483–499, 2006.
- [86] Bortolon V, Savadori T. Process for modifying Polypropylene with Maleic Anhydride. Patent NR 6,437,049, 2002.
- [87] Arbelaiz A, Fernandez B, Ramos JA, Retegi A, Llano-Ponte R, Mondragón I. Mechanical properties of short flax fibre bundle/polypropylene composites: Influence of matrix/fibre modification, fibre content, water uptake and recycling. *Composites Sci. Technol.*, 65, 1582–1592, 2005.
- [88] Van den Oevert M, Peijs T. Continuous-glass-fibre-reinforced polypropylene composites II. Influence of maleic-anhydride modified polypropylene on fatigue behaviour. *Compos. Part A*, 29, 227–239, 1998.
- [89] Rowell R, Sanadi AR, Caulfield DF, Jacobson RE. Utilization of natural fibers in plastic composites: Problems and opportunities. In *Lignocellulosic-Plastics Composites*; Leao, A.L., Carvalho, F.X., Frollini, E., Eds.; USP and UNESP: Sao Paulo, Brazil, pp. 23–51, 1997.
- [90] Qiu W, Zhang F, Endo T, Hirotsu T. Milling-induced esterification between cellulose and maleated polypropylene. *J. Appl. Polym. Sci.*, 91, 1703–1709, 2004.
- [91] Keener TJ, Stuart RK, Brown TK. Maleated coupling agents for natural fibre composites. *Compos. Part A*, 35, 357–362, 2004.
- [92] Kamaker AC, Youngquist JA. Injection molding of polypropylene reinforced with short jute fibres. *J. Appl. Polym. Sci.*, 62, 1147–1151, 1996.

- [93] Albano C, Ichazo M, Gonzalez J, Delgado M, Poleo R. Effects of filler treatments on the mechanical and morphological behavior of PP + wood flour and PP + sisal fiber. *Mater. Res. Innov.*, 4, 284–293, 2001.
- [94] Vallejos, M.E. Aprovechamiento de Integral del Cannabis Sativa Como Material de Refuerzo/Carga del Polipropileno. Master Thesis, Universidad de Girona, Girona, Spain, 2006.
- [95] Ceresa RJ. *The Chemical Modification of Polymers*, Academic Press, New York, 1978.
- [96] Hurtrez G, Wilson D J, and Reiss G, *NATO ASZ Ser., Ser. E*, 89(Polym. Blend Mixtures), 149, 1985.
- [97] Polikarpov and AP, Krul LP, *Dokl. Akad. Nauk BSSR*, 34(7), 627, 1990.
- [98] Xu G, Lin S, *Polym. Materials Sci. and Eng.*, 70, 15 1, 1993.
- [99] Mukherjee AK, Gupta BD, *Macromol. Sci. -Chem.*, A19 (7), 1069, 1983.
- [100] Hasan A, Pandey LM, *Polymer-Plastics Technol. Eng.* 2015, 54, 1358.
- [101] Guangxue Xu, Shangan Lin, *Functional Modification of Polypropylene*, *Journal of Macromolecular Science, Part C*, 34:4, 555-606, 2006.
- [102] Lazar M, Rado R, Rychly J. *Crosslinking of polyolefins*, *Adv. Polymer Sci.*, 95, 149-197, 1990.
- [103] Ivan CH, *Crosslinking of polypropylene* pp.128. in *Polypropylene*, edited by j. karger-kocsis, published by Kluwer academic publishers dordrecht/ boston/ london, 1999.
- [104] Romani F, Corrieri R, Braga V, Ciardelli F, *Polymer* 2002, 43, 1115.
- [105] Khonakdar HA, Jafari SH, Taheri M, Wagenknecht U, Jenichen D. *J Appl Polym Sci*, 100, 3264, 2006.
- [106] Kontopoulou M, Li Z. *Polym Eng Sci*, 49, 34, 2009.
- [107] Chodak, I. *Properties of crosslinked polyolefin-based materials*, *Prog. Polymer Sci.*, 20, 1165-1199, 1995.
- [108] Chodak I, Repin H, Bruls W, Janigov BI. *Mucromol. Symp.* 112, 159 166, 1996.
- [109] Wagner D, Vaia R. *Nanocomposites: issues at the interface*. *Materials Today*, © Elsevier Ltd. 2004.
- [110] Daniël Petrus Nicolaas VLASVELD, *Fibre reinforced polymer nanocomposites*, Phd thesis, 2005.
- [111] Fu S Y, Mai Y-W, Lauke B, Xu G and Yue C Y. *Combined effect of fiber content and microstructure on the fracture toughness of SGF and SCF reinforced polypropylene composites*, *J Mat Sci*, 37 (14), 3067–3074, 2002.

Chapter III
Materials and
experimental
techniques

Materials and experimental techniques

In this present chapter, all the materials and the different experimental techniques used will be presented.

III.1. General characteristics of the materials used

III.1.1. Polypropylene (PP)

Isotactic polypropylene (3050 MN1) was provided by Arkema. The glass transition temperature T_g (determined by dynamic mechanical analysis) and the melting temperature T_m (determined by differential scanning calorimetry) are 10 °C and 167°C, respectively. The average molecular weights are $M_n = 75,900 \text{ g mol}^{-1}$ and $M_w = 262,000 \text{ g mol}^{-1}$. The density determined by hydrostatic weighting is 0.946 g cm^{-3} . Wide angle X-rays scattering analyses revealed the exclusive presence of the α -monoclinic crystal of PP. Noteworthy that isotactic polypropylene (3050 MN1 grade) is used only in the study of the crosslinking of polypropylene.

The polypropylene used in the study of polypropylene / short hollow recycled PET fibers composite was polypropylene (PP) SABIC® PP 510A provided by, SABIC ARABIE SAOUDITE. The glass transition temperature T_g (determined by dynamic mechanical analysis) and the melting temperature T_m (determined by differential scanning calorimetry) are 10 °C and 165°C, respectively. The table III.1 summarized its properties.

Table III.1. Properties of the polypropylene (PP 510A) used

Property	Value	Units	Test method
Melt flow index	12	g/10 min	ISO 1133
Density	0.950	g cm^{-3}	ASTM D1505
Isotacticity	High	-	-
Tensile modulus	1700	MPa	ISO 527-2 1A

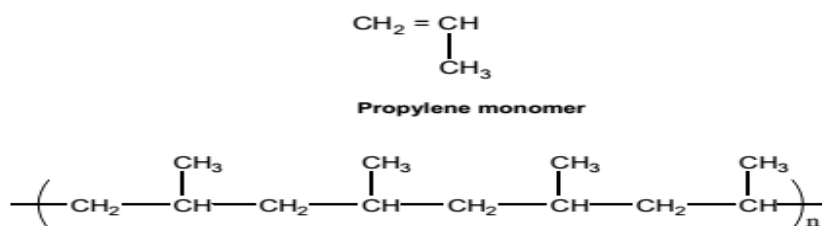
On the other hand, Polypropylene (PP) SABIC ® 510P homopolymer supplied by, SABIC ARABIE SAOUDITE was used in the study of Polypropylene / short polyamide fibers and hybrid composites. The different properties of this polypropylene are listed in table III.2.

Table III.2. Some properties of the polypropylene (PP 510P) used

Property	Value	Units	Test method
Melt flow index	10.5	g/10 min	ISO 1133
Density	0.950	g cm ⁻³	ASTM D1505
Isotacticity	High	-	-
Tensile modulus	1700	MPa	ISO 527-2 1A

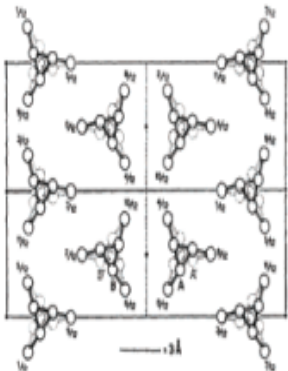
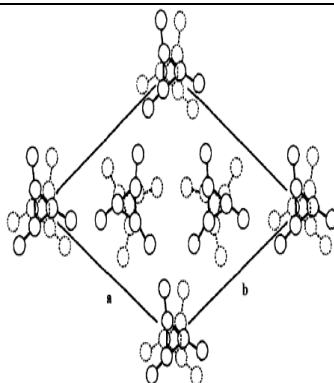
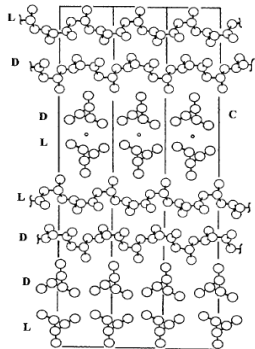
III.1.1.1. Microstructure of PP

PP can be made from the propylene monomer by a process known as Ziegler-Natta catalyzed polymerization or by metallocene catalysis polymerization. Mechanical properties, solubility and melting temperature of polypropylene can be ascertained with knowledge of the polymer tacticity [1].

**Figure III.1.** Molecular structure of Polypropylene

PP is considered to be capable of crystallizing into several isomorphous forms, abbreviated as α -PP, β -PP and γ -PP. Their characteristics are summarized in the table III.3

Table III.3. Isomorphous forms of polypropylene

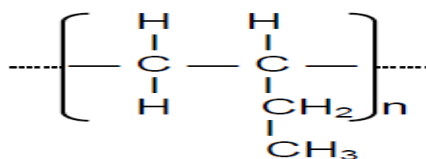
	α monoclinic	β hexagonal	γ orthorhombic
Unit cell constants	$a=6.666 \text{ \AA}$ $b=20.78$ $c=6.495$ $\alpha=90^\circ$ $\beta=99.6^\circ$ $\gamma=90^\circ$ Natta <i>et al</i> , 1960 [2]	$a=b=19.08 \text{ \AA}$ $c=6.42 \text{ \AA}$ $\alpha=90^\circ$ $\beta=90^\circ$ $\gamma=120^\circ$ Samuels <i>et al</i> , 1974 [3]	$a=8.6 \text{ \AA}$ $b=10 \text{ \AA}$ $c=6.42 \text{ \AA}$ $\alpha=90^\circ$ $\beta=90^\circ$ $\gamma=120^\circ$ Bruckner <i>et al</i> , 1989 [4]
$T_f (^\circ)$	160	150	140
$\rho_c (\text{g/cm}^3)$	0.936 [2]	0.922 [2]	0.939 [2]
unit cell structure			

III.1.2. Polybutene-1 (PB-1)

Isotactic polybutene-1 (PB 0110M) was supplied by Lyondell Basell. It is isotactic and semi-crystalline exhibiting high creep resistance and environmental stress crack resistance even at elevated temperatures. Table III.4 summarizes the density, the melt flow index (MFI) and the molecular weight of the polybutene-1 used.

Table III.4. Properties of the polybutene-1 used

Typical Properties	Value	Units	Test Method
Physical properties			
Melt Flow Rate (190 °C/2.16 kg)	0.4	g/10 min	ISO 1133
Density	0.914	-	ISO 1183
Mechanical properties			
Flexural Modulus	450	MPa	ISO 178
Tensile Strength at Break	35	MPa	ISO 8986-2
Tensile Elongation at Break	300	%	ISO 8986-2
Thermal properties			
T _{m1}	128	°C	ISO 11357-3
T _{m2}	117	°C	ISO 11357-3
weight average molecular mass	854800	g mol ⁻¹	

**Figure III.2.** Molecular structure of polybutene-1

Isotactic polybutene-1 is usually produced by solution polymerization of butene-1 with a Ziegler-Natta catalyst system [5]. Polybutene-1 (PB-1) exhibits four crystal forms [6] depending on the formation conditions: form I, twined hexagonal with a 3_1 helix [7] form I', untwined hexagonal with a 3_1 helix [8] II, tetragonal with an 11_3 helix [9] and form III, orthorhombic with a 4_1 helix [10]. Crystallization of melt at room temperature produces metastable Form-II, then gradually transforms into the stable Form-I at room temperature [6].

Table III.5 presents the structural characteristics for the crystal forms of PB-1. The helical conformations of Form-I and Form-II are shown on figure III.3.

Table III.5. Structural Characteristics for the Crystal Modifications of PB-1

Form	Crystal lattice	helix	Unit cell dimensions (nm)			T_m (°)
			A	b	c	
I	Hexagonal (twined)	3/1	1.77	1.77	0.65	120-135
I'	Hexagonal (untwined)	3/1	1.77	1.77	0.65	90-100
II	tetragonal	11/3	1.46	1.46	2.12	110-120
III	orthorhombic	4/1	1.25	0.89	0.76	90-100

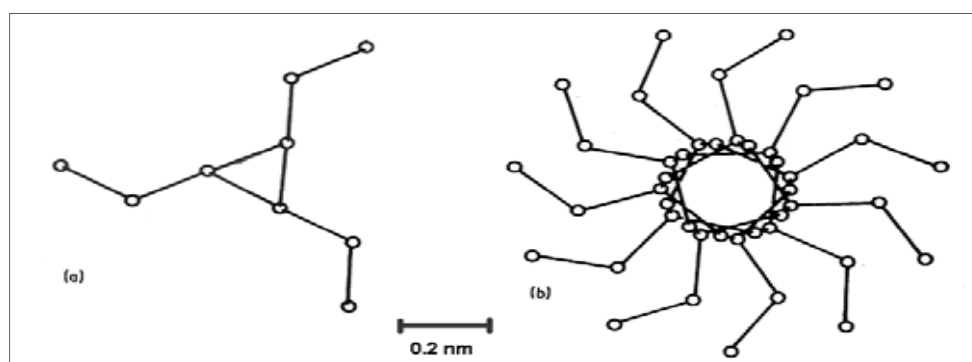


Figure III.3. Helical conformations of (a) Form-I, 3/1 helix
(b) Form-II, 11/3 helix [11]

Figure III.4 below summarizes the various crystal-crystal transformations of PB-1.

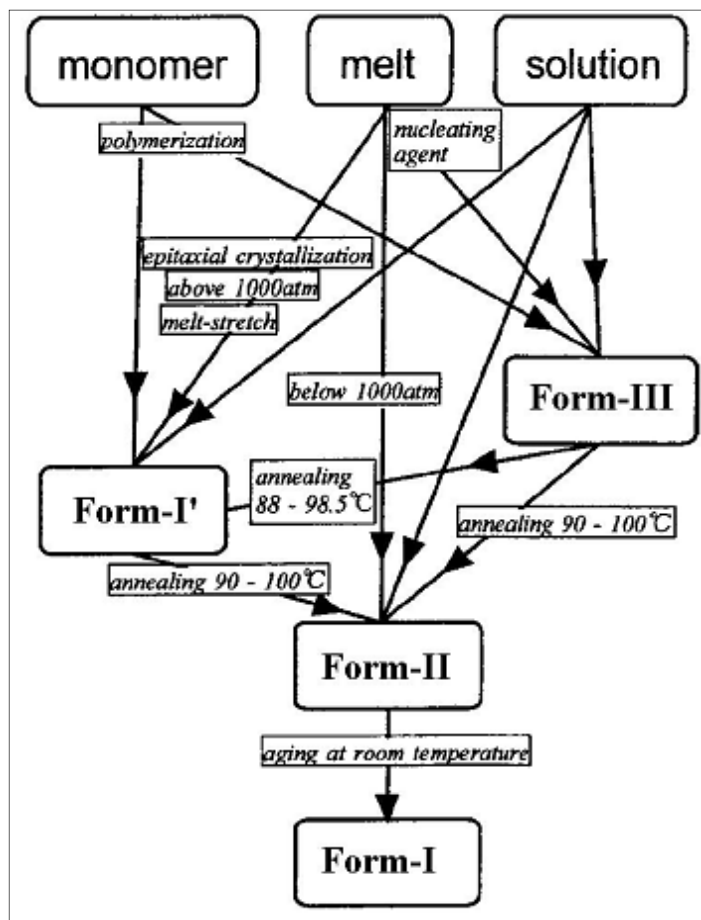


Figure III.4. Crystal-crystal transformations of PB-1 [12]

III.1.3. Hollow recycled Poly (ethylene terephthalate) fibers

The hollow recycled PET fibers (h.r-PETfs) were obtained from soft drink bottles, which were provided by the TINER-PLAST company -Setif- Algeria. The properties of these fibers are listed in table III.6. Figure III.5 shows the SEM micrograph of the hollow recycled PET fiber used in the present study.

Table III.6. Properties of the hollow recycled PET fibers

Properties	Hollow recycled PET fibers (h.r-PETfs)
Density (g/cm^3)	1.32
denier (d)	15
The breaking tenacity (g/d)	3.1
Elongation at break (%)	55
Moisture absorption (%)	0.5
T_m ($^{\circ}\text{C}$)	250

The breaking tenacity of a fiber expressed in grams per denier (g/d) or grams per tex (g/tex). Both denier and tex are units of linear density (mass per unit of fiber length) and are defined as the number of grams of fiber measuring 9000 meters and 1000 meters, respectively [13].

In general, PET fiber spun from PET pellets polymer which is the condensation product of terephthalic acid and ethylene glycol [14]. The typical fibers with special cross-section shape, commonly used, are hollow and solid fibers, meanwhile, the PET fibers for general commercial application are mostly solid fiber yarns [15, 16]. Hollow fibers are a type of core–sheath in which the core is composed of air, and they have benefit for specific applications due to the larger fiber surface/volume ratio [17].

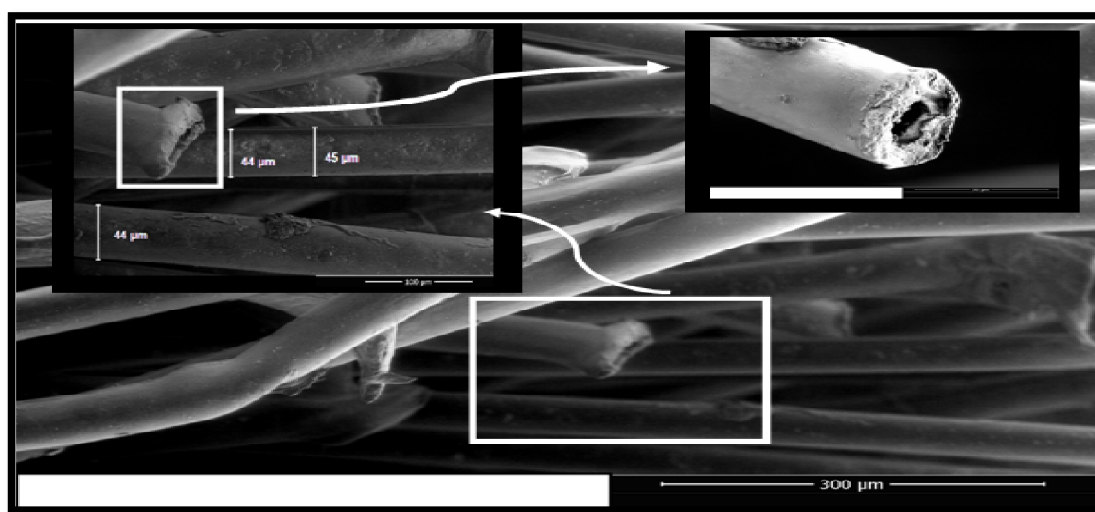


Figure III.5. SEM micrograph of the used hollow recycled PET fiber

III.1.4. Polyamide fibers (PA 6)

The polyamide 6 (PA 6) fibers were provided by Nanjing Forever Textile CO., LTD company - Jiangsu –China. The table III.7 shows their properties.

Table III.7 .Polyamide fibers (PAfs) properties

Properties	PA6 fibers
Density (g/cm ³)	1.14
denier (d)	1
The breaking tenacity (g/d)	7.2
Elongation at break (%)	45
Moisture absorption (%)	5
T _m (°C)	230

Polyamide fibers are spun from linear thermoplastic polymers having recurring amide groups made from diamines and dicarboxylic acids $(\text{CONH-R-NHCO-R}')_n$ or lactams $(\text{RCONH})_n$.

The chemical reactivity of PA 6 is a function of the amide groups and the amine and carboxyl ends. The aliphatic segment of the chain is relatively stable [18].

- **Structural models of fiber**

Aiming at describing the morphological texture of fibers, several models have been put. The model depicted in Figure III.6 is one of the basic models that have been developed [19]. The fiber consists of three distinct phases: oriented crystalline regions, amorphous regions also with preferential orientation along the fiber axis which contain tie molecules connecting crystallites, and highly extended non-crystalline molecules, called the interfibrillar phase. The interfibrillar phase will play a key role in the tensile properties of the fiber [20].

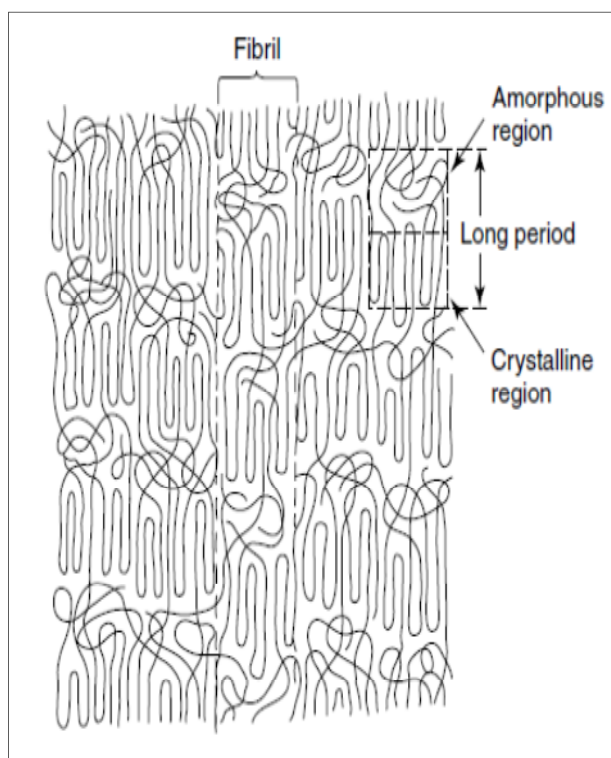


Figure III.6. Three phase model of fiber structure [20].

III.1.5. Stearic Acid

Stearic acid (octadecanoic acid) consisted of 18 carbon atoms without double bonds. It is a crystalline solid melting at $69.6\text{ }^{\circ}\text{C}$, practically insoluble in water, fairly soluble in chloroform

[0.5g / 100ml] and decreasingly soluble in other solvent as toluene. Stearic acid widely used as vulcanized activator for natural rubber and synthetic rubber products. Also used as plasticizer, softener, water – proofing agent, polishing agent and oiling agent, antistatic agent in textile industry, lubricant in metal machining, mold releasing agent in tile making etc. or used as additive for Polyethylene, Polypropylene, and PVC etc [21].

III.1.6. Montmorillonite (MMT)

Sodium montmorillonite (Na-MMT) was supplied by ENOF, Algeria. The cation exchange capacity CEC of this montmorillonite is about 1.15×10^{-3} mol/g.

Montmorillonite (MMT) is a naturally occurring 2:1 phyllosilicate, which has the same layered and crystalline structure [22]. The MMT crystal lattice consists of two-dimensional layers where a central octahedral sheet of alumina is fused to two external silica tetrahedral by the tip, so that the oxygen ions of the octahedral sheet also belong to the tetrahedral sheets, as shown in Figure III.7. Almost 1 nm is the layer thickness and the lateral dimensions may vary from 300 Å to some microns, a regular van der Waals gap is shown between these two layers, called interlayer or gallery. The sum of the single layer thickness and the interlayer represents the repeat unit of the multilayer material, called d-spacing or basal spacing (d_{001}), and is calculated from the (001) plan obtained from X-ray diffraction patterns [23-26].

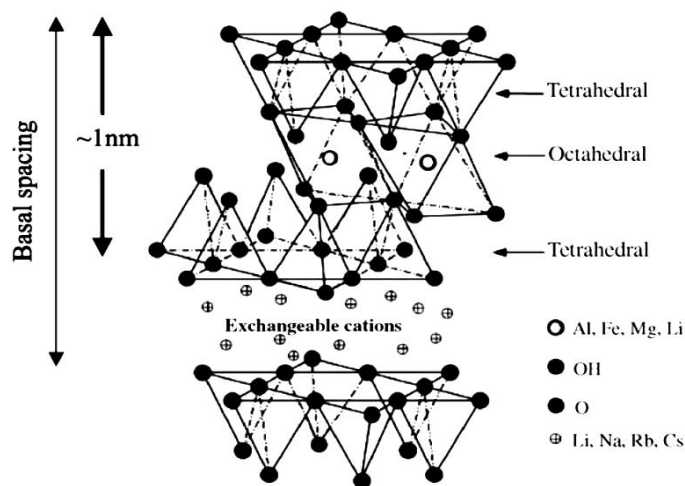
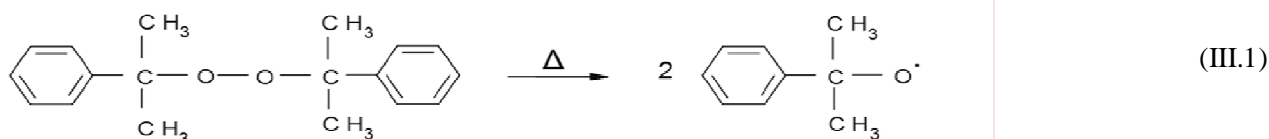


Figure III.7. Structure of Layered Silicates [25]

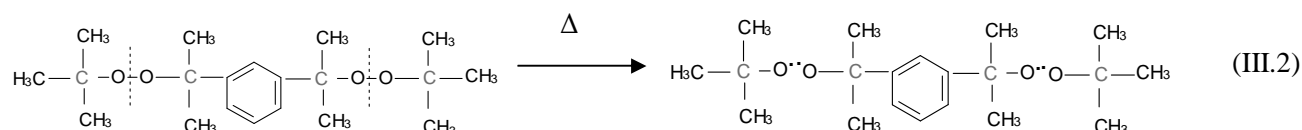
III.1.7. Crosslinking agent (Functionalizing agent)

- Peroxide

The peroxide used in the study for crosslinking of polypropylene and composites based on polypropylene matrix was Dicumyl peroxide (DCP), 96 wt % activity; supplied by Sigma-Aldrich –France. Its mechanism of decomposition is given by the scheme III.1.



On the other hand, the di(ter-butyl peroxyisopropyl) benzene (DTBPIB) peroxide was used in the study of the crosslinking of polybutene and its composites. (DTBPIB) peroxide also called Perkadox 14-40-B-gr, was provided by Akzo Nobel Polymer Chemicals B.V. Amersfoort, Netherlands. Its mechanism of decomposition is given by the scheme III.2.

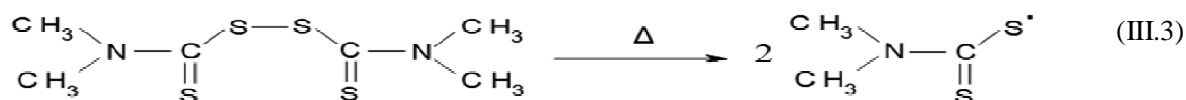


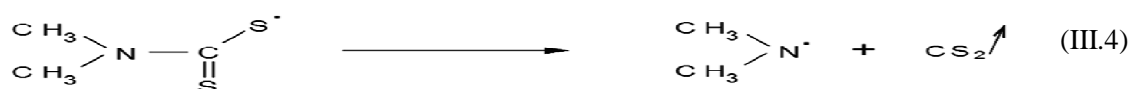
Sulfur

Sulfur (S) (vulcanizing agent for rubber) was supplied by Wuxi Huasheng Chemical Additives Factory, China.

Accelerator

The accelerator used was “Super accelerator 501” (tetramethylthiuram disulfide, TMTD), supplied by Rhone Poulenc, France. Its mechanism of decomposition is given by the schemes III.3 and III.4.





III.2. Processing method

III.2.1. Crosslinked polypropylene

For the preparation of the crosslinked polypropylene, the sulfur concentration was always equal to that of the peroxide. However, the accelerator was 1/4 of the sulfur and peroxide concentrations. crosslinking agents were mixed in the solid state, then added to the polypropylene and melt mixed at a temperature of 170 °C, a speed of 60 rpm during a mixing time of 20 min. The four prepared formulations are shown in table III.8.

Table III.8. Crosslinked PP samples designation and composition

Materials	Peroxide (wt %)	Sulfur (wt %)	TMTDS (wt %)
0.8 XPP	0.8	0.8	0.2
1.6 XPP	1.6	1.6	0.4
2.4 XPP	2.4	2.4	0.6
3.2 XPP	3.2	3.2	0.8

III.2.2. Composites preparation

a- Polypropylene (PP) matrix /short fibers composite

Before the melt mixing process, hollow PET fibers, polyamide fibers and treated fibers were dried in an oven at 60°C for 12h. Different composites were mixed in different ratios in a 60 cm³ Brabender mixer chamber to get the showed samples in table III.9. First of all the polypropylene was melted in the brabender chamber then short fibers were added and melt blended at a temperature of 190 °C, a speed of 60 rpm during a mixing time of 10 min.

❖ Surface treatment of fibers

Surface treatment of fibers was carried out using stearic acid in order to increase the number of reactive groups, and improve the fibers dispersion in the matrix. First of all, fibers were chopped into about 4 mm. Then, the obtained short fibers were washed with distilled water in order to remove the possible surface impurities and dried in vacuum oven at 60°C. 25 mg of stearic acid was dissolved in 200 ml of toluene at ambient temperature by continuous magnetic stirring of

solution for 20 min. Then, 3 g of fibers were added into toluene/stearic acid solution under a magnetic stirring at ambient temperature for 12h in order to complete the reaction between stearic acid with fibers surface and to improve the dispersion of the fibers into the solution. Following the treatment, fibers were thoroughly washed with distilled water, dried in vacuum oven at 60 °C for 8h.

Table III.9. Formulation of PP/short fibers composites

Samples	samples designation
3 wt %h.r-PETfs	3 wt % hollow recycled PET fibers /PP
7 wt% h.r-PETfs	7 wt % hollow recycled PET fibers /PP
10wt% h.r-PETfs	10 wt % hollow recycled PET fibers /PP
7wt% t-h.r-PETfs	7wt % treated hollow recycled PET fibers /PP
3 wt % PAfs	3 wt % polyamide fibers / PP
5 wt % PAfs	5 wt % polyamide fibers / PP
7 wt % PAfs	7 wt % polyamide fibers / PP

b- Crosslinked PP (XPP) matrix/short fibers composites

Table III.10. Formulation of crosslinked PP/short fibers composites

Samples	Sample designations
XPP	1.6 XPP mixed
0.5 Crosslinking agent (CA)	0.5 Peroxide +0.5 Sulfur + 0.125 TMTDS
3 wt %h.r-PETfs	3 wt % hollow recycled PET fibers + 0.5 CA /XPP
7 wt% h.r-PETfs	7 wt % hollow recycled PET fibers + 0.5 CA /XPP
10wt% h.r-PETfs	10 wt % hollow recycled PET fibers + 0.5 CA /XPP
7wt% t-h.r-PETfs	7 wt % treated recycled hollow PET fibers + 0.5 CA /XPP
3 wt % PAfs	3 wt % polyamide fibers + 0.5 CA / XPP
5 wt % PAfs	5 wt % polyamide fibers + 0.5 CA /XPP
7 wt % PAfs	7 wt % polyamide fibers + 0.5 CA /XPP

c-Hybrid composites preparation

The different composites were prepared in Brabender plastograph mixer using twin Roller blades at mixing temperature of 190°C and rotor speed of 60 rpm during 20 minutes and, then, compressed into a dreher-type Brabender. The different composites were grinded before undergoing the diverse tests. Noting that, the fillers used were dried in an oven at 60°C for 12h.

c.1- Na-MMT/PP nanocomposites preparation

A series of composites have been studied consisting of different content of the f-Na-MMT (3, 5, 7 wt %) /PP. Different composites were prepared using the conventional method. Functionalizing agent (peroxide, sulfur and accelerator) / dried Na-MMT were mixed together in the solid state, in which the functionalizing agent (FA) was added in a concentration of 1/5 of the clay. The formulations are as follows: the sulfur concentration (in wt %) was equal to that of peroxide, and the accelerator was 1/4 of the sulfur or peroxide concentration.

PP was incorporated into the Brabender plastograph chamber firstly, and then the mixture Na-MMT/FA was introduced as soon as torque indicated melting of the polymer (about 2 min).

c.2- Crosslinked PP (PP/ 1wt% FA)

The so-called “functionalizing agent of Na-MMT” which is constituted by the peroxide, sulfur, and accelerator were also used as crosslinking agent of PP. Accordingly, an additional study of crosslinked PP has been done, with a view of evaluating and explaining the effect of functionalizing agents on the structure of PP. As well as for understanding the effect of FA on neat PP structure, the same amount of functionalizing agent that was added to 5wt % Na-MMT was used to PP, The amount of sulfur and peroxide was 1 wt % and the accelerator was 1/4 of the sulfur and peroxide concentration.

c.3- PAfs/PP composites preparation

Two series of PAfs/PP composites containing 5 wt% PAfs treated and untreated fibers were prepared. The fibers were dispersed in the PP pellets in the solid state, thereafter; the obtained mixture was inserted into brabender plastograph chamber.

c.4- f-Na-MMT /PAfs /PP hybrid composites

PAfs /f-Na-MMT /PP hybrid composites were prepared by adding 5 wt % of treated polyamide fibers (t-PAfs) to different recycled nanocomposites 3, 5, 7 wt % f-Na-MMT / PP which were prepared and grinded as it was explained above in the section of f-Na-MMT/PP nanocomposites preparation .

Sample designation and composition of hybrid composites are presented in table III.11.

Table III.11. Sample designation and composition of hybrid composites.

Sample	t-PAfs (wt %)	f-Na-MMT prepared (wt %)	presented in PP nanocomposite
3 wt% hyb	5	3	
5 wt% hyb	5	5	
7 wt% hyb	5	7	

III.2.2.Crosslinked Polybutene -1

The same crosslinking agent concentrations and mixing condition that were used in the study crosslinked polypropylene was taken in the crosslinked polybutene preparation. Sample designation and composition are shown in table III.12.

Table III.12. Crosslinked PB-1 sample designation and composition

Materials	Peroxide (wt %)	Sulfur (wt %)	TMTDS (wt %)
0.8 XPB-1	0.8	0.8	0.2
1.6 XPB-1	1.6	1.6	0.4
2.4 XPB-1	2.4	2.4	0.6
3.2 XPB-1	3.2	3.2	0.8

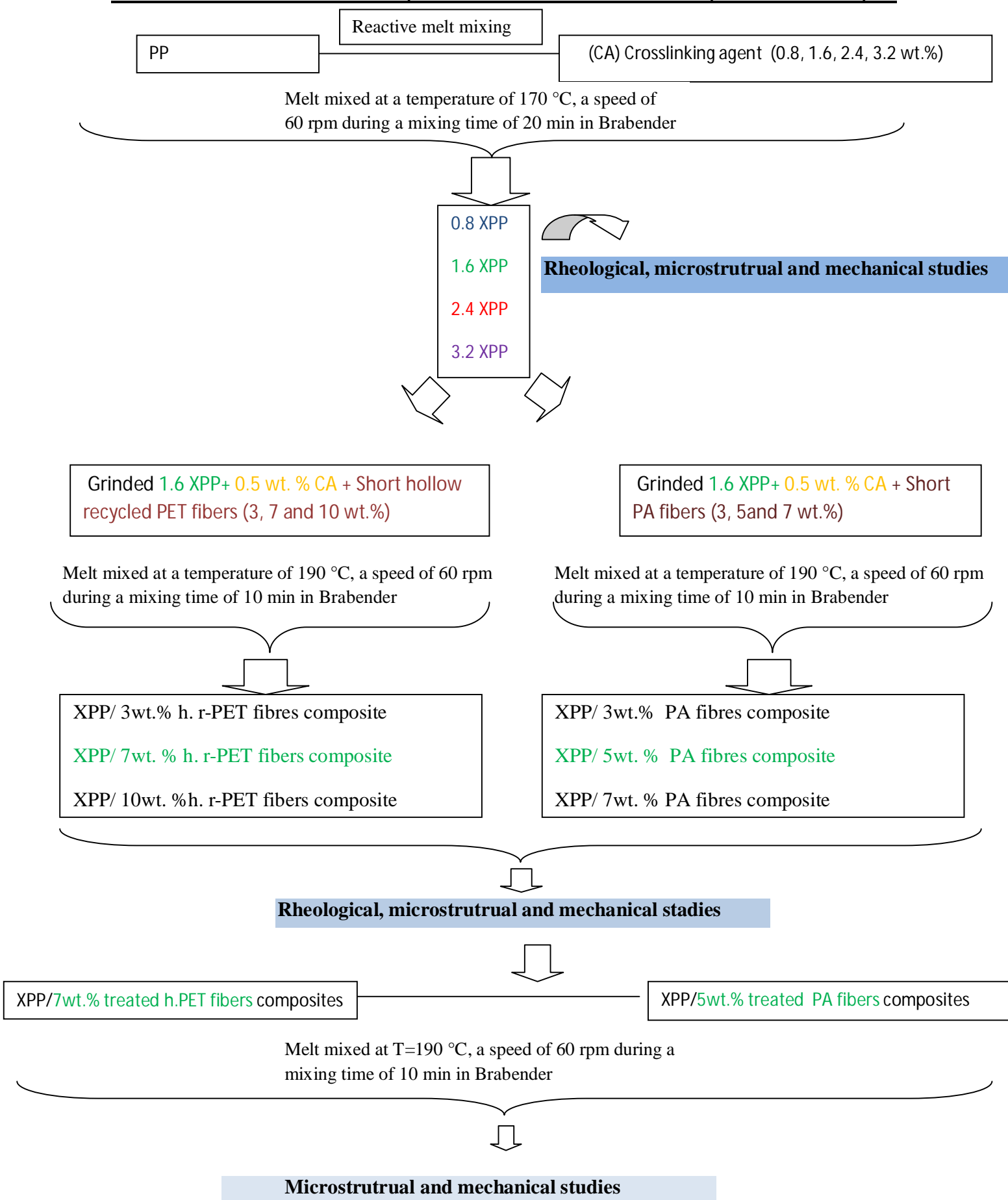
III.2.1.Polybutene-1 /hollow PET fiber/ Na-MMT hybrid composites

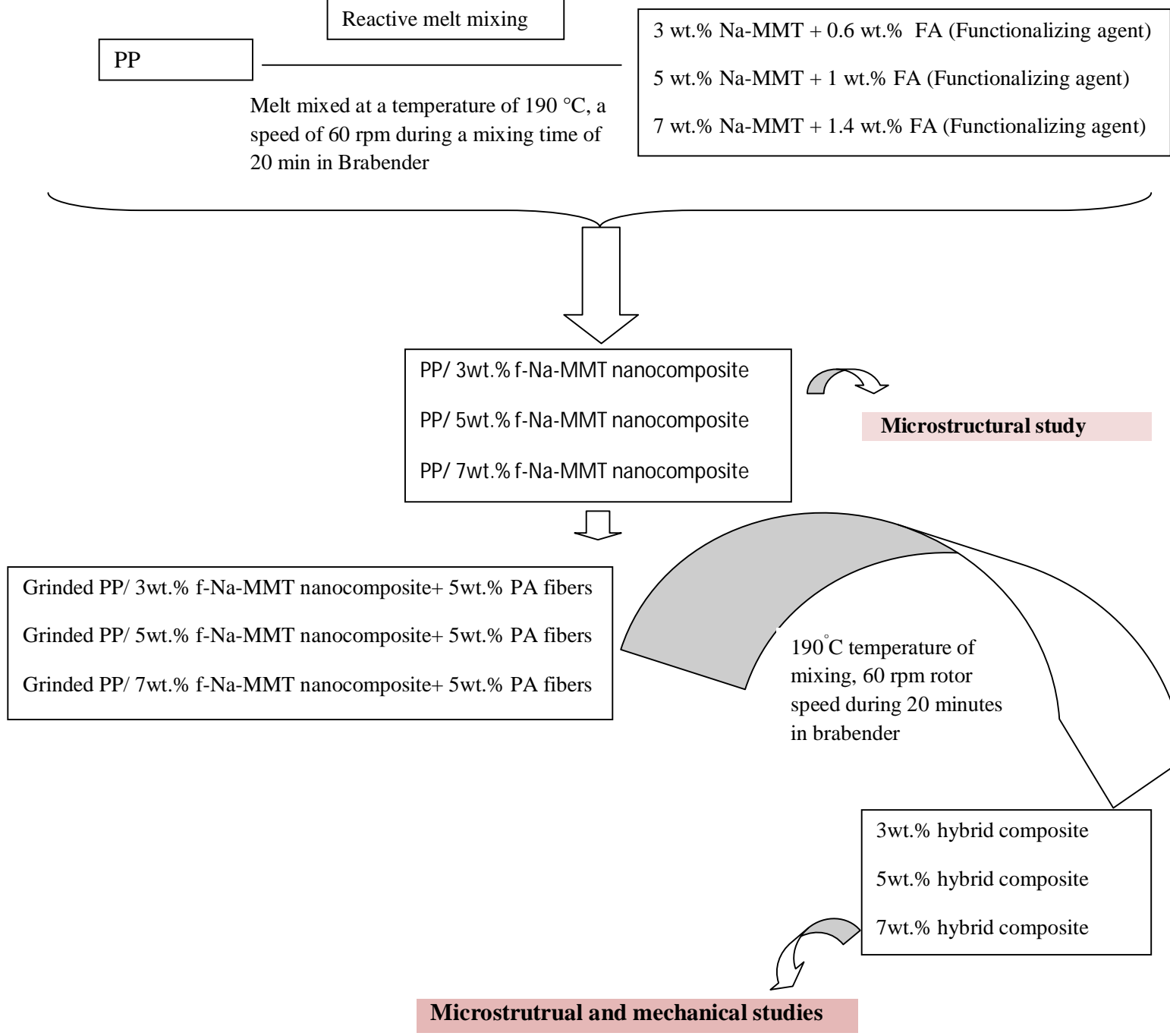
Before the reactive melt mixing in the Brabender, the fillers used were dried in an oven at 60°C for 12h. The mixing conditions were as follows: 190°C temperature of mixing, 60 rpm rotor speed during 20 minutes. The table III.13 presents the prepared formulations.

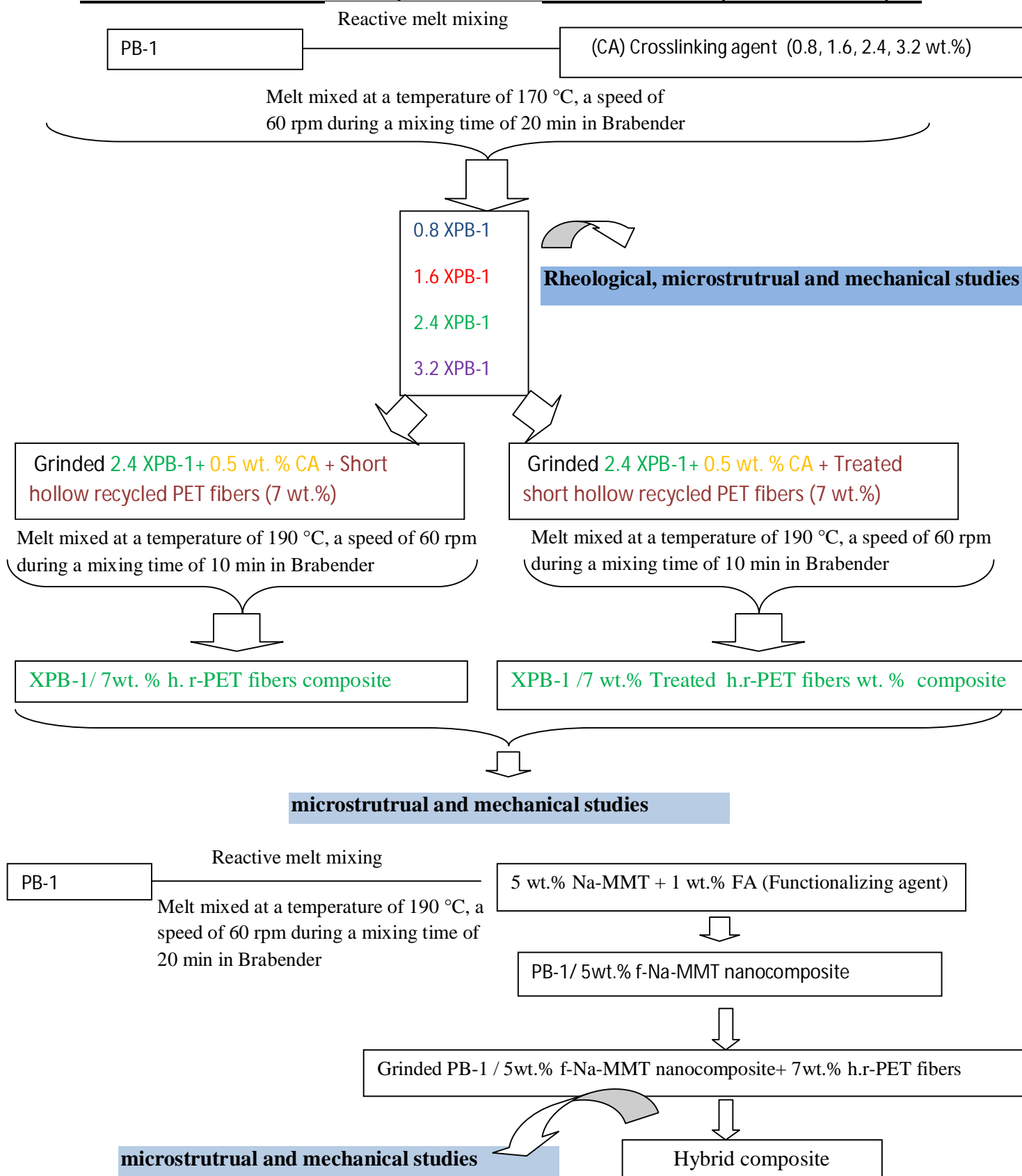
Table III.13. Formulation of PB-1/hollow PET fiber/Na-MMT hybrid composite

Samples	Designations
h.PETfs	7 wt% hollow PET fiber/ PB-1
t-h.PETfs	7 wt% treated hollow PET fiber/ PB-1
XPB-1	2.4 XPB-1 mixed
XPB-1/ t-h.PETfs	7 wt% treated hollow PET fiber/ XPB-1
Hybrid composites	
1 wt % crosslinking agent (CA)	1 wt % Peroxide + 1 wt % Sulfur + 0.25 wt % TMTDS
1 XPB-1	1 wt % CA+ PB-1
f-Na-MMT	5 wt % Na-MMT + 1 wt % CA
hyb	7 wt% treated hollow PET fiber /f-Na-MMT / PB-1

Scheme1 shows the schematic processing steps of the samples preparation in the present study.







Scheme III.1. The schematic processing steps of the different samples preparation

III.3.Experimental techniques

III.3.1.Rheological characterizations

III.3.1.1.Dynamic rheological analysis

For the dynamic rheological analysis, a Brabender type plastograph was used. The processability of the different components has been evaluated by measuring the torque required to mix the molten components in a heated chamber, under fixed conditions, i.e., temperature, time and rotor speed.

III.3.1.2.Melt flow index (MFI) measurements

Melt flow index (MFI) in (g/10min) values were measured following ASTM D 1238-82 standard. The test was performed at 230°C with a load of 2.16 kg. Values were obtained by taking the average of five extrudates.

III.3.2.Gel content

The gel content (insoluble fraction) of the crosslinked samples was determined according to standard ASTM D2765-01 [29] by extracting with xylene solvent.

III.3.3.Microstructural characterization

III.3.3.1.FTIR measurements

FTIR spectra of film samples were recorded using a Perkin Elmer Spectrum 1000 spectrometer with a resolution of 4 cm⁻¹ within 200 scans (PerkinElmer).IR spectra were obtained for different film samples in the region from 400 to 4000 cm⁻¹.

III.3.3.2. Differential scanning calorimetry (DSC)

Thermograms of all components were obtained using a Q200 instrument (TA Instruments, USA). The calorimetric runs were performed using (±10 mg) of each simple with a heating rate of 5°C/min. The samples were heated up to 200 °C and maintained at this temperature during 3 min, then samples were cooled down to 25°C with a cooling rate 5°C/min .After that, a second heating were effectuated.

The degree of crystallinity of different investigated samples was determined according to the equation III.1, in which ΔH_m is the melting enthalpy of polymers, and ΔH_m^0 presents the heat of fusion of 100% crystalline polymers, at the equilibrium melting point.

$$\frac{\Delta H_m}{\Delta H_m^{100\%}} \quad (III.1)$$

However, in the present study, the degree of crystallinity was determined with the application of a correction factor in order to take into consideration the amount of fillers (fibers and Na-MMT) in different composites. Thus, accurate values of χ_c reported were obtained from the equation III.2, where (w_f) corresponds to the weight percentage of fillers in the composite.

$$\frac{\Delta H_m}{\Delta H_m^{100\%}} \times \frac{100}{100-w_f} \quad (\text{III.2})$$

The crystallite sizes L_c can be also deduced using the melting temperature by means of Thomson-Gibbs' equation III.3 as follows:

$$L_c^{\text{DSC}} = 2\sigma T_m^0 / (T_m^0 - T_m) \Delta H_m^0 \rho_c \quad (\text{III.3})$$

For the polypropylene (PP) matrix:

$T_m^0 = 187.5^\circ\text{C}$, $\Delta H_m^0 = 165 \text{ J/g}$, σ (the fold surface free energy) = 0.1 j/m^2 the fold surface free energy and $\rho_c = 0.94 \text{ g/cm}^3$ is the crystal phase density [27].

For the polybutene-1 (PB-1) matrix:

$T_m^0 = 133^\circ\text{C}$, ΔH_m^0 (form I) = 125 J/g and ΔH_m^0 (form II) = 75.2 J/g , σ (the fold surface free energy) = 15.5 erg/cm^2 and $\rho_c = 0.914 \text{ g/cm}^3$ is the crystal phase density [28].

III.3.3.3. Wide-angle X-ray scattering (WAXS)

Crosslinked samples are analyzed by wide angle X-ray scattering (WAXS). The selected tension and the intensity are 30 kV and 40 mA, respectively. The wave length used is $K_{\alpha 1}$ copper radiation ($\lambda = 0.154 \text{ nm}$). The diffraction system used in the laboratory of IJL (Nancy, France), has two detection modes, 1D and 2D. The 2D transmission pattern, intercepted by a Fujifilm image plate normal to the beam, is revealed with the adapted scanner (Fujifilm BAS 5000) with a maximum resolution of 25 μm , the image being readily obtained in digital form with a PC microcomputer (see figure III.8).

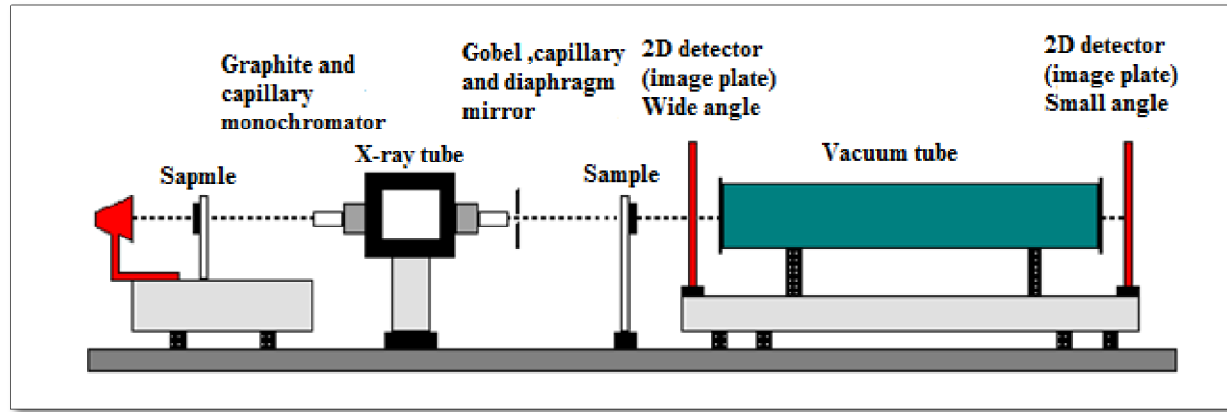


Figure III.8. Experimental device of X-ray diffraction test [29].

It is worth noting that, the crystalline structure of the different studied composites in the present thesis was determined by WAXS analysis using reflection mode. WAXS profiles were recorded on a Seifert diffractometer (RICH.SEIFERT & CO, Germany). The following conditions were employed: 40 kV, 35 mA, angular range: $^{\circ}4-35^{\circ}$ (2θ), scan rate: $0.02^{\circ}/s$.

From the WAXS patterns, the degree of crystallinity (χ_c) can be measured using the following equation III.4 [30]:

$$\chi_c^{\text{WAXS}} = I_c / (I_a + I_c) \quad (\text{III.4})$$

Where I_c and I_a present the integrated intensities of crystalline and amorphous phases, respectively, which were determined by deconvolutions of WAXS patterns. We fit the contributions of amorphous and crystalline phases by a series of Gaussian curves of different heights and widths using Fityk software.

The portion of the α and λ forms of the PP were calculated using the following equations:

$$\alpha (\%) = \frac{I_{\alpha(130)}}{\sum \text{areas}} \quad \text{and} \quad \lambda (\%) = \frac{I_{\alpha(117)}}{\sum \text{areas}} \quad (\text{III.5})$$

$$\text{where, } \sum \text{areas} = I_{\alpha(130)} + I_{\gamma(117)} \quad (\text{III.6})$$

We have also estimated the content χ_{β} of β form and χ_{γ} of the β and γ -form in all the studied composites samples according to the method of Turner-Jones and al [31, 32]:

$$\chi_{\gamma} = I_{(130)}^{\gamma} / (I_{(130)}^{\gamma} + I_{(130)}^{\alpha}) \quad (\text{III.7})$$

$$\chi_{\beta} = I_{(300)}^{\beta} / (I_{(110)}^{\alpha} + I_{(040)}^{\alpha} + I_{(130)}^{\alpha} + I_{(300)}^{\alpha}) \quad (\text{III.8})$$

To calculate the crystallinity degree (χ) of form I and form II in a partially transformed PB-1 sample, the peaks of form I, form II and amorphous are fitted using Fityk software.

The two forms are calculated using the following equations proposed by Hsiao et al [33].

Where A_I , A_{II} , A_A represent the integrated areas beneath peaks of the form I, the form II and amorphous, respectively.

$$\chi_I = \frac{A_I}{A_I + A_{II} + A_A} \quad (\text{III.9})$$

$$\chi_{II} = \frac{A_{II}}{A_I + A_{II} + A_A} \quad (\text{III.10})$$

III.3.3.4. Macromolecular orientation (2D WAXS)

The orientation degree of the crystallites can be given on a quantitative numerical basis using Hermans' orientation function. The orientation factor noted $F_{\vec{u}/\vec{x}}$ represents the relative orientation of a given crystallographic axis \vec{u} against a fixed reference direction \vec{x} . Its general expression is given in Equation (III.11) [34].

$$F_{\vec{u}/\vec{x}} = \frac{3 \langle \cos^2(\alpha_{\vec{u}/\vec{x}}) \rangle - 1}{2} \quad (\text{III.11})$$

where,

$$\langle \cos^2(\alpha_{\vec{u}/\vec{x}}) \rangle = \frac{\int_0^{\pi/2} I_{hkl} \cos^2 \varphi \sin \varphi d\varphi}{\int_0^{\pi/2} \sin \varphi d\varphi} \quad (\text{III.12})$$

and, I_{hkl} depicts the maximal intensity scattered of the (hkl) plane at a given azimuthal angle φ .

Table III.13 illustrates the remarkable values corresponding to the specific crystallographic orientation using Hermans' orientation factor [34].

Table III.14. Remarkable values of $F_{\vec{u}/\vec{x}}$ used for determining the material texture using Hermans' orientation factor [34].

$\langle \cos^2(\alpha_{\vec{u}/\vec{x}}) \rangle$	$F_{\vec{u}/\vec{x}}$	Texture
0	-1/2	\vec{u} is perpendicular to \vec{x}
1/3	0	Isotropic distribution of \vec{u} in space
1/2	1/4	Isotropic distribution of \vec{u} in the plane parallel to \vec{x}
1	1	\vec{u} is parallel to \vec{x}

III.3.3.5. Dynamic Mechanical Analysis

Dynamic mechanical analyzer (DMA) model DMA242 from NETZSCH was used to investigate the dynamic mechanical properties of the specimens, i.e. storage modulus (E'), loss tangent ($\tan \delta$) and glass transition temperature (T_g). The specimen used were manufactured from the plaques prepared using a computer-controlled milling machine (CharlyRobot CRA4). The specimens length, width and thickness were 50, 4, and 1 mm, respectively. Noteworthy that the dimensions of the specimens of the crosslinked polypropylene were 50, 4 and 4 mm, respectively. The test was performed under bending mode. The strain was applied sinusoidally with a frequency of 1 Hz, and the specimen was heated at a rate of 2°C/min from -100 to 100°C.

III.3.3.6. Scanning electron microscope (SEM)

The cross-section surfaces of the different composites were examined using an environmental SEM (MEB- FEI- QUANTA- FEG 600). Noting that cryogenic fracture in liquid nitrogen was done before SEM observation for the recycled PET fiber/PP composites. However, for the polyamide fibers/PP composites and recycled PET fiber/PB-1 composites, the analysis of the composites was performed by observation of the fractured surfaces produced after the tensile tested composites.

III.3.3.7. Optical light polarized microscopy

Polarized light microscopy examinations using an Olympus bx50 with a capture camera Micro Publisher 3.3 RTV were carried out on both sides of the cast samples.

III.3.3.8. Synchrotron X-ray tomography (SRXTM)

In situ tensile test under synchrotron radiation were performed at the Syrmep beamline located at Elettra Trieste international research center, Italy. X-ray photon energy of 10-15 keV was used, and 900 projections (≈ 1 sec/proj) were captured over the 180° of rotation. The detector was a 2048 x 2048 pixel CCD camera. The specimens were scanned at a resolution of 2.04 μm voxel edge length. Tensile speed was 5 $\mu\text{m/s}$. The tensile specimens were manufactured from the plaques prepared using a table milling machine which was managed by CAO software. The length and the width overall of specimens were 40 mm and 10 mm respectively, length and width narrow section of specimens was 4 mm (see figure III.9.a and b).

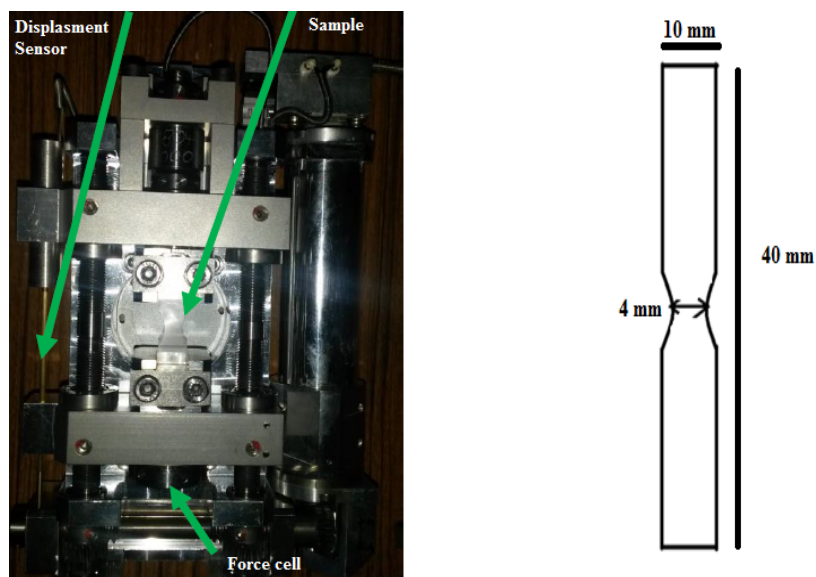


Figure III.9. a-Tensile micromachine [29] b-Sample dimensions

III.3.4. Mechanical Tests

III.3.4.1. Tensile test

III.3.4.1.1. VidéoTraction™ system

The videotraction™ system is a video-controlled mechanical testing technique invented in the laboratory of Materials Science and Metallurgy Department, Jean Lamour Institute. (1990). This system was patented by G'Sell and Winter (2001).

Tensile strength tests of the crosslinked polymer are carried out with a servo-hydraulic machine (MTS 810) using VidéoTraction™ system.

- **Specimens' preparation**
- **Preparation of plates (shaping)**

Plates were prepared by compression molding, using a specific square mold of $100 \times 100 \text{ mm}^2$ which can be used to get different plates thickness. The chosen thickness was 1 mm^2 and for 4 mm^2 for the crosslinked PB-1 and crosslinked PP respectively. The compression molding was performed in CARVAR manual press between hot plates at $200 \text{ }^\circ\text{C}$ and at a constant pressure of 8 MPa for 20 min, followed by water cooling under the same molding press.

The test specimens are machined from the polished plates using a computer-controlled milling machine (CharlyRobot CRA4) following the shape represented in Figure III.10. (a. crosslinked PB-1 samples) and (b. crosslinked PP samples). Seven dot markers, made of a fluorescent ink, are

printed on the front flat face of the sample. Five of these dots are aligned and equally spaced in the tensile direction, x_3 , while the two others are aligned with the central dot along the transverse direction, x_1 (see figure III.10.b). The traction machine is equipped with a camera that closely follows the movement of dots markers placed on the surface of the specimen (see figure III.11). In addition, the seven fluorescent markers, illuminated with an ultraviolet lamp, are followed in real time during the tensile tests by means of a CCD camera (resolution 800*600 pixels) interfaced with a microcomputer through a video interface board. Video measurements are performed locally in a specific Representative Volume Element (RVE) at the sample centre, where plastic deformation can be showed (see figure III.12) [35].

The tensile properties of specimens were determined using 5 samples for each composition, at room temperature and at strain rate of 10^{-5} s^{-1} .

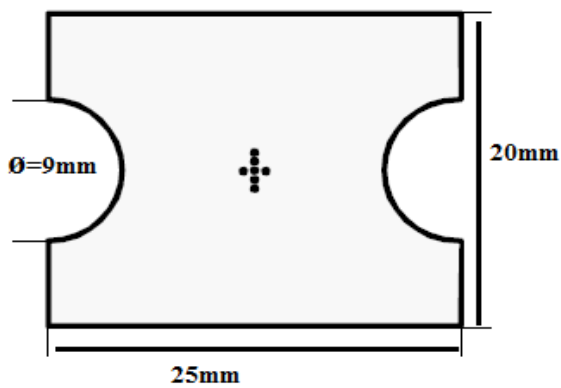


Figure III.10.a. PB tensile sample with seven markers

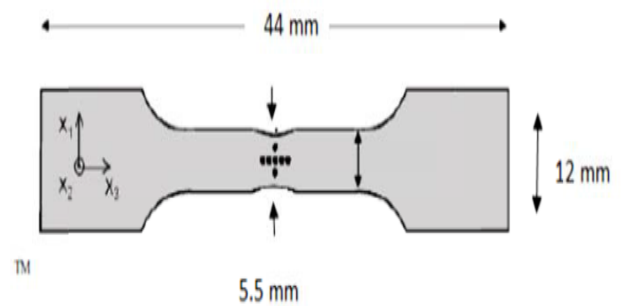


Figure III.10.b. PP Tensile sample

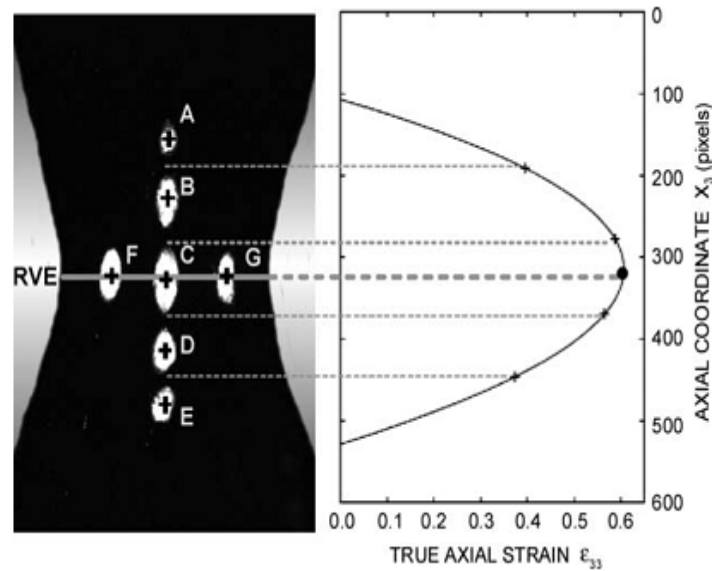


Figure III.11. Determination of the true axial strain in the representative volume element (RVE)

[35]

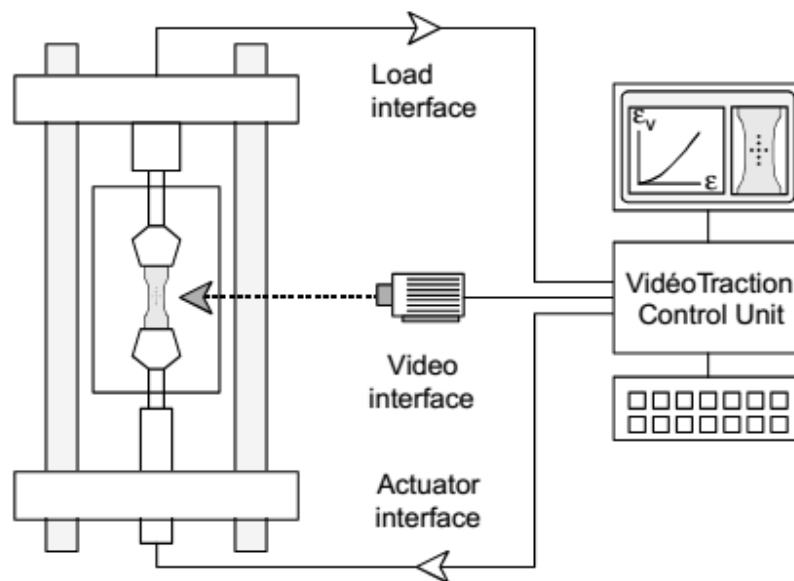


Figure III.12. General diagram of the VidéoTraction™ system [35].

The volume strain in the RVE, ε_v , is computed as the trace of the true strain tensor:

$$\varepsilon_v = \varepsilon_{11} + \varepsilon_{22} + \varepsilon_{33} \quad (\text{III.13})$$

For crosslinked PB-1 samples having a very low thickness-to-width ratio, the hypothesis is that of plane tensile testing [29], the axial strain ε_{33} in the RVE is equal to the opposite of the normal

strain ϵ_{11} in the RVE. So, the resulting axial load in the RVE is calculated using Equation (III.14):

$$\sigma_{33} = \frac{F}{S_0} \exp(\epsilon_{33}) \quad (\text{III.14})$$

However, for the crosslinked PP samples having a high thickness-to-width ratio, the hypothesis is that of uniaxial tensile testing [29], transverse strains in the RVE, ϵ_{11} and ϵ_{22} , are equal considering the realistic hypothesis that the strain field is transversally isotropic in the centre of the neck.

The axial true stress (Cauchy stress) is determined in the same RVE as the load per unit actual cross-section:

$$\sigma_{33} = \frac{F}{S_0} \exp(-2\epsilon_{11}) \quad (\text{III.15})$$

where S_0 is the initial cross-section of the tensile specimen.

III.3.4.1.2. Simple tensile test

Type I specimens of ASTM D 638, were prepared by compression molding using a CARVAR manual at a pressure of about 8 MPa and at a temperature of 200°C, the specimens were submitted to tensile test. The tensile properties of specimens were determined using 5 samples for each composition with a universal Shimadzu model WDT-/20KN testing machine at a constant cross-speed of 20 mm/min. Measurements were carried at room temperature.

III.3.4.2. IZOD impact strength tests

(V-45 ° angle) Notched (1/10 deep) specimens were prepared and submitted to the Izod impact strength testing equipment. The specimen thickness and width were 3 and 9 mm respectively. The impact strength properties of specimens were determined using 5 samples for each composition with a Microtest testing machine (ISO 180), using a 2 J hammer.

References

- [1] Arranz-Andrès J, Pena B ,Pèrez E, Cerrada M L . Influence of isotacticity and molecular weight on the properties of mettalocenic isotactic propylene.European Polymer Journal, 43 (6), 2357-2370, 2007.
- [2] Natta G, Corradini P. Structure and properties of isotactic polypropylene. Del Nuovo cimento, supplement, Vol.24, p. 917-950, 1960.
- [3] Samuels R.J. Structred polymer properties : the identification ,interpretation and application of crystalline polymer structure ,John Wiley and Sons ,New York, 1974.
- [4] Bruckner S, Meille SV. Non-parallel chains in crystalline isotactic polypropylene, Nature, 340, 455-457, 1989.
- [5] Qigu H, Fangming Z, Qing W, Shangan L. The synthesis of high molecular weight polybutene-1 catalyzed by Cp^{*}Ti(OBz)₃/MAO. Polym Int, 50, 45, 2001.
- [6] Luciani L, Sepala J, Lofgren B. Poly-1-butene: its preparation, properties and challenges. Prog Polym. Sci.13, 37, 1988.
- [7] Natta G, Corradini P, Bassi IW. Crystal Structure of Isotactic Poly-alfa-butene. Nuovo Cimento Suppl, 15, 52, 1960
- [8] Miller, RL, Holland VF. On Transformations in Isotactic Polybutene-1. Polym. Lett., 2, 519,1964.
- [9] Turner-Jones AJ. Polym. Sci., B18, 455, 1963.
- [10] Kopp S, Wittmann, JC, Lotz B. Polymer, 35, 908, 1994.
- [11] Strob G. The physics of Polymers. Springer-Verlag, Berlin, 1996.
- [12] Tosaka M., Kamijo T , Tsuji M , Kohjiya S, Ogawa T, Isoda S, Kobayashi T.Macromolecules, 33, 9666,2000.
- [13] Needles, Howard L, Textile fibers, dyes, finish, and processes, Noyes Publications, USA, 1986.
- [14] East AJ, Polyester fibres, in J.E. McIntyre (ed.), Synthetic Fibres: Nylon, Polyester Acrylic, Polyolefine, Woodhead Publishing Limited, Cambridge, England, 2005.
- [15] Sandip V. Purane, Narsingh R. Panigrahi., “Microfibres, microfilaments & their applications », AUTEK Research Journal. 3, 7, 2007.
- [16] Kothari, V.K., Textile Fibers: Development and Innovations, IAFL Publication, New Delhi, 2000.
- [17] Michael Jaffe, Anthony J. East, Polyester Fibers, in: Handbook of Fiber Chemistry, International Fiber Science and Technology Series,Taylor& Francis Group, Boca Raton, pp.20-25. 2007
- [18] Polyamide Fibers in EPST 1st ed., Vol. 10, pp. 347–460, by O. E. Snider and R. J. Richardson, Allied Chemical Corp.; Polyamides, Fibers in EPSE 2nd ed., Vol. 11, pp. 410–445.
- [19] H. Brody, Synthetic Fibre Materials, John Wiley and Sons Inc., New York, 1994.
- [20] David Godshall. Production and structure / properties of nylon-6 core / isotactic polypropylene sheath bicomponent fibers suitable for use in carpeting applications. Master thesis, Blacksburg, 1999.
- [21] Yunfeng L, Qiang P. Stearic Acid: Synthesis, Properties and Applications (Chemistry Research and Applications), Nova Science Pub Inc; UK, pp.20, 2014.
- [22] Theng, B. K. G. Formation and properties of clay-polymer complexes; Elsevier: Amsterdam,(14) Theng, B. K. G. Chemistry of clay-organic reactions; Wiley: NewYork, 1974,1979.
- [23] Beyer G. Nanocomposites: a new class of flame retardants for polymers. Plast Addit Compound,4, 22–27,2002.
- [24] McNally T, Murphy WR, Lew CY, Turner RJ, Brennan GP. Polyamide- 12 layered silicate nanocomposites by melt compounding. Polymer; 44, 2761–2772, 2003.
- [25] Solomon MJ, Almusallam AS, Seefeldt KF, Somwangthanaroj A,Varadan P. Rheology of polypropylene/clay hybrid materials. Macromolecules, 34,1864–1872, 2001.
- [26] ASTM D2765 - 01. Standard Test Methods for Determination of Gel Content and Swell Ratio of Crosslinked Ethylene Plastics. ASTM International, West Conshohocken, PA, 2001.
- [27] Wunderlich, B. Macromolecular Physics (Vol. 3: Crystal Melting), 2nd ed.; Publisher: Academic Press: New York, 1980.
- [28] Cimmino S, Lorenzo ML, Pace E, Silvestre C. Isotactic poly (1-butene)/ hydrogenated oligo (cyclopentadiene) blends: miscibility, morphology, and thermal and mechanical properties. J. Appl. Polym. Sci., 67 (8), 1369–1381, 1998.

-
- [29] Poncot M. Comportement thermomécanique de polymers charges selon different chemin de deformation et traitements thermiques. Thèse de Doctorat INPL, Nancy, 2009.
- [30] Alexander LE. X-Ray diffraction methods in Polymer Science, 2nd Ed.; Publisher: Wiley, New York, 1969.
- [31] Turner JA, Aizlewood JM, Becket DR. Crystalline forms of isotactic polypropylene. Makromol Chem, 75, 134-158, 1964.
- [32] Nam PH, Maiti P, Okamoto M, Kotaka T, Hasegawa N, Usuki A. A hierarchical structure and properties of intercalated polypropylene/clay nanocomposites. Polym, 42, 9633, 2001.
- [33] Samon JM, Schultz JM, Hsiao BS, Wu J, Khot S. Journal of Polymer Science Part B-Polymer Physics. 38,14, 2000.
- [34] Hermans PH, Weidinger A, Quantitative X-ray investigations on the crystallinity of cellulose fibers. A background analysis, J. Appl. Phys. 19, 5, 1948.
- [35] Frederic A, Abdesselam D, Christian G, Jean-Marie Hiver. Characterization of volume strain at large deformation under uniaxial tension in high-density polyethylene. Polymer 47, 4387–4399, 2006.

*Chapter IV Results
and discussions*

The present chapter deals with the results obtained and their discussions. This chapter can be divided on two important sections. The first one focuses on the composites based on the unmodified and modified polypropylene matrix, and the second one deals with composites based on the crosslinked polybutene-1 matrix.

IV.1. Composite based on modified polypropylene matrix/fibers

Polyolefin structure modification and fibers treatment appear as effective methods to provide interesting properties for polymer/short fiber composites. In this view, first the modification of the polypropylene (matrix) by crosslinking reaction using XRX method was studied, in which different concentrations of crosslinking agent were used aiming at optimizing the properties of the crosslinked matrix. Then, the selected crosslinked polypropylene which presents the appropriate structural and mechanical properties (good crystallinity degree, high impact and tensile strength) was filled by short fibers (hollow PET fibers, Polyamide fibers).

IV.1.1. Crosslinking of polypropylene (PP)

IV.1.1.1. Rheological results

1.1. Dynamic rheological analysis (DRA) results

Figure IV.1 displays the torque-time evolution for the neat PP, and the crosslinked PP with different crosslinking agent amount. First, due to the high resistance provided by the solid pellets, an increase in torque is observed. After that, the torque begins to decrease until the point A, which is assigned to the melting point. Beyond the point A (T_A), the torque shows different behavior depending on the crosslinking agent content. For the neat PP, it is observed that the torque remains constant before the appearance of an equilibrium stage (C), which indicates the final viscosity of the polymer. However, the torque of the crosslinked samples presents an increase up to a maximum value T_B (point B), which means that the maximum crosslinking reaction is taking place. Then, a partial reduction of torque is observed related to a partial destruction of the formed network, Then, the torque showing almost constant values (equilibrium torque) but it is still higher than T_A . The T_c values are proportional with the crosslinking agent amount, thus the viscosity of the crosslinked materials increases with increasing of the crosslinking agent concentration.

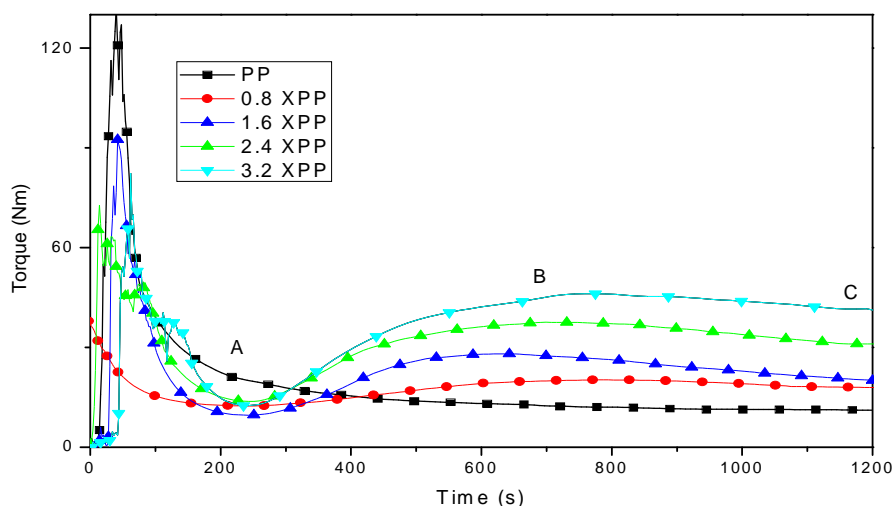


Figure IV.1. Torque-time evolution of the different crosslinked PP

1.2. Melt flow index (MFI) results

Figure IV.2 shows the variation of MFI for the neat PP and the different crosslinked PP materials. It can be seen that the crosslinking agent affects the melt flow of PP, in which, MFI decreases proportionally as function of the crosslinking agent content. Consequently the viscosity of the modified PP increases. The DRA curves are in a good agreement with the obtained MFI of all crosslinked samples.

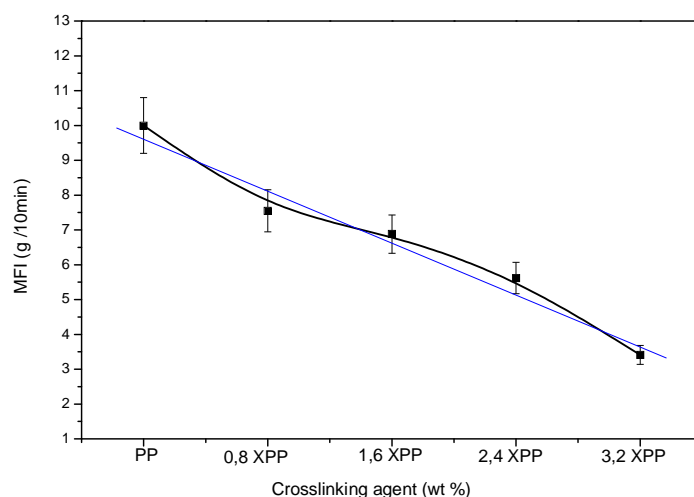


Figure IV.2. Variation of MFI for the crosslinked samples

IV.1.1.2. Gel content test

The effect of the crosslinking agent concentration on the gel content of the crosslinked PP has been also a subject of investigation. The results are displayed in table IV.1. From the obtained results, it is evident that the gel content increased linearly as the crosslinking agent content increased (see figure IV.3). This increase is due to the increasing number of the sulfur bridges and the network structure that leading to high gel products.

Table IV.1. Gel content values of the different crosslinked PP

Crosslinked PP samples	Gel content (%)
0.8 XPP	18.31
1.6 XPP	38.40
2.4 XPP	42.21
3.2 XPP	65.42

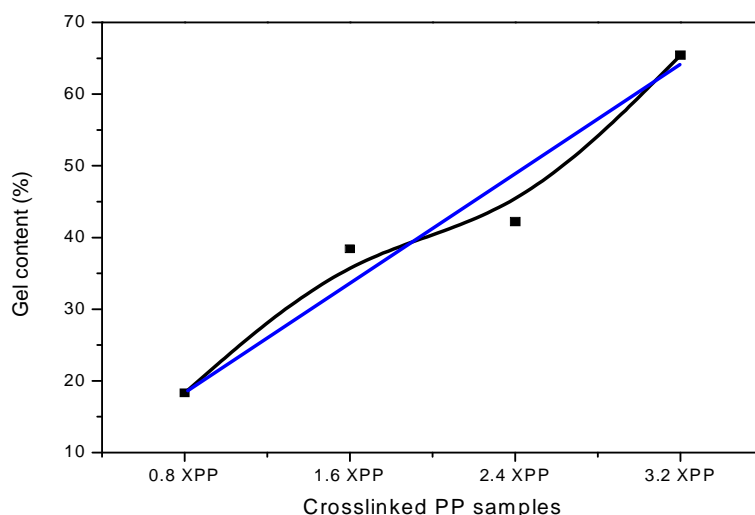


Figure IV.3. Variation of the gel content for the crosslinked samples

IV.1.1.3. Structural study of the modified polypropylene samples

3.1. DSC measurements of crosslinked PP

In order to show the influence of the melt mixing process on the structure of PP. Firstly, DSC measurements of the PP pellet (in his first state) and PP granule (obtained after one mixing cycle

in a brabender) have been compared. The DSC thermograms of both materials are shown in figure IV.4 and the results are collected in table IV.2. The mixed PP (granule) presents an increase in crystallinity degree compared to PP pellet. Accordingly, the PP granule (mixed PP) is taken as reference, because all crosslinked samples go through the same mixing conditions as PP granule.

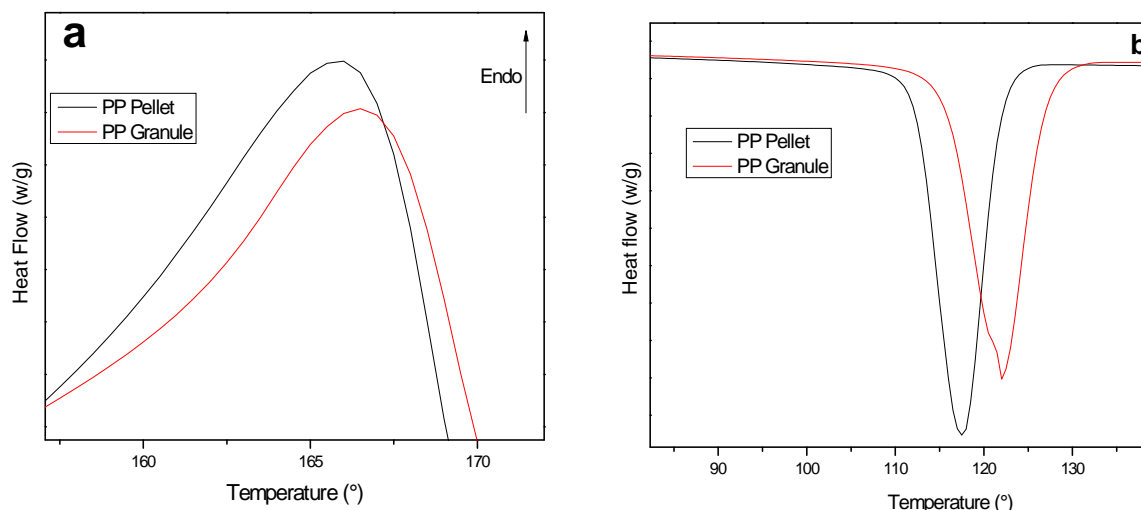


Figure IV.4. DSC thermograms of first heating (a) and cooling (b) runs of PP (pellet and granule).

Table IV.2. DSC parameters of PP (pellet and granule)

Materials	ΔH_m (J/g)	T_m (°C)	ΔH_c (J/g)	T_c (°C)	X (%)
PP Pellet	91	166	89	117	55
PP Granule	106	167	101	122	64

The DSC thermograms of the crosslinked PP samples are shown in figure IV.5 (first and second heating runs) and IV.6 (cooling run). From the obtained DSC parameters (see table IV.3). It can be seen that the melt temperatures of the modified samples decreased slightly with increasing of crosslinking agent content in both heating runs. On the other hand, the crystal lamellar thickness

decreases with the increasing of the crosslinking agent content; this can explain the diminution in the melting temperatures of the crosslinked PP.

Regarding the cooling run, the crystallization temperatures are increased inversely proportional to crosslinking agent concentration compared to the unmodified PP, thus the crosslinking agent act as nucleating agents, which increases the crystallization temperature of PP.

Table IV.3. DSC parameters of the modified PP materials

	First heat			Second heat			Cooling
	T _m (°C)	χ _c (%)	Lc (nm)	T _m (°C)	χ _c (%)	Lc (nm)	T _c (°C)
PP granule	167	64	11.3	165	61	10.8	122
0.8 PP	164	67	10.3	163	61	10.2	129
1.6 PP	162	66	9.5	163	58	9.5	127
2.4 PP	160	66	9	160	60	8.9	125
3.2 PP	158	66	8.4	158	59	8.3	124

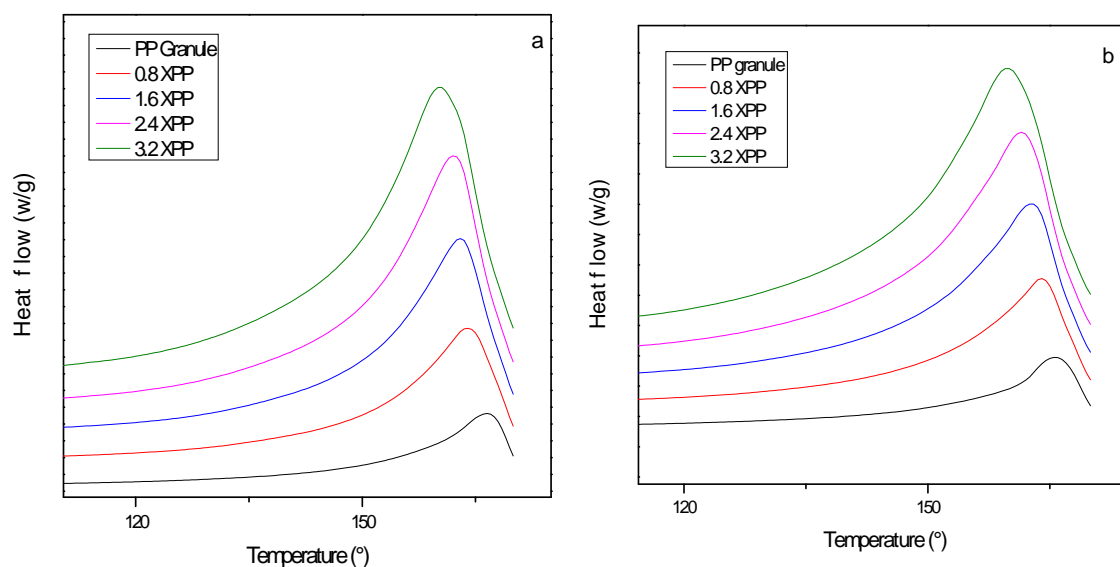


Figure IV.5. First (a) and second (b) heating runs of crosslinked PP samples

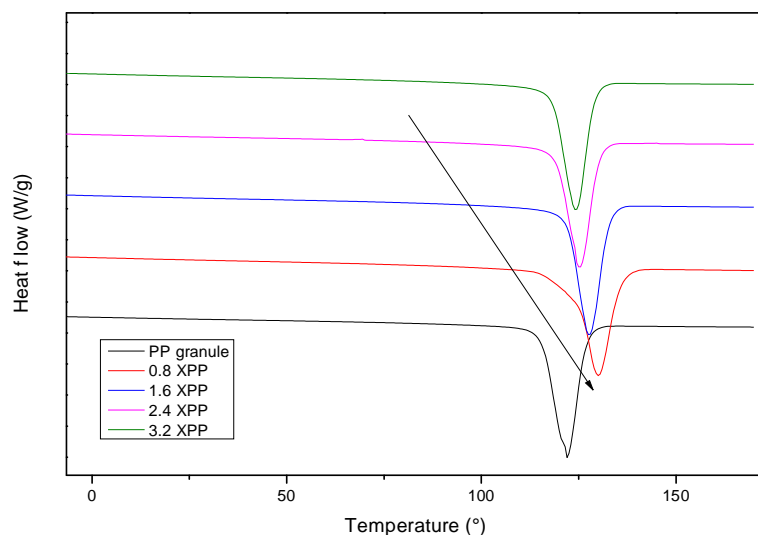


Figure IV.6. Cooling run of crosslinked PP samples

3.2. X-ray diffraction results

Figure IV.7 shows the obtained x-ray diffraction patterns of the different crosslinked samples and the unmodified PP respectively. The WAXS pattern of the neat PP shows the characteristic reflections of the monoclinic α -form of PP. However the WAXS patterns of the crosslinked PP samples exhibit a new intensities reflection of the γ form as is indicated in figure IV.6. Figure IV.8 shows the calculated portion (%) of α and γ forms as a function of the crosslinking agent content. It is clearly observed that the γ form ratio of the modified PP increased with the crosslinking agent content, meanwhile the percentage of α form decreased. According to Bruckner *et al.* [1], the formation of the γ form can be explained by the presence of short chains. It can be concluded that the short chains are produced during the scission of PP chains (reaction with the free radicals produced by peroxide decomposition). Additionally, it was proved by Marigo *et al.* [2,3] that, in the presence of the gamma phase, the thickness of the crystalline layer decreases, This is in consistent with the found crystal lamellar thickness in the DSC study above (see table IV.3).

On the other hand, it was found that the presence of ethylene comonomer enhanced the formation of γ phase [4]. This is supported by FTIR results (see figure IV.9), Bouhelal *et al* [5] confirmed also that the reversible crosslinking of PP gives rise to the generation of ethylenic chains.

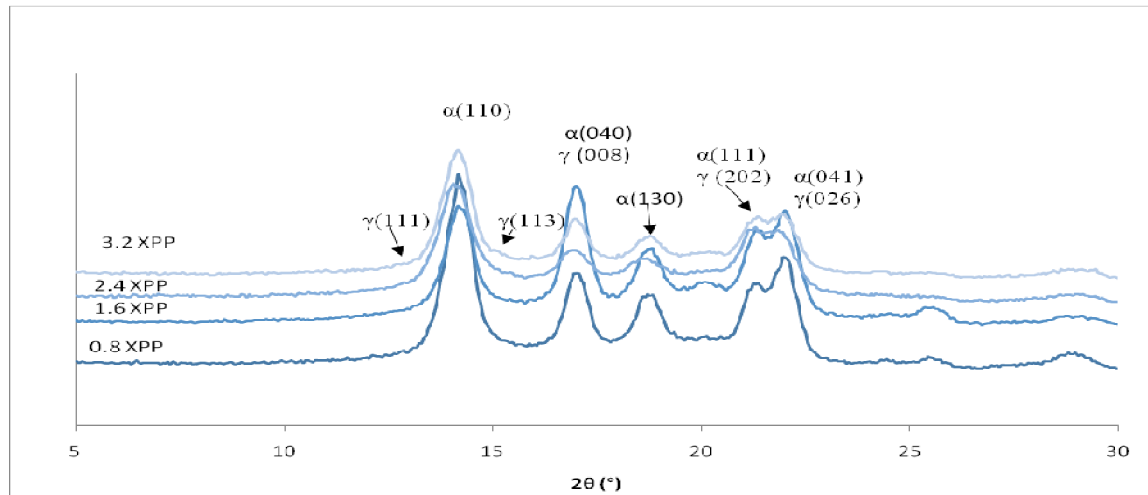


Figure IV.7. WAXS patterns of the different crosslinked PP samples

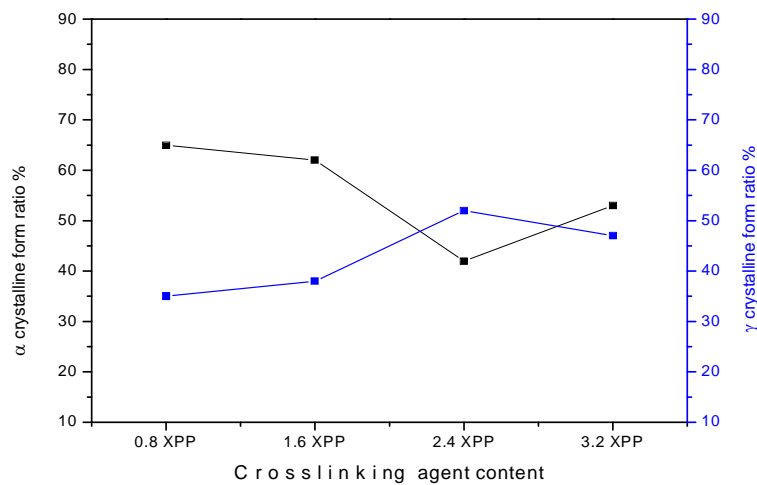


Figure IV.8. α and γ forms portion (%) as a function of the crosslinking agent content

Crystallinity degrees of the different samples are given by the table IV.4. In general, crystallinity degree of the crosslinked samples does not vary except for the ones with 0.8 and 2.4 wt % crosslinking agent in which a noticeable increase in crystallinity is obtained for the first one, and remarkable decrease of the crystallinity is showed for the second one respectively.

Table IV.4. Crystallinity degrees of modified PP materials

Materials	χ (%)
PP	55
0.8 XPP	63
1.6 XPP	58
2.4 XPP	48
3.2 XPP	57

3.3. Fourier transform infrared spectroscopy (FTIR)

Figures IV.9 and 10 (a, b, c) show the FTIR spectra of the crosslinked materials compared with the spectrum of the neat PP. From the figures new characteristic bands are shown in all the crosslinked PP. The band centered at 1745 cm^{-1} is assigned to the stretching vibration peak of the carbonyl group C=O, noteworthy that the intensity of this band increases proportionally with the crosslinking agent concentration, the carbonyl group indicates the scission of the PP chains that occurred through the peroxide decomposition.

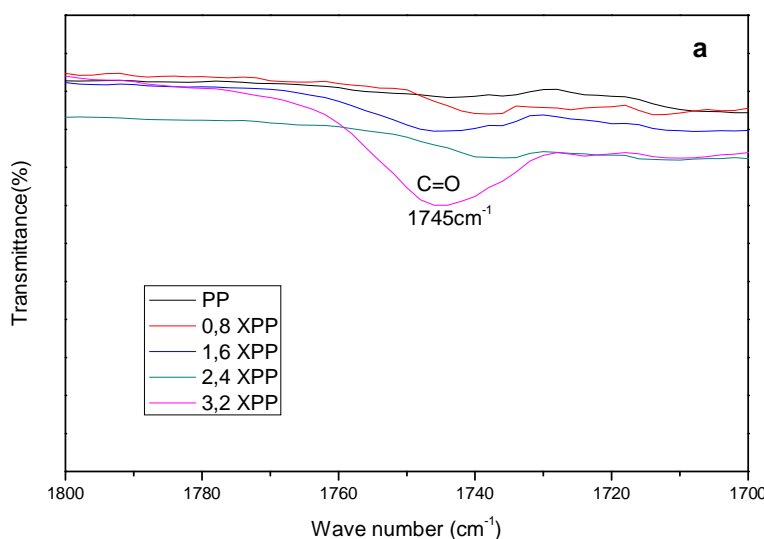


Figure IV.9. FTIR spectra of crosslinked PP samples in the region [$1800\text{-}1700\text{ cm}^{-1}$]

In Figure IV.10b a new weak band is observed in all crosslinked samples at 875 cm^{-1} assigned to the swinging of N-H emerged from the reaction with the accelerator. Figure IV.10c also shows new characteristics bands, for instance, the weak band at 730 cm^{-1} , which is characteristic of the rocking mode of the $(\text{CH}_2)_n$ sequences in ethylenic chains as a consequence of the crosslinking

process. Characteristic weak bands of C-S stretch at 700, 710 and 630 cm^{-1} . Also, new bands around 545 and 500 cm^{-1} assigned to the bonding of disulphide (S-S). Noting that, the bands intensities vary proportionally with the content of crosslinking agent.

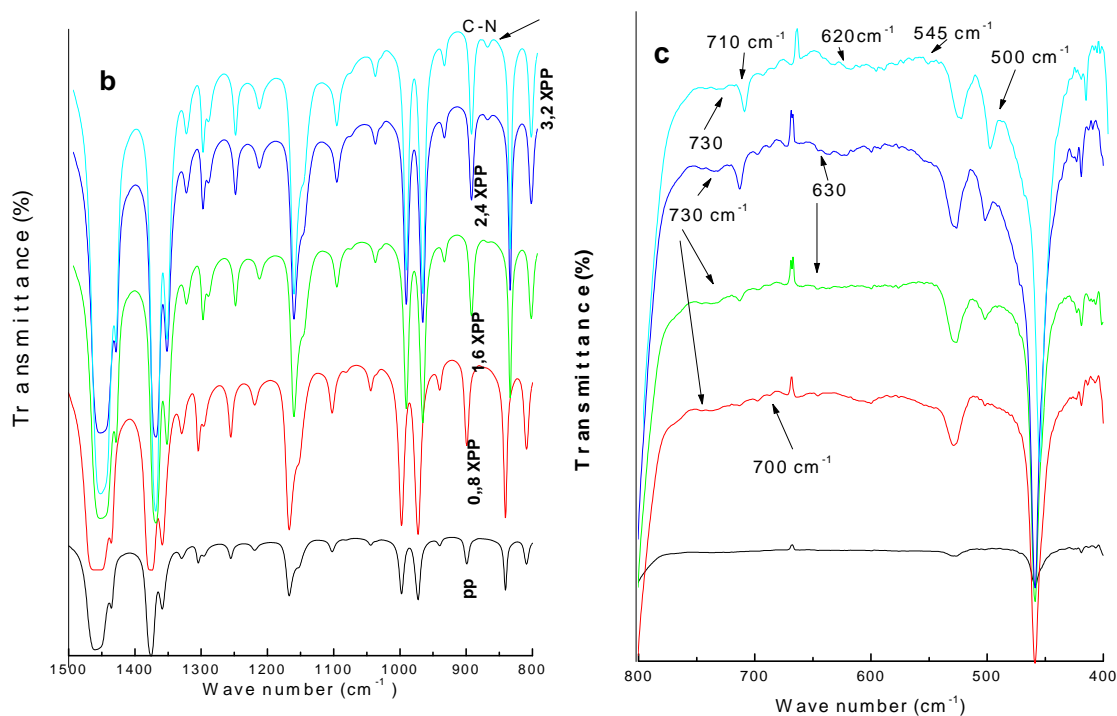


Figure IV.10. FTIR spectra of crosslinked PP samples. **b.** in the region [1500-800 cm^{-1}] **c.** in the region [800-400 cm^{-1}]

Based on the above results, a proposal mechanism of the reversible crosslinking reaction is presented in figure IV.11. The crosslinking process is a homolytic chemical reaction and the principle of the reaction consists in creating macro-radicals through peroxide decomposition process, then stabilizing them by active sulfur groups. The chains are linked by sulfur atoms (coupling reaction), through the formation of a tri-dimensional network. The bridges formed can be: a sulfur atom, a polysulfide $-(\text{S})_n-$, or a cyclic S-compound. Noteworthy that the accelerator increases the sulfur activation. So, the macro-radicals' formation and their coupling reaction with the sulfur originate approximately at the same time, which gives rise to the optimum crosslinking degree.

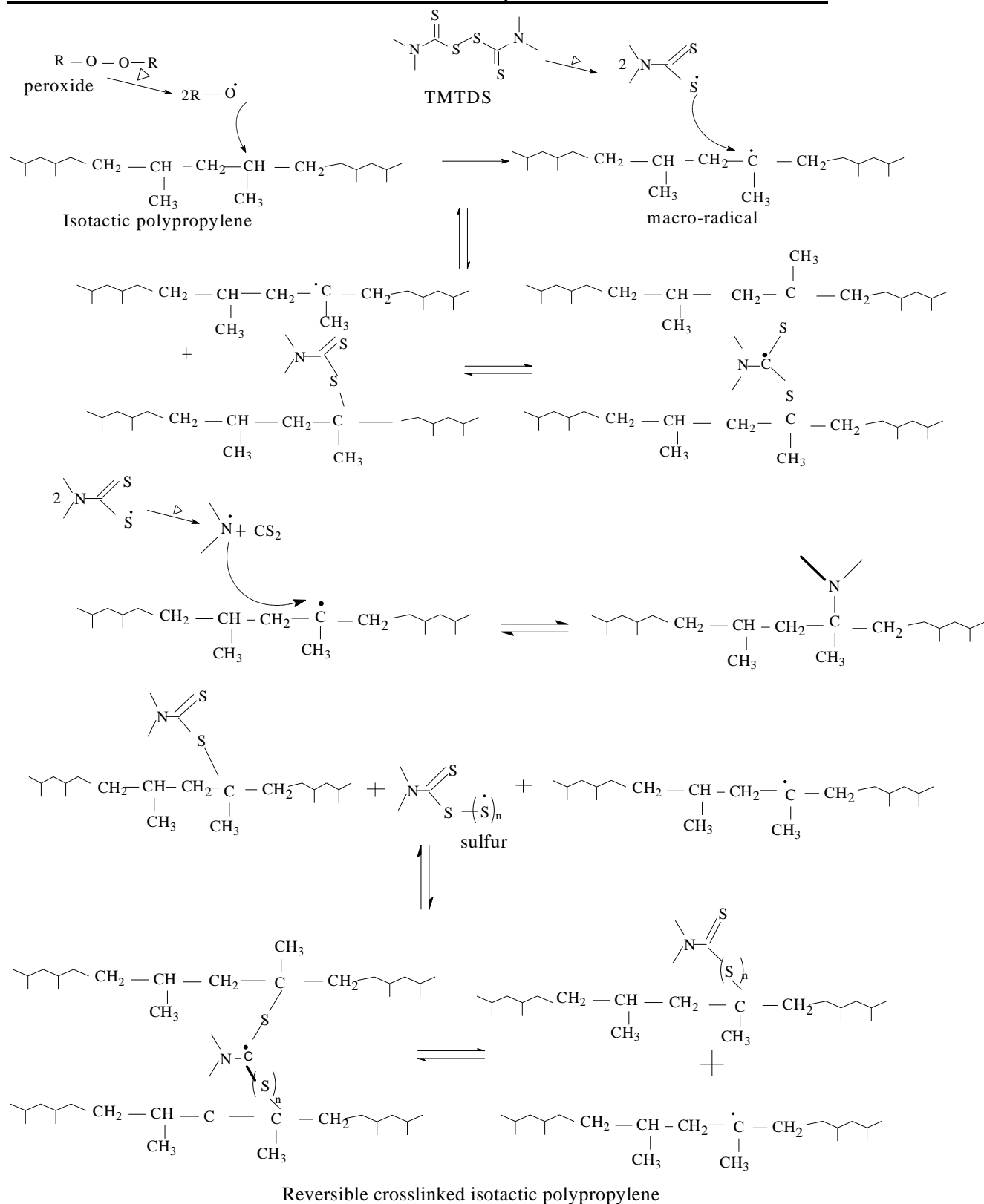


Figure IV.11. Mechanism of the reversible crosslinking reaction of polypropylene

IV.1.1.4. Mechanical study of the modified polypropylene

It is worth noting that the study of the mechanical properties of the crosslinked samples were supervised by Dr. Marc Poncot at Jean Lamour institute, University of Lorraine (Master thesis) [6]. Plates of the modified PP were prepared by molding compression as it has been explained in the experimental section. It has to be noticed that the previous X- ray diffraction test has been done using samples that was taken from the prepared plates.

4.1. 2D-WAXS

Aiming at studying the effect of the compression molding of the prepared plates on the chain orientation of the modified PP, 2D transmission patterns were examined. The 2d-WAXS patterns of the PP, 0.8 XPP and 3.2 X PP are displayed in figure IV.12. The different materials are characterized by a set of concentric circles of different homogeneous intensities. So, it can be concluded that our materials are isotropic and the shaping process does not cause any orientation.

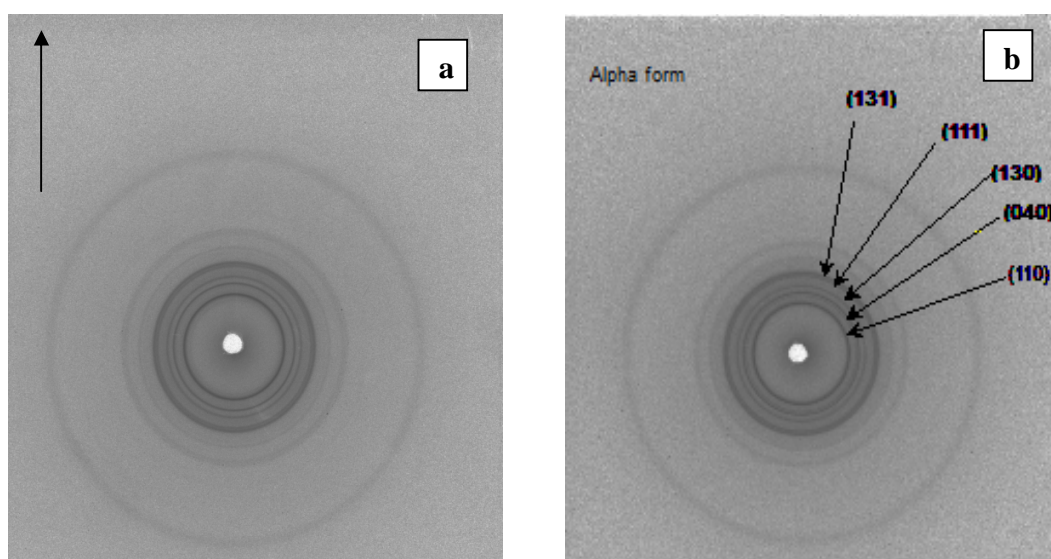


Figure IV.12. 2D WAXS patterns of a) - 0.8 XPP b) - 3.2 XPP

4.2. DMA (Dynamic mechanical analysis)

The results of dynamic mechanical analysis of the modified and unmodified PP materials are shown in figures IV.13.a and b. Figure IV.13.b shows the storage modulus values of the different

samples in the glassy and glass transition regions. It can be observed that the storage modulus values of the samples decrease in the both regions compared to the unmodified PP, except the 2.4 XPP in which the modulus increased by 1214 MPa and 435MPa in the glassy and glass transition regions respectively. 2.4 XPP is the stiffest crosslinked materials.

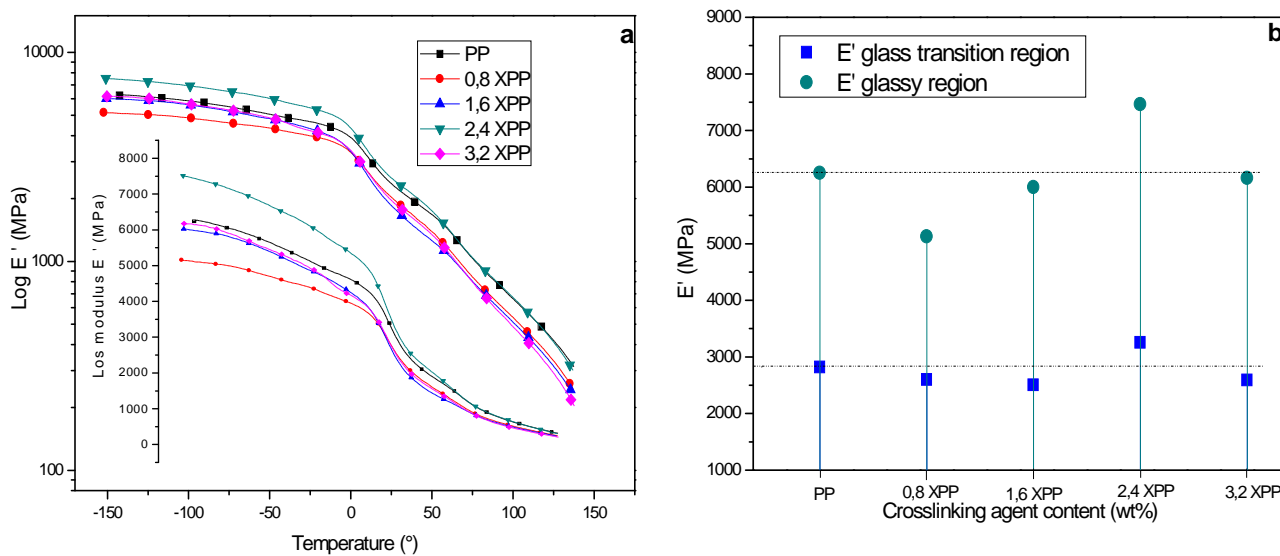


Figure IV.13. Variation of the storage modulus (a) and storage modulus values (b) as a function of temperature for the neat PP and crosslinked PP.

Figure IV.14. shows the variation of the damping factor ($\tan \delta$) as a function of the temperature for all crosslinked samples. The main structural relaxation is the glass transition of the samples, in which the transition temperature can be indicated. The transition temperatures T_g remained nearly unchanged for all crosslinked materials compared to the neat PP.

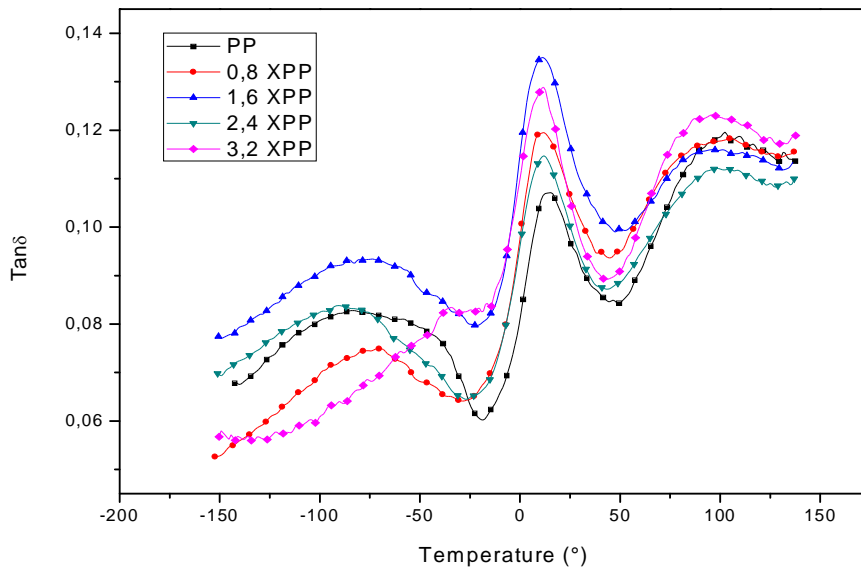


Figure IV.14. Variation of $\tan \delta$ as a function of temperature for the crosslinked PP materials

4.3. True mechanical behavior

Figure IV.15 shows the evolution of true stress versus true strain, for the crosslinked samples. In general it can be said that the tensile curves of the crosslinked PP present a similar shape to that of neat PP until the plastic plateau. For instance all materials show the same viscoelastic region from $\varepsilon = 0$ to $\varepsilon = 0.14$. Then, the plastic plateau of the materials begin at $\varepsilon = 0.2$. From 0.2 to 0.4 for 1.6 XPP, from 0.16 to 0.4 for 2.4 XPP and from 0.2 to 0.4 for 3.2 XPP. Noting that, the 0.8 XPP depicts a particular behavior with the smallest value of the strain at break.

The last region corresponds to the plastic hardening of the materials, in which it can be observed that strain-hardening takes place at large strain level. During this stage, the true stress versus true strain curves vary differently. From the obtained curves it is found that a significant increase in the toughness is found for the crosslinked materials compared to the unmodified PP. 3.2XPP reveals the highest toughness value which is presented by the maximum values of strain and stress at break $\varepsilon_b = 2.27$ and $\sigma_b = 74$ MPa respectively, followed by the 2.4 XPP with $\varepsilon_b = 2.11$ and $\sigma_b = 90$ MPa then, 1.6 XPP with $\varepsilon_b = 1.8$ and $\sigma_b = 75$ MPa. The table IV.5 summarizes the obtained mechanical parameters of the neat PP and crosslinked materials. It can be seen that the

Young modulus slightly increased in all the crosslinked samples except the 3.2 XPP, which present the lowest modulus value of 1338 MPa. It is noteworthy that 2.4XPP shows the highest Modulus value (E= 1675 MPa). In addition, the tensile curves denote that the yield stress slightly decreases for the cross-linked PP samples in comparison with the unmodified PP.

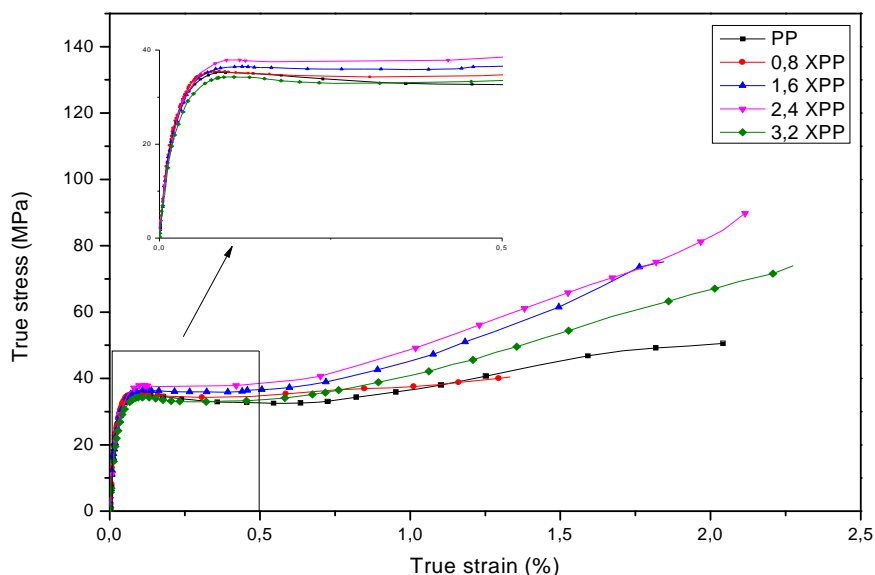


Figure. IV.15. True tensile behavior of the crosslinked samples

Table IV.5. Mechanical parameter of the cosslinked PP samples

Materials	E (MPa)	σ_b (MPa)	ϵ_b (%)
PP	1511	50.5	2.04
0.8 XPP	1563	40,4	1.3
1.6 XPP	1644	75.2	1.8
2.4 XPP	1675	90	2.1
3.2 XPP	1338	74	2.2

4.4.Impact strength

Figure IV.16 shows the variation of the Izod impact strength for the neat polypropylene as well as the different crosslinked samples. The high crosslinking agent content improved the resilience of the PP significantly. This improvement can be ascribed to the formed network which enhance the efficiency of the neat PP and absorb the required energy to stop the crack propagation.

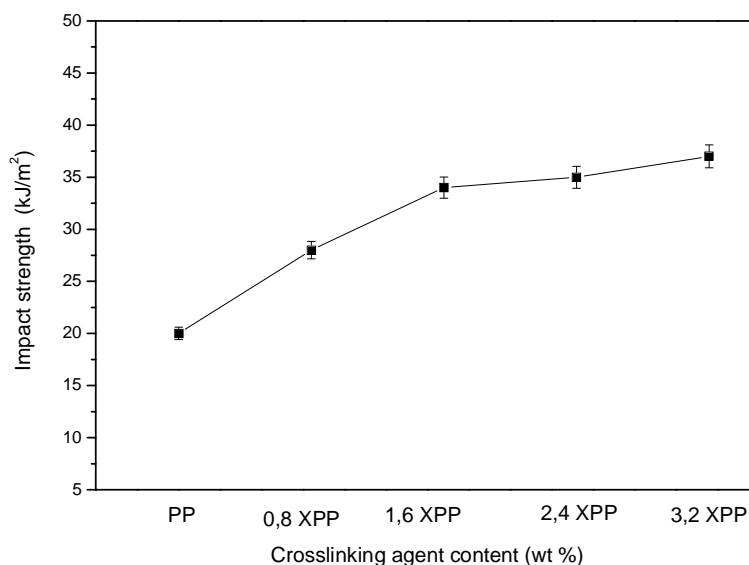


Figure IV.16. Variation of Izod impact strength for the crosslinked PP materials.

It is worth noting that DSC measurements of the samples taken from plates were carried out, with view of showing the effect of shaping on the microstructure of the crosslinked samples, however almost DSC parameters were identical as those obtained in the DSC study of granules mixed samples (see table IV.3).

IV.1.1.5. General Conclusions

From the obtained results, it can be concluded that:

- 1- The entire crosslinking agent in different content gave rise to the formation of a network (S-S and C-S bonds); the crosslinking reaction is affected by the crosslinking agent amount.
- 2- γ form has been generated from the crosslinking reaction (2.4 XPP showed the highest γ ratio).
- 3- 3-2.4 XPP presented the high modulus in both DMA and tensile tests.
- 4- The 1.6XPP, 2.4 XPP and 3.2 XPP samples shows ductile structures.

Based on these conclusions, the 1.6XPP has been selected as matrix for the forthcoming composites, because it presents intermediate properties between those of the 2.4XPP and 3.2 XPP. For instance, 1.6 XPP shows less γ ration (short chains), good crystallinity degree, almost the same mechanical properties as 2.4 XPP and 3.2 XPP.

IV.1.2. Crosslinked PP matrix/short fiber composite

IV.1.2.1. Crosslinked PP/short hollow PET fiber composite

A. Influence of the Matrix modification

A.1. Study of unmodified PP/short hollow PET fibers composite

1.2. Rheological properties of composites

2.1. DRA results

For the Dynamic Rheological Analysis, Figure IV.17 illustrates a typical Torque /time evolution of the PP/ hollow r-PETfs composites and compared with the neat PP matrix. As seen in Figure IV.17, the curves represent an abrupt rapid increase in torque, that due to the high resistance provided by the solid pellets. Beyond this point, the torque begins to decrease once the matrix has been completely melted; the torque reduced rapidly to the much lower steady state values, where it remains constant before the appearance of an equilibrium stage, value that is mentioned the stabilization torque value. A stable torque is an indicator of homogenization of fiber in the melt and final viscosity of melt composites [7]. When the stable torque values were compared, it was clearly seen that the incorporation of fibers was accompanied by decrease in the stable torque values with time for all composites compared to the neat PP. The decreases in torque values indicate that the loading of r-PETfs decreased the viscosity of PP that can be explained by the weak interactions between the fibers and the matrix [8]. The 10 wt% PETfs loading shows the lowest torque value in its stabilization stage, this is due to the agglomeration of fibers additionally to the weak adhesion between the fibers and PP. The gaps between the fibers and PP are shown on SEM observations. On the contrary, the MFI test which was done after the grinding of the formulations showed an increase of the viscosity that can be explained by the better dispersion of the fibers under the pressure during MFI test.

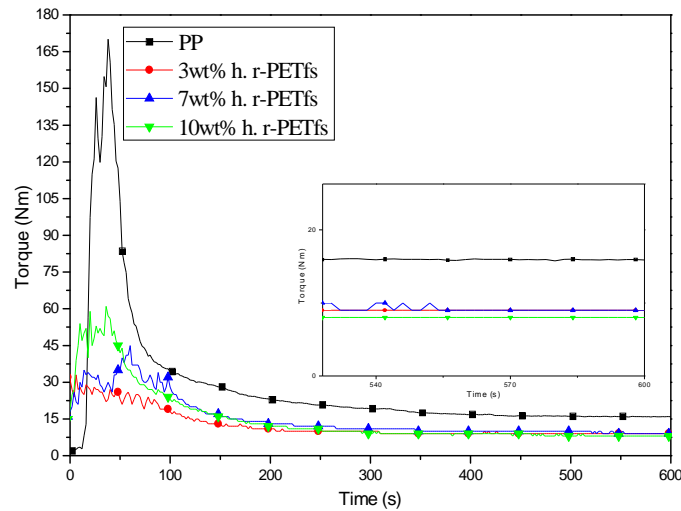


Figure IV.17. Torque vs time data of neat PP and PP/h.r-PETfs composites

2.2. MFI results

Figure IV.18 displays the MFI results of different PP/ hollow r-PETfs composites, the results show a linear decrease of MFI depending on the content of PET fibers, subsequently; the viscosity of different composites was increased compared to the neat PP.

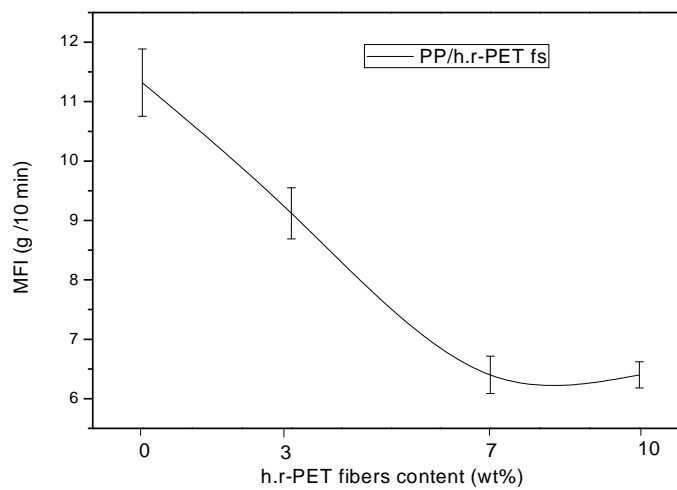


Figure IV.18. MFI of composites in function of different loading of r-PETfs

1.3. Mechanical Properties

The mechanical properties of composites suffered some variations in relation to neat PP, and the results of tests, in terms of Young's modulus, elongation at break, stress at break, strain at break and the impact strength are presented in Figures IV.19-21. Three samples with different PET fibers loading (0%, 3%, 7%, and 10%) were tested. From Figure IV.19 a significant increase in Young's modulus was found when hollow PET fibers loading are added. The young's modulus of composites increases proportionally with PET fibers loading. Accordingly, hollow r-PET fibers can be a good reinforcement candidate for high performance PP composites. Figure IV.19 shows also the results of the elongation at break measurements. The elongations at break drastically decreased after the hollow PET fibers were introduced in PP. This behavior is typical for fiber reinforced composites with weak interactions between the filler and the matrix. The values of strain and stress at break are reported in Figure IV.20. The strain at break highly decreases whereas the stress at break slightly increases for 3 and 7 PET fiber wt%. This result can be ascribed to the insufficient adhesion between the two polymer phases.

Figure IV.21 shows the variation of the Izod impact strength of the PP/ hollow r-PET fibers composites as a function of the fibers loading. In general, the impact strength of the composites decreases by adding PET fiber. Impact strength is an indication of tolerability for sudden force where the composite is subjected to rapid crack propagation through the material [9, 10]. The crack propagation is initiated through fibers agglomeration in different composites. In addition, PET fibers/ PP interactions are not strong enough to absorb the required energy to stop the crack propagation [10]. SEM micrographs shown in Figure IV.27 (a, b) prove the presence of voids between the fibers and the matrix.

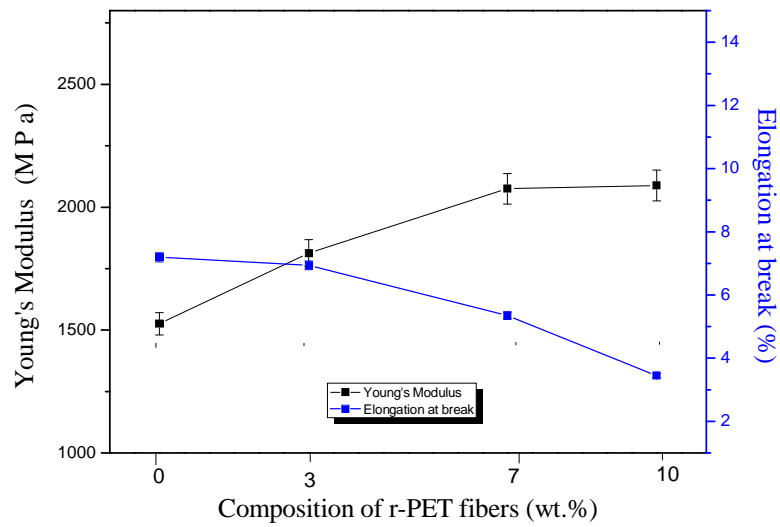


Figure IV.19. Variation of the Young's modulus and elongation at break for PP/ hollow r-PETfs (wt %) composites.

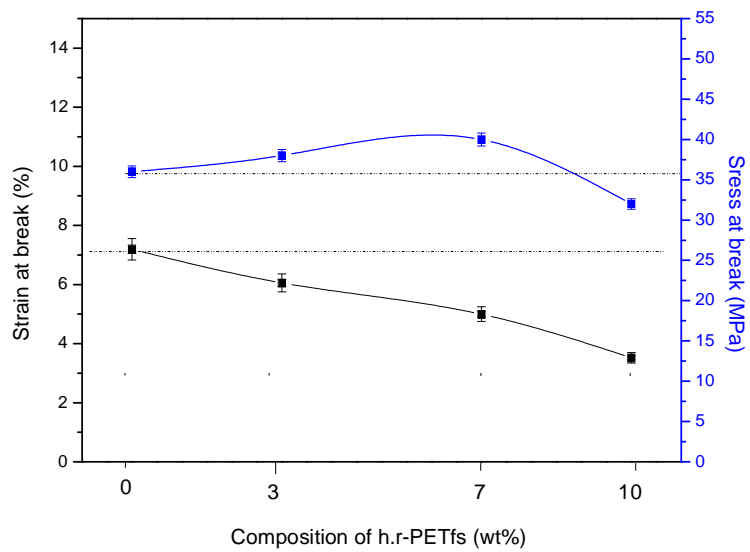


Figure IV.20. Strain and stress at break of PP/ hollow r-PETfs (wt %) composites.

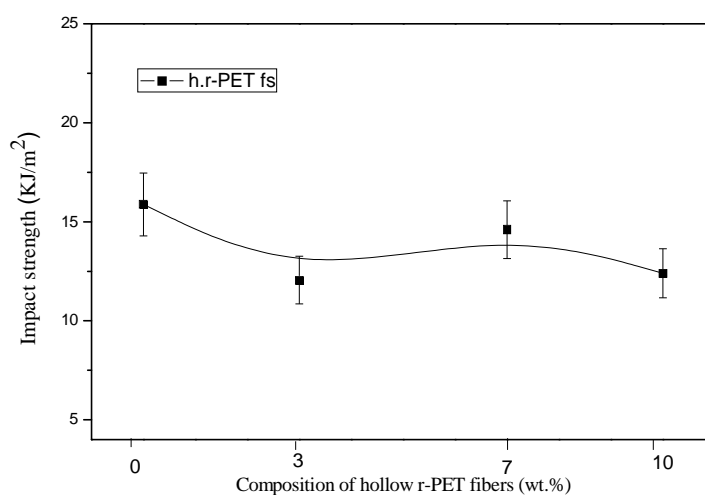


Figure IV.21. Variation of the impact strength for PP/ hollow r-PETfs (wt %) composites.

1.4. Microstructural study of the composites

4.1. Wide-angle scattering (WAXS) method

The structure of PP/ h.r-PETfs composites was evaluated by a wide-angle X-ray scattering method. From the shown patterns in Figure IV.22, it exists obvious α form peaks of PP in all patterns, which can be indexed as (110) at 2θ ($^{\circ}$) = 14.07, (040) at 16.84, (130) at 18.5, (111) at 21.11 and (041) at 21.8 and (060), (220) at about 25.3 and 28.5 respectively. No additional diffraction peaks observed in the WAXS patterns. In addition, the crystallinity degree of the different composites seems to be constant (see table IV.6). Hence, the incorporation of PET fibers does not affect the PP structure. This result is consistent with DSC results.

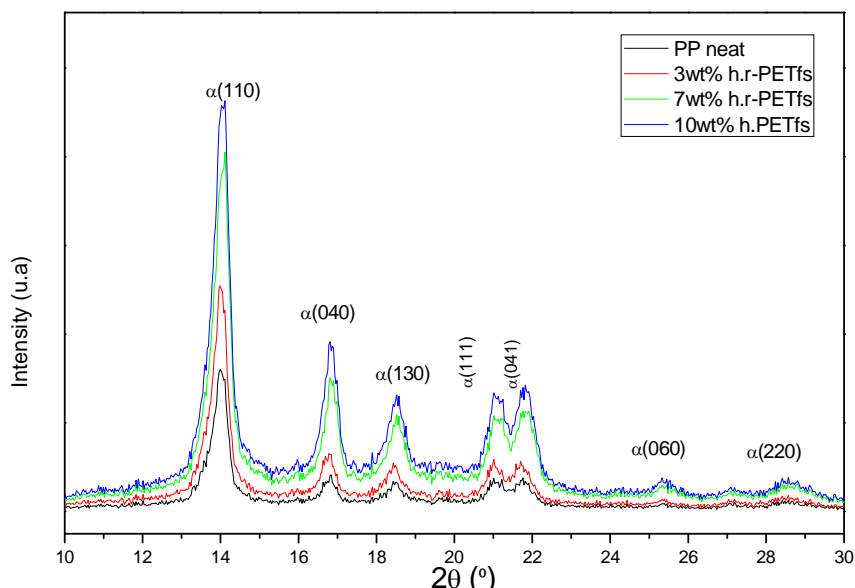


Figure IV.22. WAXS patterns of composites in different loading of r-PETfs

4.2. DSC Analysis

Figures IV.23 and IV.24 display the DSC thermographs of PP/ h.r-PETfs, and the results are collected in Table IV.6. The displayed DSC curves correspond to the second heating cycle. It is worth noting that the crystallite sizes will give the same value because the melting temperatures are almost the same for all composites (L_c DSC = 11). Results of DSC experiments gave evidence that the temperatures of melting, crystallization and crystallinity degree (χ_c) seem to be relatively constant for the different PP/ h.r-PETfs composites in comparison with the neat PP. Indeed hollow PET fibers did not act as nucleating agents.

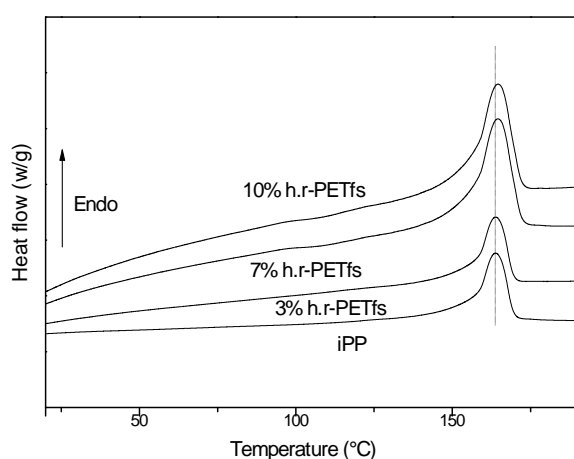


Figure IV.23. Thermograms of the second heating cycle of composites

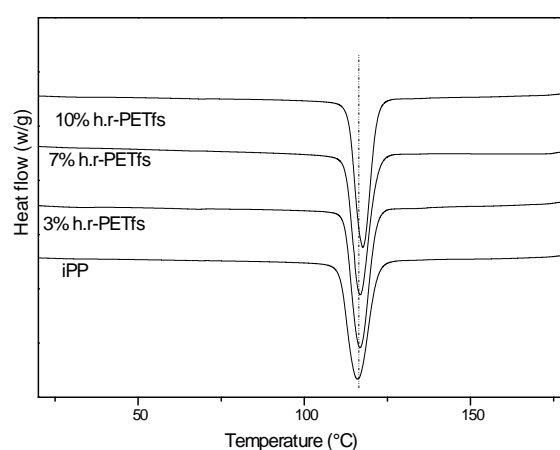


Figure IV.24. Thermograms of the cooling cycle of composites.

Table IV.6. Melting (T_m), crystallization temperatures (T_c) and enthalpies (ΔH_m , ΔH_c) for different samples and crystallinity degree (χ_c) obtained by DSC and WAXS.

Sample	T_c (°C)	T_m (°C)	ΔH_c (J/g)	ΔH_m (J/g)	χ_c^{DSC} (%)	χ_c^{Drx} (%)
iPP	117	165	100	98	59	44
iPP/3 wt%	116	166	101	100	61	44
iPP/7 wt%	118	165	98	91	62	45
iPP/10 wt%	118	165	98	90	61	45

4.3. Optical microscopy observations

Optical microphotographs of PP / 7wt % h.r-PETfs composites of polished plate and film surface are shown in figures IV.25 and IV.26 respectively. The micrographs showed a good dispersed fibers, which embedded in PP matrix. In addition some agglomeration as pointed in black circle were observed (figure IV.26). Length reduction of fibers was noticed that can be explained by the effect of the intense shearing involved in closed chamber of the brabender.

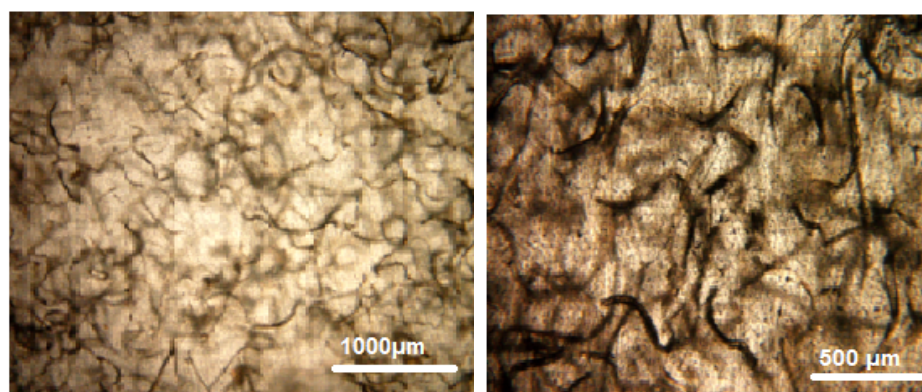


Figure IV.25. Optical microscopic images of polished plaques surface of 7wt% h.r-PETfs reinforced PP composite

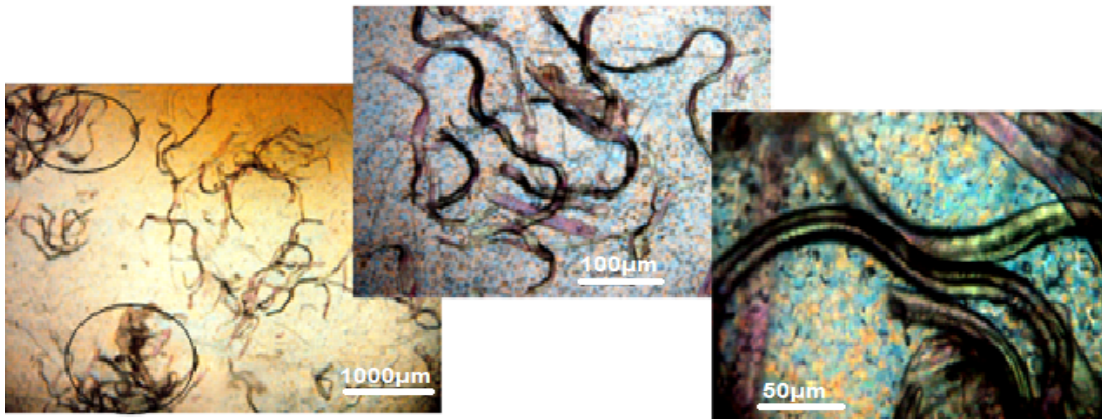


Figure IV.26.Optical microscopic images of films surface of 7wt% h.r-PETfs reinforced PP composites.

4.4. SEM Observation

The SEM micrographs of 7 wt % h.r-PETfs reinforced PP composite are shown in figure IV.27. Figure IV.27 (c, d) shows some gaps between the fibers and matrix, in which h.r-PETfs /PP debonding were shown at fiber ends and along fiber lengths indicating a very limited adhesion between PP and hollow fibers. Also, folding and bending of fibers were shown in figure IV.27(c, d, e, f), that could be explained by the flexible aspect of hollow PET fibers. Hollow fibers damage was clearly seen in figure (g, h), Von Turkovich and Erwin, 1983[11], Fu *et al.*, 1999 [12] reported the major reasons of fiber damage where they included the fiber contact with equipment surfaces as one of the reasons, which represented by palstograph's chamber in this present study. Based on SEM micrographs, we can conclude that the fiber/matrix debonding and the fiber damage caused the reduction on the mechanical properties as discussed above.

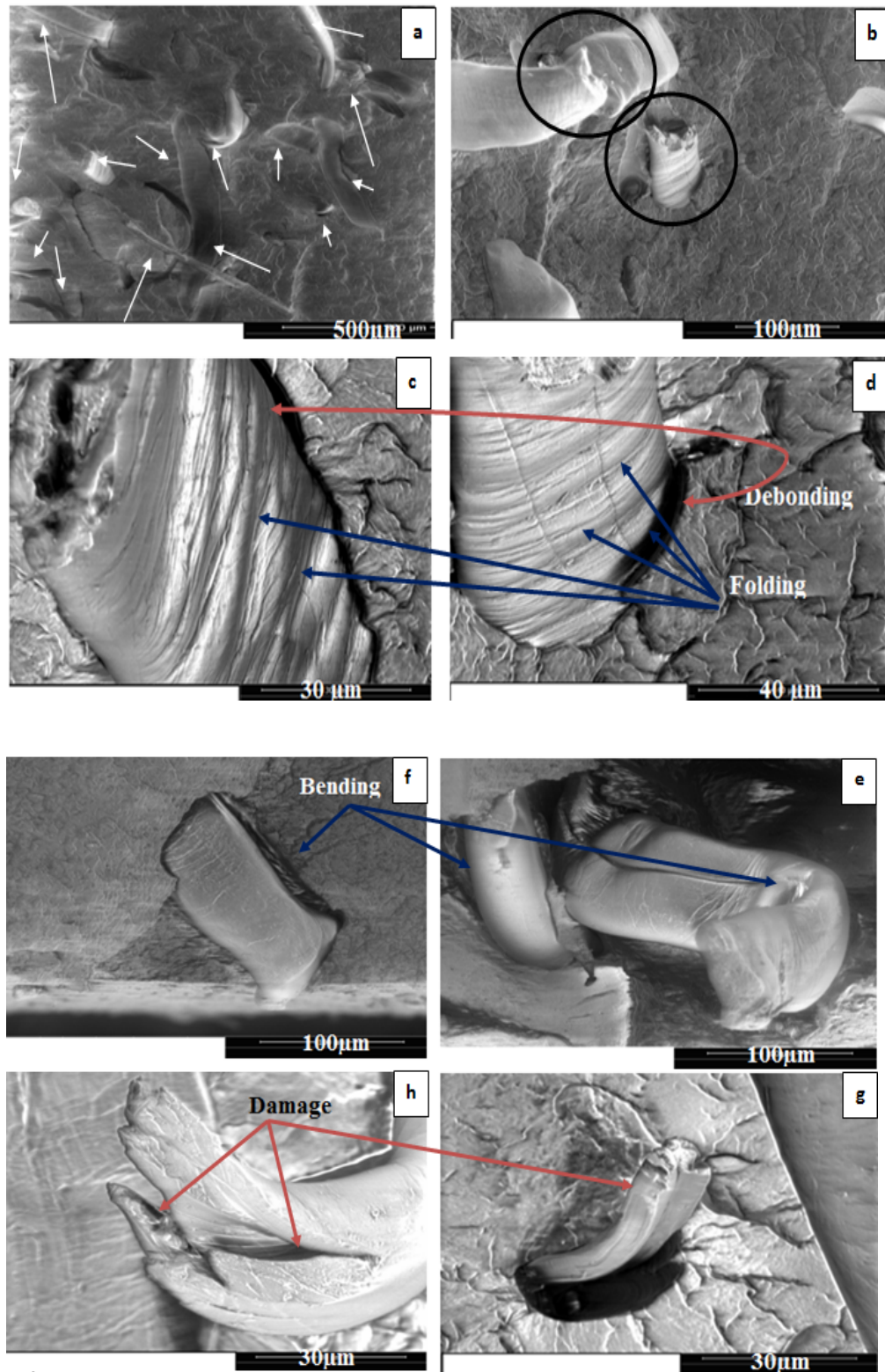


Figure IV.27. (a,b,c,d,e,f,g,h). SEM micrographs of the fractured surface of composite with 7wt%h.r-PETfs.

4.5. Synchrotron X-ray tomography (SRXTM)

Internal damage in PP/7wt%h.r-PETfs composite was observed by in situ tensile test under x-ray tomography based on synchrotron radiation. A tensile testing sample was performed to investigate the fracture process during the tensile test. The images obtained under tensile loading showed a good performance of the sample stage, in which the matrix deformation and h.r-PETfs fibers damage could be observed. In the tomography-slice images taken at the maximum stress just before the final fracture, the detachment matrix-fiber (a), matrix cracks (b), hollow fiber pull-out (c), fiber damage (d) and the hollow fiber flexibility (e) could be clearly observed as presented in figure IV.28.

The in situ tensile test allowed the observation of the growth of such defects under tensile loading. The observation revealed that the matrix was broken by propagation of the matrix cracks which might be caused by stress concentration at the ends of the short fibers as shown in Figure IV.29. In addition, the tomography-slice images showed in figure IV.28 (d, e) confirmed the flexible aspect of hollow fiber in which the elongation of fiber under tensile loading it was clearly observed. These observations are in agreement with those observed in SEM micrographs of the composite fractured surface.

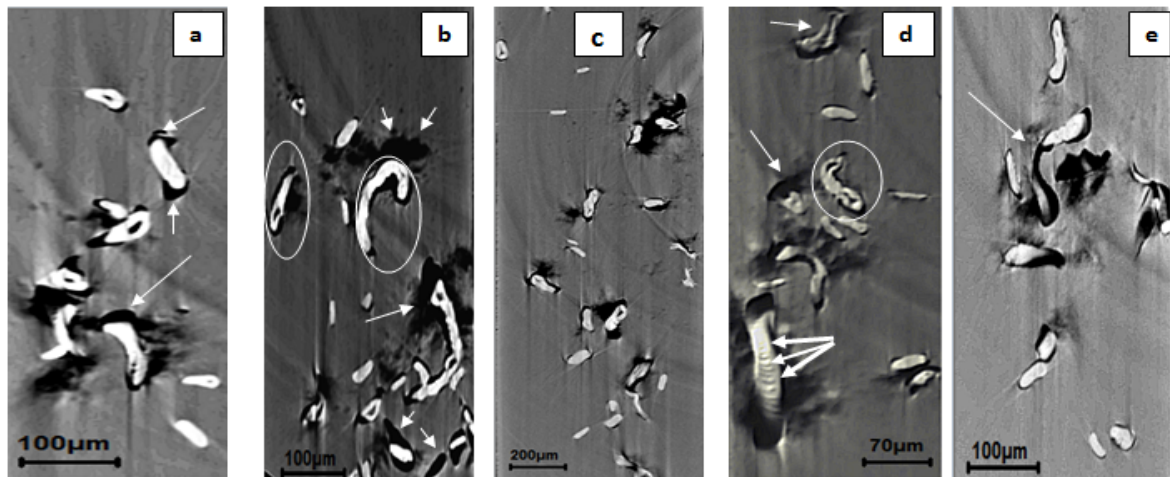


Figure IV.28. In situ tensile tomography -slice images showing different kinds of damage

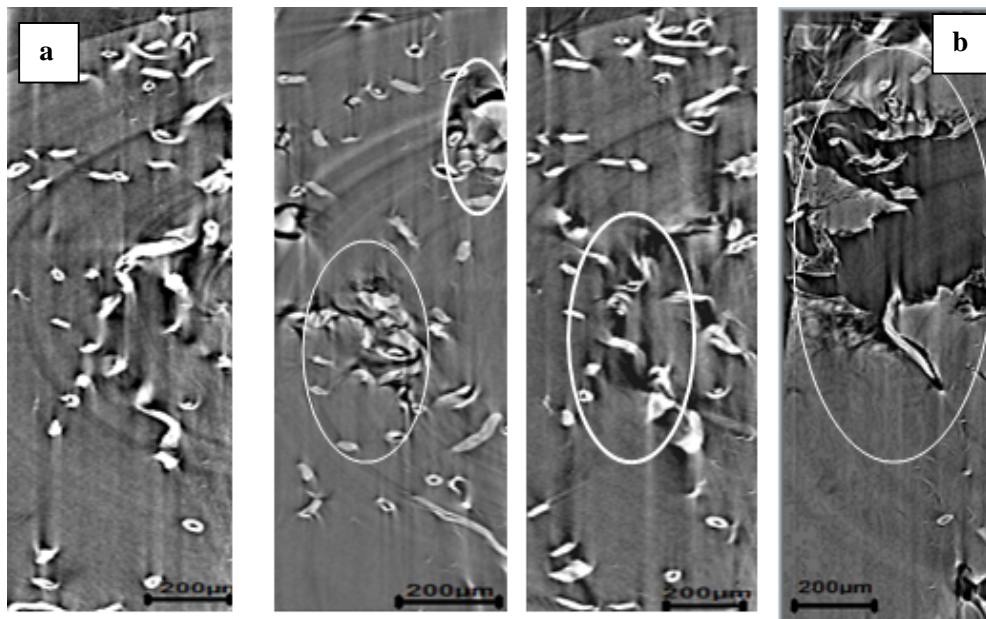


Figure IV.29. In situ tensile tomography -slice images of PP/ 7 wt% h.r-PETfs composite before loading (a) and after fracture (b).

4.6. Dynamic mechanical analysis (DMA)

Figure IV.30 shows the variation of composites' storage modulus as a function of temperature. According to this figure, an enhancement in the storage modulus (in the glassy and transition regions) with 7wt % h.r-PETfs loading was observed; this is in agreement with the Young's modulus obtained. Daiane *et al.* [13] reported that when the filler loading increased, the stress is more constantly dispersed, and therefore the storage modulus will be improved. However, the addition of 10 wt % h.r-PETfs loading shows a decrease in the storage modulus which can be ascribed to the agglomeration of fibers which increase the voids volume between the fiber and the matrix, and subsequently a decrease in the mechanical properties. Additionally, the flexible aspect (folding and bending of fibers) of 7wt % h.r-PETfs loading that has been shown on the morphological observations led also to enhance the stiffness of the composites.

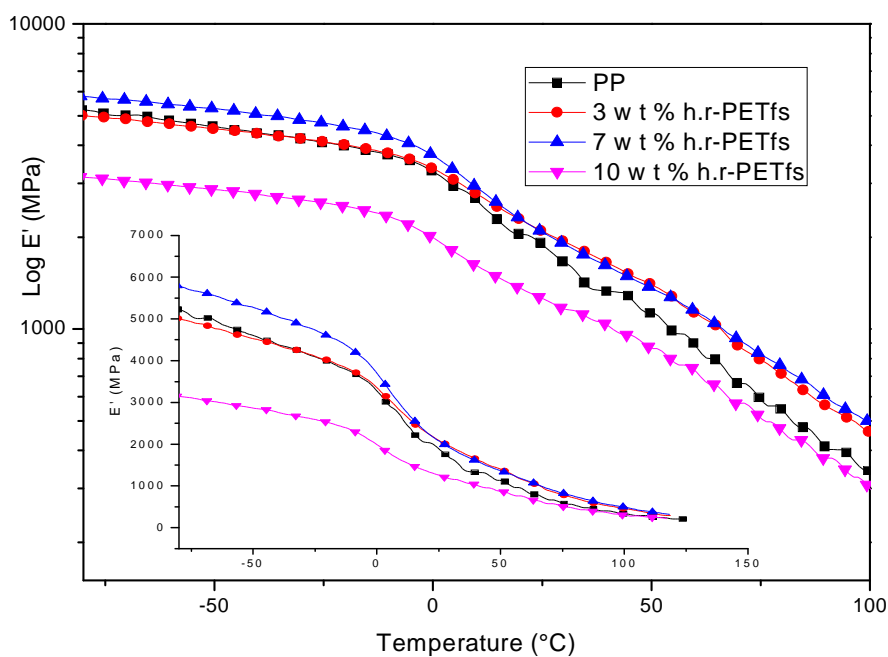


Figure IV.30. Modulus (E') curves of composites PP/h. r-PETfs composites as a function of temperature.

The tan delta as a function of temperature curves for all composites are reported in figure IV.31. The maxima in these curves correspond to the structural relaxation in the composites (glass transition of the composites) and its temperature corresponds to their T_g values. The glass transition temperatures of the composites are almost the same as that of the neat PP, accordingly, the presence of PET fiber in PP matrix does not affect the molecular mobility of PP chains; this can be attributed to the weak interactions between the PP and PET fiber. Tan delta peaks of the composites exhibit a lower value compared to the PP and this is mainly due to a restriction in the movement of the chains matrix [14].

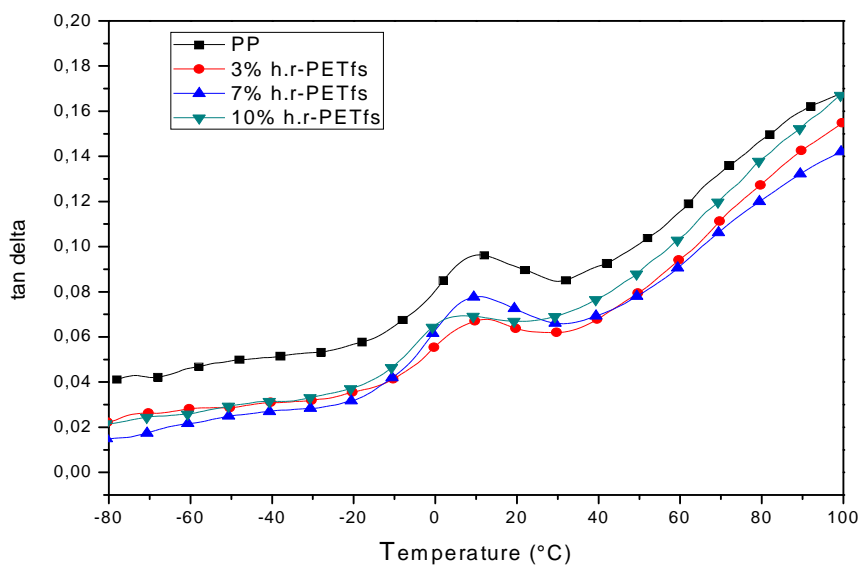


Figure IV.31. Tan delta curves of PP/h. r-PETfs composites as a function of temperature.

A.1.2. Conclusion

From the study of unmodified PP/ short hollow recycled PET fiber composites, it can be concluded that the recycled PET fibers can be efficient reinforcements of PP, showing an improvement in the stiffness of PP composites (high Young's modulus) due to their flexible aspect. However, a weak adhesion between PET fibers and PP matrix has been shown. To overcome this problem, modifications of PP matrix and/or fiber treatment are needed. Proposal treatments are presented in the forthcoming studies. It has to be noticed that 7 wt% hollow PET fibers has shown the better mechanical behavior.

A.2. Study of crosslinked PP/ short hollow PET fibers composite

2.1. Rheological properties

1.1. DRA measurement

Figure IV.32 displays the dynamic rheological analysis of the crosslinked PP matrix reinforced with 3, 7 and 10 wt% h.r-PET fibers. Beyond the melt point, the torque vs time evolution of the different composites was increased in function of the hollow fibers loading. This can be explained by two main reasons. The first one is the reversibly crosslinking reaction of the PP

matrix which increases the torque. The second reason is the fibers loading that gave rise to the viscosity of the composites. Indeed, a good dispersion of fibers it could be confirmed.

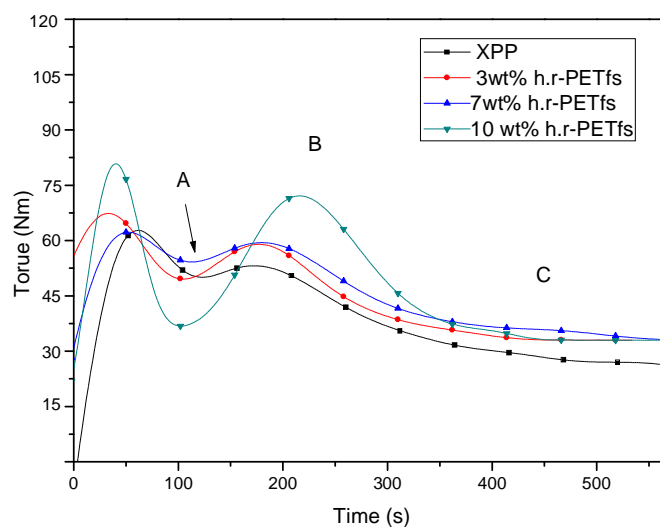


Figure IV.32. Dynamic rheological analysis of crosslinked PP/h.r-PETfs (wt %) composites

1.2. MFI Results

MFI measurements of different crosslinked PP/ r-PETfs composites are reported in Figure IV.33. The obtained results are in good agreement with the DRA discussion. As it is expected the MFI decreases with the addition of hollow fiber. This decrease is relative to the neat PP and the crosslinked PP, though, is much lower at high fiber loading. This can be simply explained by the increase of the viscosity of the composites based on the crosslinked PP matrix.

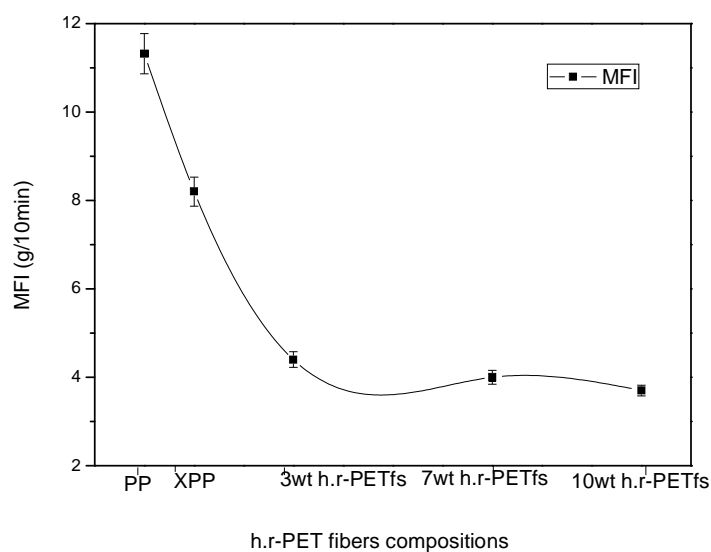


Figure IV.33. MFI measurement of crosslinked PP/h.r-PET fibers (wt %) composites

2.2. Mechanical properties

2.2.1. Tensile strength

The mechanical behavior of the different composites is showed in figures IV.34- 36. Figure IV.34 presents the Young's modulus of different hollow recycled PET fibers (3, 7 and 10 wt. %) reinforced crosslinked PP matrix and neat matrix. As expected, an increase in Young's modulus is observed for all composites. Compared to hollow fiber reinforcing neat PP matrix, it is found that crosslinked PP filled by different hollow fiber loading composites gave the most important young's modulus values. Consequently, the reversibly crosslinking reaction enhanced the interactions between PET fibers and crosslinked PP matrix. SEM observation of crosslinked PP/ Hollow PET fibers proved the enhancement of the adhesion in the case of the modified PP/PET fibers composite (see figure IV.43).

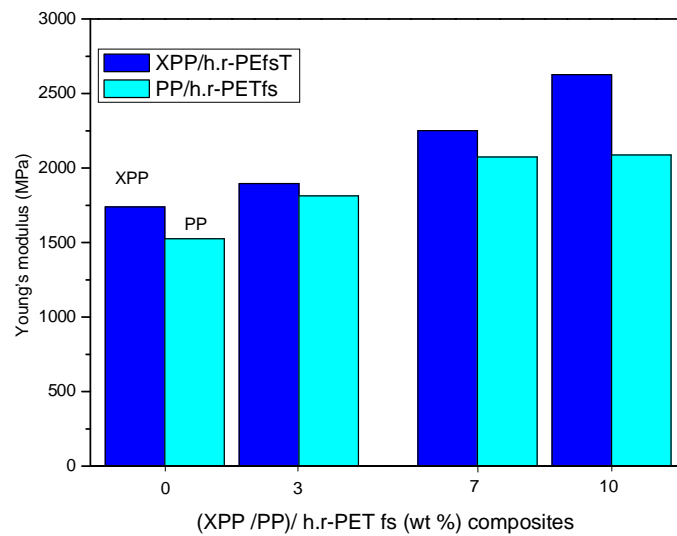


Figure IV.34. Young's Modulus of h.r-PET fibers (wt %) reinforcing (XPP/PP) matrices

The variation of the stress and strain at break of the PP/PET fiber and XPP/PET fiber composites as a function of the fiber content is shown in Figure IV.35. The modified PP matrix affects both the stress and the strain at break of composites compared to the neat PP matrix. From Figure IV.35 either the crosslinked or unmodified PP/PET fiber composites show an increase of the stress at break. On the other hand, the strain at break of the crosslinked matrix /PET fiber composites presents a significant increase compared to the composite based on neat PP matrix; whereas it slightly decreased compared to the crosslinked PP. the results proved that the modification of the PP matrix enhances the compatibility between the crosslinked PP and the PET fiber derived from the existence of polar groups in the chemical structure of the PET fiber and the modified PP by crosslinking.

Analogously, an improvement of elongation at break can be noticed in Figure IV.36, for crosslinked PP/PET fiber composites.

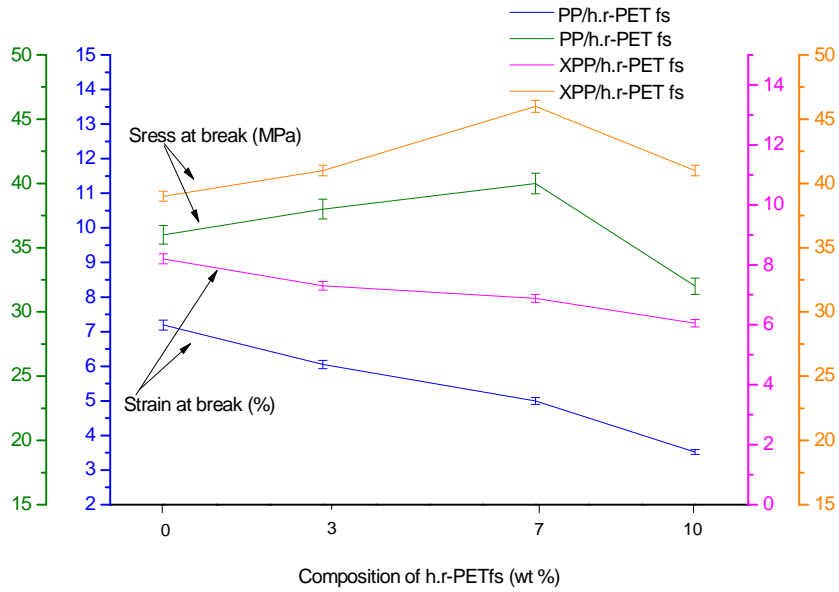


Figure IV.35. Stress and strain at break of (unmodified/modified PP) /h.r-PET fibers (wt %) composites.

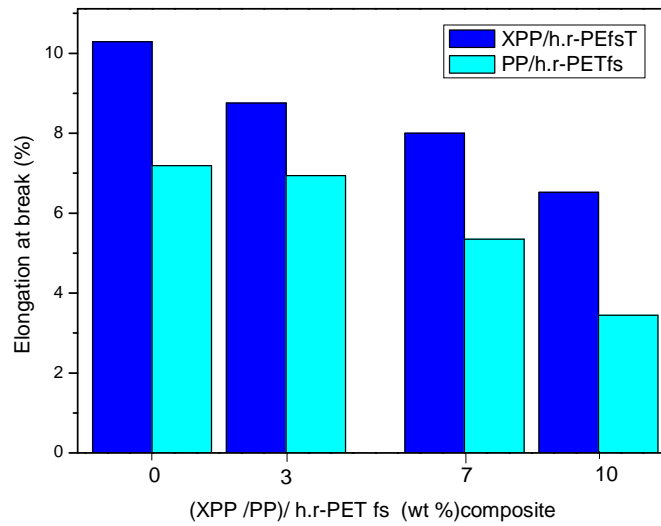


Figure IV.36. Elongation at break of (unmodified/modified PP) /h.r-PET fibers (wt %) composites.

2.2.2. Izod impact strength

Figure IV.37 shows the variation of the Izod impact strength for the crosslinked PP matrix reinforced with 3, 7 and 10 wt % recycled hollow PET fiber composites. In general, the impact strength of the composites does not vary by adding PET fiber except for 7 wt % PET fiber in which a noticeable increase in resilience is found. This trend can be ascribed to the agglomeration of the PET fibers in the crosslinked PP matrix and this seems better dispersed in the composite containing 7 wt % of PET fibers. Noteworthy that the resilience of the modified PP/PET fiber composite shows an enhancement compared to the composite based on unmodified PP matrix.

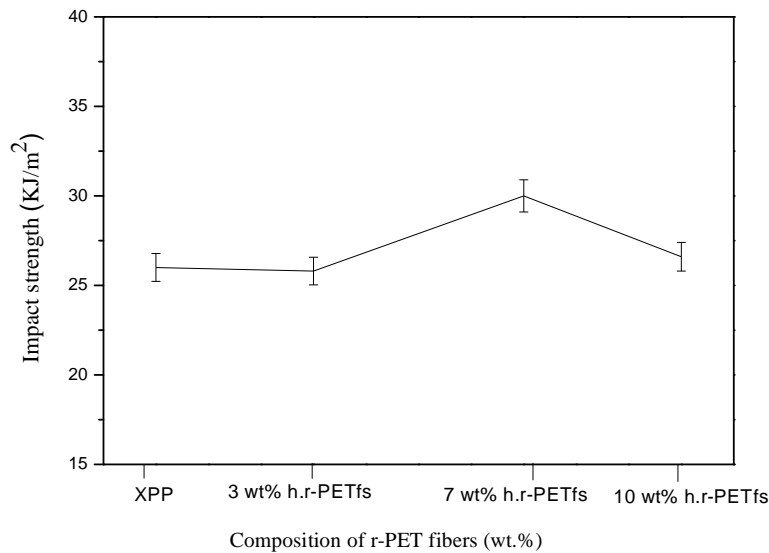


Figure IV.37. Izod impact strength of crosslinked PP/PET fibers composites.

2.2.3. Dynamic mechanical analysis (DMA)

The results of the dynamic mechanical analysis are shown figure IV.38, and IV.39. Figure IV.38 shows a slight increase in the storage modulus in the glassy and glass transition regions for the crosslinked PP/h.r-PETfs composites compared with the crosslinked PP. The higher storage modulus is shown in 7wt% h.r-PETfs loading. This enhancement is due to the restriction imposed by the fibers on the matrix, which increases the stress transfer at the fiber interface.

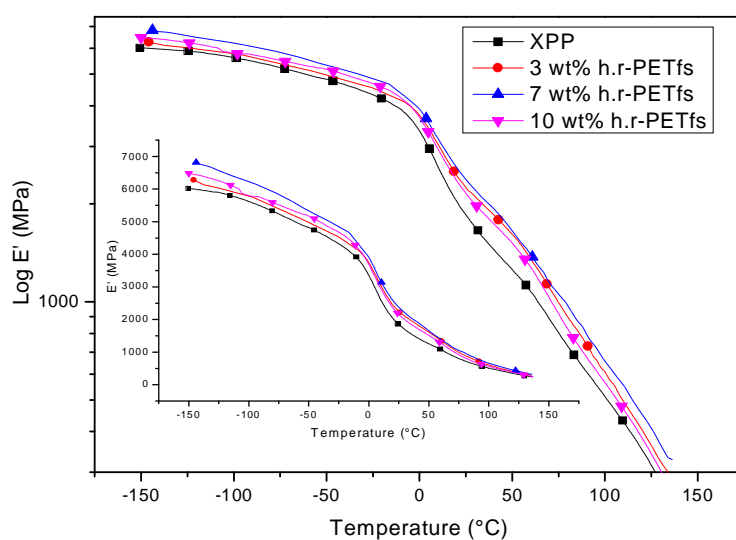


Figure. IV.38. Variation of the storage modulus as a function of temperature for crosslinked PP/hollow PET fiber composites

The tan delta curves for crosslinked PP/h.r.-PETfs composites are shown in figure. IV.39. With the addition of fibers, the tan delta peak is lowered due to greater restriction in the movement of the polymer chain caused by the presence of stiff fibers [15]. According to Pothan *et al.* [16], composites with a strong fiber–matrix adhesion tend to store more energy than the composites with poor interface bonding, i.e. greater damping indicates weaker interfacial adhesion. In Figure IV.38, the increase in fiber content showed a slight decrease in the tan delta peak because of the good interface between PET fiber and the crosslinked PP. The glass transition temperature obtained from the tan delta curve of composites did not show a clear trend. Thus, the introduction of fibers showed more influence on the tan delta peak than in the measured glass transition temperature.

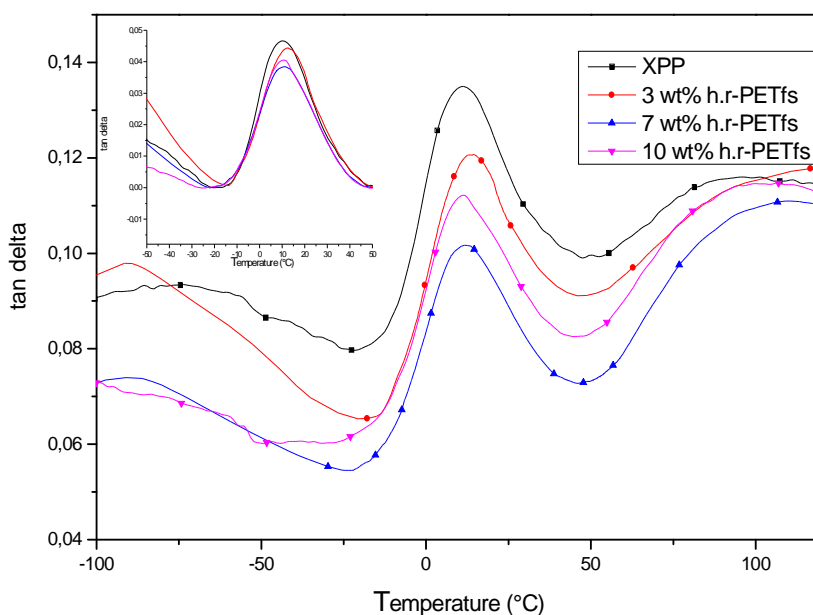


Figure. IV.39. Variation of the tan delta as a function of temperature for crosslinked PP/ hollow PET fiber composites

2.3. Structural properties

2.3.1. X-ray diffraction Results

Figure. IV.40. shows the WAXS patterns of PP, XPP and XPP/ (3, 7 and 10wt %) PET fibers. The pattern of neat PP shows 7 main peaks, in the 2θ range of $10-30^\circ$, characteristic of the monoclinic α -form. The WAXS patterns of the crosslinked PP and XPP/PET fiber composites appear additional new weak peaks at 16.2 and 20.1 (2θ) which are characteristic of the (300) plane of PP β -crystalline form and the (130) or (117) planes of the γ -crystalline respectively. It is worth noting that the β -crystalline form was not shown in the previous study of the crosslinked PP (Figure. IV.7) however it was indicated in the study of the crosslinking polypropylene conducted by Bouhelal *et al* [5]; this difference may be caused by the reversibly crosslinking reaction of the crosslinked PP. The degree of crystallinity (χ_c), X_β and X_γ are collected in the table IV.7.

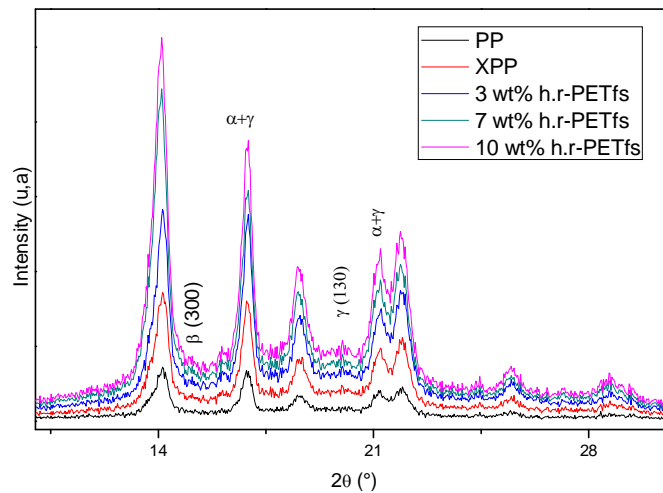


Figure. IV.40.WAXS patterns of crosslinked PP/h.r-PET fibers composites

The crosslinked PP matrix shows a slight decrease in the crystallinity degree compared to the unmodified PP. Nevertheless, the crystallinity degree of the crosslinked PP/PET fibers composites increased slightly compared to the crosslinked matrix , but it seem to be constant in comparaison with the neat PP. It is noted that the γ -form is more pronounced than the β form in all composites.

Table IV.7. WAXS measurements: (χ_c^{WAXS}), X_β of β form and X_γ of the γ -form.

Materials	χ_β (%)	χ_γ (%)	χ_c^{WAXS} (%)
PP	-	-	44
XPP	0.01	0.32	42
3wt% h.r-PETfs	0.015	0.42	47
7wt% h.r-PETfs	0.017	0.45	46
10wt% h.r-PETfs	0.017	0.45	45

2.3.2. DSC results

The main results of the DSC tests are presented in Table IV.8. The DSC thermograms corresponding to the heating and cooling runs of crosslinked PP/ h.r-PETfs composites are shown in Figures. IV.41 and 42. Accordingly, the results demonstrate that the reinforcing fibers did not significantly affect the melting temperature of the crosslinked PP matrix. On the other hand, and it has been shown in the WAXS results that an increase in the crystallinity degree of composites is noticed, which is clearly significant in 3 and 7 wt% h.r-PET fibers. Additionally, the crystallization temperature indicates a significant increasing in all composites; this increase could be related to fibers acting as nucleating agents.

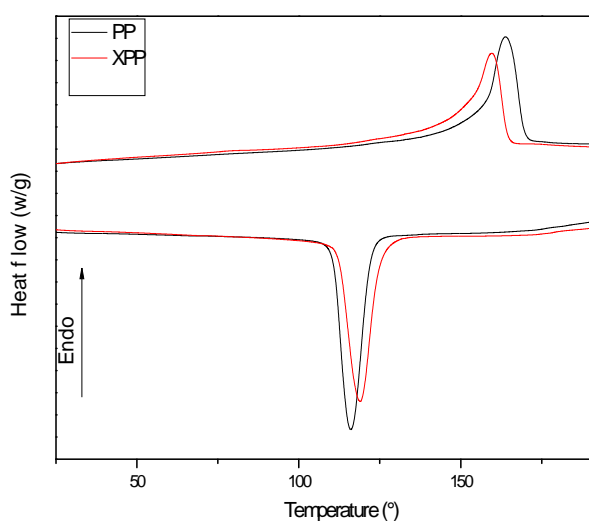


Figure. IV.41. Heating and cooling runs of unmodified and modified PP.

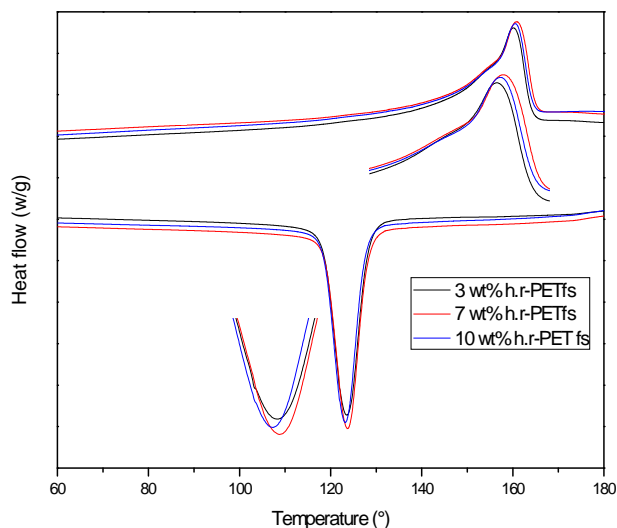


Figure. IV.42. Heating and cooling runs of crosslinked PP/h.r-PETfs (wt%) composites.

Table IV.8. Melting (T_m), crystallization temperatures (T_c) and enthalpies (ΔH_m , ΔH_c) for different samples and crystallinity degree (χ_c) obtained by DSC.

Materials	ΔH_m (J/g)	T_m (°C)	ΔH_c (J/g)	T_c (°C)	χ_c (%)
PP	98	165	100	117	59
XPP	86	160	101	119	52
3% pet	92	160	99	123	66
7% pet	85	161	99	123	63
10% pet	84	161	96	123	59

2.3.3. Optical and scanning electron microscopy

Figure IV.43.a and b show SEM and optical micrographs of crosslinked PP/ 7wt% h.r-PET fiber respectively. The dispersion of the PET fibers in crosslinked matrix was assessed by optical microscopy, the figure IV.43b clearly shows a good dispersion of PET fiber in the matrix, also and as it was shown in unmodified PP/PET fiber composite (see figure IV.25), a reduction in PET fiber length was noticed.

The interface between PET fiber and crosslinked PP matrix was examined by SEM microscopy of cryo-fractured specimens. SEM micrograph shows an enhancement of adhesion between PET fiber and the modified PP compared to the SEM micrographs that have been shown in figure IV.27 of the neat PP/PET fiber composite. Therefore, an improvement of the mechanical properties was found, in fact this would not be possible if the adhesion of the PET fiber to the crosslinked PP is not sufficiently good.

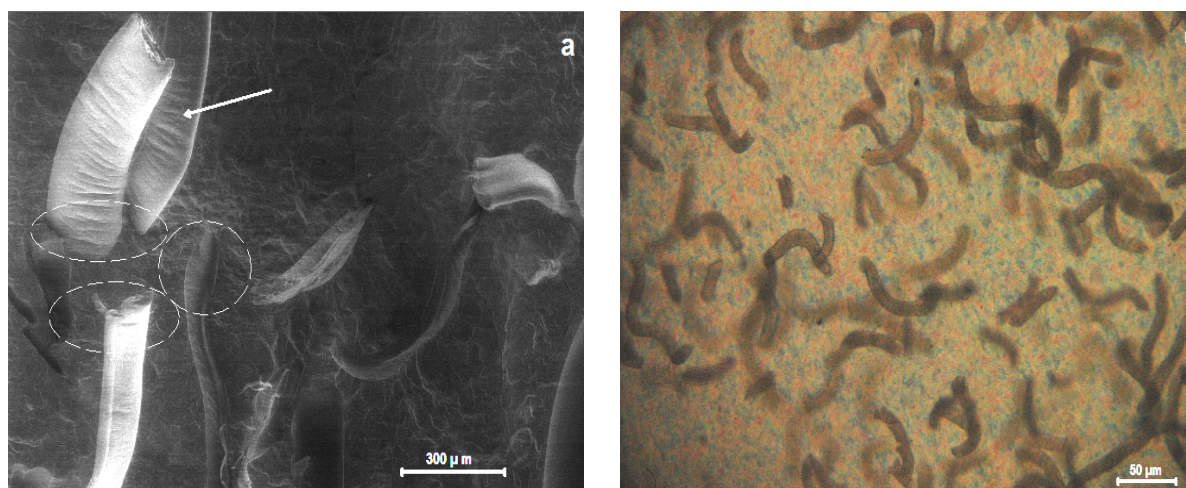


Figure. IV.43.a. SEM micrograph of 7wt% h.r-PET fiber/crosslinked PP composite **b.** optical image of 7wt% h.r-PET fiber/crosslinked PP composite.

A.2.2. Conclusion

According to the obtained results it could be concluded that the presence of hollow r-PETfs in the crosslinked PP increase relatively the mechanical properties, also an improvement of the stiffness of composites was showed. In addition, we can say that the modification of PP by crosslinking is an efficient way to increase the adhesion between the PP and hollow fibers which give rise to attractive properties of composites. Additionally, 7wt% hollow PET fiber reinforced crosslinked PP showed the optimum mechanical properties. So, the effect of the fiber surface treatment on the modified and unmodified matrix has been carried out on 7wt% hollow PET fiber only.

B- Influence of the PET fiber treatment

1. Fourier transform infrared (FTIR)

Figure. IV.44 displays the spectra of the different composites based on unmodified and crosslinked PP filled with untreated and treated PET fiber. It is shown that all composites present new bands associated with the PET fiber. For instance, the band at 1720 cm^{-1} which is attributed to the ester carbonyl bond stretching, the weak beak at 1090 cm^{-1} related to the methylene group, and the band at 725 cm^{-1} attributed to aromatic bands of PET fiber.

According to the spectrum of the crosslinked PP, it can be shown that both crosslinked PP filled by treated and untreated PET fiber present additional peaks that are related to the crosslinking reaction such as the peaks situated at 1700,875 and 730 cm^{-1} which are attributed to the carbonyl group C=O resulting from the reaction between the peroxide and PP (see the study of the crosslinked PP above figure IV.9), swinging of N-H (reaction with the accelerator), and C-S stretch respectively. The strong intensities showed in the spectrum of composites reinforced with the treated PET fiber could prove the effect of the fiber treatment on the interaction enhancement with PP matrices.

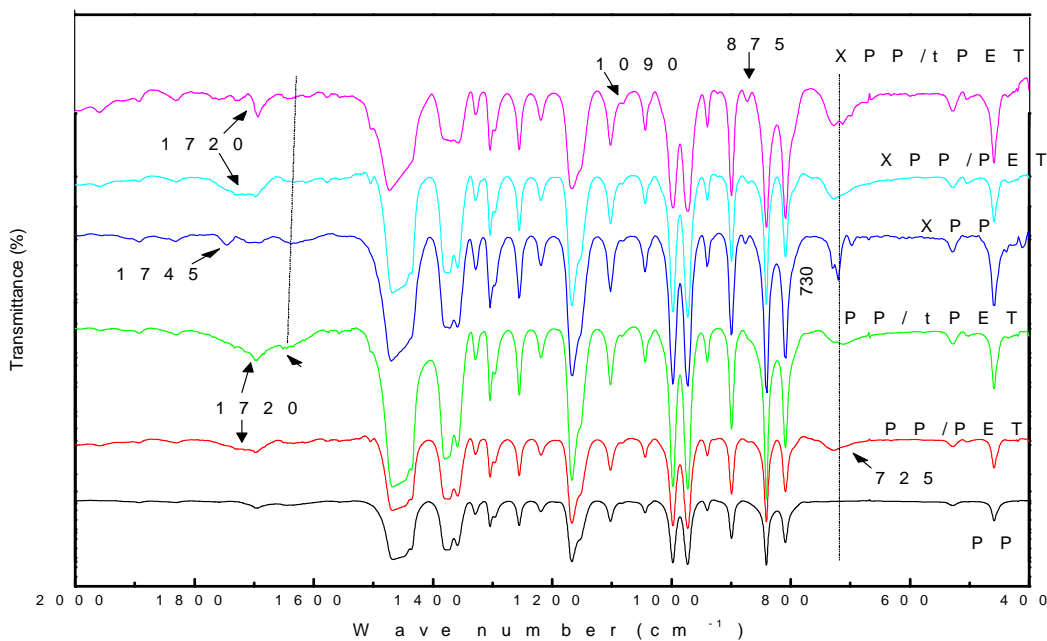


Figure. IV.44. FTIR spectra of 7wt % (treated/untreated) PET fiber/ (modified/unmodified) PP composites

2. Mechanical properties

Figure IV.45 and 46 depict the variation of the Young's modulus and elongation at break for different composites with the aim of determining the effect of the fiber treatment in both matrices (neat and crosslinked PP). The Young's modulus of treated PET fiber /unmodified PP composite shows almost the same value as that of untreated PET fiber/PP composite, In contrast the modified PP presents a noticeable enhancement in Young's modulus with the incorporation of the treated PET fiber compared to the one filled with untreated fiber.

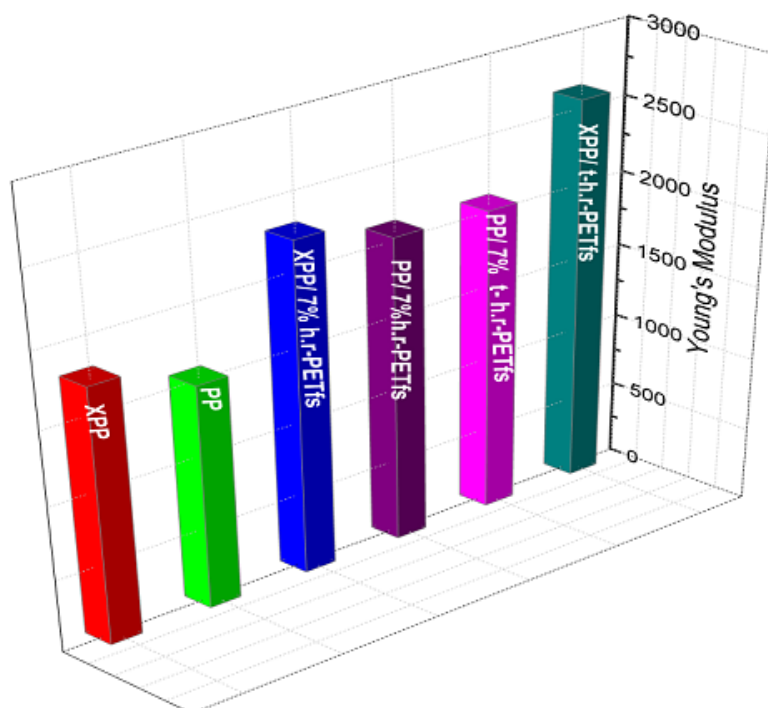


Figure IV.45. Young's modulus of 7 wt% (treated/untreated) PET fiber/ (modified/unmodified) PP composites.

The elongation at break of the treated PET fiber/crosslinked PP composite increases slightly when the treated PET fiber was added, therefore, the treatment of PET fiber improves slightly the tensile properties of the crosslinked PP. This result can be ascribed to the good dispersion of the treated PET fiber and the enhancement of the adhesion between the treated PET fiber and the modified PP as it can be shown in SEM micrographs. In contrast, the incorporation of the treated PET fiber in the neat PP matrix does not show any improvement of the elongation at break; instead a slight decrease is obtained compared to that of the untreated PET fiber/ neat PP composite.

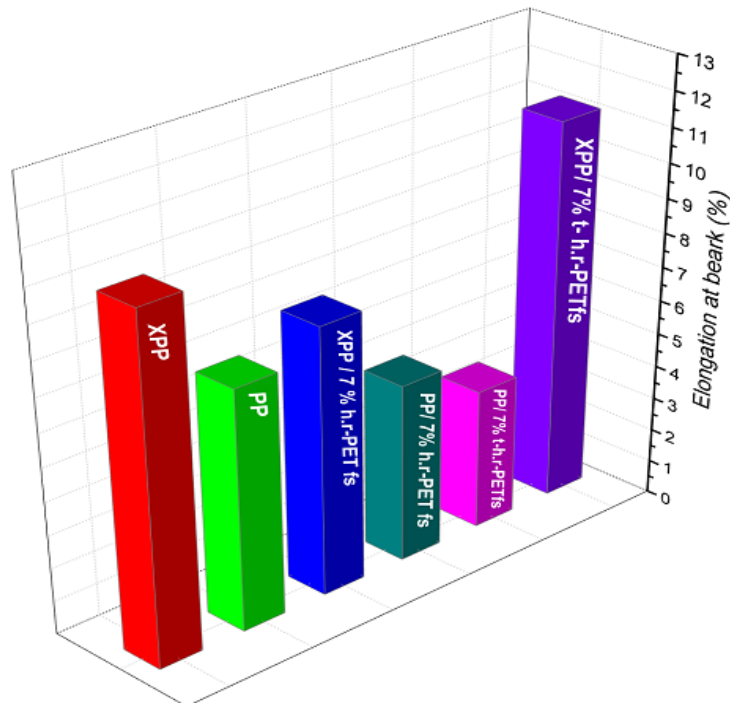


Figure IV.46. Variation of elongation at break for 7 wt% (treated/untreated) PET fiber/ (modified/unmodified) PP composites

2.2. IZOD Impact strength

The variation of Izod impact strength for the treated PET fiber filled unmodified and modified PP matrices are depicted in Figure IV.47. It is shown that the crosslinked PP/treated PET fiber composite presents fairly higher resilience compared to the unmodified one. This can be explained by the obtained large interface between treated fiber and the crosslinked PP. Additionally; it is found that the untreated PET fiber filled unmodified PP has been shown more important resilience compared to the treated fiber/unmodified PP composite.

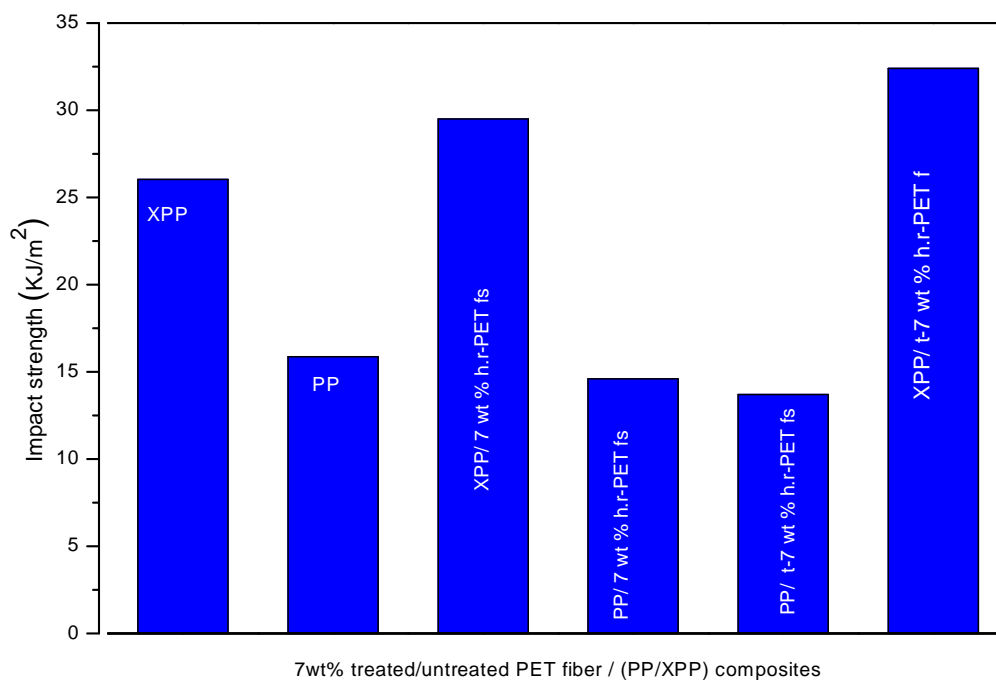


Figure IV.47. Variation of Izod impact strength for the treated PET fiber filled unmodified and modified PP matrices

3. X-ray diffraction results

Figure IV.48 depicts the WAXS patterns of 7 wt% treated PET fiber / (unmodified and modified) PP composites. As expected, only α form is shown in the composites based on the unmodified PP composite, whereas both of γ and β forms are appeared in the treated PET fiber/crosslinked PP composite. This is due to the crosslinking agent effect. The crystallinity degree of composites is given by table IV.9. Both composite shows almost the same crystallinity values as those one obtained in the untreated PET fiber/ modified PP and untreated PET fiber/ unmodified PP composites. The fiber treatment does not affect the microstructure of composites.

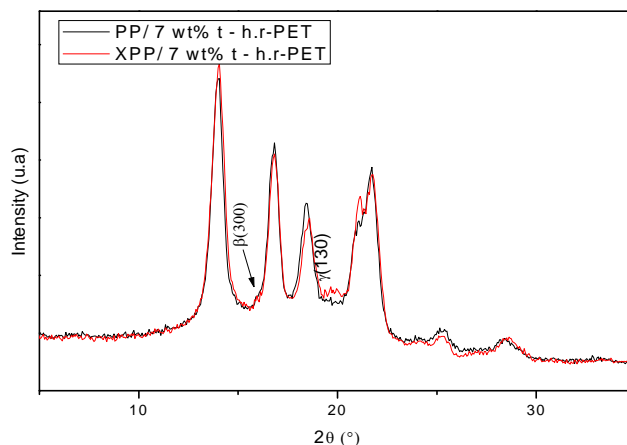


Figure IV. 48. WAXS patterns of 7 wt% treated PET fiber / (unmodified and modified) PP composites.

Table IV.9. WAXS measurements: (χ_c^{WAXS}), X_β of β form and X_γ of the γ -form

Materials	χ_β (%)	χ_γ (%)	χ_c^{WAXS} (%)
7wt%t-h.r-PETfs/ PP	-	-	43
7wt% t-h.r-PETfs/XPP	0.015	0.45	45

4. DSC Results

Figure IV.49 represents the heating and cooling runs of both treated and untreated PET fiber/ (unmodified/modified) PP composites. It is clearly shown that both composites show the same melting temperatures, and crystallinity degree values (see table IV.10). It has to be noticed that the melting temperatures of the composites based on 7 wt % untreated PET fiber are almost as the ones obtained after the fiber treatment ($\pm 2^\circ\text{C}$). As expected, in the presence of crosslinking agent, the fiber act as nucleating agent, which gives rise to the crystallization temperature of composite based on crosslinked PP.

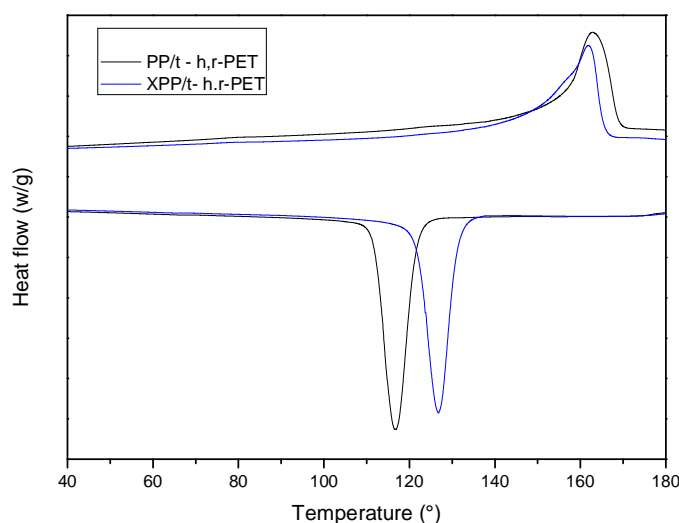


Figure IV.49. DSC thermograms of 7 wt% treated PET fiber / (unmodified and modified) PP composites

Table IV.10. DSC parameters of treated PET fiber/ modified and unmodified PP composites

Materials	ΔH_{m2} (J/g)	T_{m2} (°)	ΔH_c (J/g)	T_c (°)	χ_c (%)
PP/ t – h.r-PETfs	97	163	105	117	62
XPP/ t – h.r-PETfs	97	162	100	127	62

5. SEM observation

Fractured surface of 7 wt% treated PET fiber /XPP composite was observed under a SEM and are depicted by figure IV.50. SEM micrographs show an improvement in the adhesion between the surfaces of the PET fiber and the modified PP compared to SEM micrograph obtained in untreated PET fiber/ modified PP composite, This may due to the fact that the treated PET surface interact with PP chain in the presence of the crosslinking agent. The good adhesion could help to absorb more impact energy to overcome the fracture propagation during the impact strength, and pull out of the fibers from the matrix during the tensile test.

The splitting of the fibers result (see figure IV.50b) from their ability to withstand the applied load that is transferred from the matrix. This would not be possible if the adhesion of the fiber to the matrix is not sufficiently strong.

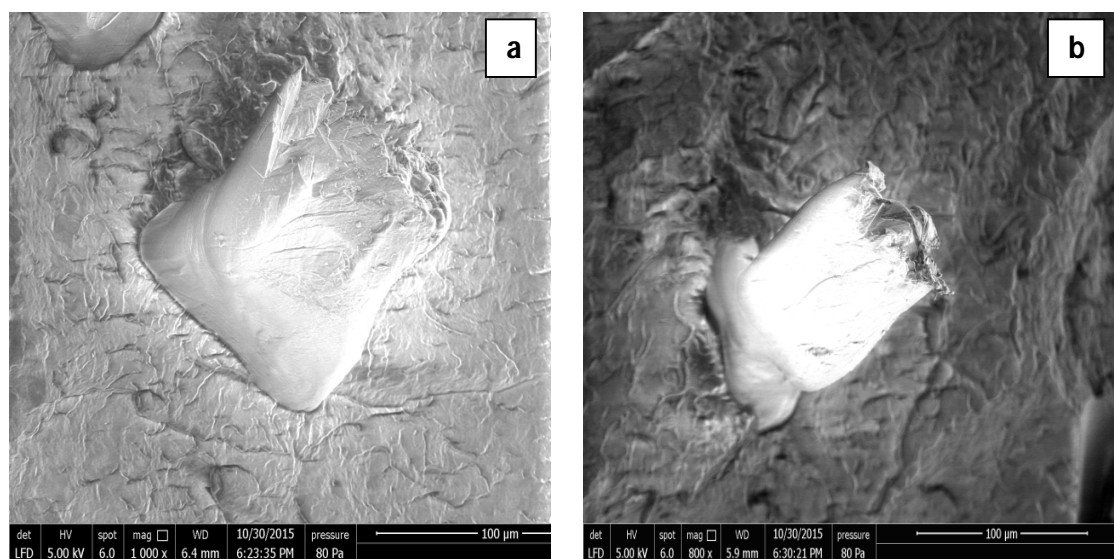


Figure IV.50. SEM micrographs of fractured surface of 7 wt% treated PET fiber /XPP composite.

B.2. Conclusion

Based on the study of the surface PET fiber treatment using stearic acid, it can be concluded that the stearic acid could play the role of a coupling agent in the presence of crosslinking agent and modified PP matrix. Furthermore, the surface treatment of PET fiber using stearic acid is a simple method which can enhance the adhesion and interaction properties of composites based on short synthetic fiber/ crosslinked PP composites.

IV.1.2.2. Crosslinked PP/short polyamide fiber composite

2.1. DRA results

Since torque is an indicator of viscosity, the effect of polyamide fiber loading or matrix modification on the rheological properties of the composites can be investigated using torque vs time data.

Figure IV.51 (a) illustrates a typical torque vs time data of (3, 5 and 7 wt% PA fibers) /PP composites. As seen in the previous DRA curves. After the complete melting of polypropylene (point A in figure), the addition of polyamide fiber in different loading is accompanied by an increase in torque, consequently the viscosity is increased. Beyond this step, torque values decreased down to a stable value that is called stabilization torque.

Figure. IV.51 (b) presents the torque evolution of (3, 5 and 7 wt% PA fibers)/ crosslinked PP composites, the variation of torque vs time for the different composites based on the modified PP show an increase in the viscosity, which is increased proportionally with the polyamide fiber loading. It is noteworthy to indicate that torque value in the stabilization of the modified PP/ polyamide fiber composites exhibits higher value than the composites based on unmodified matrix (see figure IV.51 (c)). From the SEM image an enhancement of the adhesion between the polyamide fiber and the crosslinked PP was shown, this can explained the highest value of the viscosity of the modified PP/polyamide fibers composites.

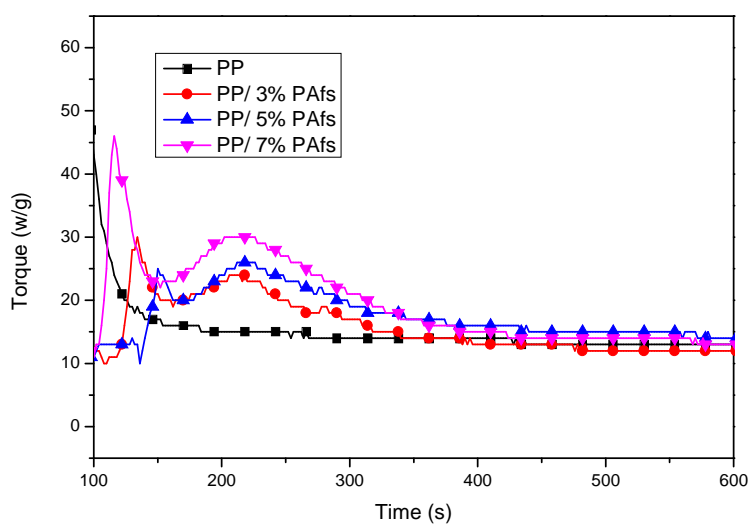


Figure IV.51.a. Torque vs time data of (3, 5 and 7 wt% PA fibers) /PP composites

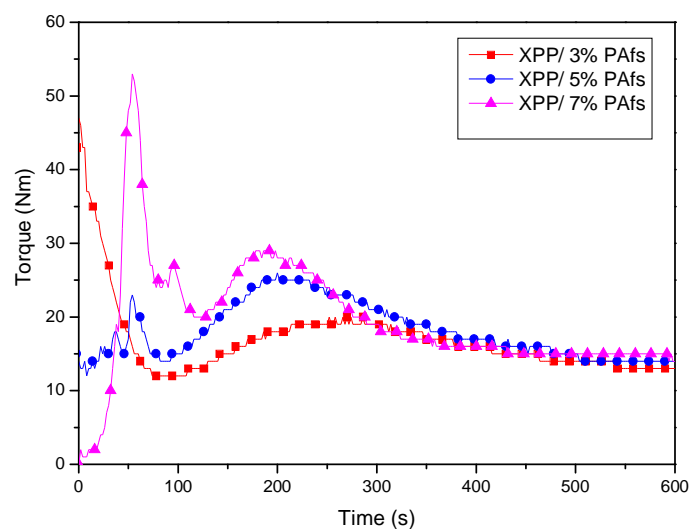


Figure. IV.51. b. Torque evolution of (3, 5 and 7 wt% PA fibers)/ crosslinked PP composites

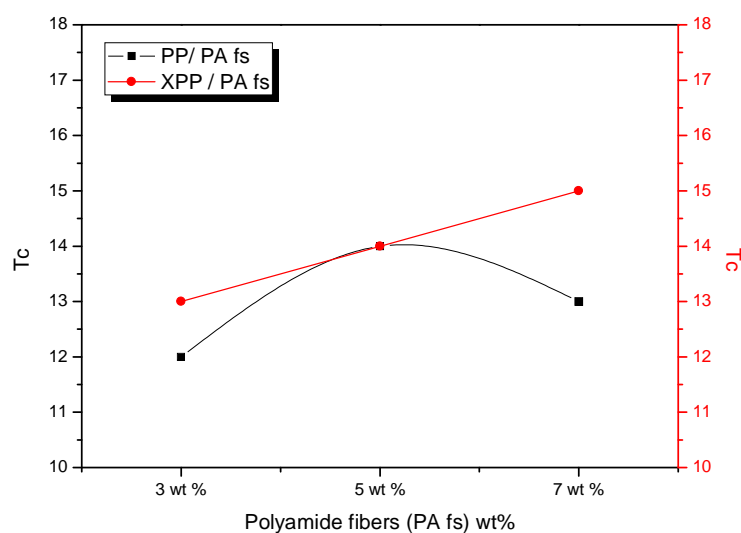


Figure IV.51.c. Torque stabilization values (T_c) of polyamide fibers/ (unmodified/crosslinked) PP composites

2.2. MFI measurement

MFI measurements are in good agreement with DRA results. Figure IV.52 reports a noticeable decrease of unmodified and modified polypropylene MFI depending on PA fibers loading. Also, as expected the crosslinked PP/polyamide fiber composites show the smallest MFI value

compared to those based on unmodified matrix. This increase of the viscosity in the modified matrix composite is more important compared to the composite based on the neat PP.

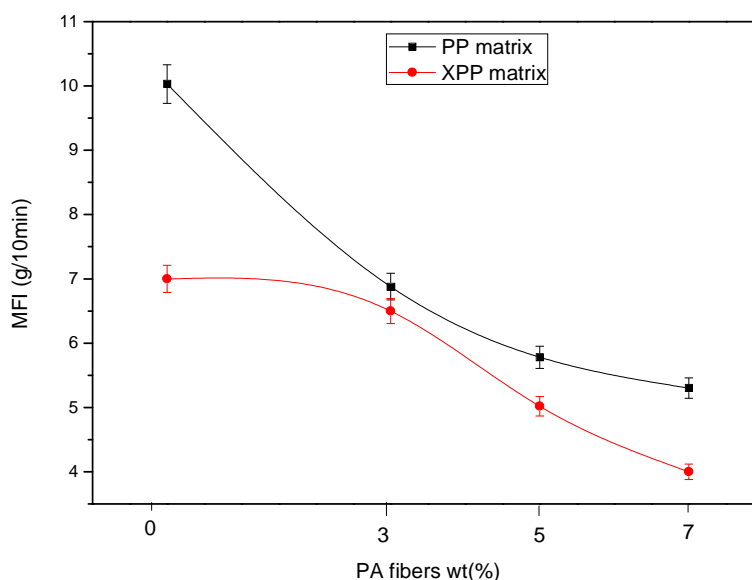


Figure IV.52. Variation of MFI values for (PP/XPP)/ wt% PAfs composites

2.3. Mechanical properties

Figures IV.53- 55 show the effect of polyamide fiber (PAfs) loading on Young's modulus, tensile strength, and izod impact strength of unmodified and crosslinked PP/ Polyamide fiber composites. Young's modulus shows an increase with fiber content in both matrices (unmodified and modified PP). It indicates that fiber loading plays a role in the strength of composites; this can be explained by the strength of polyamide fiber which is much higher than PP matrix. On the other hand, as expected the unfilled modified matrix present a higher modulus than the neat PP matrix, this is due to the fact that the crosslinking reaction of the PP gave rise to higher young's modulus (see the study of the crosslikned PP). Noteworthy, 5wt% PAfs loading shows the highest modulus in both matrices, this may be ascribed to the better dispersion of the 5 wt% fibers than 7wt% fiber loading. The variation of the tensile strength for composites as a function of the fiber content and matrix modification is displayed in figure IV.54. It is shown that the tensile strength decreases slightly in the unmodified PP/short polyamide fiber composite

compared to the neat PP, whereas it increased slightly in the crosslinked PP/polyamide fiber composite as function of fiber loading.

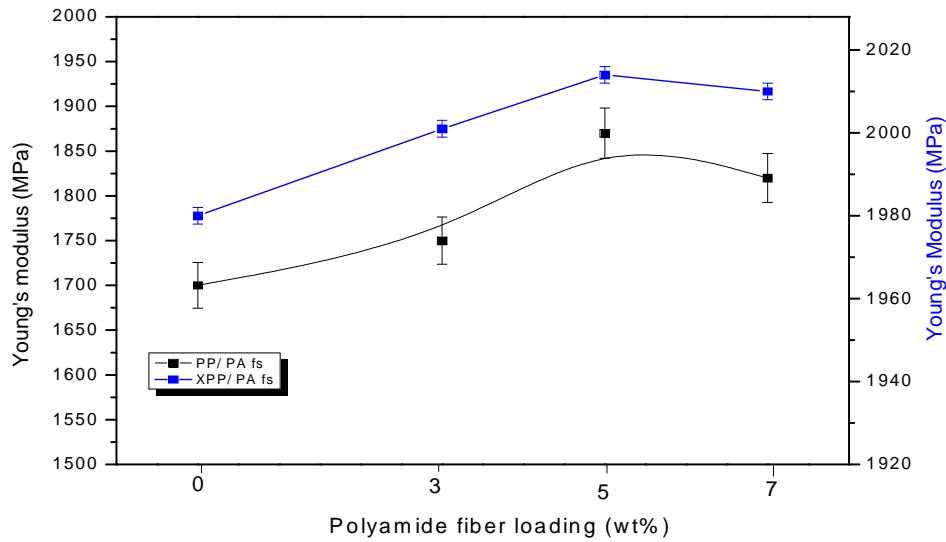


Figure IV.53. Variation of Young's modulus for (PP/XPP)/ wt% PAfs composites as a function of PAfs loading.

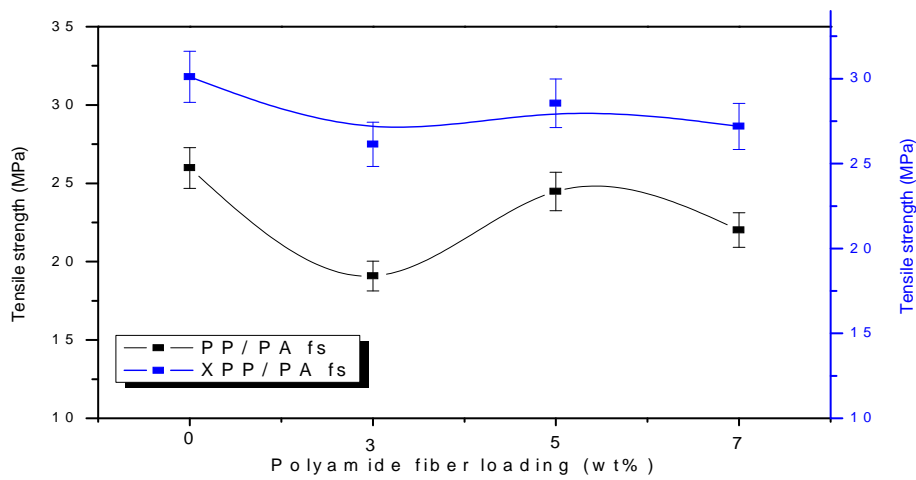


Figure IV.54. Variation of tensile strength for (PP/XPP)/ wt% PAfs composites as a function of PAfs loading.

The variation of the Izod impact strength for the different composites is presented in figure IV.55. The impact strength of PP increases slightly with the increase of polyamide fiber loading, except for the one with 7wt% polyamide fiber in which a noticeable decrease in the resilience is shown, this trend can be related with the agglomeration of fiber, which could induce voids in the composite, this behavior has been reported in the Young's modulus and tensile strength results. On the other hand, the resilience of the crosslinked PP matrix/ polyamide fiber composites shows a significant increase compared to the modified and unmodified PP. The PP modification enhances the mechanical properties of crosslinked PP/polyamide fiber composite.

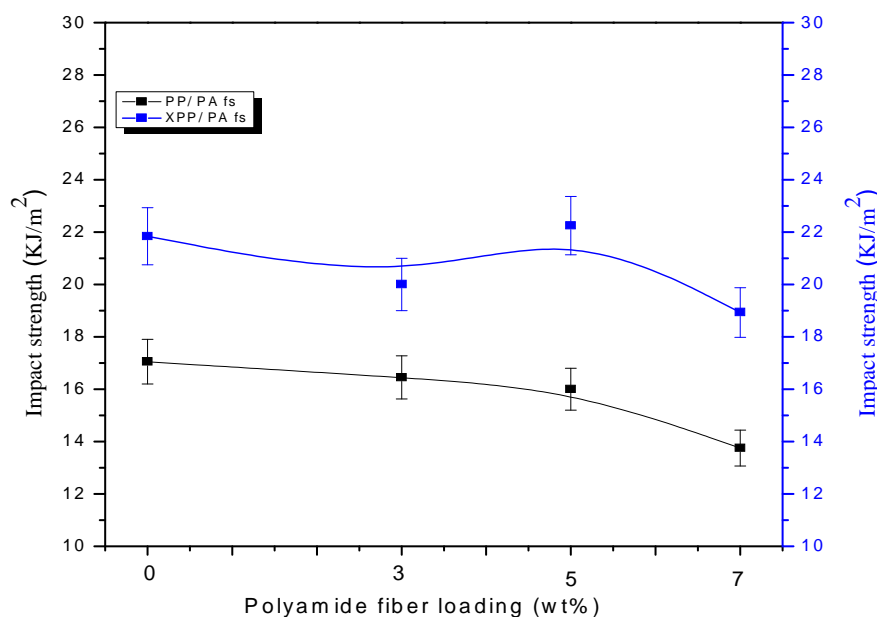


Figure IV.55. Variation of Izod impact strength for (PP/XPP)/ wt% PAfs composites

2.4. X-ray diffraction results

The X-ray diffractograms of the PP/ (3, 5 and 7 wt %) PA fiber composites presented in Figure IV.56 shows that all composites patterns are indexed in terms of characteristic crystallographic planes of the PP α monoclinic crystalline cell ((110), (040), (130), (111) and (041)). Otherwise, the diffractograms of the filled crosslinked PP depicted in figure IV.56 b present the five obvious peaks associated to α form of the PP, additionally, as it has been shown in the previous studies related to the crosslinked PP matrix, β and γ diffraction peaks are occurred in all composites.

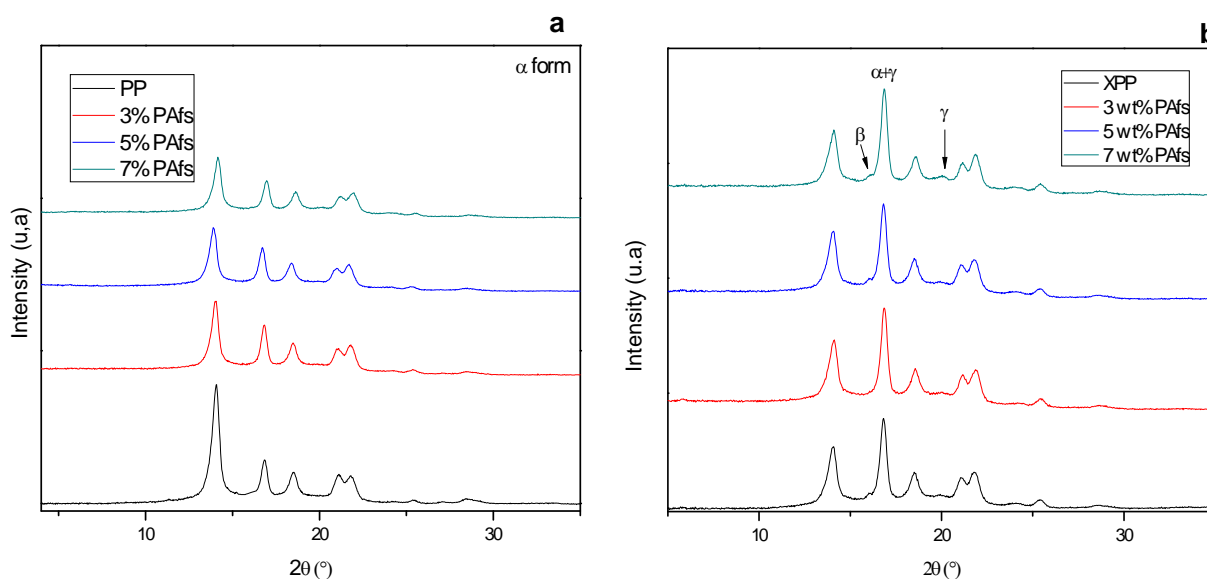


Figure IV.56. WAXS patterns of (PP/XPP)/ wt% PAfs composites

2.5. DSC measurement

DSC thermograms of unmodified and crosslinked PP matrices filled by polyamide fiber in different content are presented in figure IV.57. The values of relevant thermodynamic parameters are summarized in table IV.11. From the figure IV.56.a related to the unmodified PP/polyamide fiber composites it is shown that DSC parameters are almost the same as those of the neat PP. Noting that the 5wt% PA fiber/PP composite shows a slight increase in the crystallinity degree compared to 3 and 7 wt% fiber content. The DSC thermograms of crosslinked PP/ (3, 5 and 7wt% polyamide fiber composites) indicate that the addition of different content of polyamide fiber to crosslinked PP causes a shift in the crystallization peak toward the higher values (figure IV.57.b) because of the effect of fibers, which provides a large number of nucleation sites in the presence of the crosslinking agent. Therefore, the crystallinity degree and the crystallization temperature should be enhanced in the presence of dispersed polyamide fiber content.

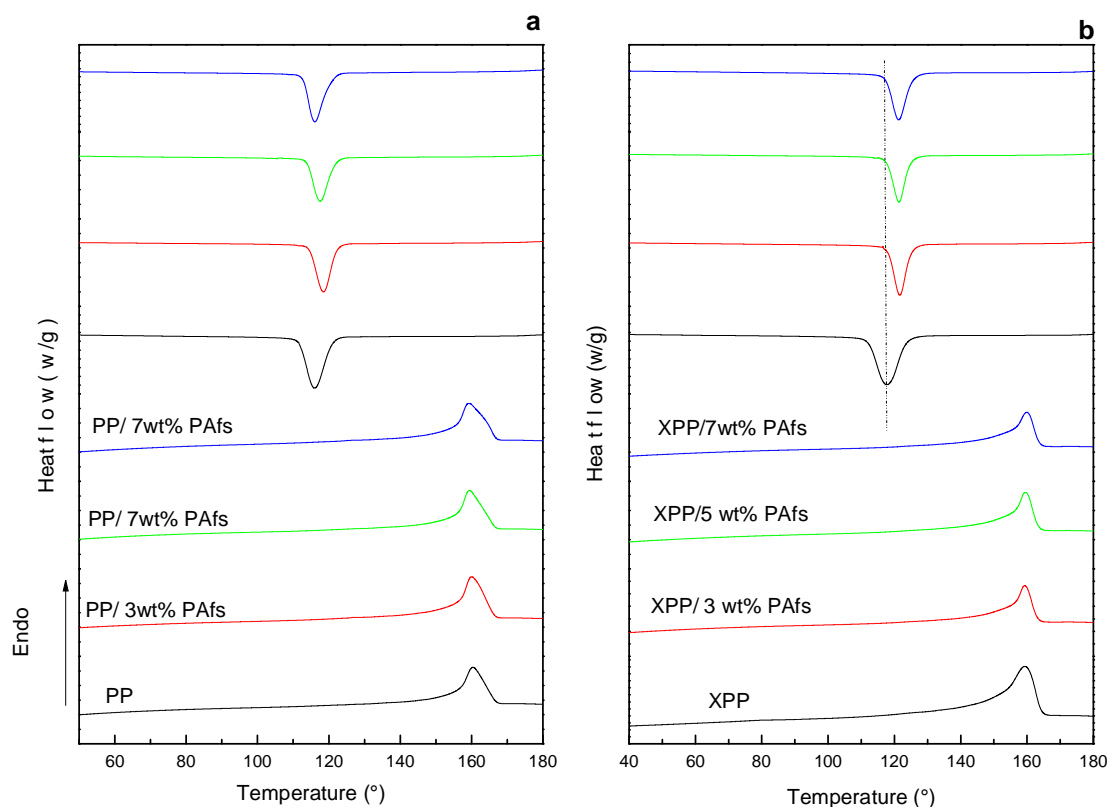


Figure IV.57. DSC thermograms of polyamide fiber/ (unmodified PP (a) and modified PP (b)) composites.

Table IV.11. DSC parameters of polyamide fiber / (unmodified and modified) PP composites

Materials	ΔH_f	T_f	ΔH_c	T_c	χ_c
PP	90	161	98	116	42
3% PAfs	81	160	105	117	40
5% PAfs	85	159	93	117	43
7% PAfs	77	159	97	116	40
XPP	66	159	69	118	31
3% PAfs	102	159	105	121	47
5% PAfs	90	159	94	121	45
7% PAfs	88	160	91	121	45

2.6. Optical and scanning electronic microscopy

The dispersion of the 5wt% polyamide fiber in the PP matrix was assessed by optical microscopy. Figure IV.58 shows a good dispersed polyamide fiber in the PP matrix.

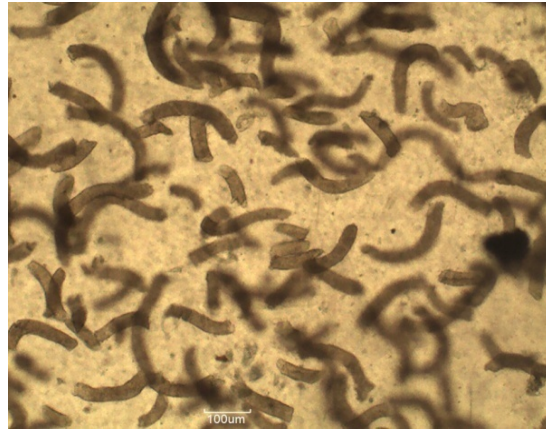


Figure IV.58.Opticl microscopy image of PP/ 5 wt% polyamide fiber composite

Aiming at examining the adhesion between polyamide fiber and PP, SEM micrographs of the fractured surfaces of 5wt% polyamide fiber/ (crosslinked and neat) PP composites is shown in Figure IV.59. According to figure IV.59.a and b, the addition of 5wt% of polyamide fiber to the crosslinked PP allows a good adhesion in the matrix. The development of strong interfacial interactions ensures a larger contact surface enabling a better stress transfer between the two phases of the composite [17-18].

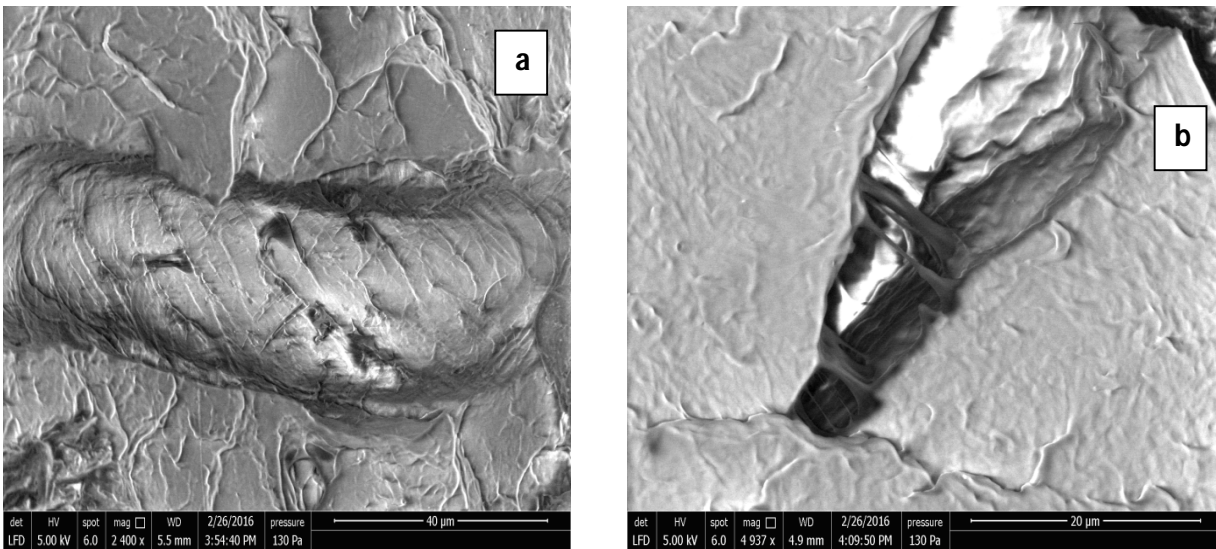


Figure IV.59.SEM micrographs of fractured surface of crosslinked PP/ 5wt% polyamide fiber composite

IV.1.2.2.2. Conclusion

According to the obtained results, it can be concluded that the reversible crosslinking reaction of PP is a good way to enhance the interaction between polyamide fiber and PP. 5wt% polyamide fiber has presented the optimum properties. Additionally; it has been shown that the modified PP matrix has given more important mechanical and structural results in comparison with those obtained in the study of modified PP/ hollow PET fiber.

Polypropylene/clay nanocomposite are another class of materials which can be prepared by using the same crosslinking agent (so-called functionalizing agent of clay), and based on the good obtained results by using crosslinked matrix /polyamide fiber, it has been proposed to study the effect of the addition of polyamide fibers to the PP/ clay nanocomposite.

IV.1.2.3. Na-Montmorillonite– short polyamide Fiber/polypropylene hybrid composite

3.1. Fourier transform infrared spectroscopy (FTIR)

Figure IV.60, shows the FTIR spectra of Na-MMT. The band at 3623 cm^{-1} produced from the O-H stretching vibration associated with Al^{3+} , Fe^{2+} or Mg^{2+} cations. The intensive band situated at 1045 cm^{-1} assigned to the Si-O stretch, and that at 529 cm^{-1} is due to Si-O bending vibrations. The band at 1113 cm^{-1} assigned to the Si-O out-of-plane stretching vibration. The hydroxyl vibrations groups of water molecules showed at two bands which situated at 3440 and 1639 cm^{-1} . The band at 798 cm^{-1} shows the quartz present in Na-MMT [19].

Figures IV.60 a, b and c display the FTIR spectra of different nanocomposites and crosslinked polypropylene (1wt% FA/PP). From the results presented in figure IV.60a, it was observed that the peak related to Na-MMT octahedral structure peak at 3623 cm^{-1} remained with a weak intensity in the spectra of 3 and 7 wt% f-Na-MMT /PP; however this peak disappeared with 5 wt% f-Na-MMT. In addition, weak peaks associated with the tetrahedral structure of Na-MMT at 1639 cm^{-1} , 1045 cm^{-1} and at 529 cm^{-1} remained in the final structure of the different nanocomposites samples with strong intensities in the case of PP/3 and 7 wt% f-Na-MMT as shown in figures IV.60b, c. This result can be explained by the reaction between the functionaliz-

ing agent used and Na-MMT which is a redox reaction that involves the octahedral crystalline portion. Thus, the organometallic components of Na-MMT octahedral structure react in the presence of cations supplied by decomposition of the peroxide and the accelerator [20]. According to Bouhelal *et al* [21], the technique of crosslinking by reactive extrusion used in this present study gave rise to a partial or total exfoliation (4 wt % clay) with absence of intercalated structure.

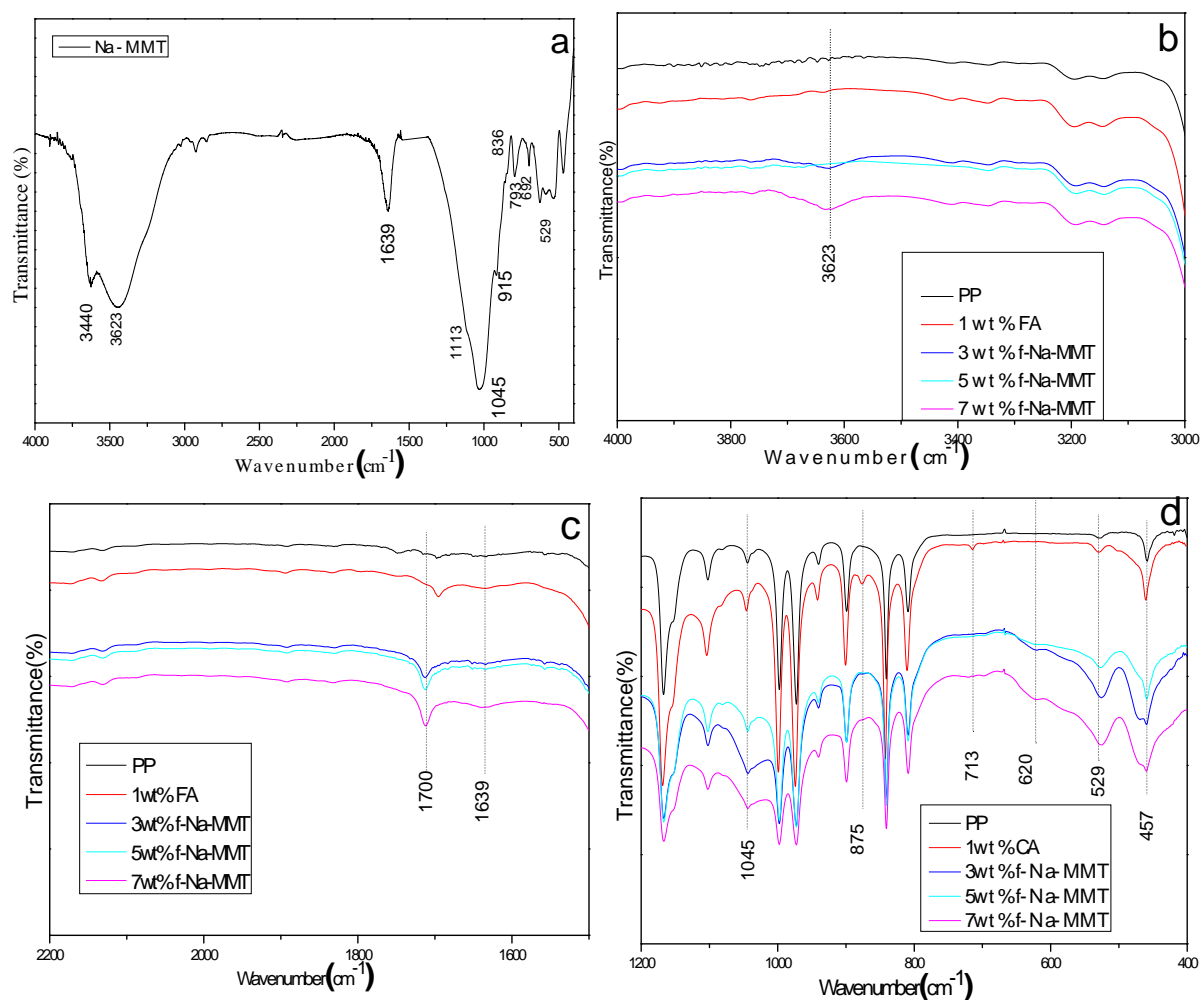


Figure IV.60. FTIR spectra of a)-Unmodified Na-MMT; b, c, d)- PP ; PP/1wt% FA crosslinked PP ; 3,5 and 7wt%f-Na-MMT nanocomposites.

The different weak bands at 1700cm^{-1} , 875cm^{-1} , 713cm^{-1} and 620cm^{-1} shown in figure IV60.c and d are related to crosslinked PP as observed in crosslinked PP spectrum. The band at 1700cm^{-1} assigned to the carbonyl group $\text{C}=\text{O}$ which resulted from the reaction between the peroxide and PP, and that at 875cm^{-1} due to the swinging of N-H , emerged from the reaction with the accelerator, the two bands at 713cm^{-1} and 620cm^{-1} attributed to C-S stretch that related with the reaction with the sulfur. From these results, we can conclude that a few portion of the FA contributed also in the chemical crosslinking process of PP, which was proved by the appearance of the β and γ -crystalline forms in the WAXS patterns of crosslinked PP and f-Na-MMT /PP nanocomposites.

Figure IV.61 displays the FTIR spectra of PP and different composites based on treated polyamide fibers (t-PAfs) and untreated polyamide fibers (PAfs) reinforced polypropylene (PP). Remarkable changes in intensities between the PP spectrum and the spectra of composites were seen. Both of composites based on PA treated fibers and untreated present a large absorption band in the interval $2960\text{--}2850\text{ cm}^{-1}$ indicates the symmetric stretching vibration peak of $(-\text{CH}_2)$ group at 2850 , and the absorption band of the asymmetric stretching vibration peak of $(-\text{CH}_2)$ group at 2919 cm^{-1} . The absorption band at 2960cm^{-1} is the anti-symmetric stretching vibration peak of $-\text{CH}_3$. The t-PAfs/PP composite shows new bands at 1700 and at 1630 cm^{-1} assigned to the stretching vibration peak of the carbonyl group $\text{C}=\text{O}$ in carboxylic acid and the combination absorbance of $\text{C}=\text{O}$ and C-N amide I stretch. These new bands showed on FTIR spectra of treated polyamide are in a good agreement with SEM observation of treated polyamide fiber, in which polyamide fibers exhibit rough surface.

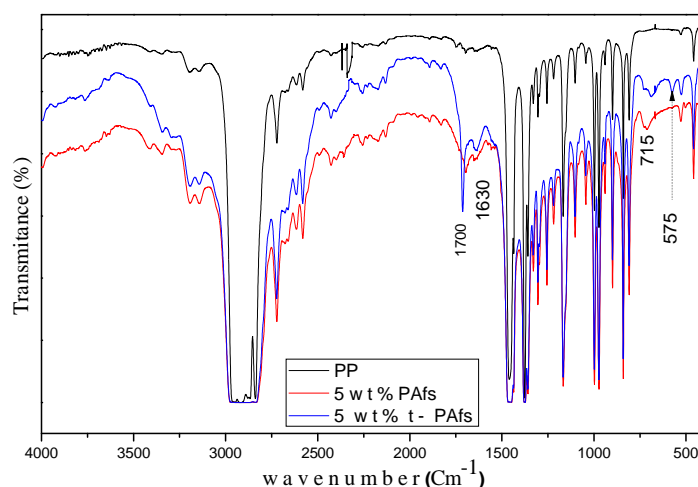


Figure IV.61. FTIR spectra of PP, PP/5wt% PAfs, PP/5wt% t-PAfs composites

FTIR spectra of PP and t-PAfs/f-Na-MMT/PP hybrid composites are shown in figure IV.62. Different bands related to tetrahedral structure of Na-MMT were clearly observed in the spectra of all composites. Two characteristic weak bands of Na-MMT at 3635cm^{-1} and at 3410cm^{-1} related to the OH of the Al-OH and to the stretching and bending vibrations for the hydroxyl groups of water molecules were respectively shown. In addition, bands at $1639,692$ and 529cm^{-1} which associated with water molecules, quartz and Si-O bending vibrations were respectively observed as seen in figure IV.60 a and b. However the band situated at 3623cm^{-1} that attributed to Na-MMT octahedral structure disappeared in the FTIR spectra of all composites. The disappearance of the characteristic peaks of the Na-MMT octahedral layers from the FTIR spectra is in good agreement with the obtained FTIR results of 5wt% f-Na-MMT/ PP nanocomposite as has been discussed above, what led to confirm the exfoliation of the Na-MMT layers in PP with the presence of t-PAfs.

Owing to the fact that the different nanocomposites were reprocessed in the second melt mixing cycle in which the polyamide fibers were added, and that the characterizations were carried out in the samples which are able to be molten again and form films using compression molding, we can conclude that the recycled f-Na-MMT/ PP nanocomposites have been successfully produced. Some bands associated with the crosslinked PP with FA as indicated above (figure IV.60) were further observed. The presence of the t-PAfs in f-Na-MMT/ PP nanocomposite matrix was proved by FTIR results, in which a new characteristic strong band at 3300cm^{-1} of bending vibration in primary amine was observed in figure VI.62 , and three bands which situated at 1700cm^{-1} , 1540cm^{-1} and 1200cm^{-1} , assigned to the stretching vibration peak of the carbonyl group (C=O) in carboxylic acid , the combination absorbance of the N-H and C-N amide II stretch and C-N stretch respectively.

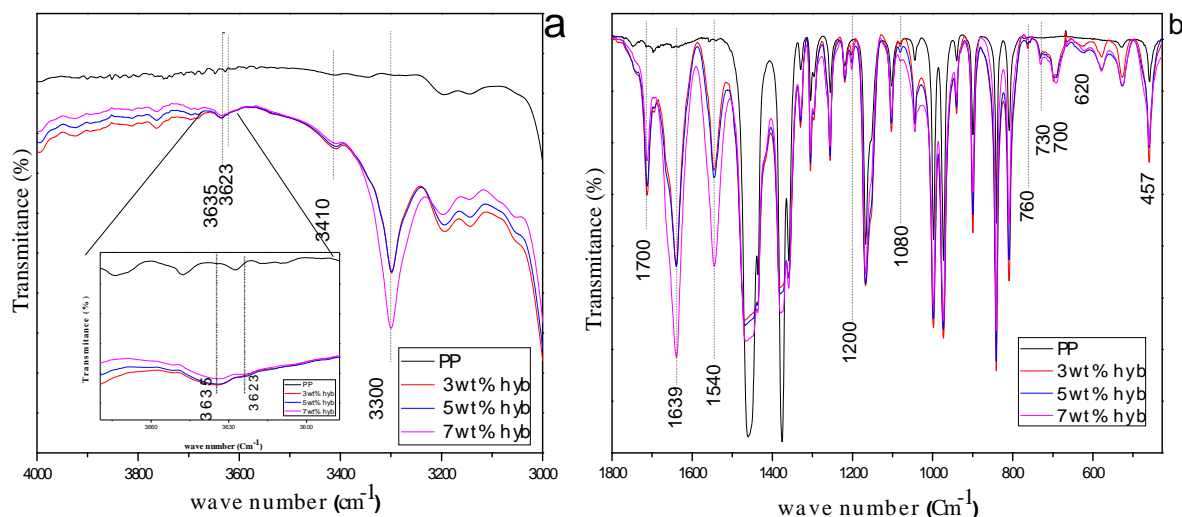


Figure IV.62. Fourier transform infrared spectroscopy (FTIR) spectra of a, b) - 5 wt % t-PAfs/ 3, 5 and 7 wt% f-Na-MMT/PP hybrid composites

3.2. Wide-angle X-ray scattering (WAXS)

The structure of PP/ 5wt % t-PAfs was evaluated by a wide-angle X-ray scattering method. On the basis of the WAXS patterns are shown in Figure IV.63.a. Only characteristic peaks of α form PP can be found, which can be indexed as (110) at 2θ ($^\circ$) = 14.07, (040) at 16.84, (130) at 18.5, (111) at 21.11 and (041) at 21.8 and (060), (220) at about 25.3 and 28.5 respectively, without any additional diffraction peaks.

The effect of FA on the structure of PP has been studied. Crosslinked PP is shown in Figure IV.63.b. The WAXS pattern appears two new weak peaks at 16.2 and 20.1 (2θ) which are characteristic of the (300) planes of PP β -crystalline form and the (130) or (117) planes of the γ -crystalline respectively. It can be seen also in Figure IV.63.b that the intensity of the reflection at 16.7 (2θ) is higher than that of PP which due to the appearance of the γ -crystalline form in the crosslinked PP, as both α - and γ - forms show a reflection in this position.

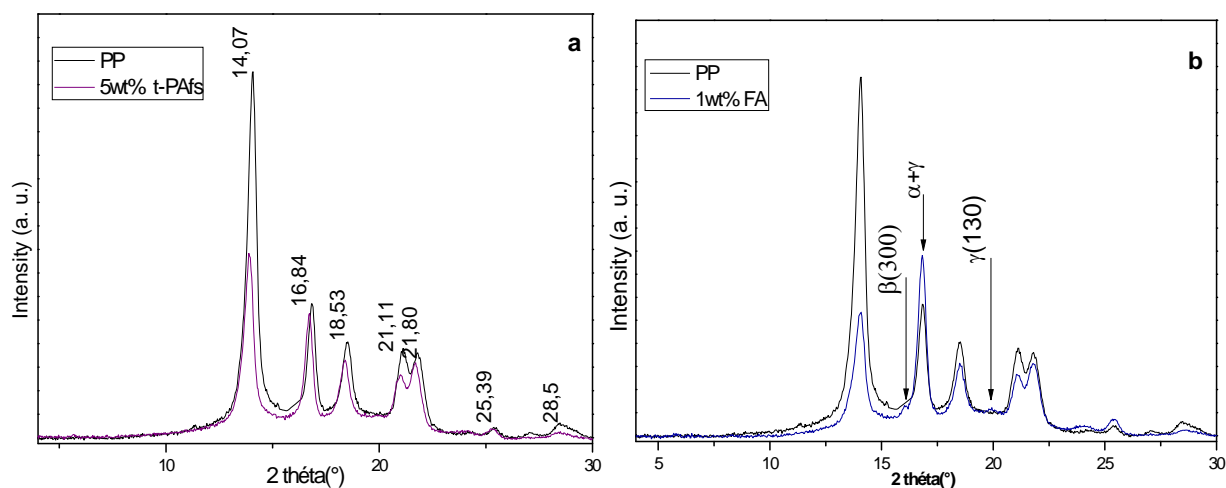


Figure IV.63. WAXS patterns of **a)**- 5 wt% t-PAfs /PP composite **b)-** 1 wt% FA /PP crosslinked PP sample.

Figure IV.64 shows the X-ray diffraction patterns of 3, 5, and 7wt% f- Na-MMT/PP nanocomposites. From this figure it was observed that the WAXD patterns exhibit the typical reflections of the α -form of PP, with four additional peaks, at 6.9, 16.2, 20.1 and 26.7 (2θ) that are characteristic of the d_{001} spacing of Na-MMT, (300) planes of the iPP β -crystalline form, (130) or (117) planes of the γ -crystalline form, and the quartz accompanying the Na-MMT which was showed with much less intensity. The characteristic peak of the d_{001} spacing of Na-MMT, indicated by an arrow appeared with a weak intensity in 7 and 3 wt % f- Na-MMT. However it disappeared in the case of PP with 5wt% f- Na-MMT. According to Giannelis *et al.* [22] the disappearance of peak indicates the separation of clay layers (exfoliated structure) and the formation of nanocomposites. The two new peaks at 16.2 and 20.1 have been already presented in the diffractogram of the crosslinked sample having no Na-MMT (Figure IV.63.b). On the work conducted by Bouhelal *et al.* [21] based on the development of iPP/clay nanocomposites, it was found that 4wt % clay gave a rise to a partial or total exfoliation in which the reactive extrusion technique was used. Further, in this present study the exfoliation of the Na-MMT layers was given with 5wt% f-Na-MMT.

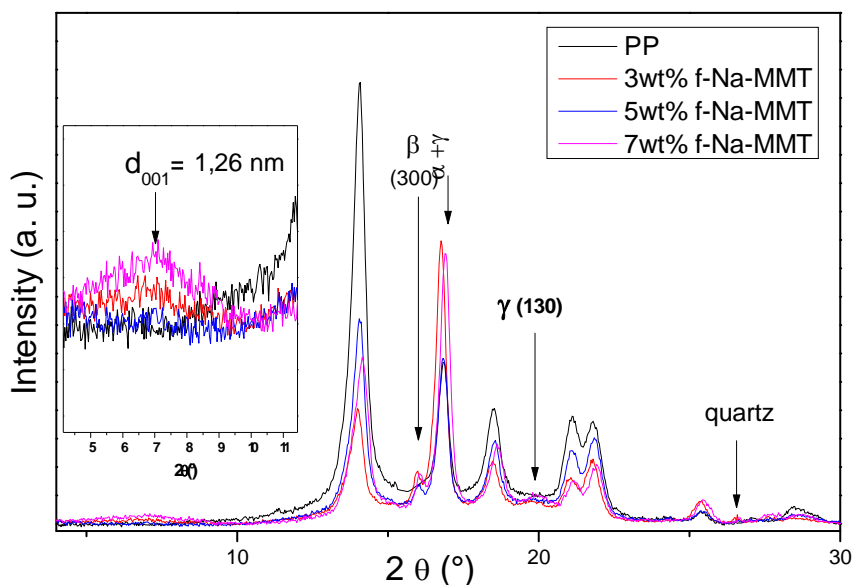


Figure IV.64. WAXS patterns of 3, 5 and 7 wt%/PP nanocomposites.

Figure IV.65 displays the WAXS patterns of t-PAfs / f-Na-MMT /PP hybrid composites. It was observed that the presence of PAfs with Na-MMT do not give any significant difference compared with the WAXS patterns of nanocomposite. The same additional peaks are showed, with the disappearance of the weak peak assigned to the quartz in nanocomposites samples and the peak related with β -crystalline form at 16.2 (2θ) in 7wt% t-PAfs/f-Na-MMT hybrid. Also, it can be seen that the characteristic peak of the d_{001} spacing of Na-MMT shifted to higher diffraction angles unlike the diffraction angle of Na-MMT which was found in the PP/Na-MMT nanocomposites. The exfoliation of the Na-MMT layers was given with 5wt% f-Na-MMT also as it has been explained above (figure IV.64).

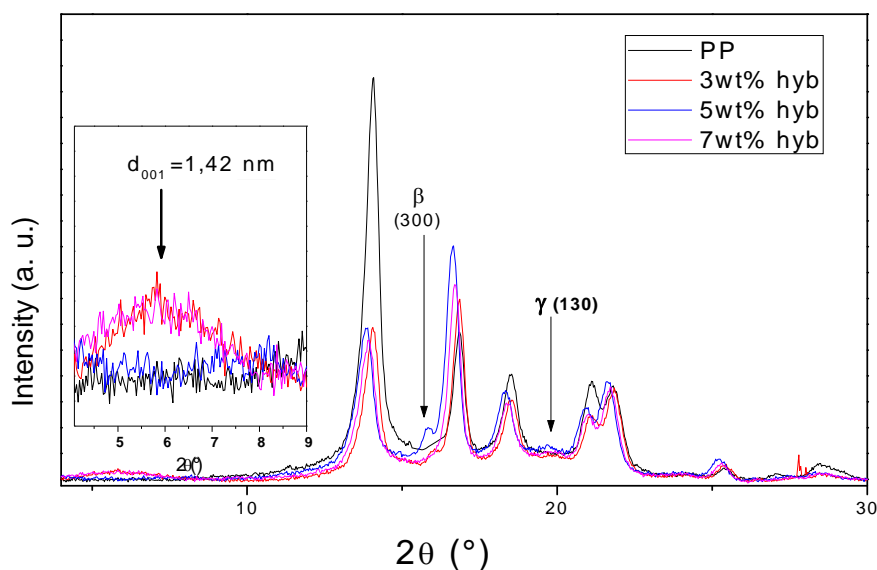


Figure IV.65. WAXS patterns of 5wt% t-PAFs/3, 5 and 7wt% f-Na-MMT/PP hybrid composites.

The obtained degree of crystallinity (χ_c), X_β and X_γ are collected in Table IV.12. It is clearly observed that the degree of crystallinity (χ_c) seem to be relatively constant with the different composites (nanocomposites and hybrid composites) in comparison with the neat PP, however it is lower in the case of t-PAFs/PP. The degree of crystallinity of different composite is consistent with DSC results. A gradual increase of X_γ value has been noted in different nanocomposite samples. It increases from 0.32 in the crosslinked PP, up to 0.55 for the samples with 3–7% of clay. While these values decrease to 0.36 and 0.45 for the 3, 7 wt% and 5wt% hybrid samples.

Concerning the X_β value, its contribution reaches the highest value in the sample with 7 wt % of Na-MMT. However, it was observed that the peak related with β -crystalline was disappeared in 7wt % Na-MMT/5wt% PAFs. It can be explained the diminution X_γ and X_β values in hybrid composites by the presence of polyamide fibers.

Table IV.12. WAXS measurements: (χ_c^{WAXS}), X_β of β form and X_γ of the γ -form.

Sample	χ_β (%)	χ_γ (%)	χ_c^{WAXS} (%)
PP	-	-	38.1
5wt % t-PAfs/PP	-	-	32.6
1wt % FA/PP	0.010	0.32	36
3wt%Na- MMT	0.017	0.50	37.7
5 wt% Na-MMT	0.016	0.53	38
7 wt% Na- MMT	0.02	0.55	38.2
3wt% hyb	0.016	0.36	38
5wt% hyb	0.016	0.45	38.5
7wt% hyb	-	0.36	38

3.3. DSC Analysis

Figures IV.66 and IV.67 display the DSC thermograms of t-PAfs/PP composite, f-Na MMT/PP nanocomposites and hybrids. The DSC results are displayed in table IV.13. It can be seen that the melting temperatures of different composites are about 159°C, slightly lower than 161°C of pure PP. the melting temperatures of f-Na-MMT/PP increased slightly with increasing of f-Na-MMT amount. However, in the case of hybrid composites, in which 5wt% of t-PAfs were added to 3, 5 and 7 wt% f-Na-MMAT /PP nanocomposites, a constant value of melting temperature is observed that is almost between the melting temperature of t-PAfs/PP composite and different nanocomposites. The crystalline peak temperature (T_c) of the pure PP is increased slightly with 5wt% t-PAfs. Meanwhile, the T_c is increased significantly with different f-Na-MMT/PP nanocomposites and hybrids. MMT and t-PAfs act as nucleating agents, which increase the crystallization temperature of PP matrix. The addition of 5wt%t-PAfs to 7wt% f-Na-MMT/PP

nanocomposite increased the T_c by up to 4°C compared to 5wt%t-PAfs/PP composite. This result indicates that the nucleating effect of MMT was further strengthened by the addition of polyamide fibers.

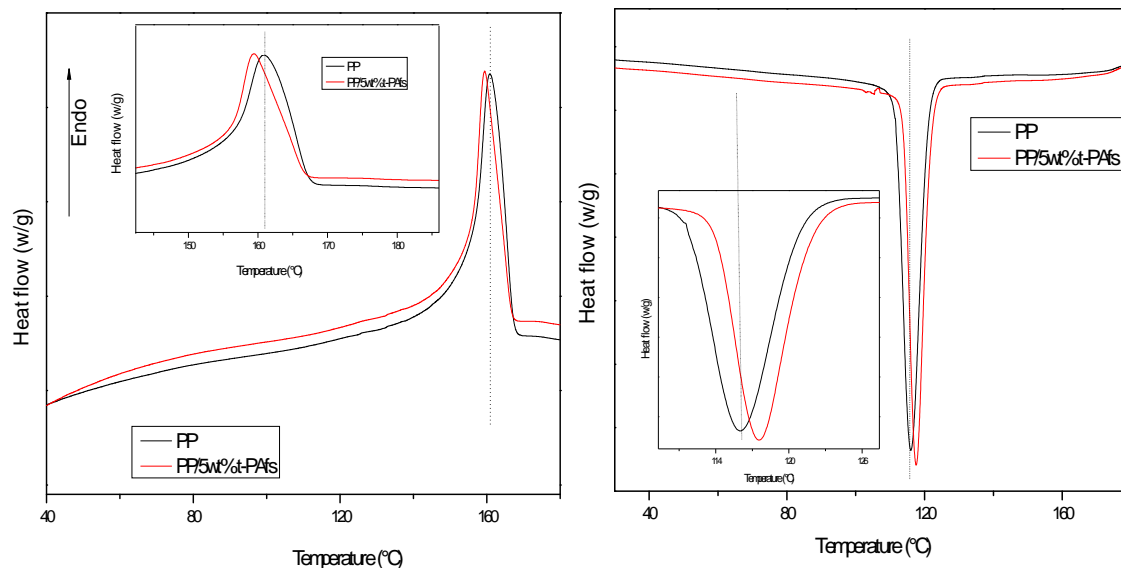
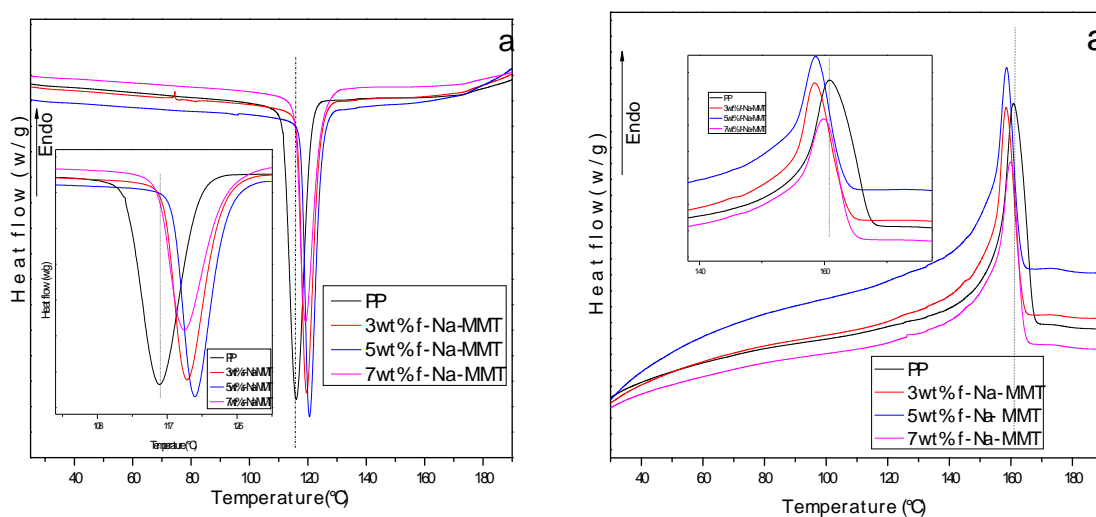


Figure IV.66. DSC thermographs of second heating and cooling runs of 5wt%t-PAfs /PP composite



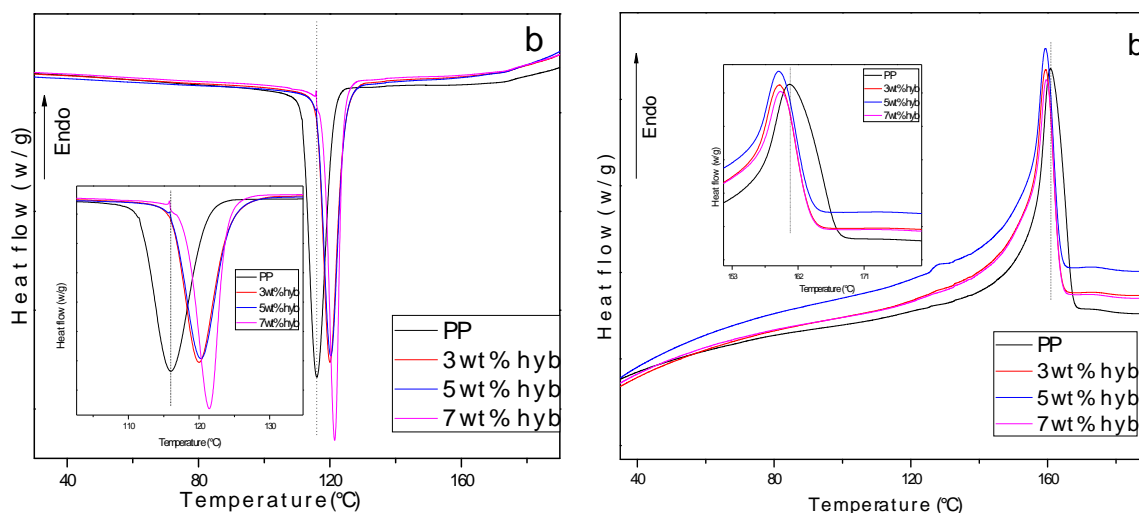


Figure IV.67. DSC thermographs of second heating and cooling runs of a)-f-Na-MMT/PP nanocomposite and b)-t-PAFs/f-Na-MMT/PP hybrid composites

Table IV.13. Melting (T_m), crystallization temperatures (T_c) and enthalpies (ΔH_m , ΔH_c) for different samples and crystallinity degree (χ_c) obtained by DSC.

Sample	ΔH_m (J/g)	T_m (C°)	ΔH_c (J/g)	T_c (C°)	χ_c^{DSC} (%)
PP	90	161	98	116	42.4
PP/5wt% t-PAFs	77	159	89	117.5	39
3wt% Na-MMT	87.9	158.3	98.3	120	43.6
5 wt% Na-MMT	83.7	158.5	98	120.8	42.3
7 wt% Na-MMT	81.7	160	92.5	119.5	42.1
3wt% hyb	87.7	159.5	102.3	120	45.6
5wt% hyb	83.5	159.3	102.1	120.3	44.7
7wt% hyb	83.1	159.5	100.1	121.4	45.2

3.4. Optical and scanning electron microscopy

To show the matrix/fiber adhesion and hybrid composite morphology, polarized optical microscopy (POM) and scanning electron microscopy (SEM) investigations were used. The POM images of 5 wt% t-PAfs/PP composite and 5wt% f-Na-MMT / 5wt% t- PAfs /PP hybrid composite are shown in Figure IV.68. The polyamide fibers generally seem to be well dispersed. Also, some agglomerations were observed (see figure IV.68.a). Figure IV.68.b shows the POM image of hybrid composite in which a good dispersed polyamide fiber was shown, and with less agglomeration than t-PAfs/PP composite due to the presence of Na-MMT in the matrix. Length reduction of fibers was observed that can be explained by the effect of the intense shearing involved in the closed chamber of the Brabender palstograph.

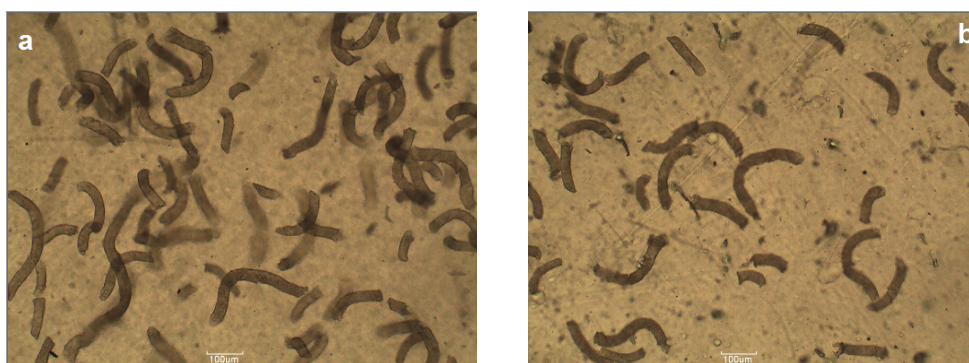


Figure IV.68. Optical micrographs of **a)** 5wt% t-PAfs/PP composite **b)** 5wt% t-PAfs / 5wt% f-Na-MMT /PP hybrid composite

Scanning electron micrographs (SEM) of untreated and treated polyamide fibers PAfs are shown in Figure IV.69. It can be observed that the untreated fibers showed a smooth surface while the images of treated surface polyamide fibers exhibit rough surfaces, which proved the affect of the treatment.

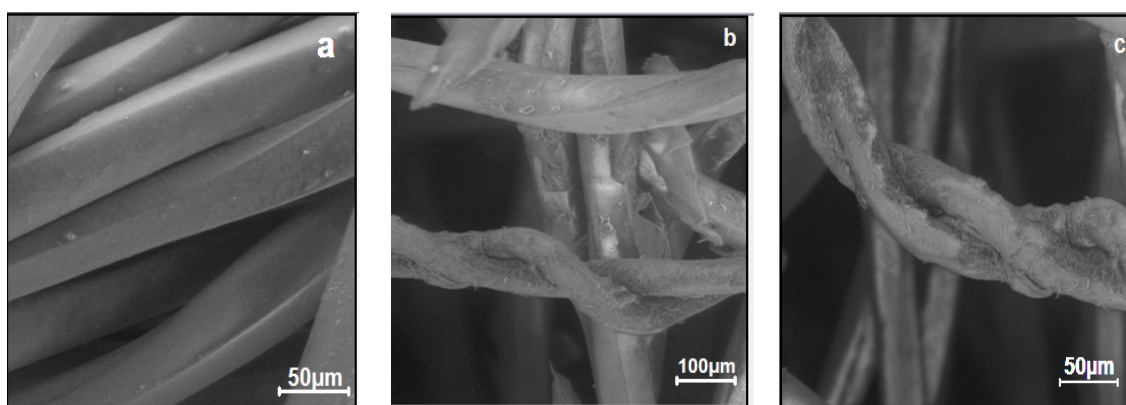


Figure IV.69. SEM micrographs of a) - Untreated PAfs b, c)-Treated PAfs

Scanning electron micrographs of the tensile fractured surface of 5 wt% PAfs/PP composite and 5wt% t- PAfs / 5wt% f-Na-MMT /PP hybrid composite are shown in Figure IV.70. Figures IV.70.a and b show the SEM micrographs of 5wt% PAfs/PP and 5 wt% t-PAfs/PP composites respectively. For the composite based on untreated polyamide fibers, fibers pull-out, the absence of polymer attached to the fiber surface and fiber fracture clearly indicate a very limited adhesion between PP and fibers (Figure IV.70a). On the other hand, in the case of t-PAfs/PP composite, fibers pull-out and debonding reduced significantly and the adhesion between fiber and matrix improved strongly. In addition, it was observed that the fibers folded with no fiber pull-out after tensile test what confirm that the interfacial adhesion of the treated fiber composites is much better than that of the untreated fiber composite (Figure IV.70b).

Figures IV.70.c and d show the SEM micrographs of the tensile fractured surface and the stretched surface of hybrid composite. It can be observed from the micrograph IV.70.c that the addition of t-PAfs in Na-MMT/PP nanocomposite give rise to a good interfacial adhesion which can be confirmed by the few voids appeared in the surface of stretched tensile specimen showed in figure IV.70.d.

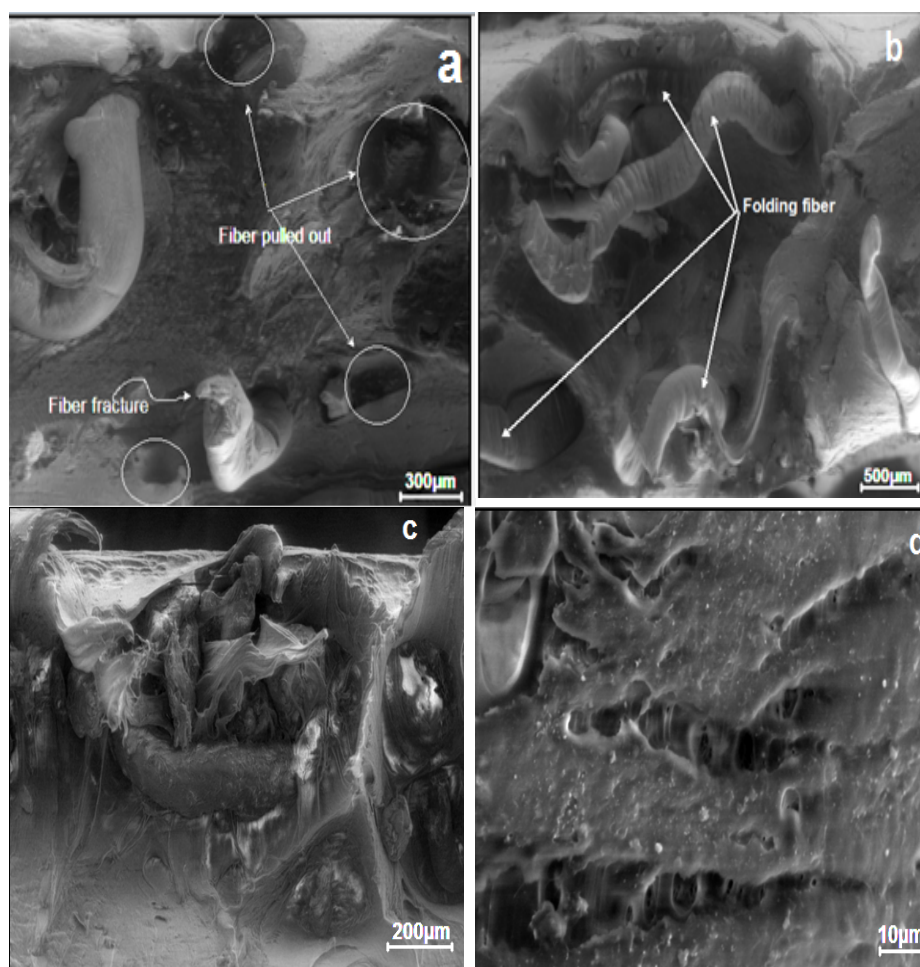


Figure IV.70. SEM micrographs of the tensile fractured surface of a) - 5wt% PAfs/PP composite b) 5wt% t-PAfs/PP composite c) 5wt% t- PAfs / 5wt% f-Na-MMT/ PP hybrid composite d) - the tensile stretched surface of hybrid composite

3.5. Mechanical properties (Tensile strength)

Figure IV.71 shows the variation of the Young's modulus for 5 wt% (untreated and treated polyamide fiber) /PP composites, 5 wt% f- Na-MMT/PP nanocomposite and the hybrid composite. It is observed that there is a slight improvement in the modulus for the different composites. The fiber treatment does not affect the modulus value of the composite compared to the untreated one, however, the addition of the treated polyamide fiber to the Na-MMT/fiber nanocomposite matrix showed an enhancement of the Young's modulus value.

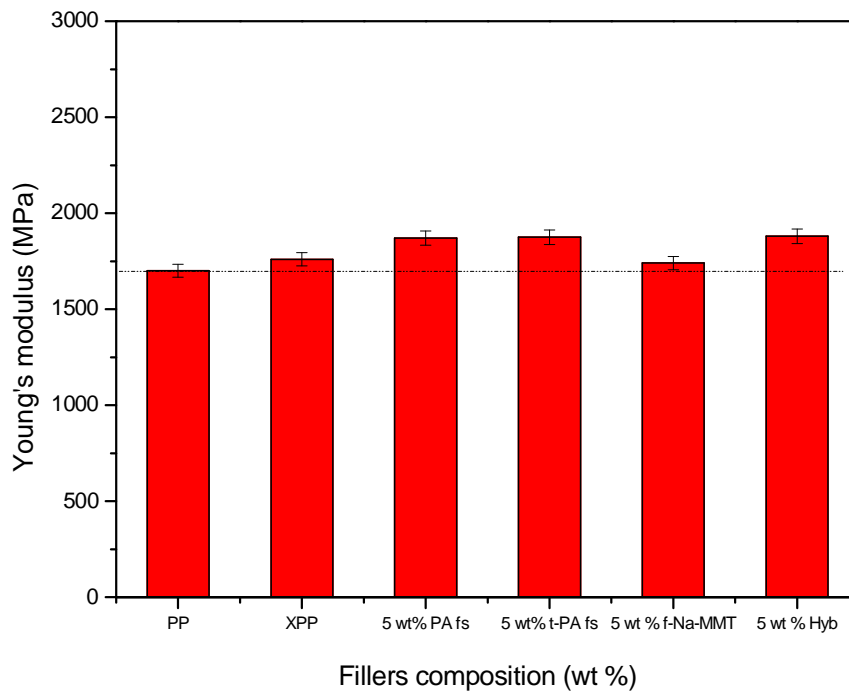


Figure IV.71. Variation of Young's modulus for the different composites

Figure IV.72 depicts the variation of the tensile strength of the different composites. An increase in tensile strength is found when 5 wt % treated polyamide fiber is added to the 5wt% f-Na-MMT nanocomposite, showing a synergistic effect for the tensile strength of the t-PA fs/PP composite and that of the nanocomposite, which can be related to the good of interfacial adhesion between the treated fiber and the PP/Na-MMT nanocomposite matrix.

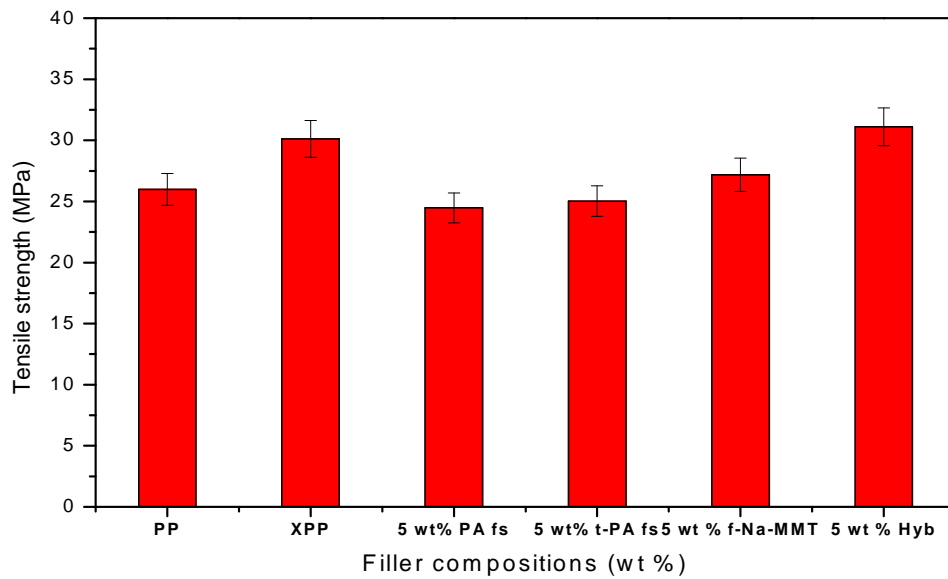


Figure IV.72. Variation of the tensile strength for the different composite.

3.5.1. Izod impact strength

The variation of the izod impact strength for the different composites is presented in figure IV. 73, it is found that the nanocomposite shows a noticeable increase in resilience; however it is clearly seen that the impact strength of the treated PA fiber/PP composite does not vary compared to that of the untreated fiber composite. Nevertheless, the addition of the treated polyamide fiber to the nanocomposite matrix increases the resilience of the PP, indicating a synergistic effect of the two fillers.

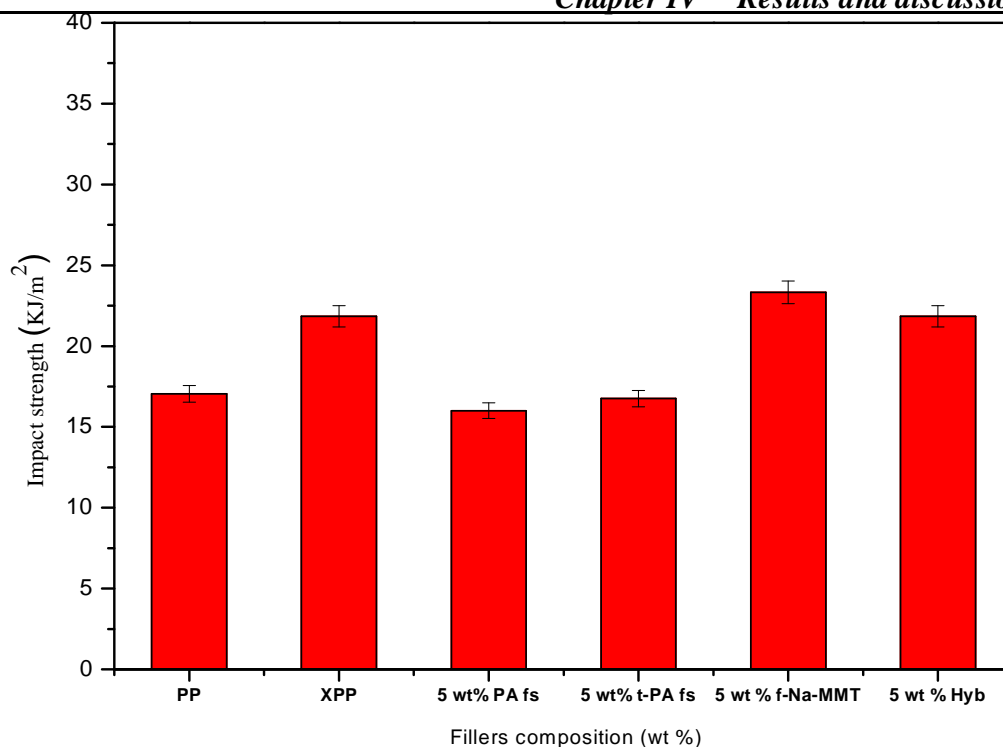


Figure IV.73. Variation of the Izod impact strength for the different composites

IV.2.3.2. Conclusion

From the obtained results by different experimental methods, the following conclusions can be summarized. The reactive melt mixing method using the functionalizing agent successfully gives rise to a total or partial exfoliation with 5wt% of f-Na-MMT as has been proven with FTIR and WAXS results. The t-PAfs can be effectively incorporated in f-Na-MMT/PP recycled nanocomposite matrix. The differential scanning calorimetry (DSC) measurements indicates the nucleating effect of f-Na-MMT and t-PAfs. The treatment of polyamide fiber surface with stearic acid is a simple and a successful method that enhances the adhesion with the f-Na-MMT/PP recycled nanocomposite. A good dispersion of the fibers with a noticeable improvement of the interfacial adhesion between PP and and treated PAfs phases were observed, showing an enhancement in the mechanical properties of the PP.

IV.1.2. Crosslinking of polybutene-1 (PB-1)

IV.1.2.1. rheological results

2.1.1. DRA results

Figure IV.74 (torque variation as a function of time) reports the rheological behavior of the different crosslinked PB-1 materials. From the figure it could be shown that all materials show an increase in torque at the beginning which explained by the effect of the solid polymer pellet resistance, then the torque decreases until the complete melting of the polymers (point A). Beyond this point, the torque of the modified samples increases by increasing the crosslinking agent content. However, the torque of the neat PP is still constant until the equilibrium torque value. The effect of the peroxide on the neat PB-1 is also evaluated, showing a lower torque value than the neat PB-1, this is due to the attack of the peroxide radicals, at the tertiary carbons of PB-1, which caused a scission chain of the polymer.

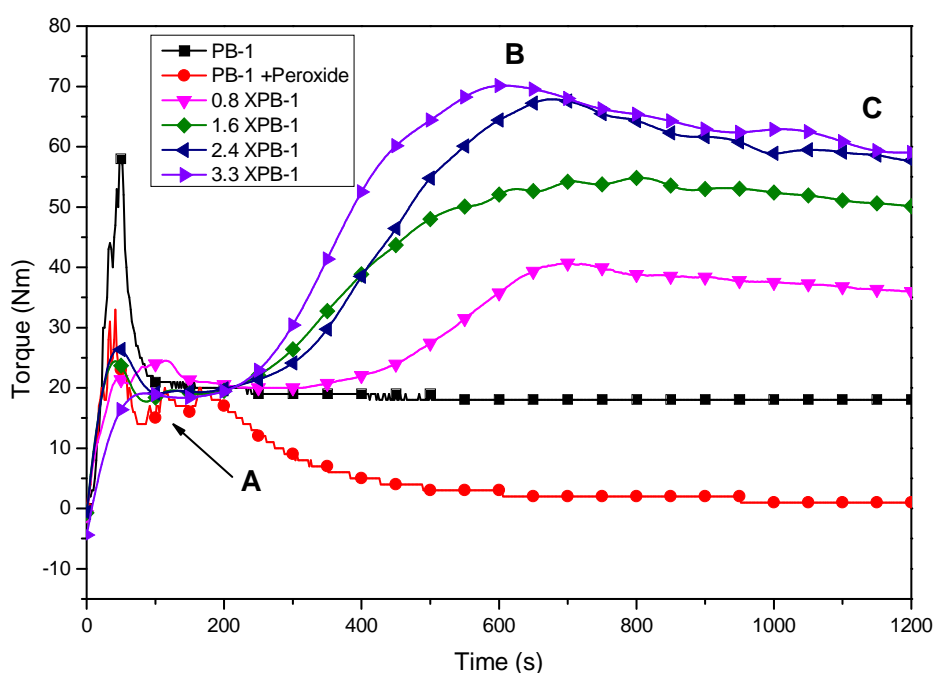


Figure IV.74. Evolution (Torque/time) for the different crosslinked PB-1 materials

Figure IV.75 depicts the T_B and T_C torque values as function of crosslinking agent, the maximum crosslinking degree (T_B) and the equilibrium torque (T_C) values depend on the crosslinking agent concentration, Therefore the viscosity of the crosslinked samples increases with the crosslinking agent content compared to the neat PB-1.

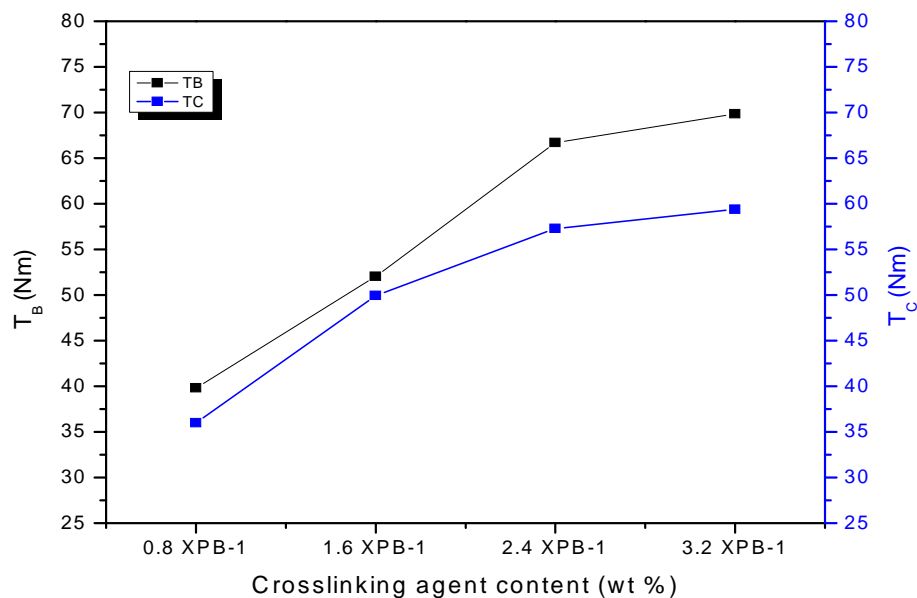


Figure IV.75. Variation of T_C and T_B torque values for the crosslinked PB-1 materials

2.1.2. MFI measurements

The MFI results of the different materials are shown in figure IV.76. As expected the MFI values of the different crosslinked samples present a significant decrease as function of the crosslinking agent amount compared to the unmodified PP, this is due to the contribution of crosslinking agent effect in increasing the polymers viscosities. MFI results prove the DRA results.

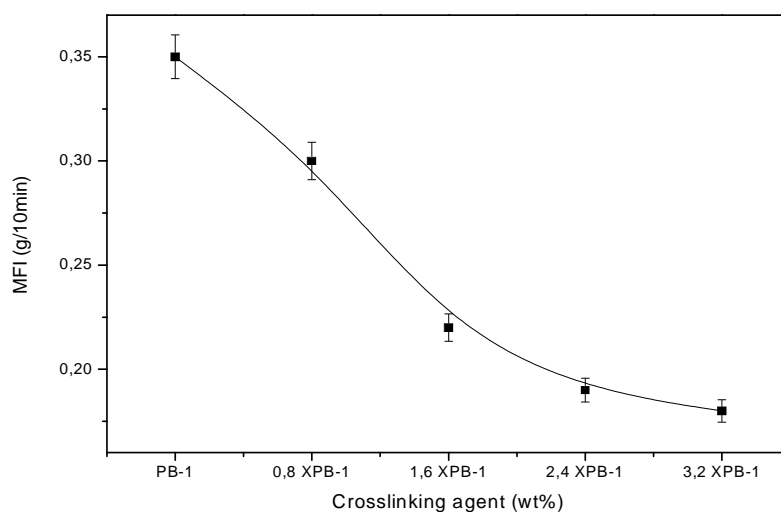


Figure IV.76. Variation of MFI values for the modified PB-1 samples

IV.1.2.2. Gel content

With aim of determining the crosslinking degree for the different compositions, gel content test was done and the obtained values are collected in table IV.14. The results clearly show that the gel content increases as the crosslinking agent content increases; we should note that the highest value of the gel content is found in the composition of 3.2 XPB. It should be mentioned that the obtained results are in good agreement with those of the DRA.

Table IV.14. Variation of gel content for the crosslinked PB-1 samples

Samples	Gel content w/w (%)
0.8 X PB-1	19.5
1.6 X PB-1	26.3
2.4 XPB-1	30.6
3.2 XPB-1	34.1

IV.1.2.3. Structural study of the modified PB-1

2.3.1. DSC measurements

a/- DSC measurement of the granules

Before studying the modified samples, it should be compared the DSC results of the pellet used polybutene-1 in his first state, and after one mixing cycle in the Brabender (mixed granules), with a view of showing the effect of the mixing process on the thermal properties of PB-1. Figure IV.77 shows the DSC thermograms of the neat PB-1 before and after one mixing cycle in the Brabender. The thermogram of the PB-1 pellet presents a lower melting temperature than that of the mixed granules polymer, whereas the crystallinity degree of the pellet shows higher value than the mixed one (see table IV.15). It is worth noting that the mixed PB-1 granules were aged for 3 months at room temperature, thus the melting temperature found corresponds to the stable form I of PB-1. So, the mixed PB-1 granules are taken as reference, because all crosslinked samples go through the same mixing conditions as PB-1 granules.

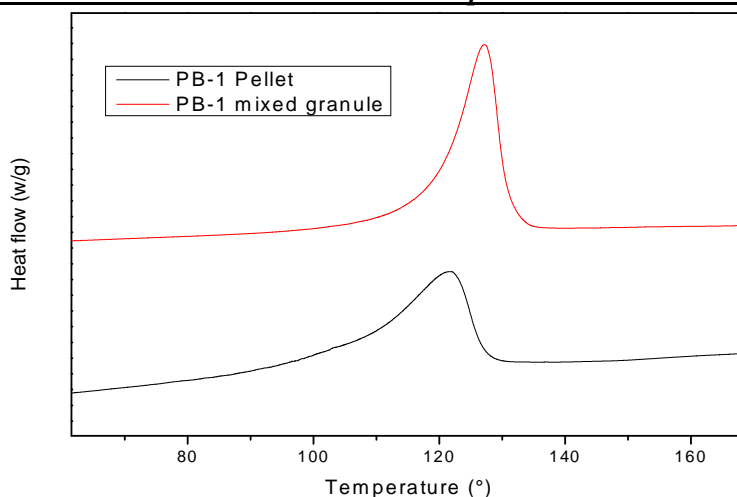


Figure IV.77. DSC thermograms of the neat PB-1 before and after one mixing cycle in the Brabender (pellet and mixed granule).

Table IV.15. DSC parameters of PB-1 pellet and granule (mixed)

Materials	T_m (°C)	ΔH_m (J/g)	χ_c (%)
PB-1 pellet	121	60	47
PB-1 mixed granule	127	56	44

Figure IV.78a and b show the DSC thermograms corresponding to the first and second heating runs of the different aged crosslinked PB-1. During the first heating run, the thermograms of the crosslinked PB-1 present the melting point of the stable crystalline form I of PB-1. However, and as it is expected the melting point of the unstable crystalline form II is shown in the second heating run. From the both heating runs a decrease in the melting temperature (-10°C) is shown in the 2.4 and 3.2 XPB-1 samples. According to the table IV.16, the 3.2XPB-1 sample exhibits the lowest crystallinity degree and crystal thickness value compared to all materials including unmodified PB-1. This may be due to the high peroxide content which produced a small crystal that formed from the chains session. The 1.6 XPB-1 present an increase in the crystallinity degree (+7%) followed with a stable melting temperature and crystal thickness in comparison with unmodified PB-1. Regarding the crystallization temperature of the modified samples, an inversely increase of T_c with the crosslinking agent content is shown compared to the neat PB-1 (see figure IV.79), the crosslinking agent acted as nucleating agent. From the obtained results it

can be concluded that the high crosslinking agent content affects the crystallization process of the PB-1.

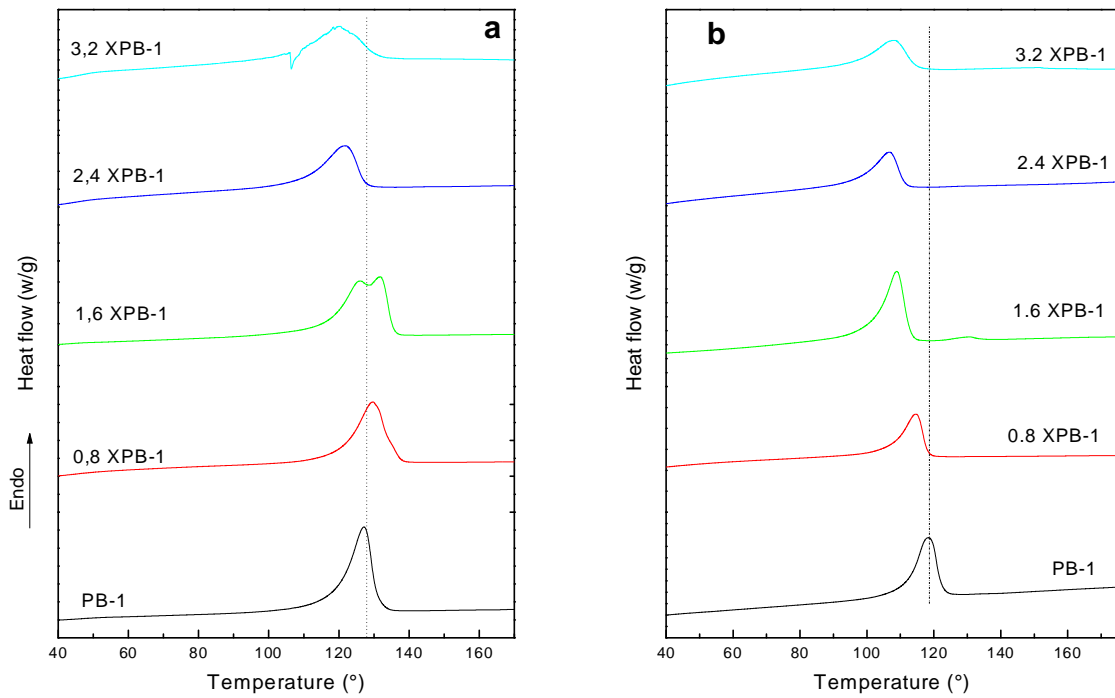


Figure IV.78.DSC thermograms of the first (a) and second (b) heating runs of the crosslinked PB materials

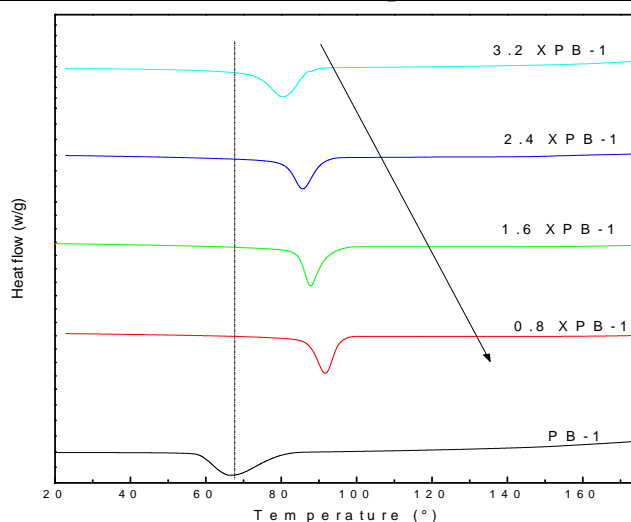


Figure IV.79. DSC Thermograms of the cooling run of the crosslinked samples

Table IV.16. DSC results of the modified PB-1 samples

Sample	T _{m1} (°C)	ΔH _{m1} (J/g)	L _c ^{DSC} (nm)	χ _c ¹ (%)	T _{m2} (°C)	ΔH _{m2} (J/g)	L _c ^{DSC} (nm)	χ _c ² (%)	T _c (°C)	ΔH _c (J/g)
PB-1	130	56	11	44	117	33		44	69	37
0.8 XPB-1	130	60	11	47	115	31		41	91	34
1.6 XPB-1	129	66	8	52	110	31		41	87	30
2.4 XPB-1	122	54	4	43	107	31		41	85	28
3.2 XPB-1	120	50	3	40	107	25		33	80	20

b/ DSC measurement of the plates

As it has been mentioned in the experimental section, plates with dimension of 100*100*1 mm³ were prepared by compression molding using the mixed granules studied above. Therefore, DSC thermograms of the plates are also investigated with aim of showing the effect of the plates shaping on the structure of the modified samples. Noteworthy, that the prepared plates were aged at room temperature for 4 weeks before undergoing the diverse tests.

Figure IV.80a depicts the DSC thermograms of the first heating run of the different materials. Table IV.17 shows the obtained DSC parameters. From the figure, it can be seen that all melting temperatures are corresponding to the stable form I of PB-1. Also, the melting temperatures of the pellet and granules are similar as those found in the DSC measurement of the mixed granules

before shaping (see table IV.16), and both of them give higher crystallinity degree. This observation is almost the same for the modified samples, where they present the same melting temperature as the mixed granules (see table IV.16) whereas their crystallinity degrees show a significant increase, also the 1.8 XPB sample shows the most important crystallinity degree as it has been found also in the 1.8 XPB mixed granule. The second heating run is shown in figure IV.79b, it can be clearly seen that all the melting temperatures are related to the unstable form II, however a weak second peak of the melting temperature of the stable form I is appeared at 128 °C in all materials thermograms including the neat PB-1.

The crystallization temperatures of the crosslinked samples show an inversely increase of T_c with the crosslinking agent content (see figure IV.81).

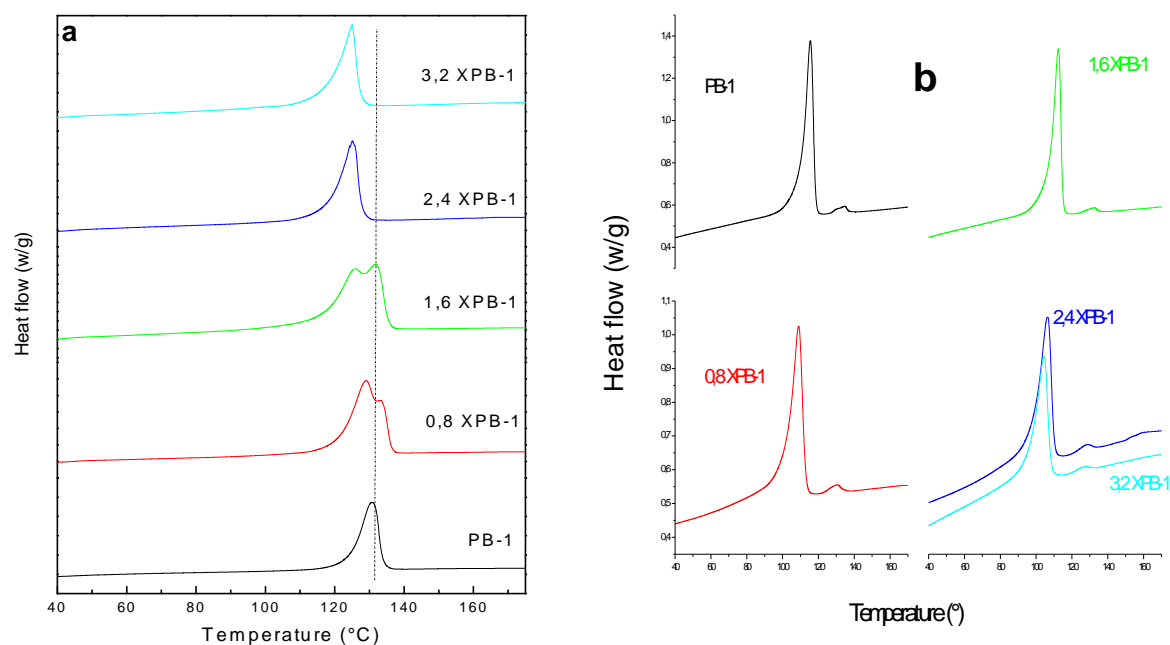


Figure IV.80. DSC thermograms of the first (a) and second (b) heating runs of the crosslinked samples (plates)

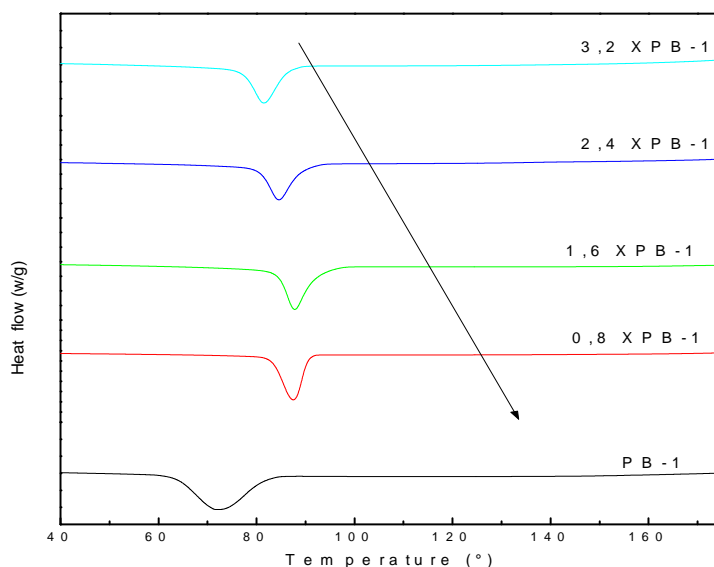


Figure IV.81. DSC Thermograms of the cooling run of the crosslinked samples (plates)

Table IV.17. DSC results of the modified PB-1 samples (plates)

Sample (plates)	T _{m1} (°C)	ΔH _{m1} (J/g)	L _c ^{DSC} (nm)	χ _c ¹ (%)	T _{m2} (°C)	ΔH _{m2} (J/g)	L _c ^{DSC} (nm)	χ _c ² (%)	T _c (°C)	ΔH _c (J/g)
PB-1 pellet	121	73	-	58	117	36		48	71	37
PB-1 mixed granules	129	66	8	52	117	30		34	70	34
0.8 XPB-1	129	70	8	55	112	33		34	87	34
1.6 XPB-1	130	65	11	52	108	30		33	87	33
2.4 XPB-1	125	56	7	44	106	25		27	84	27
3.2 XPB-1	125	46	7	37	104	23		24	81	24

2.3.2. X-ray diffraction Results (Plates)

Figure IV.82 shows X-ray diffraction profiles of the different crosslinked PB-1. As it has been mentioned the crosslinked materials were aged for four weeks at room temperature before the X-ray diffraction test, therefore, it is expected that the II→I transition is completed [23, 24]. Thus, from the WAXS patterns it can be observed that the hexagonal phase I is characterized by three main peaks at 9.9, 17.3, 20.2 °θ, originated by the (110), (300), (220) planes, respectively [25]. In addition, the reflection relative to the tetragonal phase II has been observed at 11.9 and 18.48 2θ, corresponding to the (200) and (301) planes respectively [25]. The crystallinity degree of the crosslinked samples decreases as function of crosslinking agent content (see table IV. 18). Also,

it is found that the crosslinking agent increases the crystallinity of the form II, the form I crystallinity decreases, whereas that of the form II increases by the addition of the crosslinking agent (see figure IV.83). The 2.4 XPB sample shows the same crystallinity ratio of the both forms.

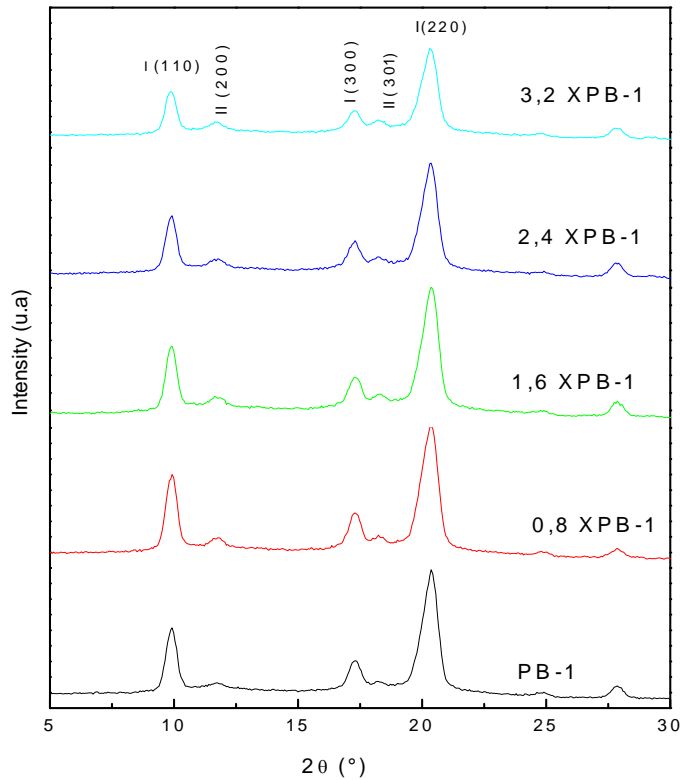


Figure IV.82 .WAXS profiles of the crosslinked PB-1 samples

Table IV.18. χ_I , χ_{II} and crystallinity degree of the modified PB-1 materials

Materials	χ_I(%)	χ_{II}(%)	χ(%)
PB-1	20	12	33
0.8 XPB-1	19	14	32
1.6 XPB-1	17	16	33
2.4 XPB-1	14	14	28
2.3 XPB-1	12	14	26

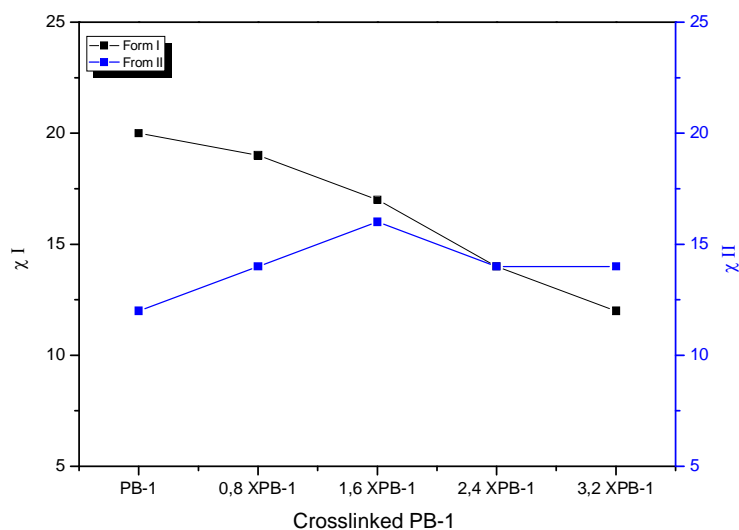


Figure IV.83. Variation of the crystallinity degree for form I and II of the crosslinked PB samples

2.3.3. FTIR Results

Figures IV.84 (a and b) display the FTIR spectra of the crosslinked PB-1 samples. New characteristic weak bands are shown, for instance, the band at 1110 cm^{-1} assigned to C-S stretch, and at 875 cm^{-1} due to the swinging of N-H, produced from the reaction with the accelerator (see figure IV.84 a). Characteristic weak bands of C-S stretch at 713 and 670 cm^{-1} . Additionally, the characteristic bands of S-S disulphide bonding are shown around 500 , 524 and 470 cm^{-1} (see figure IV.84 b). On the other hand, it can be shown in figure IV.84a that the intensity of the peak at 905 cm^{-1} decreases and the intensity of the peak at the 923 cm^{-1} increases after the ageing at room temperature. The band at 905 cm^{-1} is a characteristic band of form-II and the band at 924 cm^{-1} is a characteristic band of form-I. Form-II is completely transformed into form-I upon ageing at room temperature as it has been also found in the WAXS results.

The principle of the reversibly crosslinking reaction of the polybutene-1 is the same of that presented in the crosslinking mechanism of the polypropylene which consists in forming macro-radicals through peroxide decomposition process, then stabilizing them by active sulfur groups. The bridges formed can be: a sulfur atom, a polysulfide $-(S)_n-$, or a cyclic S-compound. Figure IV.85 summarizes the principle steps of the crosslinking reaction of the polybutene-1.

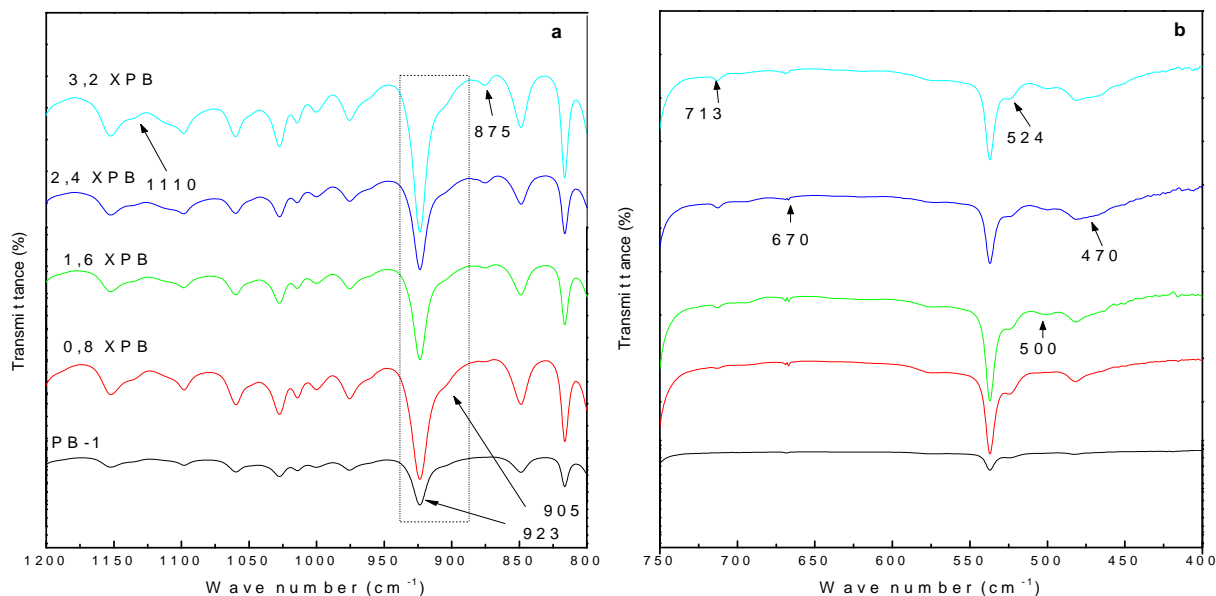


Figure IV.84. FTIR spectra of the crosslinked PB-1 samples **a-** in the region [1200- 800 cm^{-1}] and **b-** in the region [750 - 400 cm^{-1}]

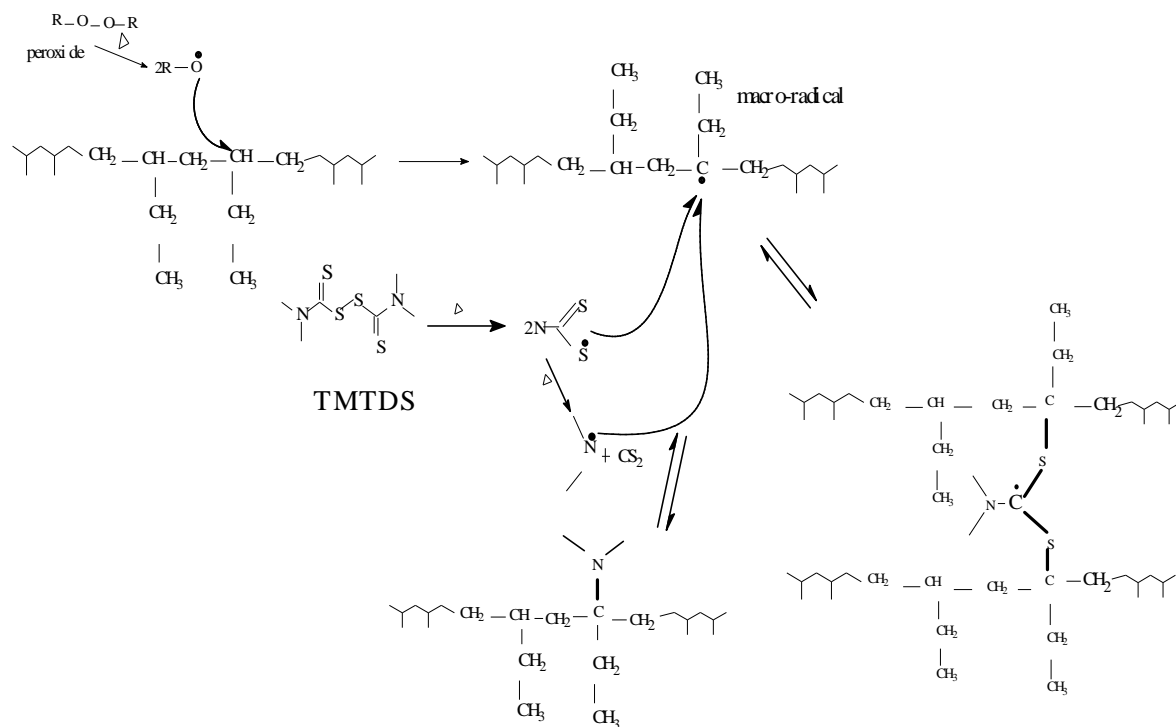


Figure IV.85. Mechanism of the crosslinking reaction of the polybutene-1.

2.3.4. 2D WAXS result

With the aim of determining the effect of the compression molding on the chain orientation of the modified PB-1, 2D transmission patterns of the prepared plates were examined. The 2D-WAXS patterns of the different plates are shown in figure IV.86.

It is found that three crosslinked samples show an initial orientation texture induced by the forming process by compression molding. $F_{(110)}^{\rightarrow} / \rightarrow_x = -0.07, -0.14$ and -0.06 for 1.6 XPB, 2.4 XPB and 3.2 XPB respectively.

Tensile tests are then machined out in the manner that this crystalline orientation of the macromolecular chains is taken as the stretching direction.

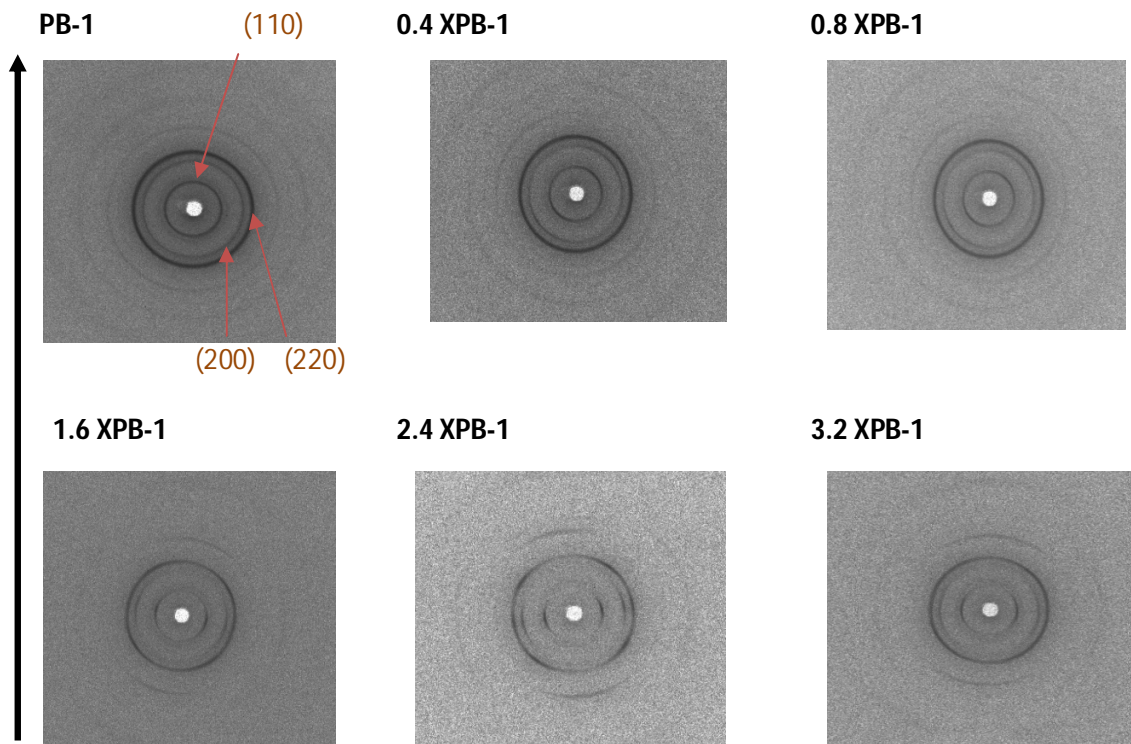


Figure IV.86. 2D WAXS patterns of the modified PB-1 samples

2.3.5. DMA results

In order to evaluate the viscoelastic behavior of the crosslinked PB-1 samples as function of temperature, DMA test was performed. Figure IV.87 a, b represent, respectively, the variations of the storage modulus and $\text{Tan } \delta$ as a function of temperature for the different crosslinked samples. It is found that the storage modulus of the crosslinked samples increases in both region (glassy and transition regions) as function of crosslinking agent (see table IV.19). The crosslinked materials with high degree of crosslinking give rise to the high storage modulus. In figure IV.87b, the maxima in these plots correspond to the structural relaxations in the materials. The main structural relaxation corresponds to the glass transition of the samples T_g (glass temperature) values, are given in Table IV.19. It is clearly observed that t_g of the crosslinked polybutene-1 shifted up to a high values. Based on the study conducted by Roman *et al* [26] the crosslinked chain exhibits a high T_g values.

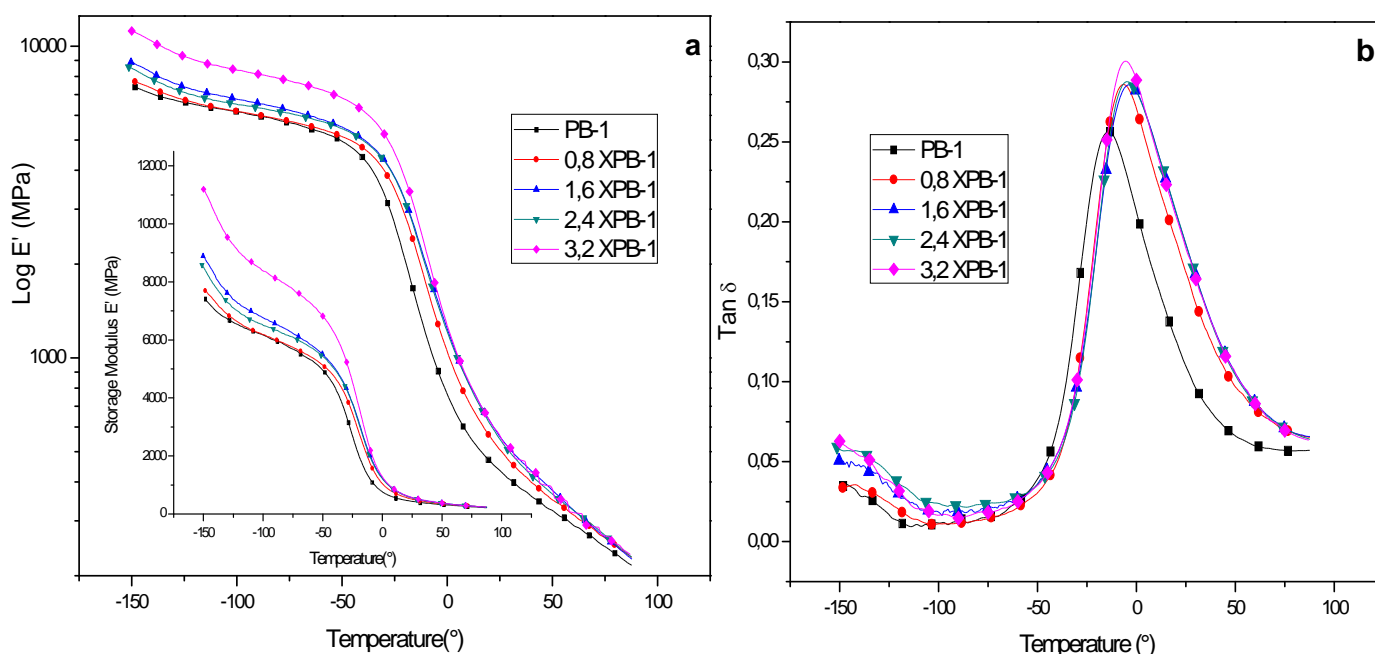


Figure IV.87. Variation of the storage modulus (a) and $\text{tan } \delta$ (b) as a function of temperature for the crosslinked materials

Table IV.19. DMA parameters of the modified PB-1 samples

Materials	E g	E0	Tg
PB-1	7399	3267	-14
0.8	7699	3304	-7
1.6	8886	3605	-5
2.4	8585	3197	-4
3.2	11191	3925	-5

2.3.6. True Stress-Strain behavior

Figure IV.88 depicts the true stress- true strain curves of the modified PB-1 materials, the curves can be divided into three region, the first one is preyielding region, which can be shown before the yield point at a strain of about 0.1, then the second region so –called strain softening region from a strain of about 0.1 to about 0.6, and finally strain-hardening region up to specimens break. For the first region, it is shown that the yield stress of the crosslinked samples increased compared to that of the neat PB, 1.6 XPB-1 and 2.4 XPB present the high yield stress. 3.2 XPB-1 and 0.8 XPB-1 show approximately the same yield stress value.

3.2 XPB-1 and 0.8 XPB-1 samples also show the less stress in the strain- hardening region. Moreover, they present a very limit elongation. The 3.2 XPB-1 seems to be stretched in the opposite direction of chain orientation. 2.4 XPB and 1.6 XPB show the highest strain and stress values.

It is worth noting that, Izod impact tests were carried out for the different crosslinked samples, and it was found that all modified samples including the neat PB-1 did not break during the impact test, that is due to the ductile behavior of the samples.

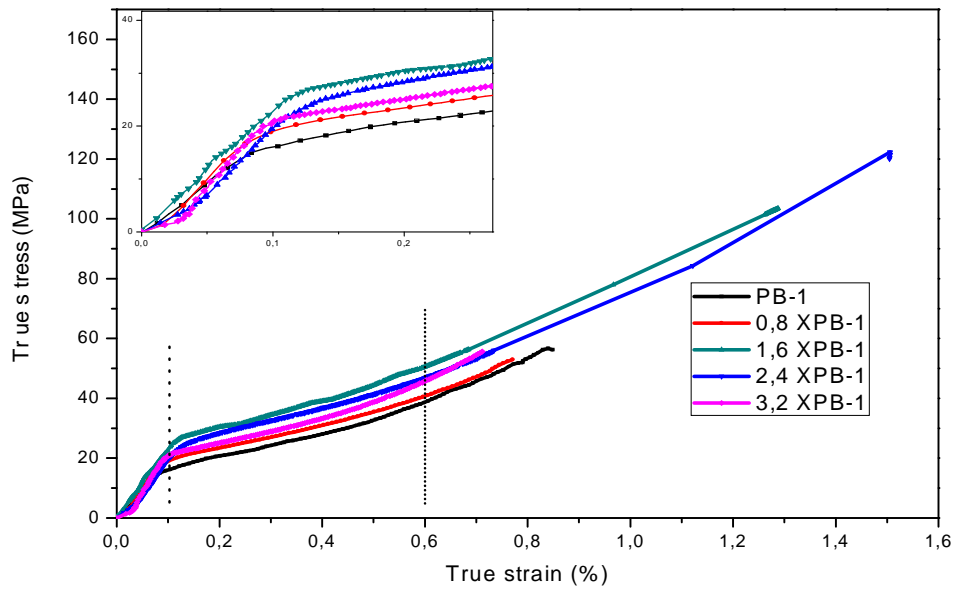


Figure IV.88. True stress- true strain curves of the modified PB-1 materials

2.3.7. SEM observation

SEM micrographs of 0.8 XPB-1 and neat PB-1 are shown in figure IV.89. Unlike the neat PB-1, the crosslinked sample shows some droplets coalesce together indicating a difference in the morphology of the modified polybutene materials.

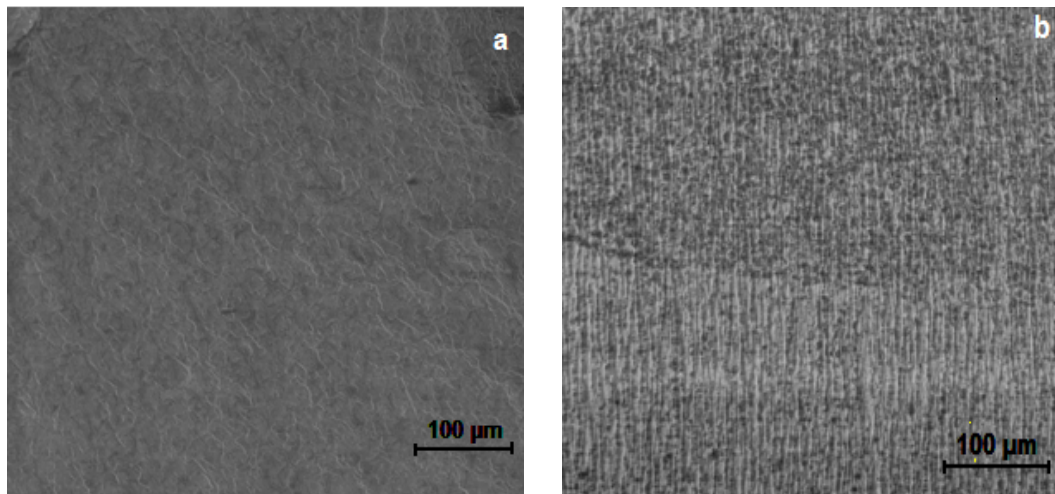


Figure IV.89. SEM micrographs of a-neat PB-1 and b- 0.8 XPB-1 samples

IV.1.2.4. Conclusion

According to the results obtained, it can be concluded that, the crosslinking reacton degree can be affected by the crosslinking agent content .Also; it has clearly seen that the crosslinking process has affected the microstructure of the polybutene-1.2.4 XPB-1

IV.2.2. Crosslinked PB-1/hollow PET fiber/clay Hybrid composites

2.1. DRA measurement

Figure IV.90 depicts the torque evolution for PB-1, PB-1/7wt % treated hollow PET, PB-1/5wt % f-Na-MMT and hybrid composites. Compared to the torque of PB-1, it is clear that the hybrid composite and PB-1/7wt % hollow PET fiber composite show the higher and lower torques in the stability region, respectively. PB-1/5wt % f-Na-MMT nanocomposite presents intermediate torque value between that of the hybrid and PB-1/7wt % hollow PET fiber composites. The torque in stability can be affected by the fillers addition, dispersion and adhesion which provide a high viscosity to the composites.

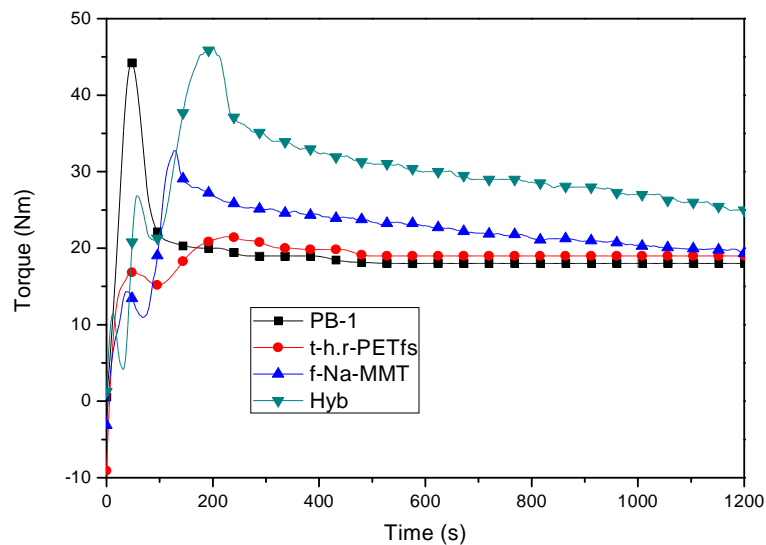


Figure IV.90. Torque evolution of the different composites samples

2.2. MFI measurement

The variation of the MFI values of the presented composites in DRA curves above are illustrated in figure IV.91. It is clearly seen that the viscosity of the studied composites increased compared to that of the neat PB-1. The hybrid composite shows the highest viscosity value. The obtained results are in consistent with the DRA results.

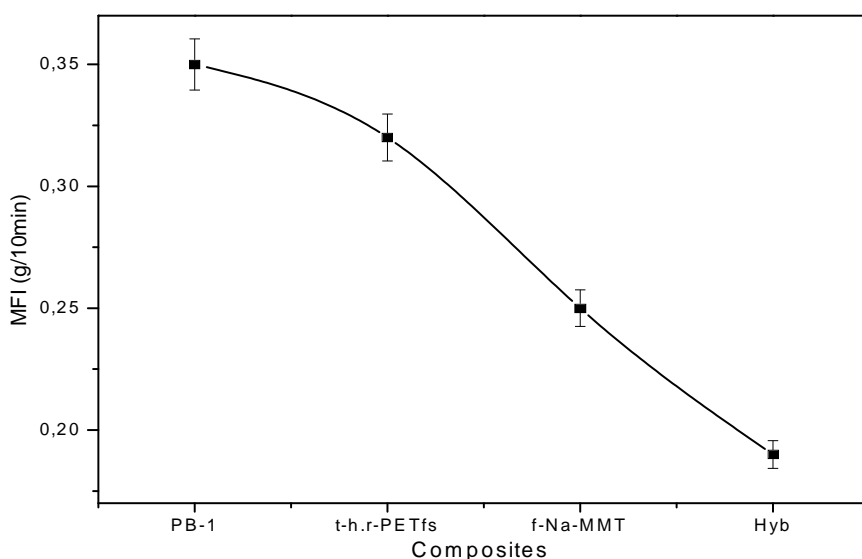


Figure IV.91. Variation of MFI for the different composites samples

2.3. DSC Measurements

Figure IV.92 displays the first and second heating runs of the crosslinked PB-1, modified and unmodified PB-1 / treated PET fibers composites, in which the influence of the modification of the polybutene matrix by the crosslinking was investigated. From the data of the first run (see table IV.20), it can be seen that the crosslinked PB-1/PET fiber composite present almost similar melting temperature as the composite based on unmodified PB-1, however it is higher than that of the modified PB-1. Thus, the incorporation of the treated PET fiber on the crosslinked PB-1 increases the melting temperature and the crystallinity degree of the crosslinked PB-1. It is worth noting that the melting temperatures of the different compositions correspond to the stable form I of the polybutene-1. Crystallization temperatures of composites show an increase in both filled matrices compared to the neat PB-1, this because of PET fiber and crosslinking agent acted as a nucleating agent in the composite.

Chapter IV Results and discussions

Regarding the second heating run, all melting temperatures are related to the unstable form II of polybutene -1. As it has been shown in the study of the crosslinked PB-1 a lower melting temperatures are found in both crosslinked PB-1 and its composite.

Table IV.20. DSC parameters of modified and unmodified PB-1/PET fiber composites

Materials	ΔH_{m1}	ΔH_{m2}	ΔH_C	T_{m1}	T_{m2}	T_c	χ_{c2}	χ_{c1}
	(J/g)	(J/g)	(J/g)	(°C)	(°C)	(°C)	(%)	(%)
PB-1	66	30	34	129	117	70	40	52
7wt% h.r- PETfs	71	37	36	127	113	89	52	60
2.4 XPB-1	58	30	28	125	106	84	40	46
XPB-1 /t- h.rPET fs	64	29	32	128	107	77	41	54

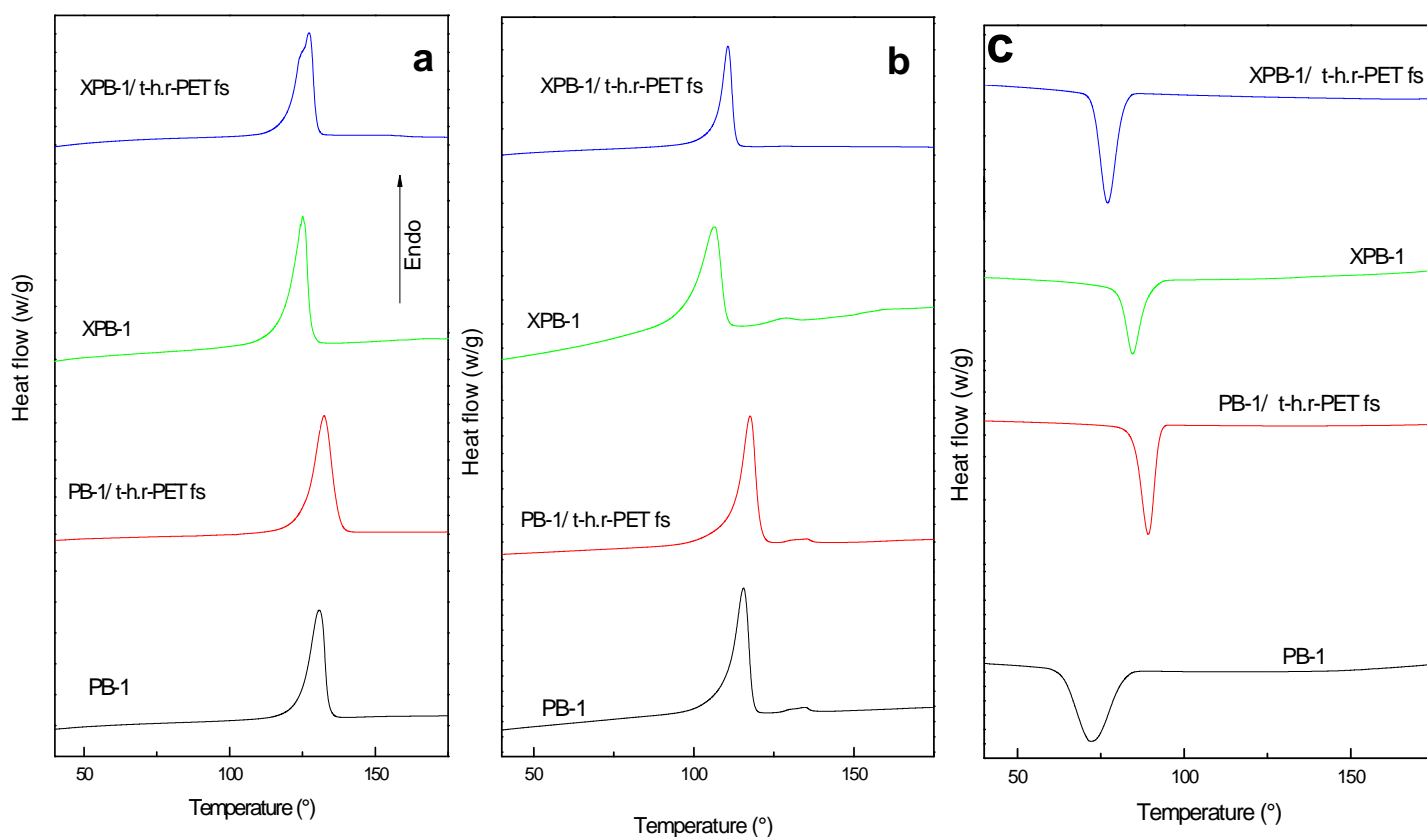


Figure IV.92. First and second heating runs of the crosslinked PB-1, modified and unmodified PB-1 / treated PET fibers composites

Figure IV.93 depicts the first and second heating runs of PB-1/f-Na-MMT nanocomposite, PB-1 /7wt% hollow PET fibers composite and the hybrid composite. From the DSC parameters (table IV.21). The melting temperature of the hybrid composite increases compared to the neat polymer, it is noticed that this temperature is almost between the melting temperatures of the nanocomposite (PB-1/ f-Na-MMT) and composite (PB-1/ h.PETfs) samples. Additionally, the crystallinity degree of the hybrid composite increased. PB-1/ f-Na-MMT nanocomposite shows the highest crystallization temperature degree (see figure IV.94) and crystallinity value, this could be explained by the nucleating effect of the exfoliated clay nanolayers on the PB-1 matrix.

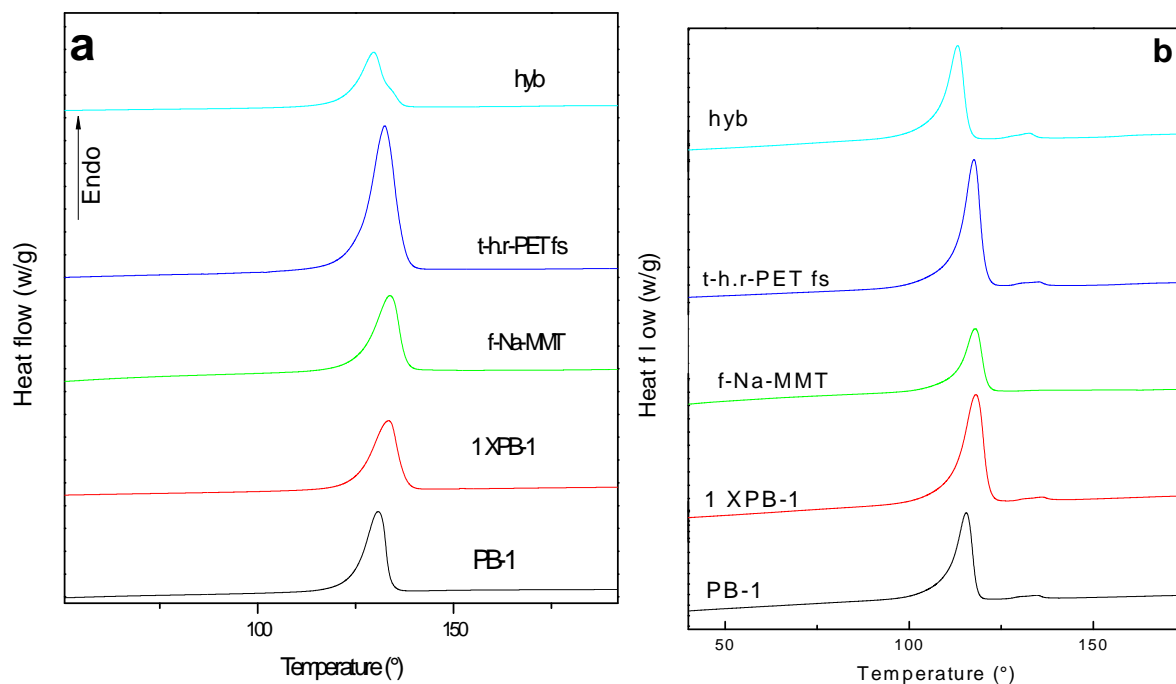


Figure IV.93. First and second heating runs of PB-1/f-Na-MMT nanocomposite, PB-1 /7wt% hollow PET fibers composite and the hybrid composite.

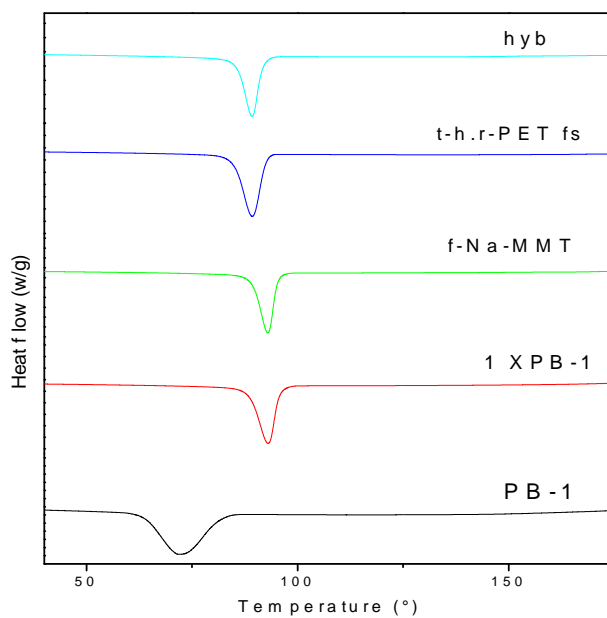


Figure IV.94. Cooling run of PB-1/f-Na-MMT nanocomposite, PB-1 /7wt% hollow PET fibers composite and the hybrid composite.

Table IV.21. DSC parameters of the composites investigated

Materials	ΔH_{m1} (J/g)	ΔH_{m2} (J/g)	ΔH_c (J/g)	T_{m1} (°C)	T_{m2} (°C)	T_c (°C)	χ_{c2} (%)	χ_{c1} (%)
PB-1	66	30	34	129	117	70	40	52
1 XPB-1	83	32	41	133	118	93	42	66
f-Na-MMT	91	40	40	133	118	93	62	72
t-r.PETfs	71	37	36	127	117	89	52	60
Hyb	67	42	31	130	113	89	62	60

2.4. X-ray diffraction

Figures IV.95 a and b illustrate the X-ray diffraction patterns of the different composites, All samples show characteristic peaks of form I and II of polybutene-1. The peaks at 2θ values of 9.9, 17.3, 20.2 and 21.6 correspond to planes (110), (300), (220) and (211), respectively, of form I, whereas, the peaks at 2θ values of 11.9, and 18.48 correspond to planes (200), (301) respectively, of form II. Very weak peaks of form II are shown in the neat PB-1. Based on figure IV.94.a, it can be clearly seen that the characteristic peak of the d_{001} spacing of Na-MMT at 6.9° disappeared in the both nanocomposite (5wt% Na-MMT) and hybrid composite. This indicates the separation of clay layers and the formation of nanocomposites. The crystallinity degree (see table IV.22) of the different composites do not show a clear trend compared to that of the neat PB-1, except for the nanocomposite and PB-1/t-PET fibers composites ones so that an increase of the crystallinity degree is shown in the nanocomposite sample, indicating the nucleation effect of the nanoclay in the PB-1, whereas, the incorporation of the treated PET fibers shows a decrease of the crystallinity degree of the polymer.

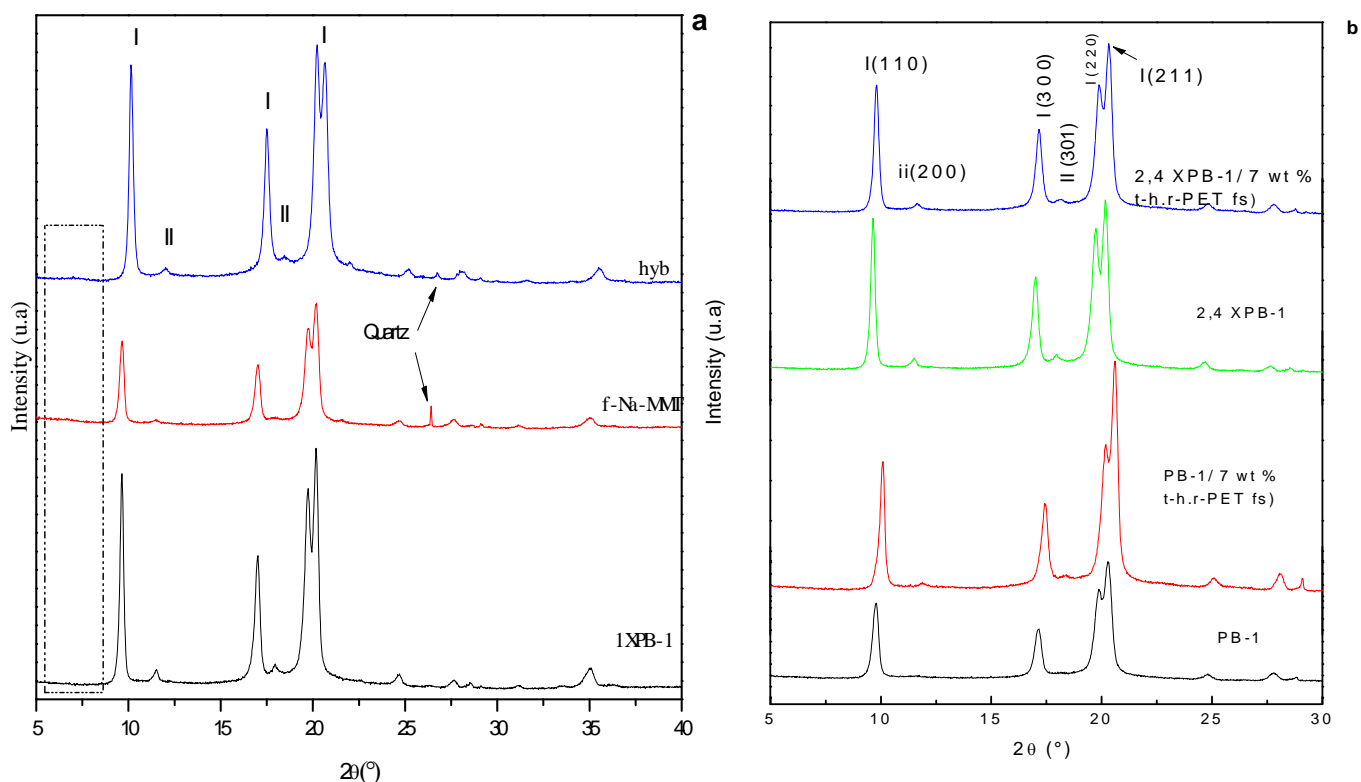


Figure IV.95. WAXS patterns of the different composites.

Table IV. 22. Crystallinity degree of the different composites

Composites	χ (%)
PB-1	30
PB-1/t-h.r-PETfs	25
2,4 XPB-1	28
2,4 XPB-1/ t-h.r-PETfs	28
1 XPB-1	30
f-Na-MMT	34
Hyb	30

2.5. Mechanical properties

Figure IV.96 shows the variation of Young's modulus for the different composites. For the PB-1/PET fiber composite, the Young's modulus shows an enhancement in the composite based on the treated fiber. On the other hand, the Young's modulus of the PB-1/f-Na-MMT nanocomposite

almost does not vary compared to that of the neat matrix. On the other hand, it is clear that the modified matrix reinforced by the treated PET fiber improves the modulus of the composite; this is due to the strong interaction between the polar group in PET fiber and the crosslinked PB-1. Since the crosslinking reaction is reversible, the interactions between the modified PB-1 and the treated PET fiber are expected to be good. The improvement of the adhesion between the two phases can also be shown from the scanning electron micrographs of the fractured surface of crosslinked PP/treated PET fiber composites (Figure IV.99 (b,d)). Moreover, the incorporation of the treated PET fiber on the melted PB-1/ f-Na-MMT nanocomposite gave rise to the Young's modulus of the hybrid composite. This can be explained by the improvement of the nanocomposite rigidity by adding the treated PET fiber.

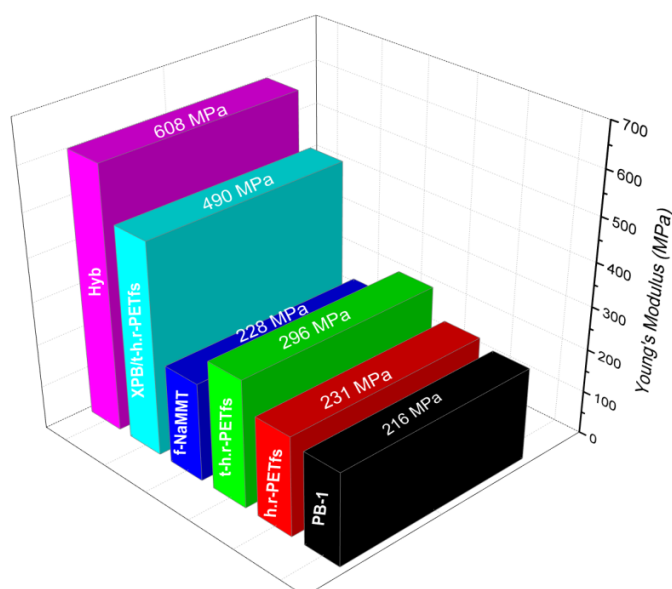


Figure IV.96. Variation of Young's modulus for the different composites, nano and hybrid composite samples.

The values of stress and strain at break of the investigated composites are shown in Figure IV.97. A significant increase in the stress at break is observed when the treated PET fiber was incorporated to the crosslinked PB-1, in addition this composite shows a good strain value. So, a good adhesion between the treated fiber and the modified PB-1 can be confirmed, the SEM micrographs are in good agreement with this result (see figure IV.100).The f-Na-MMT/PB-1 nanocomposite also presents a high stress and strain at break values what can be explained by the structural affinity of the functionalized nanoclay. Analogously, an enhancement in stress and strain at break can be noticed in the hybrid composite sample.

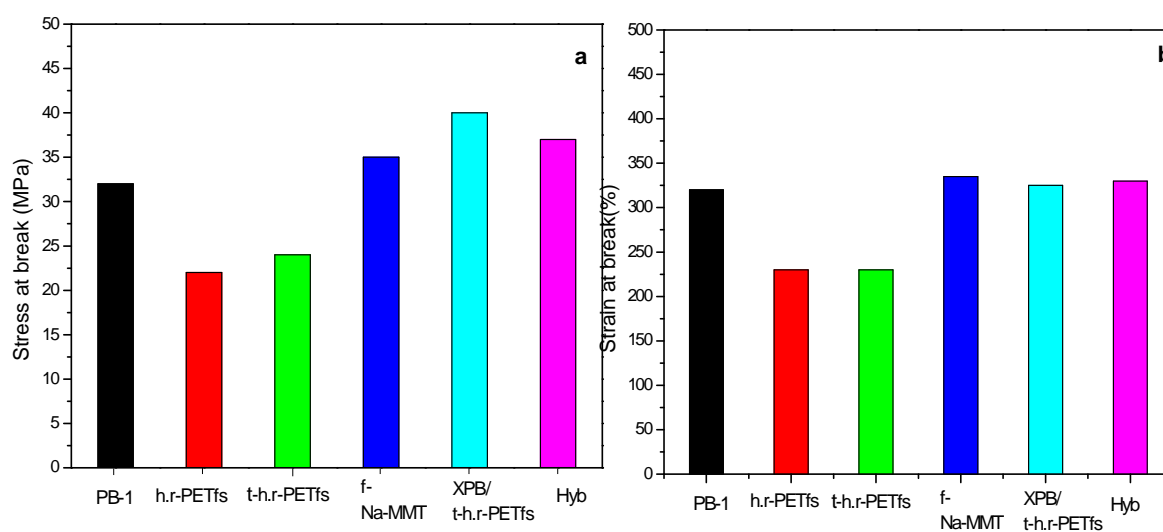


Figure IV.97. Variation of the stress (a) and strain (b) at break of the investigated composites

2.6. Impact strength

The Impact strength values of the studied composites are listed in table IV.23. The modified PB-1 /treated PET fiber composite shows an important resilience value. This is due to the interfacial bond strength between the crosslinked PB-1 /treated PET fiber. SEM micrographs illustrate the good interface existing between the two phases. Neat PB-1 and PB-1/ f-Na-MMT did not break whereas the hybrid composite sample shows a significant improvement of the resilience compared to that of the composites.

Table IV.23. Impact strength of the different composites

Materials	Impact strength (KJ/m²)
PB-1	No break
h.r-PETfs	12
t-h.r-PETfs	15
f-Na MMT	No break
XPB-1/ t-h.r-PETfs	25
Hyb	32

2.7. DMA results

The storage modulus E' represents the stiffness of a viscoelastic material. Figure IV.98 (a) and (b) depict, respectively, the variations in the storage modulus and the damping factor ($\tan \delta$) as function of temperature for the different composites. In the glassy region (E_g), both unmodified and modified PB-1/treated PET fiber exhibit the lowest storage modulus of about 6888 and 6941 MPa respectively. On the other hand, the nano and the hybrid composites give the highest storage modulus values which are 8598 and 10728 MPa respectively (the storage modulus values are summarized in table IV.23). Then, all composites present a downward trend as the temperature increased, which represent glass transition region (E_0). In this region the nano and hybrid composites are still indicating the highest storage modulus of about 4160 and 5100MPa respectively. The storage modulus enhancement is due to the higher restriction imposed by the fillers on the PB-1 matrix; subsequently the stress transfer at the fillers interface will be increased, which increases the stiffness of the composite.

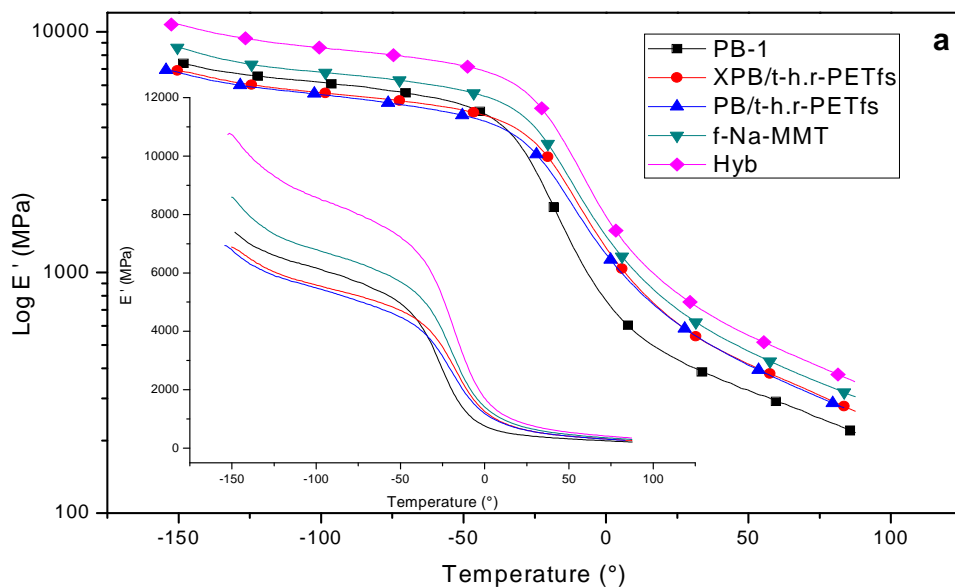


Figure IV.98.a. Storage modulus of the different composites as a function of temperature

The glass transition temperatures obtained from the tan delta curve of the composites, indicate a slight increase compared to that of the neat matrix. According to Almeida *et al.* [27], systems containing more restrictions and a higher degree of reinforcement tend to exhibit higher T_g. A similar trend was obtained by Chieruzzi *et al.* [28] on studying UPR/montmorillonite (MMT) nanocomposites and they attributed the increase of the T_g to the good adhesion between the clay and the matrix. The tan delta peak of the neat matrix is lowered with the incorporation of the PET fiber and the nanoclay; this is due to the restriction in the movement of the polymer molecules caused by the presence of fillers.

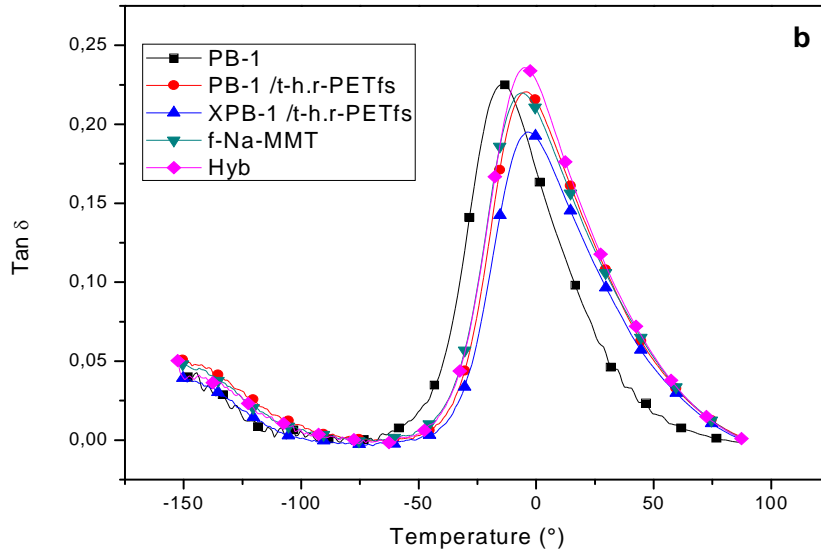


Figure IV.98. b. The damping factor ($\tan \delta$) of the composites as a function of temperature

Table IV.23. DMA parameters of the different composites

Composites	Eg (MPa)	E0 (MPa)	Tg (°)
PB-1	7384	3469	-14
PB-1/t-h.r-PETfs	6898	2962	-4
XPB-1/t-h.r-PETfs	6904	3312	-4
f-Na-MMT	8598	4159	-6
Hyb	10728	5097	-4

2.8. SEM observations

The effect of the surface treatment of PET fiber on the interface between the PB-1 and the PET fibers was studied by examining the tensile fractured surfaces of the specimens using SEM. SEM micrographs of the tensile fractured surface of the treated and untreated PET fiber composites containing 7 wt% PET fibers can be seen in Figure IV.99. Both treated and untreated fibers are well dispersed in the matrix indicating the efficient mixing of filler within the polybutene matrix. The examination of the fractured surface of untreated PET fiber composites (figures 99 (a,b)) indicates that there are voids between fiber and matrix. Also, fibers pull out is shown which is an

Chapter IV Results and discussions

evidence of poor adhesion. On the other hand, SEM micrographs of the treated PET fiber composites (figures 99 (c,d)) clearly indicate that there are still voids around the fiber, however, it is shown that the fiber present more elasticity aspect during tensile strength test, in addition it can be seen that the treated fibers embedded inside the matrix more than the untreated ones.



Figure IV.99. SEM micrographs of the tensile fractured surface of the untreated (a, b) and treated (c, d) 7 wt% PET fiber /PP composites

Tensile fractured surface examinations of treated PET fiber/crosslinked PB-1 composite show the best results in term of interfacial adhesion. As shown in figure IV100, treated PET fiber was well surrounded by the matrix without voids and the matrix fibrillation takes place, which is a

Chapter IV Results and discussions

good indicator of better interfacial adhesion between fiber and matrix as shown in Figure 100 (a). In addition, it can be clearly seen that the matrix locked inside the treated hollow PET fiber, which proves the good adhesion between fiber and matrix (Figure 100 (b, d)). All these observations are consistent with the mechanical test results.

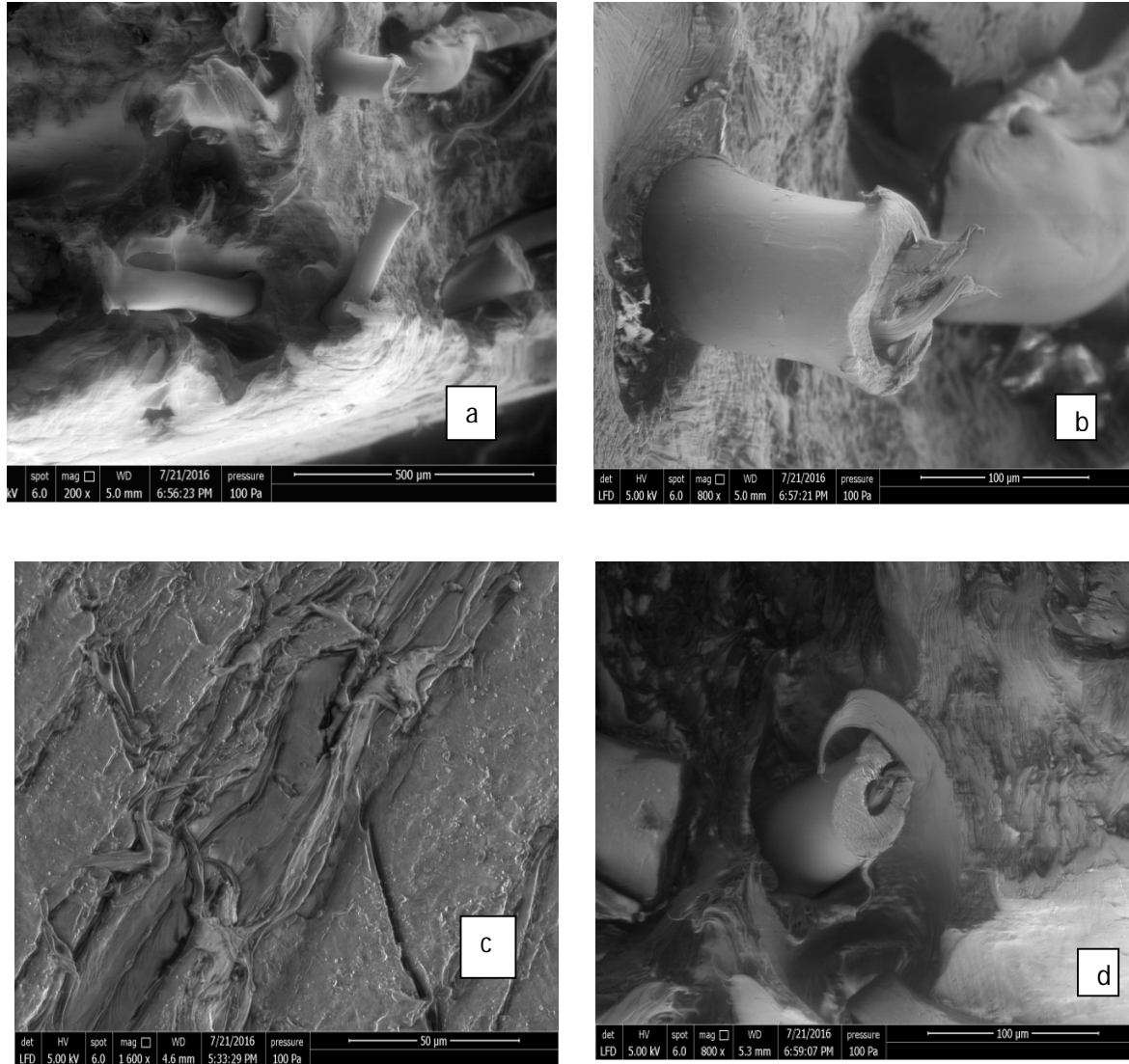


Figure IV.100 (a,b,c,d). SEM micrographs of the tensile fractured surface of 7 wt% treated PET fiber/crosslinked PB-1 composite.

IV.2.3. Conclusion

Tests analysis of the study of f-Na-MMT/r-PET fiber/PB-1 hybrid composites reveals that the reactive melt mixing method using the functionalizing agent successfully gives rise to a total or partial exfoliation with 5wt% of f-Na-MMT. Also, the addition of the treated PET fiber to the f-Na-MMT/PB-1 nanocomposite matrix enhances the adhesion between fibers and PB-1, which leads to the improvement of the mechanical properties of the hybrid composite sample. Additionally, a good interfacial adhesion between the treated fiber and the crosslinked PB-1 matrix was observed.

References

- [1] Bruckner S, Meille S. Non-parallel chains in crystalline γ -isotactic polypropylene. *J Nature*, 340, 455–457, 1989.
- [2] Marigo A, Marega C, Saini R, Camurati I. Influence of regioirregular structural units on the crystallization of isotactic polypropylene. *J Appl Polym Sci*, 79, 375–384, 2001.
- [3] E. Nedkov, T. Dobрева, Wide and small-angle X-ray scattering study of isotactic polypropylene gamma irradiated in bulk. *European Polymer Journal*, 40, 2573–2582, 2004.
- [4] Turner-Jones, A. Aizlewood, J.M. Beckett, D.R. Crystalline forms of isotactic polypropylene. *Makromo. Chem*, 74, 134-158, 1964.
- [5] Bouhelal S, Cagiao ME, Benachour D, Calleja FJB. Structure modification of isotactic polypropylene through chemical crosslinking: Toughening mechanism. *Journal of Applied Polymer Science*, 103, 2968-2976, 2007.
- [6] M'bouroukounda G. Élaboration de composites innovants multicouches à matrice thermoplastique, Mémoire de Master, Institut Jean Lamour, France, 2014.
- [7] Joseph PV, Joseph K, Thomas S. Effect of processing variables on the mechanical properties of sisal-fiber-reinforced polypropylene composites. *Composites science and technology*, 59, 1625-40.1999.
- [8] Demira H, Atiklera U, Balkosea D, Tihminhog ˘lua F. The effect of fiber surface treatments on the tensile and water sorption properties of polypropylene–luffa fiber composites. *J Compo PartA*, 37, 447-456, 2006.
- [9] Ahmad I, Abu Bakar DR, Mokhilas SN, Ramli A. Recycled PET for Rice Husk/Polyester composites, *J sci techn develop*, 22 (4), 345-353, 2005.
- [10] Nasr-Isfahani M, Latifi M, Amani-Tehran M, Warnet L, Halvaei M. Enhancement of composite performance by hollow polyester fibers. *Journal of textiles and polymers*, 2 (2), 45-50, 2014.
- [11] Von Turkovich R, Erwin L. Fiber fracture in reinforced thermoplastic processing. *Polym eng sci*. 23, 743-749, 1983.
- [12] Fu SY, Hu X, Yue CY. Effects of fiber length and orientation distributions on the mechanical properties of short-fiber-reinforced polymers. *Mater sci eng res inter*, 5, 74-83, 1999.
- [13] Romanzini D, Lavoratti A, Heitor L, Ornaghi Jr, Sandro C. AAmico, Ademir J. Zattera. Influence of fiber content on the mechanical and dynamic mechanical properties of glass/ramie polymer composites, *Mater Des*. 47, 9-15, 2013.
- [14] Ornaghi Jr HL, Bolner AS, Fiorio R, Zattera AJ, Amico SC. Mechanical and dynamic mechanical analysis of hybrid composites molded by resin transfer molding. *J App Polym Sci*, 118, 887–896, 2010.
- [15] Ornaghi Jr HL, Bolner AS, Fiorio R, Zattera AJ, Amico SC. Mechanical and dynamic mechanical analysis of hybrid composites molded by resin transfer molding. *J Appl Polym Sci*, 118, 887–896, 2010.
- [16] Pothan LA, Oommen Z, Thomas S. Dynamic mechanical analysis of banana fiber reinforced polyester composites. *Compo sci technol*, 63, 283–293, 2003.
- [17] Mortaigne B, Bourbigot S, Bras ML, Cordellier G, A. Baudry. Fire behaviour related to the thermal degradation of unsaturated polyesters, *Polym. Degrad. Stab*, 64, 443, 1999.
- [18] Johnson K, Yang L. Preparation, properties and applications of unsaturated polyesters, In *Modern Polyesters: Chemistry and Technology of Polyesters and Copolyesters*, J. Scheirs and T.E. Long, Eds., Wiley, Chichester, 699, 2003.

- [19] Hari Prasad, K, Senthil Kuma M. Thermal Characterization of PP/Na⁺-MMT Composite Materials. *J. Mater. Sci. Eng*, 5, 80-86, 2011.
- [20] Zouai, F, Bouhelal S, Cagiao ME, Benabid FZ, Benachour D, Cagiao ME. Study of nanoclay blends based on poly(ethylene terephthalate)/poly(ethylene naphthalene 2,6-dicarboxylate) prepared by reactive extrusion. *J Polym Eng*, 34,431–439, 2014.
- [21] Bouhelal S, Cagiao M, Benachour D, Djellouli B, Rong L, Hsiao BS, Baltà-Calleja FJ. SAXS Study Applied to Reversibly Crosslinked Isotactic Polypropylene/Clay Nanocomposites. *J. Appl. Polym. sci*, 117, 3262–3270,2010.
- [22] Giannelis EP, Krishnamoorti R., Manias E. Polymer-Silicate Nanocomposites: Model Systems for Confined Polymers and Polymer Brushes. *Adv. Polym. Sci*, 138, 107–111,1999.
- [23] Boor J, Mitchell JCJ. Kinetics of crystallization and a crystal-crystal transition in poly-1-butene. *Polym. Sci., Part A*, 1, 59,1963.
- [24] Powers J, Hoffman JD, Weeks JJ, Quinn FA. Crystallization kinetics and polymorphic transformations in polybutene-1 .*J Res Natl Bur Stand*, 69A, 335,1965.
- [25] Azzurri F, Alfonso GC, Gomez MA, Martí MC, Ellis G, Marco C. Polymorphic transformation in isotactic 1-butene/ethylene. *Copolymers. Macromolecules*, 37, 3755, 2004.
- [26] Roman F, Calventus Y, Colomer P, Hutchinson JM. *Thermochim. Acta*, 54, 76, 2012.
- [27] Bismarck A, Mohanty A, Askargorta IA, Czapla S, Misra M, Hinrichsen G. Surface characterization of natural fibers; surface properties and the water up-take behavior of modified sisal and coir fibers. *Springer, Green Chem.*, 3, 100, 2001.
- [28] Chieruzzi M, Miliozzi A, Kenny. Effects of the nanoparticles on the thermal expansion and mechanical properties of unsaturated polyester/clay nanocomposites, *J. Compos. Part A*, 45, 44, 2013.

General conclusions

General conclusions

Data analysis derived from the study of the reversibly crosslinking reaction of polypropylene and polybutene-1, confirm that the crosslinking process affects the microstructure of both polymers:

- ✓ The crystal lamellar thickness decreases with increasing of the crosslinking agent content.
- ✓ The crystallization temperatures are increased inversely proportional to crosslinking agent concentration (the crosslinking agent act as nucleating agent).
- ✓ Generation of new forms :
 - γ and β forms in the crosslinked PP samples.
 - Increasing the crystallinity degree of the unstable form-II in the crosslinked PB-1.
- ✓ The formation of a network (S-S and C-S bonds).

The crosslinked samples show an improvement in the mechanical properties (tensile and impact strength).

Based on the study of the crosslinked PP and PB-1/treated short fibers (PA and hollow PET) composites, it was found that:

- The reversibly crosslinking reaction is an efficient way to improve the adhesion between PP/PB-1 crosslinked polymers and hollow PET fibers/ PA fibers, leading to the enhancement of the tensile and impact strength properties.
- The surface fibers treatment using stearic acid is a simple method that can improve the interactions between fiber and polymer matrix phases (stearic acid could play the role of a coupling agent in the presence of crosslinking agent and crosslinked matrix).
- The surface treatment of fibers by stearic acid gives rise to the good dispersion of fibers in the matrix.

The study of the Na-MMT/(PP & PB-1)/short fiber (PA and hollow PET fiber) hybrid composites shows that :

- The reactive melt mixing method using the functionalizing agent successfully gives rise to a total or partial exfoliation with 5wt% of Na-MMT.
- 5wt % f-Na-MMT/ (PP& PB-1) nanocomposites matrices can be reinforced with treated short fibers (PA and hollow PET).

- Synergistic effect of f-Na-MMT and short fibers (PA and PET) in reinforcing properties of polypropylene and polybutene-1 matrices was found.

Recommendations

Recommendations

The following additional studies could be recommended with view of determining the durability performance of the materials prepared and better understanding the microstructure of the composites investigated:

- ✓ The effect of the functionalized Na-MMT on crystallization, spherulitic structures and polymorphism of PB-1.
- ✓ Nonisothermal crystallization kinetics of crosslinked polybutene-1 and polypropylene samples
- ✓ The study of the crosslinking process effect on the crystalline lamellar thickness of the crosslinked polymers.
- ✓ Kinetic study of the II-I phase transition of the crosslinked isotactic polybutene-1 samples.
- ✓ Study of durability performance of the hybrid composites prepared in this present work.
- ✓ Internal damage in the hybrid composites has to be investigated using in situ tensile test under synchrotron X-ray tomography.
- ✓ Study of the microstructure of the different composites prepared after and during tensile test.
- ✓ Study of the recyclability of crosslinked PP and PB-1, crosslinked (PP/PB-1)/treated short PA and PET fibers composites and Na-MMT/fibers/(PP& PB-1) hybrid composites.

Abstract

Development of (PP and PB-1)/clay/short fibers (PA, hollow PET fibers) hybrid composites for the purpose of obtaining a lightweight and recyclable material which achieves strong interfacial interactions between fillers and matrix, fibers dispersion and clay layer exfoliation in polymer matrix is the topic of this study. To enhance filler interactions within PP and PB-1 matrices, a functionalizing agent (FA) and a coupling agent were added to the Na-MMT and PA fibers respectively. An organic peroxide/ sulfur mixture and tetramethyl thiuram disulfide as an activator for sulfur, were used to functionalize Na-MMT; on the other hand, the PA fibers surface was treated using stearic acid. Morphological, rheological and mechanical properties of the different composites prepared were carried out, showed a synergistic effect of f-Na-MMT and short fibers (PA and PET) in reinforcing properties of polypropylene and polybutene-1 matrices.

Keywords: hybrid composite; functionalized sodium montmorillonite; treated synthetic fiber; PA fiber, PET fiber, nanocomposite; crosslinked PP, crosslinked PB-1, reactive melt mixing.

Résumé

Afin d'obtenir un matériau qui présente des propriétés spécifiques de hautes performances sur le plan mécanique, rhéologique, et allègement des structures, tout en étant recyclable, une proposition de faire renforcer une polyoléfine utilisant des fibres (micro) et l'argile (nano) a été étudiée dans ce présent travail. Dans ce but, différents composites hybrides ont été élaborés par l'extrusion réactive, utilisant l'argile et fibres (PA, PET). L'argile a été fonctionnalisée utilisant trois réactifs à savoir (peroxyde, soufre et un accélérateur). Aussi la surface des fibres utilisées a été traitée par l'acide stéarique afin d'avoir une adhésion entre la matrice polymère/argile fonctionnalisée nanocomposites et les fibres traitées. Plusieurs techniques de caractérisation ont été utilisées afin d'étudier tous les paramètres discutés. Des résultats encourageants ont été trouvés concernant l'effet du traitement de surface des fibres et aussi à propos de l'exfoliation de l'argile, qui va améliorer les propriétés mécanique du polymère.

Mots clés : composite hybride, argile fonctionnalisée, fibre courte traitée, fibre PA, fibre PET, nanocomposite, PP réticulé, PB-1 réticulé, extrusion réactive.

الملخص

بهدف الحصول على مواد تتميز بخصائص تشمل الميكانيكية منها والخفة و ايضا قابلية الرسلكة ..تم اقتراح هذه الدراسة التي اقترحنا فيها جمع حمولتين مختلفتين في نفس المادة المبلورة بحيث قمنا بتحميل البوليمار باللياف اصطناعية معالجة مع تربة غنية بالمعادن بهدف منح البوليمار خصائص ميكانيكية عالية..التربة المعدنية ايضا تمت عملية معالجتها بثلاث مواد البيروكسيد وغيره بهدف خلق روابط بين المصفوفة أي البوليمار و الالياف و بنفس الوقت مع التربة المعدنية ايضا..مما يجعل الحصول على خصائص ميكانيكية كبيرة محتمل جدا..في هذا الاطار قمنا بعدة تحليلات للعينات التي قمنا بتحضيرها مخبريا حيث اجرينا العديد من التحاليل.ووجدنا وجود نتائج ايجابية بشأن الورايط مع المصفوفة و ايضا بشأن الخصائص الميكانيكية .

Research Article

Study of Na-Montmorillonite–Polyamide Fiber/Polypropylene Hybrid Composite Prepared by Reactive Melt Mixing

Samia Kerakra,¹ Said Bouhelal,¹ and Marc Ponçot²

¹Unit of Emergent Research Materials, Ferhat Abbas Sétif 1 University, Sétif, Algeria

²Materials Science and Engineering–Metallurgy Department, Jean Lamour Institute, UMR 7198 CNRS, University of Lorraine, Nancy, France

Correspondence should be addressed to Samia Kerakra; samiakerakra@gmail.com

Received 23 May 2017; Revised 28 August 2017; Accepted 25 September 2017; Published 30 October 2017

Academic Editor: Cornelia Vasile

Copyright © 2017 Samia Kerakra et al. This is an open access article distributed under the Creative Commons Attribution License, which permits unrestricted use, distribution, and reproduction in any medium, provided the original work is properly cited.

Hybrid composites of polypropylene (PP)/sodium montmorillonite (Na-MMT)/short polyamide fibers (PAfs) were prepared by reactive melt mixing in a Brabender plastograph. To enhance filler interactions within polypropylene, a functionalizing agent (FA) and a coupling agent were added to the Na-MMT and PAfs, respectively. An organic peroxide/sulfur mixture and tetramethylthiuram disulfide as an activator for sulfur were used to functionalize Na-MMT; on the other hand, the PAfs surface was treated using stearic acid. The aim of this study is to investigate how the morphology and the structural properties of 3, 5, and 7 wt% recycled functionalized sodium montmorillonite nanocomposites (f-Na-MMT) are affected by the presence of 5 wt% treated short polyamide fibers (t-PAfs). According to the obtained results, 5 wt% recycled f-Na-MMT/5 wt% t-PAfs/PP hybrid composite showed Na-MMT layers exfoliation. The nucleating effect of f-Na-MMT and t-PAfs was indicated by the differential scanning calorimetry (DSC) measurements. Morphological analysis of the hybrid composites was performed using scanning electron microscope (SEM) and optical polarized microscopy (POM), showing a good dispersion of the fibers with an interesting interfacial adhesion between the PP and t-PAfs phases. Hybrid composites of PP/f-Na-MMT/t-PAfs are considered for automotive industry.

1. Introduction

The increasing demand in recent years for new lightweight, recyclable, and performing materials has guided the search for reinforced polymer systems [1]. Polymers are traditionally reinforced with synthetic or natural inorganic fillers in order to improve their properties and reduce their costs [2]. Commonly used fillers are clay, talc, mica [3, 4] and fibrous-like glass, carbon fibers, aramid, and jute fillers [5, 6]. In order to improve or modify certain thermomechanical properties of polymers for specific applications, composites based on short fibers reinforced polymers find increasing applications in engineering and consumer products [7]. Increasing the adhesion between fiber and polymer matrix is one of the most effective ways to increase the degree of reinforcement by fibers [8]. Numerous studies have been reported concerning the enhancement of the interfacial interaction between the polymer/fibers phases [9–12]. On the other hand, nowadays we are witnessing increasing use of nanoscale composites

that can enhance selected properties of related polymers [13]. Nanocomposites based on clay and layered silicates have been most widely investigated [14]. Montmorillonite (MMT) is one of the most used layered silicates. It is a 2 : 1 aluminosilicate, which is formed by two silica tetrahedral layers shared an octahedral sheet of aluminium or magnesium hydroxide [15, 16]. Stacked between the two layers is a regular Van der Waals gap called interlayer space or gallery.

Currently, the melt mixing is the most widely used method for preparing clay/PP nanocomposite [16, 17]. The clay is incompatible with most polymers due to its strong hydrophilic character. Thus, a direct melt mixing of both components is not realizable. To overcome this difficulty, as a first step, the surface of the clay has to be modified by using an organophilic agent, thus giving rise to the so-called organophilic clay or organoclay [18, 19]. On the work conducted by Kawasumi et al. [18], a new approach to prepare organoclay/PP nanocomposite has been reported, in which they expected to use a compatibilizer between the matrix and

filler [19]. In that approach, nanocomposites were prepared by melt mixing due to its lower cost than the in situ polymerization method [20]. The research work of Toyota Company's research center developed the formation of organoclay/PP hybrid composites by direct melt mixing. The organoclay used in their study was montmorillonite (MMT), and the PP used was PP grafted with maleic anhydride (PP-g-MA) or hydroxyl groups with the aim of facilitating exfoliation and improving properties [19, 21].

Our laboratory developed a new route based on reversibly crosslinking reactive extrusion, which is applied for both the crosslinking of PP and the development of iPP/clay nanocomposites [22, 23]. The developed method consists on the preparation of a functionalizing agent, capable of exfoliating the raw clay without any restricted working conditions; then the functionalized raw clay/PP nanocomposite was prepared by reactive melt mixing [24, 25]. Production of hybrid polymer composites systems based on fibers and nanoclay has shown recent achievements and activities. Eslami-Farsani et al. [26] studied the effect of nanoclay/basalt fiber on the mechanical properties of polypropylene. The authors proved that the presence of the layered structure in basalt fiber/propylene composite improved the interfacial adhesion of nanoclay and the fiber, therefore, improving the mechanical properties of composite. Chowdary and Kumar [27] analyzed the mechanical and morphological properties of nanoclay/S-glass fiber/polyester hybrid composite, in which they studied the effect of nanoclay content on S-glass fiber/polyester composite. The obtained results of their study showed that the incorporation of nanoclay had a significant effect on the mechanical behavior of composites. Several researches focused on this type of composites mainly processed by the combination of fiber with clay fillers in the same polymer matrix due to their easy availability and their low cost and also to enhance the physical and mechanical composites properties [28–30].

Development of hybrid composites based on polypropylene/clay/short polyamide fiber for the purpose of obtaining a lightweight and recyclable material which achieves strong interfacial interactions between filler and matrix, fiber dispersion, and clay layer exfoliation in PP matrix is the topic of this study.

The recycled 3, 5, and 7% f-Na-MMT/5w t-% PAFs/PP hybrid composites were prepared by reactive melt mixing in a Brabender plastograph. The microstructure and thermal properties of f-Na-MMT/t-PAFs/PP hybrid composites were studied. Fourier transform infrared (FTIR) and wide-angle X-ray scattering (WAXS) were used to investigate the obtained hybrid structure. Morphological study of different composites was determined by scanning electron microscopy (SEM) and optical microscopy (OM). The melting and crystallization process of composites were tested by differential scanning calorimetry (DSC). The obtained results indicated that 5 wt% f-Na-MMT nanocompositions showed Na-MMT layers exfoliation, also a good dispersion of the treated fibers and an adhesion between the two polymer phases was observed. Automotive components (bumpers, step-assist) can be produced using f-Na-MMT/t-PAFs/PP hybrid

composites; therefore, a mechanical study is recommended in order to test the mechanical properties of the obtained materials in this present study.

2. Materials and Methods

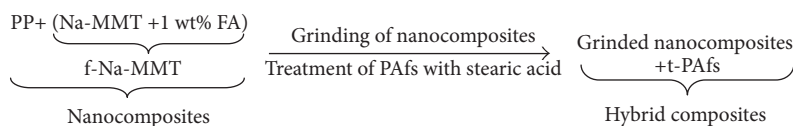
2.1. Materials. The commercial polypropylene SABIC RAF-FIA 510P homopolymer was purchased from SABIC Arabie Saoudite. Its melt flow index (MFI) is 13.1 g/10 min (230°C, 2.16 kg). PA6 fiber was provided by Nanjing Forever Textile Co., Ltd. company, Jiangsu, China. Sodium montmorillonite Na-MMT, an unmodified nanoclay, was purchased from the Algerian region of Maghnia, supplied by ENOF, Algeria. The cation exchange capacity CEC of this montmorillonite is about 1.15×10^{-3} mol/g. Dicumyl peroxide (DCP) (96 wt% activity) was supplied by Sigma-Aldrich, France. Sulfur (S) (vulcanizing agent for rubber) was supplied by Wuxi Huasheng Chemical Additives Factory, China. The accelerator used was "Super accelerator 501" (tetramethylthiuram disulfide, TMTD), supplied by Rhône Poulenc, France.

2.2. Composites Preparation. The different composites were prepared in Brabender plastograph mixer using twin Roller blades at mixing temperature of 190°C and rotor speed of 60 rpm during 20 minutes and, then, compressed into a dreher-type Brabender. The different composites were grinded before undergoing the diverse tests. The films were prepared by compression molding using a CARVAR manual press between hot plates at 200°C and at a pressure of 2 MPa for 8 min. A quench was applied to the films from the melt to room temperature.

2.2.1. f-Na-MMT/PP Nanocomposites Preparation. A series of composites have been studied consisting of different content of the f-Na-MMT (3, 5, and 7 wt%)/PP. Different composites were prepared using a conventional method [24]. Functionalizing agent (peroxide, sulfur, and accelerator)/dried Na-MMT were mixed together in the solid state, in which the functionalizing agent (FA) was added in a concentration of 1/10 of the clay. The formulations are as follows: the sulfur concentration (in wt%) was equal to that of peroxide, and the accelerator was 1/4 of the sulfur or peroxide concentration.

PP was incorporated into the Brabender plastograph chamber firstly, and then the mixture Na-MMT/FA was introduced as soon as torque indicated melting of the polymer (about 2 min).

Crosslinked PP (PP/1 wt% FA). The so-called "functionalizing agent of Na-MMT" which is constituted by the peroxide, sulfur, and accelerator was also used as crosslinking agent of PP [22]. Accordingly, an additional study of crosslinked PP has been done, with a view of evaluating and explaining the effect of functionalizing agents on the structure of PP. Also for understanding the effect of FA on neat PP structure, the same amount of functionalizing agent that was added to Na-MMT was used to PP. The amount of sulfur and peroxide was



SCHEME 1: The final obtained hybrid composites.

1 wt% and the accelerator was 1/4 of the sulfur and peroxide concentration.

2.2.2. PAfs/PP Composites Preparation

Surface Treatment of Polyamide Fibers (PAfs). Surface treatment of the polyamide fibers was carried out by stearic acid in order to increase the number of reactive groups and improve the fibers dispersion in f-Na-MMT/PP nanocomposite. First of all, PAfs were chopped into about 4 mm. Then, the obtained short fibers were washed with distilled water in order to remove the possible surface impurities and dried in vacuum oven at 60°C. 25 mg of stearic acid was dissolved in 200 ml of toluene at ambient temperature by continuous magnetic stirring of solution for 20 min. Then, 3 g of PA fibers was added to toluene/stearic acid solution under a magnetic stirring at ambient temperature for 12 h in order to complete the reaction between stearic acid with polyamide fibers surface and to improve the dispersion of the fibers into the solution. Following the treatment, PAfs were thoroughly washed with distilled water and dried in vacuum oven at 60°C for 8 h.

Two series of PAfs/PP composites containing 5 wt% PAfs treated and untreated fibers were prepared. The fibers were dispersed in the PP pellets in the solid state; thereafter, the obtained mixture was inserted into Brabender plastograph chamber.

2.2.3. f-Na-MMT/PAfs/PP Hybrid Composites. PAfs/f-Na-MMT/PP hybrid composites were prepared by adding 5 wt% of treated polyamide fibers (t-PAfs) to different recycled nanocomposites 3, 5, and 7 wt% f-Na-MMT/PP which were prepared and grinded as it was explained above in the section of f-Na-MMT/PP nanocomposites preparation. Sample designation and composition of hybrid composites are presented in Table 1.

Scheme 1 shows the schematic processing steps of the hybrid composite preparation.

3. Characterizations

3.1. FTIR Measurements. FTIR spectra of film samples were recorded using a Perkin Elmer Spectrum 1000 spectrometer with a resolution of 4 cm⁻¹ within 200 scans (PerkinElmer, USA). IR spectra were obtained for different composites film samples in the region from 400 to 4000 cm⁻¹.

3.2. Wide-Angle X-Ray Scattering (WAXS). The crystalline structure was determined by WAXS analysis. WAXS profiles were recorded on a Seifert diffractometer (Rich. Seifert & Co.,

TABLE 1: Sample designation and composition of hybrid composites.

Sample	t-PAfs (wt%)	f-Na-MMT presented in PP nanocomposite prepared (wt%)
3 wt% hyp	5	3
5 wt% hyp	5	5
7 wt% hyp	5	7

Germany). The following conditions were employed: 40 kV, 35 mA, angular range of 4–35° (2θ), and scan rate of 0.02°/s.

3.3. Differential Scanning Calorimetry (DSC) Measurement. Thermograms of all composites were obtained using a Q200 instrument (TA Instruments, USA). The calorimetric runs were performed using (±10 mg) of each sample with a heating rate of 5°C/min. The samples were heated up to 200°C and maintained at this temperature during 5 min and then samples were cooled down to 25°C with a cooling rate 5°C/min. After that, a second heating was effectuated.

3.4. Optical Light Polarized Microscopy. Polarized light microscopy (Olympus bx50, USA) examinations were carried out on both sides of the cast samples.

3.5. Scanning Electron Microscope (SEM) Observation. The cross section of the tensile fractured surface of specimens was examined using an environmental scanning electron microscope (QUANTA- FEG 600, FEI Company, France).

4. Results and Discussions

4.1. Fourier Transform Infrared Spectroscopy (FTIR). Figure 1(a) shows the FTIR spectra of Na-MMT. The band at 3623 cm⁻¹ produced from the O-H stretching vibration associated with Al³⁺ Fe²⁺ or Mg²⁺ cations. The intensive band situated at 1045 cm⁻¹ was assigned to the Si-O stretch, and that at 529 cm⁻¹ is due to Si-O bending vibrations. The band at 1113 cm⁻¹ was assigned to the Si-O out-of-plane stretching vibration. The hydroxyl vibrations groups of water molecules showed two bands situated at 3440 and 1639 cm⁻¹. The band at 798 cm⁻¹ shows the quartz present in Na-MMT [31].

Figures 1(a), 1(b), and 1(c) display the FTIR spectra of different nanocomposites and crosslinked polypropylene (1 wt% FA/PP). From the results presented in Figure 1(a), it was observed that the peak related to Na-MMT octahedral structure peak at 3623 cm⁻¹ remained with a weak intensity in the spectra of 3 and 7 wt% f-Na-MMT/PP; however, this peak disappeared with 5 wt% f-Na-MMT. In addition, weak peaks associated with the tetrahedral structure of Na-MMT

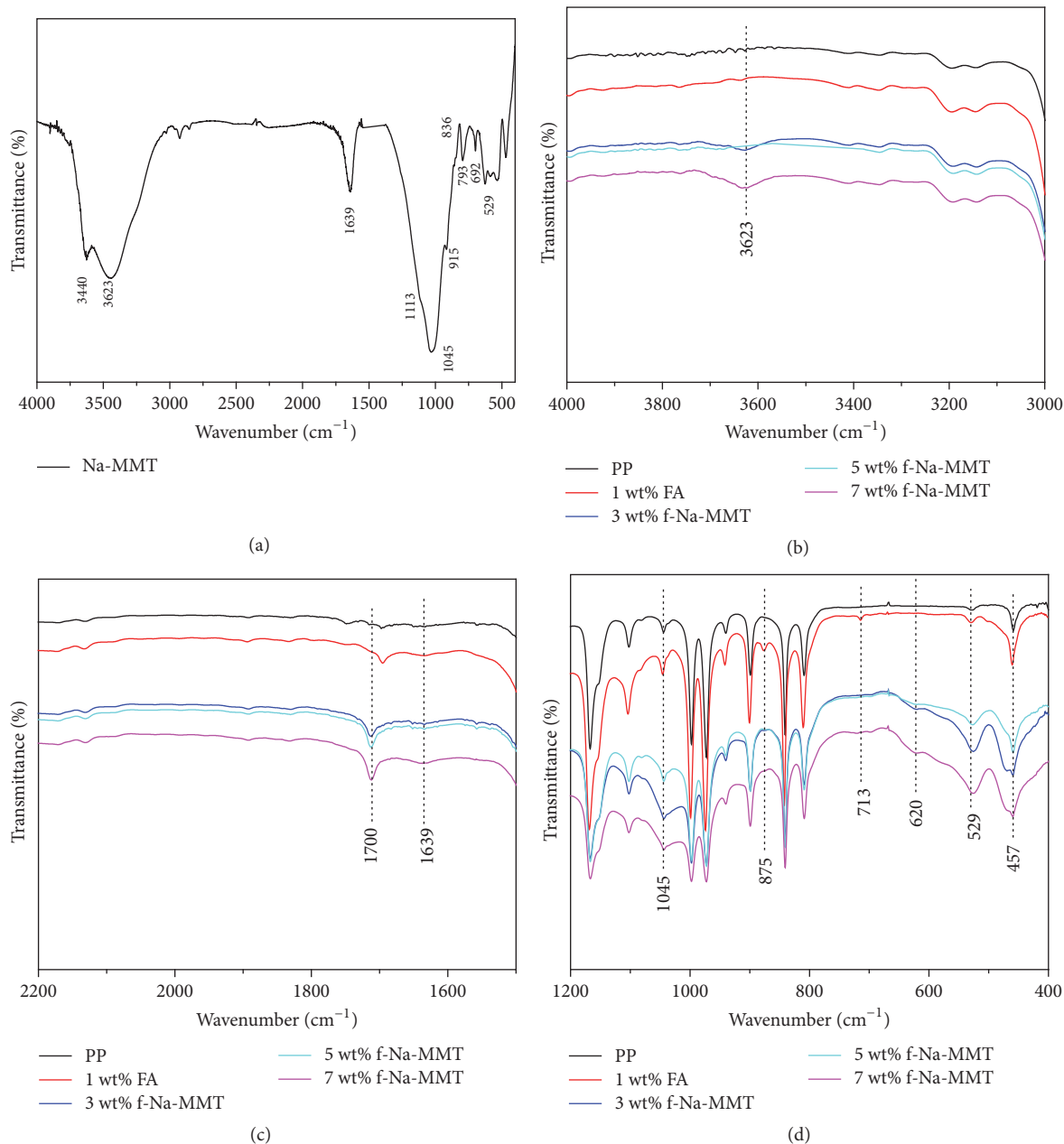


FIGURE 1: Fourier transform infrared spectroscopy (FTIR) spectra of (a) unmodified Na-MMT; (b, c, d) PP; PP/1 wt% FA crosslinked PP; 3, 5, and 7 wt% f-Na-MMT nanocomposites.

at 1639 cm^{-1} , 1045 cm^{-1} , and at 529 cm^{-1} remained in the final structure of the different nanocomposites samples with strong intensities in the case of PP/3 and 7 wt% f-Na-MMT as shown in Figures 1(b) and 1(c). This result can be explained by the reaction between the functionalizing agent used and Na-MMT which is a redox reaction that involves the octahedral crystalline portion. Thus, the organometallic components of Na-MMT octahedral structure react in the presence of cations supplied by decomposition of the peroxide and the accelerator [32]. According to Bouhelal et al. [24], the technique of crosslinking by reactive extrusion that has been used in this present study gave rise to a partial or total exfoliation

(4 wt% clay) with the absence of intercalated structure [25].

The different weak bands at 1700 cm^{-1} , 875 cm^{-1} , 713 cm^{-1} , and 620 cm^{-1} shown in Figures 1(c) and 1(d) are related to crosslinked PP as observed in crosslinked PP spectrum. The band at 1700 cm^{-1} assigned to the carbonyl group C=O which resulted from the reaction between the peroxide and PP and that at 875 cm^{-1} due to the swinging of N-H emerged from the reaction with the accelerator; the two bands at 713 cm^{-1} and 620 cm^{-1} attributed to C-S stretch that related to the reaction with the sulfur. From these results, we can conclude that a few a portion of the FA contributed

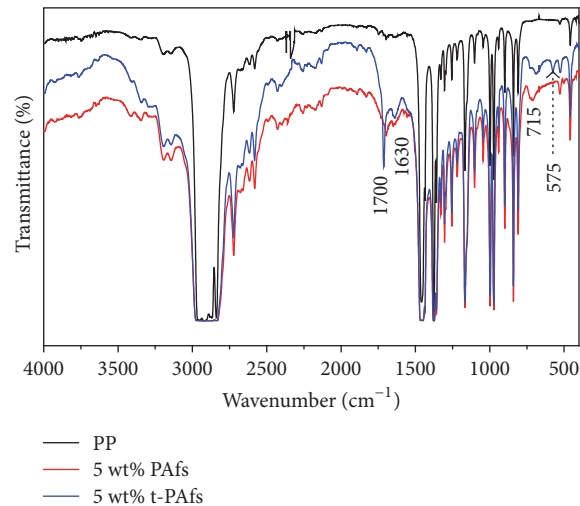


FIGURE 2: Fourier transform infrared spectroscopy (FTIR) spectra of PP, PP/5 wt% PAfs, and PP/5 wt% t-PAfs.

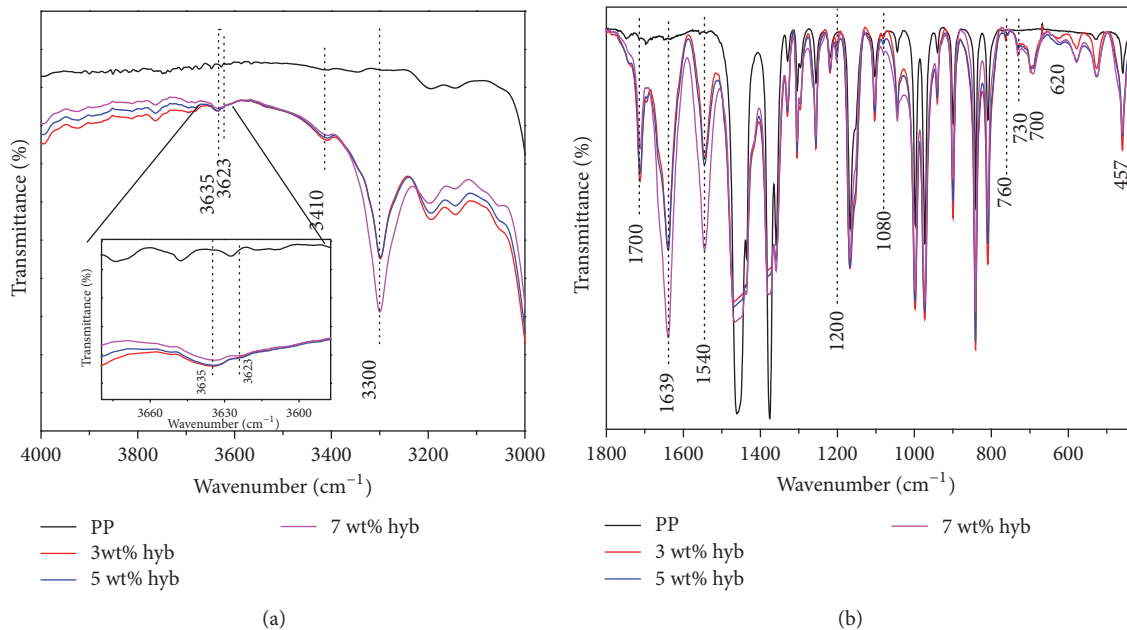


FIGURE 3: Fourier transform infrared spectroscopy (FTIR) spectra of (a, b) 5 wt% t-PAfs/3, 5, and 7 wt% f-Na-MMT/PP hybrid composites.

also in the chemical crosslinking process of PP, which was proved by the appearance of the β and γ -crystalline forms in the WAXS patterns of crosslinked PP and f-Na-MMT/PP nanocomposites.

Figure 2 displays the FTIR spectra of PP and different composites based on treated polyamide fibers (t-PAfs) and untreated polyamide fibers (PAfs) reinforced polypropylene (PP). Remarkable changes in intensities between the PP spectrum and the spectra of composites were seen. Both composites based on PA treated fibers and untreated fibers present a large absorption band in the interval 2960–2850 cm^{-1} which indicates the symmetric stretching vibration peak of ($-\text{CH}_2^-$) group at 2850, and the absorption band of the asymmetric stretching vibration peak of ($-\text{CH}_2^-$) group at 2919 cm^{-1} . The

absorption band at 2960 cm^{-1} is the antisymmetric stretching vibration peak of $-\text{CH}_3$. The t-PAfs/PP composite shows new bands at 1700 and at 1630 cm^{-1} assigned to the stretching vibration peak of the carbonyl group C=O in carboxylic acid and the combination absorbance of C=O and C–N amide I stretch. These new bands showed that FTIR spectra of treated polyamide are in good agreement with SEM observation of treated polyamide fiber, in which polyamide fibers exhibit rough surface.

FTIR spectra of PP and t-PAfs/f-Na-MMT/PP hybrid composites are shown in Figure 3. Different bands related to tetrahedral structure of Na-MMT were clearly observed in the spectra of all composites. Two characteristic weak bands of Na-MMT at 3635 cm^{-1} and at 3410 cm^{-1} related to the OH

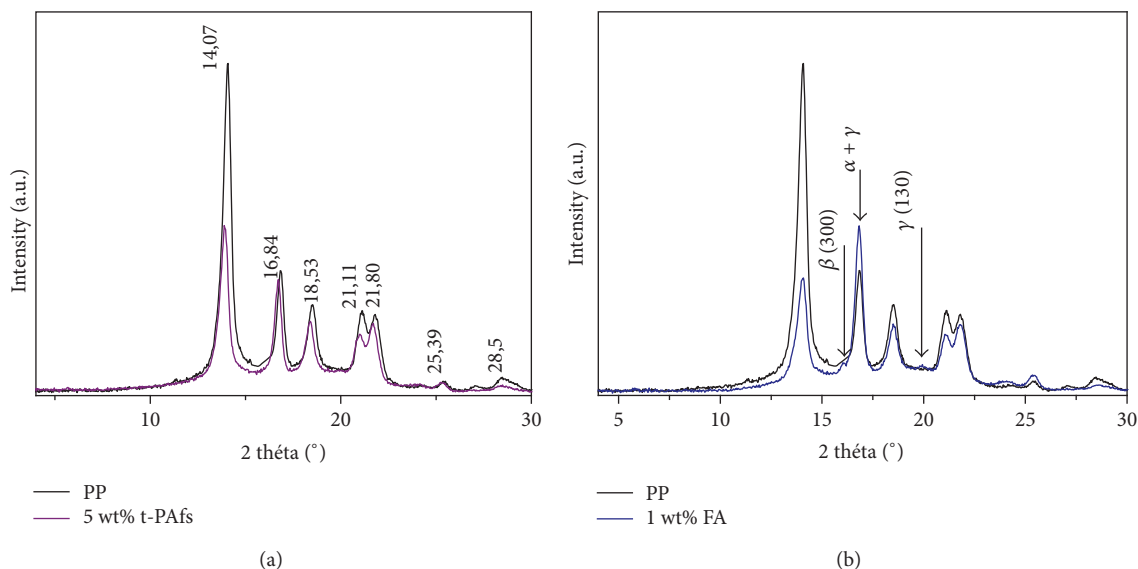


FIGURE 4: WAXS patterns of (a) 5 wt% t-PAFs/PP composite and (b) 1 wt% FA/PP crosslinked PP.

of the Al-OH and to the stretching and bending vibrations for the hydroxyl groups of water molecules were, respectively, shown. In addition, bands at 1639, 692, and 529 cm^{-1} associated with water molecules, quartz, and Si-O bending vibrations were, respectively, observed as seen in Figures 3(a) and 3(b). However, the band situated at 3623 cm^{-1} that attributed to Na-MMT octahedral structure disappeared in the FTIR spectra of all composites. The disappearance of the characteristic peaks of the Na-MMT octahedral layers from the FTIR spectra is in good agreement with the obtained FTIR results of 5 wt% f-Na-MMT/PP nanocomposite as has been discussed above, what led to confirm the exfoliation of the Na-MMT layers in PP with the presence of t-PAfs. Owing to the fact that the different nanocomposites were reprocessed in the second melt mixing cycle in which the polyamide fibers were added and that the characterizations were carried out in the samples which are able to be molten again and form films using compression molding, we can conclude that the recycled f-Na-MMT/PP nanocomposites have been successfully produced. Some bands associated with the crosslinked PP with FA as indicated above in crosslinked PP spectrum (Figures 1(b) and 1(c)) were further observed. The presence of the t-PAfs in f-Na-MMT/PP nanocomposite matrix was proved by FTIR results, in which a new characteristic strong band at 3300 cm^{-1} of bending vibration in primary amine was observed in Figure 3(a), and three bands situated at 1700 cm^{-1} , 1540 cm^{-1} , and 1200 cm^{-1} were assigned to the stretching vibration peak of the carbonyl group (C=O) in carboxylic acid, the combination absorbance of the N-H and C-N amide II stretch and C-N stretch, respectively.

4.2. Wide-Angle X-Ray Scattering (WAXS). The structure of PP/5 wt% t-PAfs was evaluated by a wide-angle X-ray scattering method. On the basis of the WAXS patterns are shown in Figure 4(a). Only characteristic peaks of α form PP

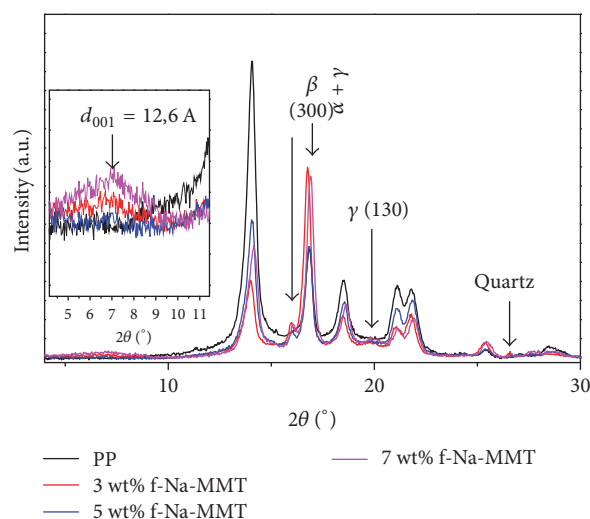


FIGURE 5: WAXS patterns of 3, 5, and 7 wt%/PP nanocomposites.

can be found, which can be indexed as (110) at 2θ ($^\circ$) = 14.07, (040) at 16.84, (130) at 18.5, (111) at 21.11, and (041) at 21.8 and (060), (220) at about 25.3 and 28.5, respectively, without any additional diffraction peaks.

The effect of FA on the structure of PP has been studied. Crosslinked PP is shown in Figure 4(b). The WAXS pattern shows two new weak peaks at 16.2 and 20.1 (2θ) which are characteristic of the (300) planes of PP β -crystalline form and the (130) or (117) planes of the γ -crystalline, respectively. It can be seen also in Figure 4(b) that the intensity of the reflection at 16.7 (2θ) is higher than that of PP which is due to the appearance of the γ -crystalline form in the crosslinked PP, as both α - and γ -forms show a reflection in this position.

Figure 5 shows the X-ray diffraction patterns of 3, 5, and 7 wt% f-Na-MMT/PP nanocomposites. From this figure it

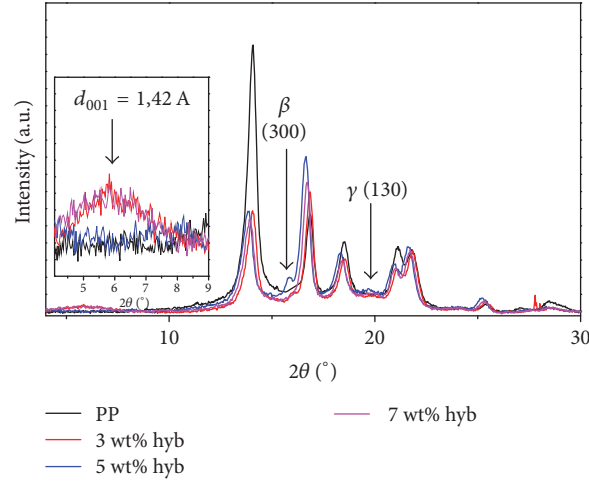


FIGURE 6: WAXS patterns of 5 wt% t-PAFs/3, 5, and 7 wt% f-Na-MMT/PP hybrid composites.

was observed that the WAXD patterns exhibit the typical reflections of the α -form of PP, with four additional peaks, at 6.9, 16.2, 20.1, and 26.7 (2θ) that are characteristic of the d_{001} spacing of Na-MMT, (300) planes of the iPP β -crystalline form, (130) or (117) planes of the γ -crystalline form, and the quartz accompanying the Na-MMT which was shown with much less intensity. The characteristic peak of the d_{001} spacing of Na-MMT, indicated by an arrow, appeared with a weak intensity in 7 and 3 wt% f-Na-MMT. However, it disappeared in the case of PP with 5 wt% f-Na-MMT. According to Giannelis et al. [16, 33] the disappearance of peak indicates the separation of clay layers (exfoliated structure) and the formation of nanocomposites. The two new peaks at 16.2 and 20.1 have been already presented in the diffractogram of the crosslinked sample having no Na-MMT (Figure 4(b)). On the work conducted by Bouhelal et al. [24] based on the development of iPP/clay nanocomposites, it was found that 4 wt% clay gave a rise to a partial or total exfoliation in which the reactive extrusion technique was used. Further, in this present study the exfoliation of the Na-MMT layers was given with 5 wt% f-Na-MMT.

Figure 6 displays the WAXS patterns of t-PAFs/f-Na-MMT/PP hybrid composites. It was observed that the presence of PAfs with Na-MMT do not give any significant difference compared with the WAXS patterns of nanocomposite (Figure 5). The same additional peaks are shown, with the disappearance of the weak peak assigned to the quartz in nanocomposites samples and the peak related to β -crystalline form at 16.2 in 7 wt% t-PAFs/f-Na-MMT hybrid. Also, it can be seen that the characteristic peak of the d_{001} spacing of Na-MMT shifted to higher diffraction angles unlike the diffraction angle of Na-MMT which was found in the PP/Na-MMT nanocomposites. The exfoliation of the Na-MMT layers was given with 5 wt% f-Na-MMT also as it has been explained above in the X-ray diffraction patterns of f-Na-MMT/PP nanocomposites (Figure 5).

From the WAXS patterns, the degree of crystallinity (χ_c) can be measured using the following equation [34]:

TABLE 2: WAXS measurements: (χ_c^{WAXS}), X_β of β form and X_γ of the γ -form.

Sample	X_β	X_γ	χ_c^{WAXS} (%)
PP	—	—	38.1
5 wt% t-PAFs/PP	—	—	32.6
1 wt% FA/PP	0.010	0.32	36
3 wt% Na- MMT	0.017	0.50	37.7
5 wt% Na-MMT	0.016	0.53	38
7 wt% Na- MMT	0.02	0.55	38.2
3 wt% hyb	0.016	0.36	38
5 wt% hyb	0.016	0.45	38.5
7 wt% hyb	—	0.36	38

$$\chi_c^{\text{WAXS}} = \frac{I_c}{(I_a + I_c)}, \quad (1)$$

where I_c and I_a present the integrated intensities of crystalline and amorphous phases, respectively, which were determined by deconvolutions of WAXS patterns.

We have also estimated the content X_β of β form and X_γ of the γ -form in all the studied samples according to the method of Jones et al. [35, 36] (Table 2):

$$X_\gamma = \frac{I^{\gamma}_{(130)}}{(I^{\gamma}_{(130)} + I^{\alpha}_{(130)})}, \quad (2)$$

$$X_\beta = \frac{I^{\beta}_{(300)}}{(I^{\alpha}_{(110)} + I^{\alpha}_{(040)} + I^{\alpha}_{(130)} + I^{\alpha}_{(300)})}.$$

The obtained degree of crystallinity (χ_c), X_β , and X_γ are collected in Table 3. It is clearly observed that the degree of crystallinity (χ_c) seems to be relatively constant with the different composites (nanocomposites and hybrid composites) in comparison with the neat iPP; however, it is lower in the case of t-PAFs/PP. The degree of crystallinity of different composite is consistent with DSC results.

TABLE 3: Melting (T_m), crystallization temperatures (T_c), and enthalpies (ΔH_m , ΔH_c) for different samples and crystallinity degree (χ_c) obtained by DSC.

Sample	ΔH_m (J/g)	T_m (°C)	ΔH_c (J/g)	T_c (°C)	χ_c^{DSC} (%)
PP	90	161	98	116	42.4
PP/5 wt% t-PAfs	77	159	89	117.5	39
3 wt% Na-MMT	87.9	158.3	98.3	120	43.6
5 wt% Na-MMT	83.7	158.5	98	120.8	42.3
7 wt% Na-MMT	81.7	160	92.5	119.5	42.1
3 wt% hyb	87.7	159.5	102.3	120	45.6
5 wt% hyb	83.5	159.3	102.1	120.3	44.7
7 wt% hyb	83.1	159.5	100.1	121.4	45.2

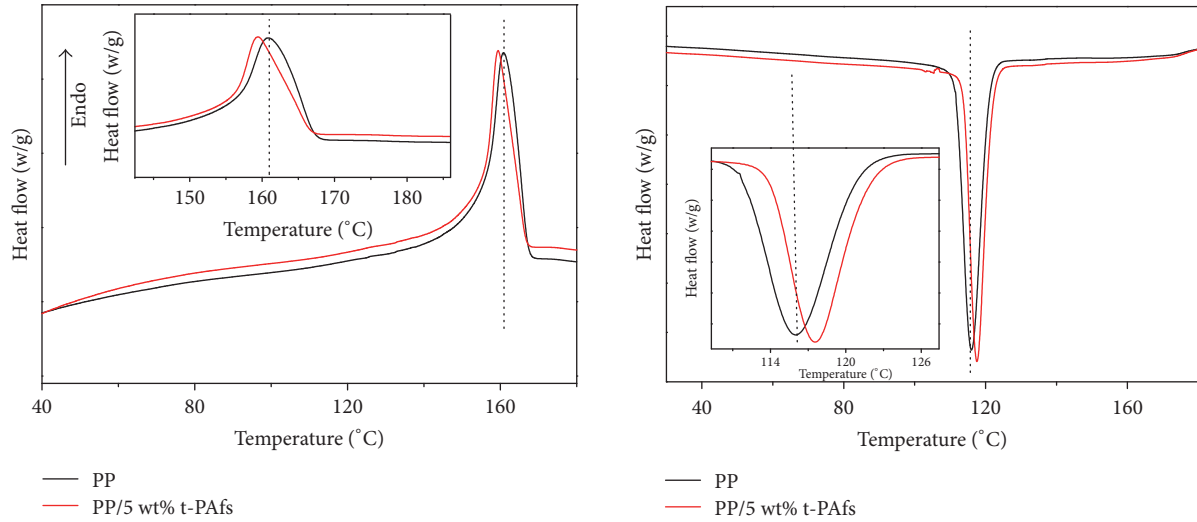


FIGURE 7: DSC thermographs of second heating and cooling runs of 5 wt% t-PAfs/PP composite.

A gradual increase of X_γ value has been noted in different nanocomposite samples. It increases from 0.32 in the crosslinked PP, up to 0.55 for the samples with 3–7% of clay, while these values decrease to 0.36 and 0.45 for the 3 and 7 wt% and 5 wt% hybrid samples.

Concerning the X_β value, its contribution reaches the highest value in the sample with 7 wt% of Na-MMT. However, it was observed that the peak related to β -crystalline disappeared in 7 wt% Na-MMT/5 wt% PAfs. The diminution X_γ and X_β values in hybrid composites can be explained by the presence of polyamide fibers.

4.3. DSC Analysis. Figure 7 displays the DSC thermographs of t-PAfs/PP composite, f-Na-MMT/PP nanocomposites, and hybrids. The DSC results are displayed in Table 3. The degree of crystallinity of PP and different composites was determined according to (3), in which ΔH_m is the melting enthalpy of PP and ΔH_m^0 presents the heat of fusion of 100% crystalline polypropylene, at the equilibrium melting point, $T_m^0 = 187.5^\circ\text{C}$. A literature value of 207.33 J/g ΔH_m^0 was used (Wunderlich [37]):

$$\frac{\Delta H_m}{\Delta H_m^{100\%}} \cdot \quad (3)$$

However, in the present study, the degree of crystallinity was determined with the application of a correction factor in order to take into consideration the amount of fillers (PAfs and Na-MMT) in different composites. Thus, accurate values of χ_c reported were obtained from the following equation, where (w_f) corresponds to the weight percentage of fillers in the composite:

$$\frac{\Delta H_m}{\Delta H_m^{100\%}} \times \frac{100}{100 - w_f}. \quad (4)$$

It can be seen in Figures 7 and 8 and Table 3 that the melting temperatures of different composites are about 159°C , slightly lower than 161°C of pure PP. The melting temperatures of f-Na-MMT/PP increased slightly with increasing of f-Na-MMT amount. However, in the case of hybrid composites, in which 5 wt% of t-PAfs was added to 3, 5, and 7 wt% f-Na-MMT/PP nanocomposites, a constant value of melting temperature is observed that is almost between the melting temperature of t-PAfs/PP composite and different nanocomposites. The crystalline peak temperature (T_c) of the pure PP is increased slightly with 5 wt% t-PAfs. Meanwhile, T_c is increased significantly with different f-Na-MMT/PP nanocomposites and hybrids. MMT and t-PAfs act as nucleating agents, which

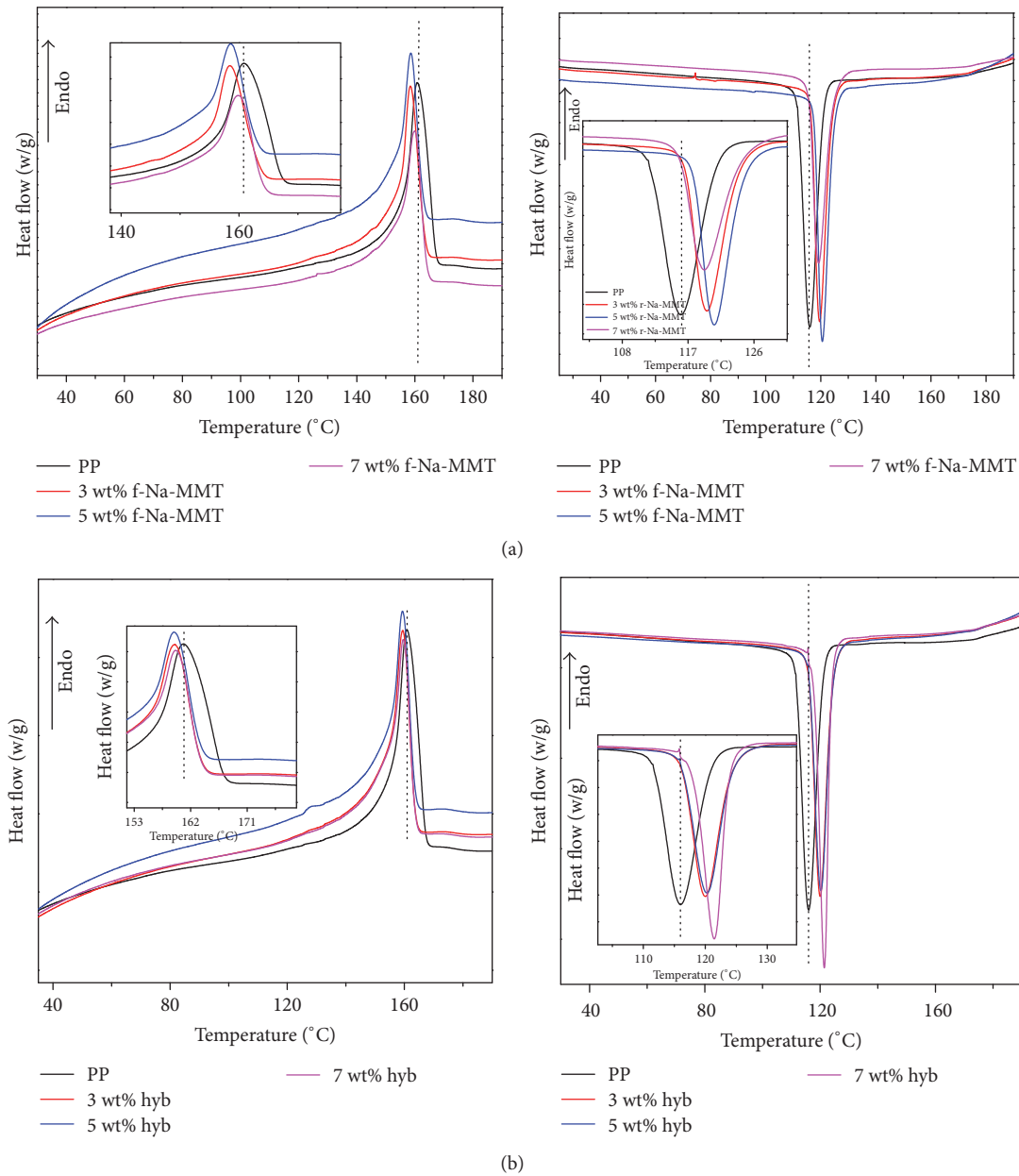


FIGURE 8: DSC thermographs of second heating and cooling runs of (a) f-Na-MMT/PP nanocomposite and (b) t-PAfs/f-Na-MMT/PP hybrid composites.

increase the crystallization temperature of PP matrix. The addition of 5 wt% t-PAfs to 7 wt% f-Na-MMT/PP nanocomposite increased T_c by up to 4°C compared to 5 wt% t-PAfs/PP composite. This result indicates that the nucleating effect of MMT was further strengthened by the addition of polyamide fibers.

4.4. Optical and Scanning Electron Microscopy. To show the matrix/fiber adhesion and hybrid composite morphology, polarized optical microscopy (POM) and scanning electron microscopy (SEM) investigations were used. The

POM images of 5 wt% t-PAfs/PP composite and 5 wt% f-Na-MMT/5 wt% t-PAfs/PP hybrid composite are shown in Figure 9. The polyamide fibers generally seem to be well dispersed. Also, some agglomerations were observed (see Figure 9(a)). Figure 9(b) shows the POM image of hybrid composite in which a good dispersed polyamide fiber was shown and with less agglomeration than t-PAfs/PP composite due to the presence of Na-MMT in the matrix. Length reduction of fibers was observed that can be explained by the effect of the intense shearing involved in the closed chamber of the Brabender plastograph.

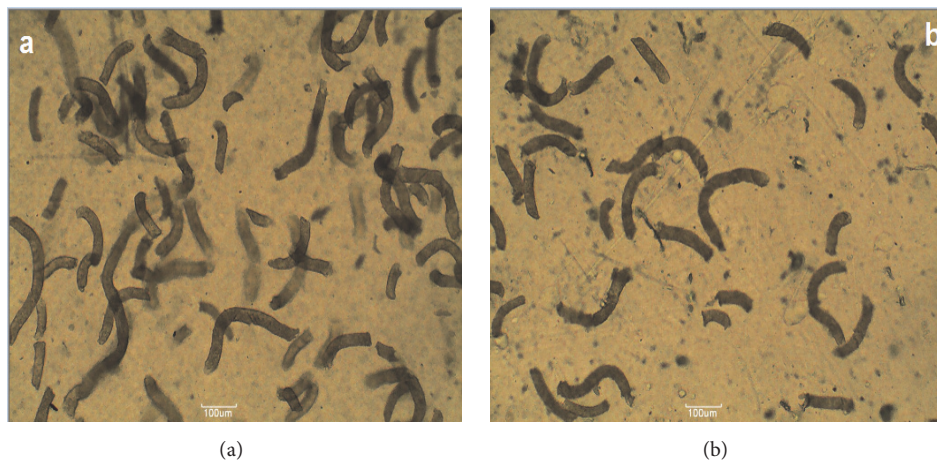


FIGURE 9: Optical micrographs of (a) 5 wt% t-PAFs/PP composite and (b) 5 wt% t-PAFs/5 wt% f-Na-MMT/PP hybrid composite.

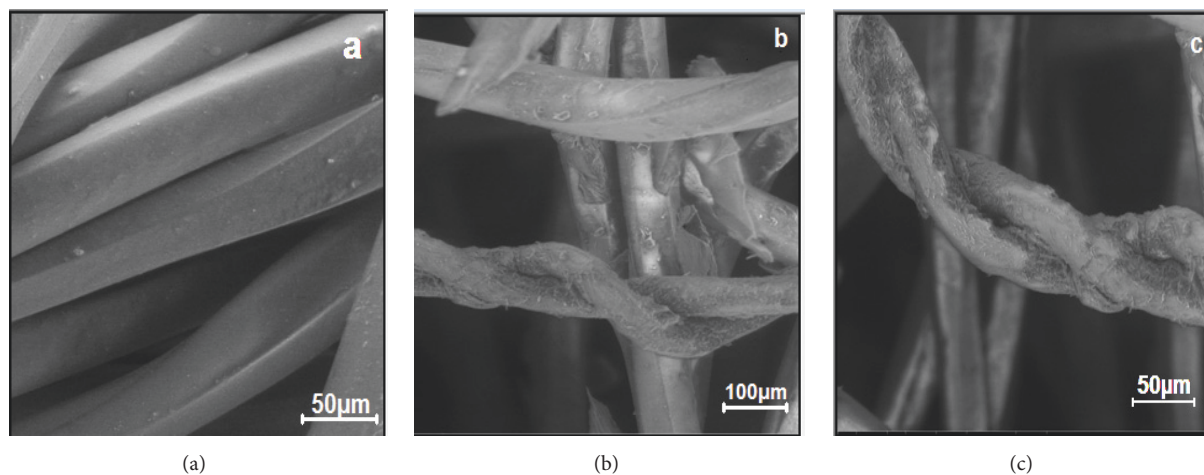


FIGURE 10: SEM micrographs of (a) untreated PAfs and (b, c) treated PAfs.

Scanning electron micrographs (SEM) of untreated and treated polyamide fibers PAfs are shown in Figure 10. It can be observed that the untreated fibers showed a smooth surface while the images of treated surface polyamide fibers exhibit rough surfaces, which proved the effect of the treatment.

Scanning electron micrographs of the tensile fractured surface of 5 wt% PAfs/PP composite and 5 wt% t-PAfs/5 wt% f-Na-MMT/PP hybrid composite are shown in Figure 11. Figures 11(a) and 11(b) show the SEM micrographs of 5 wt% PAfs/PP and 5 wt% t-PAfs/PP composites, respectively. For the composite based on untreated polyamide fibers, fibers pull-out, the absence of polymer attached to the fiber surface, and fiber fracture clearly indicate a very limited adhesion between PP and fibers (Figure 11(a)). On the other hand, in the case of t-PAfs/PP composite, fibers pull-out and debonding reduced significantly and the adhesion between fiber and matrix improved strongly. In addition, it was observed that the fibers folded with no fiber pull-out after tensile test what confirm that the interfacial adhesion of the treated fiber composites is much better than that of the untreated fiber composite.

Figures 11(c) and 11(d) show the SEM micrographs of the tensile fractured surface and the stretched surface of hybrid composite. It can be observed from the micrograph Figure 11(c) that the addition of t-PAfs in Na-MMT/PP nanocomposite gives rise to a good interfacial adhesion which can be confirmed by the few voids appearing in the surface of stretched tensile specimen shown in Figure 11(d).

5. Conclusions

From the obtained results by different experimental methods, the following conclusions can be summarized. The reactive melt mixing method using the functionalizing agent successfully gives rise to a total or partial exfoliation with 5 wt% of f-Na-MMT as has been proven with FTIR and WAXS results. The t-PAfs can be effectively incorporated in f-Na-MMT/PP recycled nanocomposite matrix. The differential scanning calorimetry (DSC) measurements indicate the nucleating effect of f-Na-MMT and t-PAfs. The treatment of polyamide fiber surface with stearic acid is a simple and a successful method that enhances the adhesion with the f-Na-MMT/PP

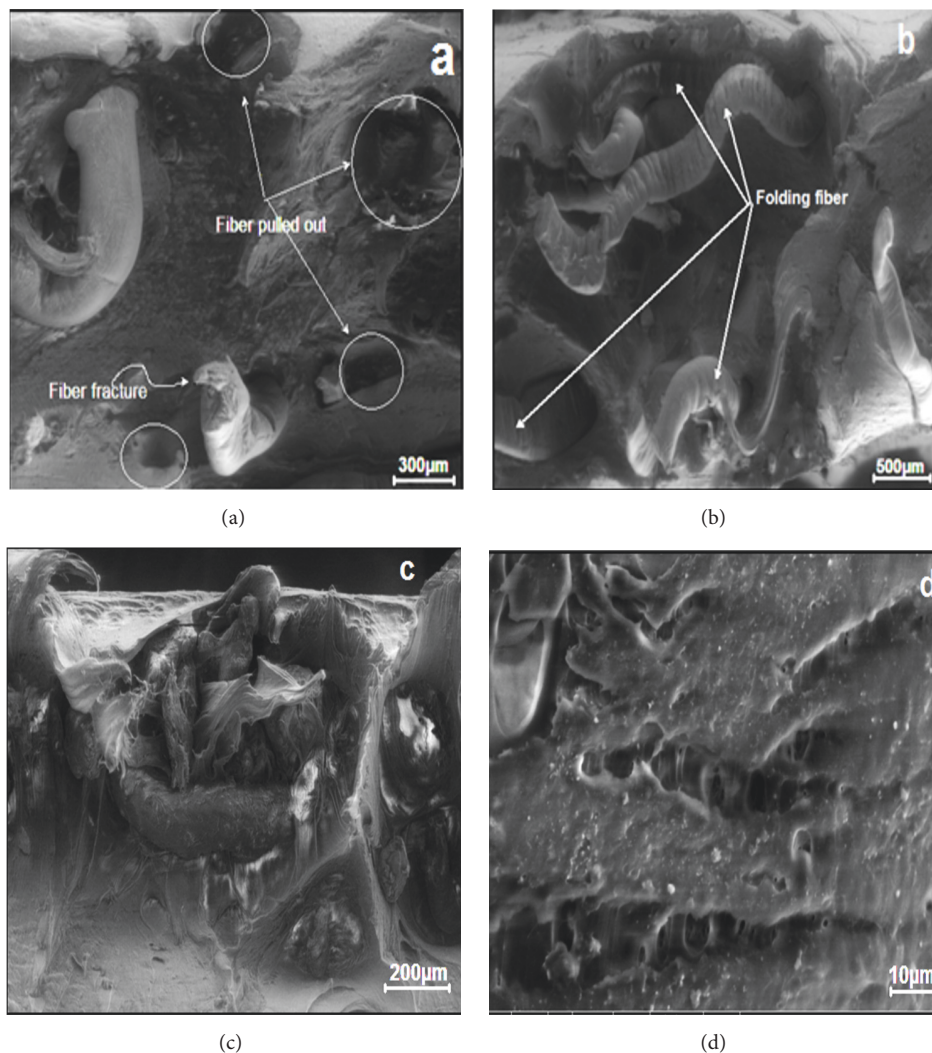


FIGURE 11: SEM micrographs of the tensile fractured surface of (a) 5 wt% PAFs/PP composite, (b) 5 wt% t-PAFs/PP composite, (c) 5 wt% t-PAFs/5 wt% f-Na-MMT/PP hybrid composite, and (d) the tensile stretched surface of hybrid composite.

recycled nanocomposite. A good dispersion of the fibers with a noticeable improvement of the interfacial adhesion between PP and treated PAFs phases was observed.

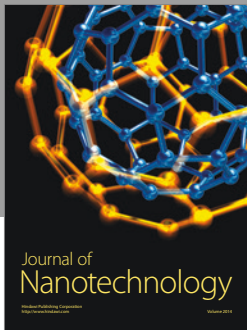
Conflicts of Interest

The authors declare that there are no conflicts of interest regarding the publication of this paper.

References

- [1] R. A. Weiss, "Mechanical properties of polypropylene reinforced with short graphite fibers," *Polymer Composites*, vol. 2, no. 3, pp. 95–101, 1981.
- [2] S. Pavlidou and C. D. Papaspyrides, "A review on polymer-layered silicate nanocomposites," *Progress in Polymer Science*, vol. 33, no. 12, pp. 1119–1198, 2008.
- [3] J. I. Velasco, J. A. De Saja, and A. B. Martínez, "Crystallization behavior of polypropylene filled with surface-modified talc," *Journal of Applied Polymer Science*, vol. 61, no. 1, pp. 125–132, 1996.
- [4] W. Qiu, K. Mai, and H. Zeng, "Effect of silane-grafted polypropylene on the mechanical properties and crystallization behavior of Talc/polypropylene composites," *Journal of Applied Polymer Science*, vol. 77, no. 13, pp. 2974–2977, 2000.
- [5] M. M. Thwe and K. Liao, "Durability of bamboo-glass fibre reinforced polymer matrix hybrid composites," *Composites Science and Technology*, vol. 63, no. 3-4, pp. 375–387, 2003.
- [6] A. K. Rana, A. Mandal, B. C. Mitra, R. Jacobson, R. Rowell, and A. N. Banerjee, "Short jute fiber-reinforced polypropylene composites: effect of compatibilizer," *Journal of Applied Polymer Science*, vol. 69, no. 2, pp. 329–338, 1998.
- [7] P. K. Mallick, *Fiber Reinforced Composites Materials. Manufacturing, and Design*, Taylor and Francis group, Boca Raton, London, UK, 3rd edition, 2007.
- [8] S. Jiang, Q. Li, Y. Zhao, J. Wang, and M. Kang, "Effect of surface silanization of carbon fiber on mechanical properties of carbon fiber reinforced polyurethane composites," *Composites Science and Technology*, vol. 110, pp. 87–94, 2015.

- [9] M. J. John, C. Bellmann, and R. D. Anandjiwala, "Kenaf-polypropylene composites: effect of amphiphilic coupling agent on surface properties of fibres and composites," *Carbohydrate Polymers*, vol. 82, no. 3, pp. 549–554, 2010.
- [10] O. M. L. Asumani, R. G. Reid, and R. Paskaramoorthy, "The effects of alkali-silane treatment on the tensile and flexural properties of short fibre non-woven kenaf reinforced polypropylene composites," *Composites Part A: Applied Science and Manufacturing*, vol. 43, no. 9, pp. 1431–1440, 2012.
- [11] N. Chand and U. K. Dwivedi, "Effect of coupling agent on abrasive wear behaviour of chopped jute fibre-reinforced polypropylene composites," *Wear*, vol. 261, no. 10, pp. 1057–1063, 2006.
- [12] M. Prakash and G. Pravin, "The effect of coupling agent on the properties of short non-woven PET micro fiber reinforced polypropylene (PP) composites," *International Journal of Chemical, Environmental and Biological Sciences*, vol. 2, pp. 2320–4087, 2014.
- [13] W. S. Chow and Z. A. Mohd Ishak, "Mechanical, morphological and rheological properties of polyamide 6/organomontmorillonite nanocomposites," *Express Polymer Letters*, vol. 1, no. 2, pp. 77–83, 2007.
- [14] G. Gorrasi, M. Tortora, V. Vittoria, G. Galli, and E. Chiellini, "Transport and mechanical properties of blends of poly(ϵ -caprolactone) and a modified montmorillonite-poly(ϵ -caprolactone) nanocomposite," *Journal of Polymer Science Part B: Polymer Physics*, vol. 40, no. 11, pp. 1118–1124, 2002.
- [15] A. Okada and A. Usuki, "Twenty years of polymer-clay nanocomposites," *Macromolecular Materials and Engineering*, vol. 291, no. 12, pp. 1449–1476, 2006.
- [16] E. P. Giannelis, "Polymer layered silicate nanocomposites," *Advanced Materials*, vol. 8, no. 1, pp. 29–35, 1996.
- [17] P. Reichert, H. Nitz, S. Klinke, R. Brandsch, R. Thomann, and R. Mülhaupt, "Poly(propylene)/organoclay nanocomposite formation: influence of compatibilizer functionality and organoclay modification," *Macromolecular Materials and Engineering*, vol. 275, no. 1, pp. 8–17.
- [18] M. Kawasumi, N. Hasegawa, M. Kato, A. Usuki, and A. Okada, "Preparation and mechanical properties of polypropylene–clay hybrids," *Macromolecules*, vol. 30, no. 20, pp. 6333–6338, 1997.
- [19] M. Kato, A. Usuki, and A. Okada, "Synthesis of polypropylene oligomer-clay intercalation compounds," *Journal of Applied Polymer Science*, vol. 66, no. 9, pp. 1781–1785, 1997.
- [20] D. H. Kim, P. D. Fasulo, W. R. Rodgers, and D. R. Paul, "Structure and properties of polypropylene-based nanocomposites: effect of PP-g-MA to organoclay ratio," *Polymer Journal*, vol. 48, no. 18, pp. 5308–5323, 2007.
- [21] A. Usuki, M. Kato, A. Okada, and T. Kurauchi, "Synthesis of polypropylene-clay hybrid," *Journal of Applied Polymer Science*, vol. 63, no. 1, pp. 137–139, 1997.
- [22] S. Bouhelal, US patent, No. 7,517,942, 2009.
- [23] S. Bouhelal, patent, No. 7,550,526, 2009.
- [24] S. Bouhelal, M. E. Cagiao, S. Khellaf et al., "Nanostructure and micromechanical properties of reversibly crosslinked isotactic polypropylene/clay composites," *Journal of Applied Polymer Science*, vol. 115, no. 5, pp. 2654–2662, 2010.
- [25] S. Bouhelal, M. E. Cagiao, D. Benachour et al., "SAXS study applied to reversibly crosslinked isotactic polypropylene/clay nanocomposites," *Journal of Applied Polymer Science*, vol. 117, no. 6, pp. 3262–3270, 2010.
- [26] R. Eslami-Farsani, S. M. Reza Khalili, Z. Hedayatnasab, and N. Soleimani, "Influence of thermal conditions on the tensile properties of basalt fiber reinforced polypropylene-clay nanocomposites," *Materials and Corrosion*, vol. 53, pp. 540–549, 2014.
- [27] M. S. Chowdary and M. S. R. N. Kumar, "Effect of nanoclay on the mechanical properties of polyester and s-glass fiber (Al)," *International Journal of Advanced Science and Technology*, vol. 74, pp. 35–42, 2015.
- [28] K. Majeed, M. Jawaid, A. Hassan et al., "Potential materials for food packaging from nanoclay/natural fibres filled hybrid composites," *Materials and Corrosion*, vol. 46, pp. 391–410, 2013.
- [29] M. Pracella, D. Chionna, I. Anguillesi, Z. Kulinski, and E. Piorkowska, "Functionalization, compatibilization and properties of polypropylene composites with Hemp fibres," *Composites Science and Technology*, vol. 66, no. 13, pp. 2218–2230, 2006.
- [30] H. Ku, H. Wang, N. Pattarachaiyakoo, and M. Trada, "A review on the tensile properties of natural fiber reinforced polymer composites," *Composites Part B: Engineering*, vol. 42, no. 4, pp. 856–873, 2011.
- [31] K. H. Prasad and M. S. Kumar, "Thermal Characterization of PP/Na⁺-MMT Composite Materials," *Journal of Materials Science and Engineering*, vol. 5, pp. 80–86, 2011.
- [32] F. Zouai, S. Bouhelal, M. E. Cagiao, F. Z. Benabid, D. Benachour, and F. J. B. Calleja, "Study of nanoclay blends based on poly(ethylene terephthalate)/poly(ethylene naphthalene 2,6-dicarboxylate) prepared by reactive extrusion," *Journal of Polymer Engineering*, vol. 34, no. 5, pp. 431–439, 2014.
- [33] E. P. Giannelis, R. Krishnamoorti, and E. Manias, "Polymer-silicate nanocomposites: Model systems for confined polymers and polymer brushes," *Advances in Polymer Science*, vol. 138, pp. 108–147, 1999.
- [34] L. E. Alexander, *X-ray diffraction methods in Polymer Science*, vol. 19, Wiley, New York, NY, USA, 2nd edition, 1969.
- [35] A. T. Jones, J. M. Aizlewood, and D. R. Beckett, "Crystalline forms of isotactic polypropylene," *Die Makromolekulare Chemie*, vol. 75, no. 1, pp. 134–158, 1964.
- [36] P. H. Nam, P. Maiti, M. Okamoto, T. Kotaka, N. Hasegawa, and A. Usuki, "A hierarchical structure and properties of intercalated polypropylene/clay nanocomposites," *Polymer Journal*, vol. 42, no. 23, pp. 9633–9640, 2001.
- [37] B. Wunderlich, *Macromolecular Physics*, vol. 3, Academic Press, New York, NY, USA, 2nd edition, 1980.



Hindawi

Submit your manuscripts at
<https://www.hindawi.com>

